NEUTRALIZATION OF BAFF AND APRIL WITH ENGINEERED SOLUBLE BCMA DECOY RECEPTOR FOR THE TREATMENT OF B-CELL MALIGNANCIES

Xin Eric Zhang

St Cross College

Thesis submitted to the University of Oxford in accordance with the requirements for the degree of Doctor of Philosophy in Oncology

Trinity Term, 2023

University of Oxford

Supervisors

Professor Amato J. Giaccia

Professor Ester M. Hammond

Examiners

Internal:

Professor Claire Edwards, Nuffiled Department of Surgical Sciences

External:

Professor Erinn B. Rankin, Department of Radiation Oncology, Stanford University

Study presented in this thesis was performed at the CR-UK & MRC Oxford Institute for Radiation Oncology, Department of Oncology, University of Oxford.

ABSTRACT

Neutralization of BAFF and APRIL with Engineered Soluble BCMA Decoy Receptor for the Treatment of B-cell Malignancies

Submitted for the Degree of Doctor of Philosophy

Xin Eric Zhang, St Cross College, Trinity Term, 2023

B-cell activation factor (BAFF) and A proliferation-inducing ligand (APRIL), two cytokines regulating B-cell homeostasis, are known to play important roles in the pathogenesis of B-cell malignancies. In B-cell malignancies, significant up-regulation and receptor-mediated signalling of BAFF and APRIL have been shown to facilitate tumour proliferation, treatment-resistance, and contribute to immune suppression in the tumour microenvironment (TME). Multiple myeloma (MM) and diffuse large B-cell lymphoma (DLBCL) are two of the most prevalent types of B-cell malignancies. Despite recent approvals of novel therapeutics such as CAR T-cell therapy (CAR T), disease relapse and treatment resistance continue to pose clinical challenges, often resulting in patient mortality. Here, we found elevated expression levels of BAFF, APRIL and their receptors, and observed the resulting activation of critical survival signalling pathways in patient specimens of MM and DLBCL. To effectively neutralize BAFF and APRIL-mediated signalling, we adopted a ligand trap approach, and developed a decoy receptor by fusing the extracellular cysteine rich domain (ECD) of the BCMA (B-cell maturation antigen) receptor (soluble BCMA, or sBCMA) with a human IgG1 Fc domain, to initially test our hypothesis. Next, to enhance the therapeutic efficacy of the approach, we engineered a mutant sBCMA, and developed a second-generation Fc fusion protein with significantly increased binding affinities toward BAFF and APRIL. *In vitro* and *in vivo* studies demonstrated that our sBCMA-

Fc ligand trap approach is efficacious at inhibiting tumour growth with minimal off-target normal tissue toxicities, providing preclinical evidence to support the use of our molecules as a treatment for MM and DLBCL.

ACKNOWLEDGMENTS

I would like to commence this acknowledgement by extending my deepest gratitude to my supervisors, Professor Amato Giaccia and Professor Ester Hammond. Their insightful guidance and unwavering support throughout my DPhil journey have been indispensable. They have been nothing short of inspirational and have played a pivotal role in my professional development within the realm of translational biology research.

Moreover, I owe a particular debt of gratitude to my mentor, Dr. Yu Rebecca Miao. Her expert insights into this project, coupled with her assistance with the *in vivo* experiments integral to this thesis, have been invaluable.

My heartfelt appreciation also goes out to my esteemed collaborators, whose critical contributions to the studies were vital in making this thesis a reality. I am indebted to Dr. Kaushik Thakkar, Dr. Dadi Jiang, Dr. Kazue Mizuno, Dr. Caiyun Grace Li, and Professor Albert Koong for their collaborative efforts.

Further, I wish to acknowledge my colleagues at the Giaccia Lab for an enriching and memorable experience. To Hala, Nuria, Yanyan, Yizhou, Fariha, and Jiyoung, I extend my sincere gratitude. Similarly, my thanks go to Dr. Ejung Moon at the Oxford Institute of Radiation Oncology, whose guidance and support have been nothing short of exceptional.

Reflecting upon my journey, I can confidently assert that I couldn't have wished for a more fulfilling DPhil experience.

TABLE OF CONTENTS

LIST OF FIGURES AND TABLES

CHAPTER 1 INTRODUCTION

1.1 Cancer

Cancer can be described as a group of complex and heterogenous diseases that arise when abnormal cells in the body acquire the ability to undergo aberrant and uncontrolled growth, leading to the formation of tumours and the invasion of other tissues and organs. Hanahan and Weinberg in their seminal and subsequent publications described six hallmarks of cancer which became the foundation for understanding the biology of the disease and developing new strategies for cancer prevention and treatment. The six hallmarks, summarized in Figure 1.1, when acquired, lead to a cell's aberrant proliferation, invasiveness, and enhanced survival.

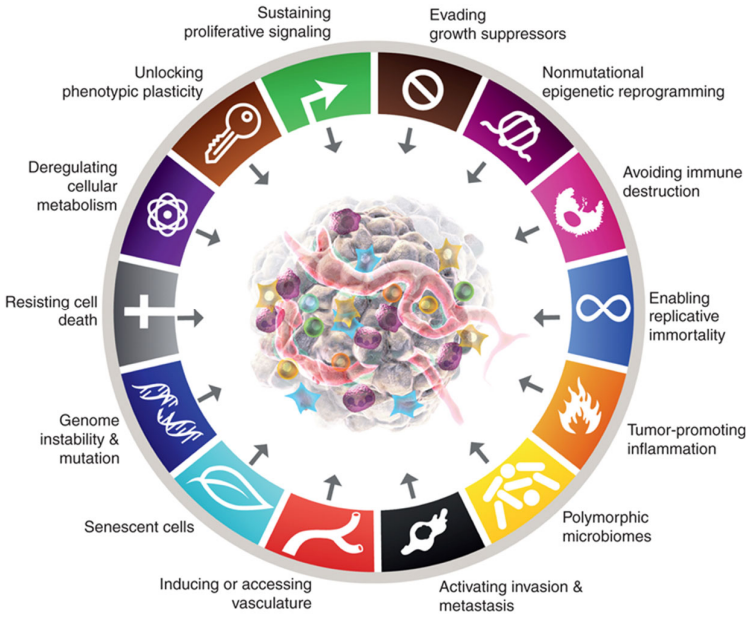

Figure 1.1. The hallmarks of cancer
The hallmark capabilities of cancer proposed in the original 2000 publication, with newly added enabling characteristics including 'genomic instability & mutation', 'tumour-promoting inflammation', 'unlocking phenotypic plasticity', and 'senescent cells'. Adapted and reprinted from Cancer Discovery, vol 12, issue 3, 12 January 2022, Hanahan, D. and Weinberg, R.A., Hallmarks of Cancer: New Dimensions, 31-46. Copyright (2022) with permission from American Association for Cancer Research. License Number: 5560231101835.

Arguably, the most prominent challenge facing the development of novel cancer therapeutics is the malignant cells' ability to acquire sustained proliferative signalling, evade growth suppressors and immune destruction, and resist cell death. While traditional options such as chemo-cytotoxic drugs and radiation therapy have long been utilized to induce cell death in cancer treatments, the recent breakthroughs in cancer therapeutics, such as targeted and cell therapies, have achieved significant improvements in overall survival rates for cancer patients. Unfortunately, most patients eventually develop resistance to treatments and face poor outcomes. Moreover, the drug-related adverse effects of novel treatment options, including CAR Ts and antibody-drug conjugates (ADCs), make these therapies unsuitable for frail and elderly patients, who constitute a significant proportion of the cancer patient population. Therefore, there is an urgent unmet demand for safe and efficacious therapies for patients who exhaust current treatment options.

1.2 B-cell malignancies

B-cell malignancies continue to be one of the most prevalent types of cancer worldwide. Non-Hodgkin's lymphoma (NHL) is the most common type of haematological malignancy worldwide, with B-cell NHL accounting for nearly 80% of all NHL cases[1]. Cancer Research UK reported that, between 2016 and 2018, there were about 14,000 new cases of NHL in the United Kingdom every year, accounting for 4% of all new cancer cases, ranking NHL as the 6th most common cancer in the country. DLBCL is the most common type of NHL, accounting for 30% - 40% of all NHL cases worldwide[2, 3]. The average age of diagnosis for NHL was 67, with over half of newly diagnosed patients aged over 65 years old[1].

MM, the second most common hematologic malignancy after DLBCL, is a cancer of plasma cells[4-6]. Although less prevalent compared to NHL, the incidence of the disease is expected to rise with an aging population globally[7]. Between 2016 and 2018, there were approximately 6,000 new cases of MM annually in the United Kingdom, accounting for roughly 2% of all new cancer cases in the country, as reported by Cancer Research UK. Similar to NHL, the median age of patients at diagnosis is approximately 66 – 70 years. Over half of new patients were over 65 years old[8].

Despite recent therapeutic advancements, MM remains incurable, and 100% of MM patients experience treatment relapse and eventually succumb to the cancer[6, 9-11]. Similarly, nearly half of DLBCL patients will relapse after initial treatment, and the current 5-year survival rate is about 60% - 70%[2, 3].

1.2.1 Multiple myeloma

MM, as the second most common type of B-cell malignancy, accounts for about 1% of all cancers and 10% of all hematologic malignancies worldwide[8, 12]. MM is characterized by excessive growth and accumulation, in the bone marrow (BM), of clonal, malignant plasma cells, which produce excessive monoclonal immunoglobulins (paraproteins, or M proteins).

Plasma cell dyscrasias encompass a range of diseases from a relative indolent precursor stage termed monoclonal gammopathy of undetermined significance (MGUS), to an intermediate asymptomatic but more advanced pre-malignant stage known as smouldering MM (SMM), to the eventual malignant disease of MM[8, 13, 14]. However, MGUS may progress directly to MM without passing through the SMM stage. In other cases, individuals may be diagnosed with SMM without a prior MGUS diagnosis[15, 16].

MGUS is a condition in which there is a small amount of monoclonal protein in the blood (< 3 g/dL), but no end organ damage or features of MM[12]. Since MGUS is asymptomatic, over 50% of individuals who are diagnosed with MGUS have had the condition for over 10 years prior to clinical diagnosis[16]. SMM is a condition in which there are higher levels of M protein in the blood, and there may be other signs of myeloma such as abnormal plasma cells or bone lesions, but the patient does not yet have symptoms or organ damage. SMM is considered the immediate precursor to MM, and patients with SMM are more likely to develop active myeloma or related conditions. SMM is defined as either the presence of serum M protein >= 3 g/dL or >= 10% monoclonal plasma cells in the BM. Similar to MUGS, not all cases of SMM evolve to MM, however, all cases of MM evolve from SMM[8].

MGUS is typically considered a benign condition with a low risk of progression to MM, while SMM patients tend to have a higher risk of developing MM. MGUS patients are monitored off therapy, as the risk of progression is 1% yearly[17]. Closer following off treatment is needed for SMM patients, as the risk of progression is 10% per year in the first 5 years, dropping to about 3% thereafter[8, 18, 19].

Clinical manifestations of MM result from excessive production of M proteins into the blood and/or urine by malignant plasma cells, infiltration of BM by neoplastic clones, and aberrant cytokine secretion[16, 20, 21]. MM's common clinical presentations include hypercalcemia, renal dysfunctions, anaemia resulting from bone marrow failure, abnormal bleedings due to platelet dysfunction, osteolytic bone lesions, and abnormal immune suppression indicated by recurrent infections. In rare cases, patients develop hyper viscosity syndrome that results in conditions such as ischemia, heart failure and neurological problems, and amyloid diseases such as carpal tunnels syndrome[5, 8, 12, 20, 22]. MM induced bone disease is the main cause of morbidity for MM patients[23].

In addition to clinical symptoms, diagnosis of MM requires either 10% or more clonal plasma cells in bone marrow examination or a biopsy-proven plasmacytoma. Also, 3 typical biomarkers are considered as evidence of MM: clonal bone marrow plasma cells >= 60%; serum free light chain ratio >= 100 (provided involved FLC level is >= 100 mg/L), and more than one focal lesion on MRI. Previous studies have shown that each biomarker is associated with approximately 80% risk of progression to more serious symptomatic end-organ damage stage of MM in 2 years[12, 16, 20, 21].

The cause of MM is currently unclear. Previous studies have reported radiation, exposure to industrial / agricultural toxins, and viral infections as likely contributing factors. However, proof is insufficient. Age, gender, and family history have also been considered potential risk factors, as MM appears to be more common in older adults

with the average age of diagnosis being around 70 years, and male are slightly more likely to develop MM than female[8, 22].

Although MM is still considered a single disease, in reality MM can be considered a collection of several different cytogenetically distinct plasma cell (PC) malignancies[20, 24]. Trisomies and IgH (immunoglobulin heavy chain) translocations are considered the primary cytogenetic abnormalities, and occur at the time of MGUS establishment[16]. According to previous studies that used fluorescent *in situ* hybridization (FISH) analysis, around 40% of MM cases involve neoplastic plasma cells with trisomies (known as hyperdiploid MM), while the remaining patients mostly have translocations affecting the IgH locus on chromosome 14q32 (known as IgH translocated MM). A small subset of MM patients exhibit both trisomies and IgH translocations[16, 25-28]. Additional secondary cytogenetic changes also occur along disease progression, including gain(1q), del(1p), del(17p), del(13) and secondary translocations involving MYC[16]. MM patients can be stratified into groups by levels of risk based on cytogenetic characteristics. For example, features of the high risk group typically include the presence of t(14;16), t(4;14) and del(17p)[12, 16].

MM patients at diagnosis typically demonstrate multiple different subclones of malignant PCs, which most commonly exhibit mutations in the driver genes KRAS, NRAS and BRAF. Clones undergo varying prominence with disease progression and response to treatment. As such, the conception of MM has evolved from one of linearly progressive disease with increasing resistance to treatment to one in which a “Darwin” selection process eliminates clones suppressed by therapy, and eventually new clones resistant to treatment dominate[12, 16, 29].

Due to the complexity of MM, patients are typically assessed along several dimensions, including host characteristics, tumour burden, biology, and response to therapy. Disease biology is best reflected by the hyperdiploid / IgH subtypes, and the presence

of secondary cytogenetic abnormalities as described above[16, 30-32]. In addition, markers associated with aggressive disease biology, such as elevated serum lactate dehydrogenase, and circulating plasma cells (plasma leukaemia), are often monitored[16].

1.2.2 Diffuse large B-cell lymphoma

DLBCL is the most common subtype of aggressive lymphoma in adults, accounting for about 30% – 40% of all NHL cases diagnosed worldwide, and representing a considerable socioeconomic burden affecting millions of people[2, 3, 33]. The incidence rates of NHL in the United States and Western Europe, including UK, France, Germany, Italy, and Spain, are among the highest worldwide[34]. According to the latest statistics from the American Cancer Society, approximately 80,550 people, including 44,880 males and 35,670 females, will be diagnosed with NHL in 2023, and about 20,180 people will succumb to the disease. In 2020, the number of incidents was estimated to be about 72,035 for Western Europe combined. As described previously, according to Cancer Research UK, NHL was ranked as the 6th most common cancer in the UK, account for 4% of all new cancer cases between 2016 and 2018. The number of DLBCL cases in the US is projected to reach 32,443 from 29,108, and in Western Europe from 26,078 to 27,981, from 2020 to 2025, related to an aging general population[34].

DLBCL is a highly heterogeneous disease with marked biological, pathological and clinical variability between patients[35]. The initial classification of DLBCL was established with respect to the microscopic appearance of cell size, nuclear morphology, and pattern of growth[36]. For instance, based on morphology, several variants of DLBCL have been described, including centroblastic, immunoblastic, anaplastic, and rare variants. The centroblastic variant accounts for about 80% of all DLBCL cases[2]. Immunophenotypic evaluation by either immunohistochemistry (IHC) or flow cytometry shows DLBCL cells express surface antigens such as CD19, CD20, CD22. Diagnosis is made when large, transformed B-cells (CD19+, CD20+ and CD79+), with prominent nucleoli, diffuse growth pattern, and a high proliferation fraction are seen in tissue biopsy[37].

DLBCL can occur de novo or result from development from a more indolent lymphoma[38]. Under the former setting, DLBCL is postulated to largely arise from the malignant transformation of mature B-cells that have experienced the germinal centre (GC) reactions[39]. The GC is the site within a lymph node where antigen-exposed B-cells undergo antibody affinity maturation and diversification, and develop the ability to produce high-affinity antibodies[40]. The GC B-cells are at risk of malignant transformation due to processes essential to immunoglobulin (Ig) affinity maturation including attenuation of certain DNA damage and cell proliferation checkpoints. These processes pose a significant risk to the genome of B-cells, which must endure high replication stress while undergoing multiple DNA mutation, breakage, and recombination events. Consequently, when critical regulatory checkpoints fail, the GC processes tend to become the genesis of most mature B-cell malignancies, including DLBCL[39].

Based on gene expression profiling (GEP) reflective of B-cell development stages, DLBCL can be classified by cell of origin (COO) into two major subtypes, germinal centre B-cell (GCB) DLBCL, or activated B-cell (ABC) DLBCL – a classification scheme also adopted by the World Health Organization. Patients with GCB DLBCL tend to have a better survival outcome than ABC DLBCL patients[2]. GCB DLBCL expresses genes that define germinal centre B-cell signatures and lack the expression of early post-GC markers. For example, recurrent t(14; 18) translocation and amplification of the c-rel gene on chromosome 2p are found exclusively in this subtype. In ABC DLBCL, cells' transcriptional signature resembles that of post-GC B-cells blocked from terminal differentiation into plasma cells. Recurrent trisomy 3, deletion of INK4A / ARF locus resulting in increased cellular proliferation and reduced apoptosis, and constitutive activation of the pro-survival B-cell receptor (BCR) signalling and consequently the NF-κB pathway, are defining hallmarks of ABC

DLBCL[40, 41]. A small subset of tumours without defining genetic features of GCB or ABC DLBCL, falls into a third group of Unclassified DLBCL[35]. It is worthy of noting that COO does not necessarily reflect the time point in B-cell differentiation at which the critical driver mutations were accrued, but rather the time point at which differentiation is arrested[39].

GCB DLBCL is more reminiscent of centroblasts and centrocytes in the dark zone and light zone of GC, respectively, due to the apparent lack of post-GC markers as mentioned previously. ABC DLBCL, on the other hand, is thought to correspond to GC-experienced B-cells ready for terminal differentiation into plasma cells[39, 42-44]. ABC DLBCL pathogenesis is characterized by two events, the constitutive activation of NF-κB, and the blockade of terminal differentiation[45-47]. For GCB DLBCL, the drivers appear to be more complex and genetic-related. One example is the translocation of the BCL2 gene detected in approximately 40% of GCB DLBCL, resulting in over expression of the BCL2 protein that protects cancer cells from apoptosis[48-51]. Clinical data showed that ABC DLBCL is associated with worse patient outcomes, as the five-year OS rate for ABC DLBCL patients is reported to be about 56%, and that for GCB DLBCL patients is about 78% following R-CHOP treatment[39].

In recent years, researchers have further analysed and classified DLBCL based on frequently occurring genetic alterations. For example, within ABC DLBCL, a subtype is strongly enriched for MYD88 and CD79B mutations, giving rise to aberrant activation of NF-κB pathway. In another subtype of ABC DLBCL, BCL6 translocation and NOTCH2 activation mutations are common, which facilitate tumour survival and proliferation. In GCB DLBCL, a subtype is characterized by pro-tumour BCL2 translocations and EZH2 mutations. EZH2 is one of the most frequently mutated genes in human lymphomas accounting for about 30% of patients with GCB DLBCL. EZH2

gain-of-function mutations repress genes involved in B-cell proliferation checkpoints, and terminal differentiation into plasma cells[35, 52-54]. The genetic subtypes lead to different tumour phenotypes and have differential impacts on patient outcomes. For example, the subtype with MYD88 and CD79B mutations tends to respond poorly to immuno-chemotherapy[52-54]. Furthermore, within GCB DLBCL, a subgroup with concurrent translocations of MYC and BCL2 and/or BCL6, termed Double-Hit Lymphoma or Triple-Hit Lymphoma, has been reported to have an aggressive and refractory clinical progression, and poor overall survival; and was assigned to a new class known as High Grade B-cell Lymphoma, representing approximately 10% of the DLBCL patient population[35, 39-41, 49]. The overexpression, instead of translocation, of MYC / BCL2 / BCL6 in Double / Triple Expressor DLBCL, appears to be of a lesser clinical importance compared to translocations[41, 55-58]. However, Double Expressor DLBCL has been reported to account for approximately one third of de novo DLBCL and up to 50% of relapsed / refractory DLBCL[35, 59, 60].

Clinically, most DLBCL patients present with a rapidly growing tumour mass involving one or more lymph nodes and extra-nodal sites. Approximately 40% of patients present with extra-nodal case. Gastrointestinal tract appears to be the most common site, although any tissue organ can be the primary site of DLBCL. About one-third of DLBCL patients suffer from B symptoms such as fever, weight loss, and night sweats. Some patients have symptoms related to organ(s) involvement. About half of patients present with stage I – II disease, while the rest present stage III – IV disease. The frequency of bone marrow involvement has been reported to be 10 – 20%, and takes the concordant form in DLBCL, which is associated with poor patient overall survival[2].

1.3 Overview of the therapeutic landscape for MM and DLBCL

1.3.1 Multiple myeloma

Treatment of symptomatic newly diagnosed MM is determined by the patient's eligibility for autologous stem cell transplant (ASCT), and primarily involves the use of the current standard-of-care (SOC) triplet regimens consisting of bortezomib (Velcade), lenalidomide (Revlimid), and dexamethasone, (VRd); or daratumumab, lenalidomide (Revlimid) and dexamethasone, (DRd). For MM patients eligible for ASCT, 3 – 4 cycles of induction therapy with VRd / DRd are typically indicated prior to stem cell harvest. After harvest, patients can either complete ASCT or resume induction therapy to delay ASCT until first relapse[12, 16].

Bortezomib belongs to a class of therapeutics known as proteasome inhibitors (PIs). Similar to normal cells, malignant cells such as MM require mechanisms for the degradation of misfolded or unfit proteins. Accumulation of misfolded proteins is typically inhibited by the unfolded protein response (UPR) pathway, which aims to resolve proteotoxic stress in the endoplasmic reticulum (ER). One of the mechanisms activated by the UPR pathway is ERAD (Endoplasmic Reticulum-Associated Degradation), which transports misfolded and unfit proteins out of the ER for degradation at the proteasome[61-63]. The proteasome is a large, multi-subunit protein complex that plays a critical role in degrading proteins that are no longer needed or that may be harmful to the cell, such as misfolded or damaged proteins, as well as regulatory proteins that control cell growth and division. The proteasome accomplishes this by recognizing and selectively breaking down targeted proteins into eventual amino acids that are subsequently reused by the cell. This process is essential for maintaining the proper functioning of cells and preventing the build-up of potentially harmful proteins[64-66]. Suppression of proteasome inhibits the ERAD mechanism, and results

in the accumulation of harmful misfolded proteins in the ER, which eventually leads to ER stress and cell death.

In MM, proteasome inhibition results in the accumulation of misfolded immunoglobulins and create stress to MM cells, which, if prolonged, leads to cell cycle arrest and apoptosis. Since proteasome inhibition-related induction of apoptosis correlates with the amount of immunoglobulins produced, MM cells are preferentially sensitive to PIs as they produce an aberrant amount of paraproteins. Bortezomib was approved in 2003 for the treatment of MM as the first PI approved for this indication[61, 67-70].

Lenalidomide belongs to a class of therapeutics knowns as immunomodulatory drugs (IMiDs). IMiDs are capable of inhibiting the NF-κB signalling pathway, which has been reported as a critical driver of MM pathogenesis. NF-κB regulates expressions of key growth factors for MM, including IL-6 and BAFF. IL-6 enhances proliferation and survival of malignant plasma cells mainly in early development of MM[61, 71-73]. Upregulation of BAFF due to aberrant activation of NF-κB results in further activation of NF-κB in a positive feedback loop, as well as the activation of AKT and MAPK signalling, which together facilitate tumour survival and proliferation. Furthermore, the constitutive activation of NF-κB enables the continuous proliferation of MM cells[73]. NF-κB also regulates various proteins involved in bone destruction (e.g., MIP-1α), cell cycle dysregulation (e.g., c-Myc and cyclin D, which are overexpressed in both MGUS and MM), and angiogenesis (e.g., VEGF)[74-77].

IMiDs have been shown to inhibit NF-κB signalling through several mechanisms, including direct binding to cereblon to activate cereblon E3 ligase, resulting in the rapid ubiquitination and degradation of B-cell transcription factors IKZF1 and IKZF3, which leads to subsequent downregulation of NF-κB signalling. Also, this degradation of

IKZF1 and 3 may cause direct cytotoxicity by inducing free radical-mediated DNA damage[16]. IMiDs have also been shown to modulate the activity of the IKK complex via inhibition of upstream TNFα or IL-1β signals. This leads to the downregulation of NF-κB signalling and decrease in the expression of NF-κB target genes. For instance, IMiDs have been shown to inhibit IL-6 secretion which is regulated by the NF-κB pathway[78].

Dexamethasone is a glucocorticoid that has anti-inflammatory, immunosuppressive, and anti-cancer properties. Dexamethasone works by binding to the glucocorticoid receptor that is present in most types of cells. Activation of the glucocorticoid receptor typically reduces normal immune system functions. In MM, the use of dexamethasone has an inhibitory effect on the proliferation of MM cells. In addition, dexamethasone has been known to reduce inflammation associated with MM, which can help to relieve pain and improve overall quality of life for patients; enhance MM cells' sensitivity to IMiD and PI treatments; and prevent the rejection of transplanted stem cells for MM patients receiving ASCT as part of their treatment[12, 16, 21].

Daratumumab is an anti-CD38 monoclonal antibody (mAB). CD38 was initially discovered in 1980 and is a Type II transmembrane receptor. CD38 plays a role in cell migration, receptor-mediated adhesion upon binding with cognate ligand CD31 or hyaluronic acid, and activation and proliferation of leukocytes[79-81]. In addition, CD38 has been reported to have bifunctional ecto-enzymatic activity, and play a role in CD38-dependent adenosine production in immune suppression mediated by NK cells and MDSCs[80, 82].Under normal conditions, CD38 is expressed at relatively low levels on myeloid and lymphoid cells, and certain non-hematopoietic tissues. However, normal plasma cells and MM cells were found to have high levels of CD38 expression, thus making CD38 a therapeutic target for MM[79, 83].

When bound to CD38 on cell surface, daratumumab disrupts the expression balance of Bcl-2 family proteins in MM cells, resulting in apoptosis. As an mAB, daratumumab can also kill tumour cells via Fc-dependent immune effector mechanisms including antibody-dependent-cellular cytotoxicity (ADCC), complement dependent cytotoxicity (CDC) and antibody-dependent cellular phagocytosis (ADCP)[79]. ADCC is induced by recruiting NK cells when the Fc receptors of NK cells bind to the Fc domain of daratumumab. Upon Fc engagement with daratumumab bound to CD38 on MM cell surface, NK cells release cytotoxic granules containing perforin and granzymes, which can penetrate MM cells and induce apoptosis. NK cells can also secrete cytokines that stimulate other immune cells and enhance the immune response against MM[79, 80, 84]. In addition, daratumumab can induce CDC against MM cells by activating the complement system. The complement system consists of a complex series of proteins that can be activated in response to foreign or abnormal cells. When bound to CD38 on tumour cell surface, daratumumab triggers the complement cascade, resulting in the formation of a membrane attack complex (MAC) on MM cell surface, which can create pores in MM cell membrane, leading to cell lysis and death[85]. Daratumumab is considered the most effective inducer of CDC of all currently available anti-CD38 mABs[79, 80]. Similar to ADCC, CDC also promotes further anti-tumour immune responses by releasing cytokines and chemokines that attract and activate other immune cells, such as macrophages and dendritic cells[85]. In the process of ADCP, phagocytosis of antibody-opsonized tumour cells occurs via interaction between the Fc domain of the anti-CD38 mAB and the Fc receptors which are present on monocytes and macrophages[79, 86]. Finally, in addition to Fc-dependent cytotoxic effects, isatuximab, a more recently approved anti-CD38 mAB, has been reported to be capable of mediating direct tumour cell apoptosis via the classical caspase-dependent and lysosomal cell death pathways[82, 87].

For newly diagnosed MM patients who are ineligible for ASCT due to age or other comorbidities, options for initial treatment are also VRd and DRd, similar to patients who are eligible for ASCT. VRd is typically preferred as the initial therapy administered for approximately 8 – 12 cycles, followed by maintenance therapy with lenalidomide. DRd is an alternative to VRd but adds cost and toxicity as a long-term treatment. For high-risk patients, bortezomib plus lenalidomide are used for maintenance treatment[16].

Despite effective initial ASCT and first-line SOC treatments, almost all MM patients eventually relapse. The duration of remission following each line of treatment decreases with each regimen. MM patients who were refractory or relapsed after initial therapy with lenalidomide and bortezomib had a reported median progression-free survival (PFS) of 5 months and overall survival (OS) of 9 months, based on previous studies[88]. The choice of second-line treatment depends on the patient's time of relapse, response to previous line of therapy, aggressiveness of the relapse, and performance status. Triplet regimens with bortezomib or daratumumab as the backbone[89, 90] and containing at least two new drugs, such as carfilzomib and pomalidomide described below, that the patient is not refractory to, should be used. Bortezomib-based triplets are recommended for relapsed patients with a longer initial remission[16, 91]. Also, ASCT or a second ASCT could be considered for eligible patients[16, 92].

Carfilzomib (Kyprolis), as a novel keto-epoxide tetrapeptide PI, was approved in 2013 by the FDA as a treatment for relapsed MM patients with previous exposure to bortezomib and lenalidomide[16, 93]. An analogue to lenalidomide, pomalidomide, was approved by the FDA in 2013 for relapsed refractory MM. For instance, pomalidomide triplets such as DPd and KPd are used for patients who are lenalidomide-refractory. For frail patients and patients with more indolent relapse, the

doublet Pd is often considered[16]. Ixazomib is a novel PI in oral formulation. Compared to bortezomib, ixazomib appears to have a more favourable safety profile and ease of administration. In 2015, ixazomib was approved for use with Rd for MM patients who have received at least one prior line of treatment[94, 95]. Elotuzumab is a novel mAB against SLAMF7. Although lacking single agent efficacy, elotuzumab was approved in 2015 by the FDA due to the therapeutic's synergistic effects in combination with Rd, for MM patients who have received one to three prior lines of treatments[81, 96]. Isatuximab is a anti-CD38 mAB that was approved by the FDA in 2020 for MM patients who have received at least two prior lines of treatment including R and a PI. Isatuximab is comparable to daratumumab in terms efficacy and safety; and the choice between either depends on cost to the patient, ease of access and scheduling[16, 81, 95, 97].

In recent years, CAR Ts emerged as a novel and promising option for relapsed / refractory (r/r) MM patients[4, 5, 10, 98]. Abecma (idecabtagene vicleucel), a BCMA-targeting CAR T, was granted full approval by the FDA in 2021 for the treatment of adult patients with r/r MM who have received at least four prior therapies, including an IMiD, a PI, and an anti-CD38 mAB. The approval was based on the results of the pivotal Phase 2 KarMMa clinical trial, which showed that Abecma induced deep and durable responses in a significant proportion of patients with heavily pre-treated MM. Among 128 patients in the KarMMa trial, the overall response rate (ORR) was 73%, and 33% of patients had a complete response (CR) or better. The median progression-free survival (mPFS) was 8.8 months. A similar BCMA-targeting CAR T, cilta-cel (CARVYKTI), was approved by the FDA in 2022 for the treatment of adult patients with r/s MM after four or more prior lines of therapy, including a proteasome inhibitor, an immunomodulatory agent, and an anti-CD38 monoclonal antibody. Cilta-cel in a

pivotal phase 2 study showed slightly better efficacy results than Abecma, although at the cost of slightly higher rates of treatment-related adverse effects[81, 99].

It's worth noting that the toxicities related to CAR Ts could be prohibitive for frail patients. Cytokine release syndrome (CRS) and neurotoxicity are the two main categories of CAR T related toxicities. CRS is an excessive inflammatory response caused by over-activation of immune effector cells that result in elevated secretion of cytokines including IL-1, IL-2, IL-6, IL-15, INF-γ and TNF-α. Symptoms include fevers, general malaise, hypertension, and hypoxia. In severe cases, irreversible organ damage and death can occur. IL-6 antibody or IL-6R antibody are typically used to manage CRS. Similar to CRS, neurotoxicity appears to be driven by cytokines such as IL-2; and typical symptoms include confusion, obtundation, and headaches[3, 100-102]. For instance, during the KarMMa study, CRS of varying degrees was reported for 84% of patients; and 18% of patients experienced neurotoxicity[16, 103].

Selinexor is a selective inhibitor of nuclear export (SINE) that works by blocking exportin 1 (XPO1), resulting in the inhibition of the export of tumour suppressor proteins which eventually induce MM cell death. Also, selinexor can inhibit NF-κB signalling. The FDA approved selinexor for MM based on the results of the STORM clinical trial, which showed that the combination of selinexor and dexamethasone induced responses in a significant proportion of heavily pre-treated patients with r/r MM, with an overall response rate of 25.4% and a median duration of response of 3.8 months. However, selinexor can have significant drug-related adverse effects, such as fatigue, nausea, anorexia, thrombocytopenia, and hyponatremia, and requires careful monitoring by a healthcare provider[16, 104].

Other notable investigational novel agents in clinical studies include BCMA-targeting ADCs such as belantamab mafodotin, and bispecific T-cell engagers (BiTEs) such as

AMG-701, REGN 5458 and TNB-383B. Belantamab mafodotin is a humanized anti-BCMA mAB that is conjugated to monomethyl auristatin-F, a microtubule disrupting agent. BiTEs typically target a cell-surface antigen such as BCMA on MM cells, and simultaneously bind to CD3 on T-cells thereby enabling T-cell recruitment and T-cell-mediated cytotoxicity against MM cells[4, 5, 81, 105].

1.3.2 Diffuse large B-cell lymphoma

The first-line SOC therapy for DLBCL patients is R-CHOP, which stands for Rituximab, an anti-CD20 mAB; cyclophosphamide, a chemotherapy agent that interferes with the DNA in cancer cells thus stopping cell division and growth; doxorubicin (hydroxydaunorubicin), a DNA-damaging chemotherapy agent; vincristine (oncovine), a chemotherapy agent that disrupts the ability of cancer cells to divide and grow; and prednisone, a steroid that helps to reduce inflammation and can also have a direct effect on cancer cells, causing apoptosis or growth inhibition[2]. Rituximab was approved by the FDA in 2006 for use as a first-line treatment in combination with CHOP for DLBCL. Rituximab binds with high affinity and specificity to CD20 expressed on the majority of normal and malignant B-cells. Rituximab achieves anti-tumour effect via several critical mechanisms, including ADCC, CDC, and non-classical apoptosis by triggering the cross-linking of multiple CD20 molecules, which in turn induces cell death via pathways involving Src kinases [33, 106].

With R-CHOP treatment, typically 60 – 70% of DLBCL patients are initially cured of disease. However, about 30 – 40% of patients will relapse or become refractory to R-CHOP treatment. The reported median OS is only about 6 months for DLBCL patients refractory to first-line treatment; and historical data showed that about 80% of r/r patients eventually succumb to the disease[33, 35, 107, 108]. Traditionally patients who progress after first-line R-CHOP treatment receive combination salvage chemotherapy, such as R-ICE, R-DHAP and R-GDP. About 50% of patients respond to second-line treatment, and of which about 50% proceed to undergo ASCT, which is often recommended for r/r DLBCL patients in suitable health conditions post first-line therapy. However, elderly patients with poor health are typically not suitable for this

option; and a substantial proportion of eligible patients are not cured by stem cell transplant[37, 109-111].

In recent years, several agents have received FDA approval for the treatment of r/r DLBCL, including anti-CD19 mAB tafasitamab-cxix (Monjuvi), SINE inhibitor Selinexor (XPOVIO), CD19b-targeting ADC polatuzumab vedotin-piiq (Polivy), and CD-19 CAR T-cell therapies Kymirah and Yescarta. Similar to CD20, CD19 is a transmembrane receptor that is expressed specifically by B-cells and on nearly all malignancies of B-cell origin. Unlike CD20, CD19 is expressed by B-cells throughout the maturation process[112-114], from the late pro-B to early pre-B-cell stages, with increasing expression as B-cells matures[115-118]. Although its level of expression is lower than CD20, CD19 is expressed on a broader range of malignant B-cells due to its onset beginning from the earlier phases of B-cell development[113, 114, 119]. Furthermore, CD19 expression is retained at relatively high levels on most B-cell tumours, including DLBCL[115].

By virtue of its extensive cytoplasmic domain, CD19 establishes intrinsic B-cell signalling thresholds and regulates BCR-dependent and independent signalling pathways[120]. However, whether CD19 expression itself contributes to the development of B-cell malignancies remains to be further investigated[115]. CD19 does not have a known natural ligand but is an important signalling component of B-cell surface complexes including CD21, CD81 and CD225, which can enhance B-cell activation[121-123]. For instance, humans genetically deficient of CD19 have B-cells that are hyporesponsive to transmembrane signals and generate weak T-cell dependent humoral responses. On the other hand, transgenic mice that overexpress CD19 have hyperresponsive B-cells and develop autoantibodies with age[124, 125]. Thus, CD19 expression appears to be required for normal signal transduction, cellular development, and functions[115].

Similar to rituximab, anti-CD19 mAB such as Monjuvi's key mechanisms of action include ADCC, CDC, and ADCP. In addition, inhibition of CD19 interaction results in reduced B-cell survival and proliferation via the receptor's impact on BCR activation pathways. For example, previous research reported a positive feedback loop between CD19 and c-Myc, one of the most frequently dysregulated and overexpressed proteins in B-cell malignancies[115].

In addition, clinical studies are being conducted for novel therapeutics with proven modalities, including CAR NK-cell therapies, CAR Ts targeting additional cell surface antigens, such as CD20 and CD30, BiTEs targeting CD19 or CD20 on tumour cells, IMiDs such as lenalidomide, immune checkpoint inhibitors such as anti-PD-1 mABs, novel mABs and ADCs, as well as molecular pathway inhibitors against the BCR pathway, such as BTK, NF-κB, and PI3K/AKT/mTOR inhibitors, as well as BCL-2 inhibitors[33].

As mentioned earlier, about one-third of DLBCL patients will fail first-line R-CHOP treatment. Although novel therapeutics such as CAR Ts are promising, and efforts to explore combination treatments involving novel agents in clinical trials are underway[33, 37], treatment resistance still remains as the major challenge[35]. For example, research has reported that about 50 – 60% of DLBCL patients will not achieve a complete response or will relapse after CAR T-cell therapy.

Similar to BCMA-targeting CAR Ts for MM, one mechanism of DLBCL CAR T therapy relapse is antigen escape, as CD19-negative B-cell malignancy relapses have been reported. Furthermore, the loss of CD19 antigen could be caused by splicing / mutation mechanisms. Another potential mechanism of CAR T relapse could be the upregulation of PD-1 / PD-L1 expressions that was observed in relapsed patients post CAR T treatment[3, 126-129]. Similar to challenges facing MM, due to dose-limiting

normal tissue toxicities associated with CAR Ts and ADCs, only a small fraction of r/r DLBCL patients are eligible for treatment[3]. Furthermore, the hefty costs associated with CAR T-cell therapy could severely limit patient access to this novel therapy. For instance, the cost of the CAR T product alone is about $375,000 without accounting for cost of hospitalization and treatment of drug-related complications such as CRS, which could incur hundreds of thousands of dollars of additional expenses[3, 130].

For patients who are not suitable for ASCT and CAR T or ADC treatments, salvage chemotherapies appear to be ineffective. For example, previous analysis of pooled outcomes from several large clinical studies with r/r DLBCL patients (n=636) treated with various salvage chemotherapies showed an ORR of 26% and a median overall survival (OS) of about 6 months[37, 108, 131]. Similarly, molecular inhibitors typically lack specificity thus result in off-target toxicities and thus are not suitable for frail patients. Therefore, novel targeted therapeutics with tolerable toxicity profile for r/r and frail DLBCL patients are needed[37].

1.4 BAFF and APRIL are important regulators of normal B-cell homeostasis

1.4.1 Characterization of BAFF

BAFF is a member of the TNF Ligand Super Family (TNFLSF). Initially discovered in the 1990s from a human neutrophil / monocyte-derived complementary DNA library, BAFF is also known as B lymphocyte stimulator (BLyS) protein, TNF and apoptosis ligand-related leukocyte-expressed ligand-1 (TALL-1) and TNF homolog that activates apoptosis, NF-κB and c-Jun NH2-terminal kinase (THANK)[9, 132-134]. BAFF is expressed primarily by cells in the microenvironment, including myeloid cells, such as monocytes, macrophages, neutrophils, dendritic cells (DC); osteoclasts, stromal cells, epithelial cells, and a subset of T-cells[9, 132, 134-137]. Previous research reported that several cytokines such as IFN-α, IFN-γ, IL-10, CD40-L and granulocyte colony stimulating factor, as well as lipopolysaccharide (via the production of reactive oxygens) and peptidoglycans can activate BAFF production by macrophages, neutrophiles and DCs[138, 139].

Human BAFF is a 285-amino acid protein. In the human BAFF gene, exon 1 codes for the transmembrane domain and flanking regions, exon 2 codes for the furin processing site, and exons 3 – 6 codes for the TNF homology domain, which binds to receptors[9, 140]. In the cell membrane-bound form, BAFF is a Type II, single-pass, transmembrane protein. However, surface-bound BAFF can be cleaved and released as a soluble ligand upon proteolytic processing by furin. Furin cleavage can generate both trimeric and monomeric forms of BAFF, depending on the specific cleavage site that is targeted. When furin cleaves BAFF between amino acid residues 72 and 73, which lies within the region of the protein that is responsible for trimerization, the resulting soluble protein will be in a trimeric form, as the three monomers will remain connected by disulfide bonds. However, there are alternative cleavage sites within the BAFF

protein that can be targeted by furin, which could result in the generation of monomeric forms of the protein. For example, cleavage at a site within the stalk region of the protein could release a monomeric form of BAFF from the cell surface[132, 136, 140].

It is important to note that while BAFF can exist as a soluble monomer which is able to bind to cognate receptors on B-cell surface and promote survival and maturation albeit at a lower affinity, soluble BAFF commonly exists in a trimeric form, which is the more biologically potent form of the protein with a higher binding affinity toward cognate ligands[132, 140, 141]. BAFF trimerization is a critical step in its ability to activate B-cells, and it occurs through the formation of disulphide bonds between the individual monomers on cell surface[142]. The balance between soluble monomeric and trimeric forms of BAFF can be influenced by a number of factors, including the expression and activity of enzymes that regulate BAFF trimerization, as well as the presence of soluble receptors such as TACI, which has been reported to bind to monomeric soluble BAFF at a higher affinity than trimeric soluble BAFF[132, 134, 140, 143, 144]. Overall, trimeric BAFF is the primary active form of the protein in effecting biological functions[136, 138, 140, 141]. At neutral or basic pH, 20 homotrimers of soluble BAFF can associate into a 60-mer virus-like structure. The association is dependent on the "Flap" loop that is unique to BAFF in the TNFLSF. At acidic pH, the 60-mer virus-like BAFF structure irreversibly dissociates back into trimers. The 60-mer BAFF structure is a biologically active ligand that binds to receptors, and has been reported to be moderately more active than trimers *in vitro*[137, 140, 145, 146]. Despite well studied biological functions of soluble BAFF, the functions of membrane-bound BAFF remain to be investigated, although reported potential functions may include regulation of peritoneal B-cells, production of basal levels of IgA, expression level of CD23, and differentiation of B-cells[132, 147]. Previous studies have reported alternative splicing leads to a short variant of BAFF,

which in soluble state forms inactive heterotrimers with BAFF and negatively regulates BAFF signalling by blocking normal soluble BAFF homotrimer formation[138, 148, 149].

1.4.2 Characterization of APRIL

APRIL, also known as TNFSF13A, is a closely related family member to BAFF. The sequence similarity between APRIL and BAFF within the receptor binding TNF Homology Domain (THD) is approximately 50%[137]. However, APRIL and BAFF do not appear to be the result of a gene duplication event, since BAFF is located on human chromosome 13q32-44, while APRIL is located close to the telomeric end on human chromosome 17p13, in close proximity to TWEAK, another TNFLSF member. Furthermore, APRIL does not form 60-mer virus-like structures[2, 136]. Human APRIL, which consists of 250 amino acids, shares a similar exon structure with BAFF. Analysis of the receptor binding sites of APRIL and BAFF revealed that the electrostatic potential on the surface of APRIL is positively charged while that of BAFF is negatively charged. This may account for the inability of APRIL to bind to BAFFR[140].

APRIL was originally identified as a growth promoter in various cancer cell lines[9, 150]. Similar to BAFF, APRIL is primarily secreted from cells of the myeloid lineage in the microenvironment, such as macrophages, monocytes, dendritic cells, and osteoclasts. In addition, research has shown that BM stromal cells and T-cells also produce APRIL[5]. Distinct from BAFF and most TNF family members, full-length APRIL is cleaved intracellularly in the Golgi apparatus by a furin protease initially, and then secreted as a soluble homotrimer[151]. As such, APRIL normally exists in a soluble trimer form once secreted outside of the cell of origin[139]. Similar to BAFF, APRIL secretion by cells of origin can be stimulated by cytokines such as IFN-α, IFN-γ, IL-10, CD40-L and granulocyte colony stimulating factor, as well as lipopolysaccharide (via the production of reactive oxygens) and peptidoglycans[138].

Previous studies have identified alternatively sliced forms of APRIL containing deletions. For example, APRIL-δ was generated when exon 1 of APRIL was combined with an alternative acceptor site in exon 3. APRIL-δ was reported to be a malignant isoform lacking a furin cleavage site, and bound to leukaemia precursor cell membrane. APRIL-β, with omission of exon 3, on the other hand, appear to be a homologue of δ-BAFF and by analogy should negatively regulate APRIL activity in a dominant-negative manner; and has been reported to bind to BAFFR at low affinity[138]. In addition to isoforms, TWE-PRIL, a combined form of APRIL and TWEAK that brings the first six exons of TWEAK together with exons 2 – 6 of APRIL, was discovered as a cell-surface protein on activated and resting primary T-cells and monocytes[136, 152]. Since TWE-PRIL contains the complete THD of APRIL, the fusion protein is expected to be trimeric and to bind with APRIL's cognate receptors. The functional significance of TWE-PRIL remains to be investigated[136]. Interestingly, heteromeric structures containing both BAFF and APRIL have been discovered previously and were shown to be biologically active *in vitro*[142]. The origin of the BAFF-APRIL structure as well as its receptor-binding activities are worthy of further investigation.

1.4.3 Cognate receptors for BAFF and APRIL

While BAFF is the only identified ligand for BAFFR, both BAFF and APRIL are capable of binding to and activating BCMA and TACI[9]. Trimeric BAFF binds to primary receptor BAFFR, and weakly to BCMA; while 60-mer BAFF can bind to BAFFR, TACI, and with low affinity to BCMA[153]. APRIL is the primary ligand for BCMA, and activates TACI when bound to heparan sulphate proteoglycans (HSP) on cell surface and oligomerized[154]. TACI activation requires BAFF 60-mers, and multimerized APRIL bound to HSP; and BAFF trimers and APRIL trimers were reported to be less effective at activating TACI[155] (Figure 1.2). In the following sections, we will discuss characteristics of receptors BAFFR, BCMA, and TACI, and their biological functions effected via ligand-mediated activation.

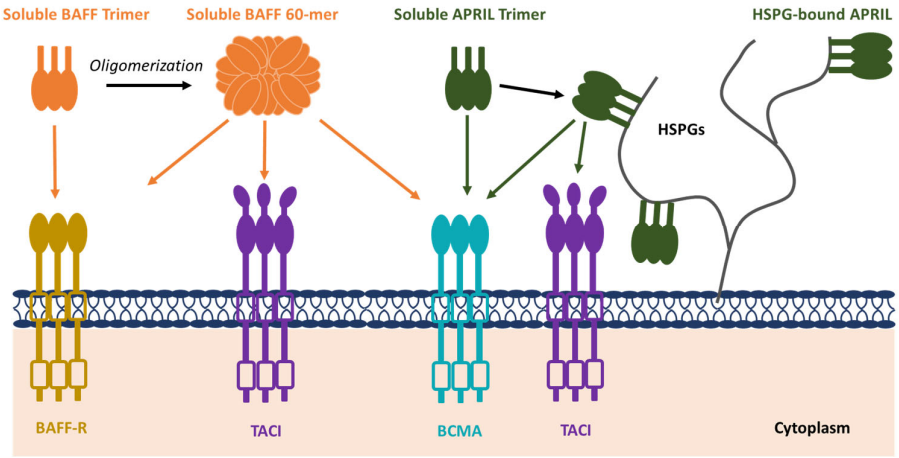

Figure 1.2. BAFF, APRIL and their receptors
Ligand-receptor interactions between BAFF, APRIL and their receptors BAFFR, BCMA, and TACI.

1.4.4 Ligand-mediated receptor activation in normal B-cell physiology

1.4.4.1 Characterization of BAFFR

BAFFR, also known as BR3 and TNFRSF13C, is a Type III transmembrane single-pass protein containing four cysteine rich residues in the extracellular ligand binding domain, but lacks a signal peptide[140, 156]. It is interesting to note that structurally BAFFR is atypical of the TNFRSF, since members of the family are typically characterized by several extracellular cysteine rich domains (CRDs), which function as ligand binding sites and as ligand-independent assembly of receptor monomers into dimers, trimers or multimers. Unlike other members of the TNFRSF, BAFFR has a partial CRD for cognate ligands and self-assembly[134, 157].The BAFFR gene is located at chromosome 22q13.1 – 13.31. Exon 1 encodes the ligand-binding domain, exon 2 encodes the transmembrane domain and flanking regions, while exon 3 encodes the intracellular domain. Previous research reported that the BAFFR protein is composed of 185 amino acids. The extracellular domain of BAFFR consists of 41 amino acids, while the transmembrane domain consists of 23 amino acids, and the intracellular domain consists of 121 amino acids. Biological functions of BAFFR are mediated through a sequence motif "PVPAT" within the cytoplasmic domain[140].

BAFFR is almost exclusively and widely expressed on most types of B-cells except for BM plasma cells[132-134]. Along the B-cell development spectrum (Figure 1.3), BAFFR expression is absent on B-cell precursors in the bone marrow but is gained and starts when immature B-cells acquire a functional B-cell receptor (BCR) in the bone marrow, and develop into transitional B-cells in the spleen, which critically depend on pro-survival signalling by BAFFR for rescue from premature cell death[134]. BAFFR expression levels are upregulated as transitional B-cells mature to become naïve or GC B-cells[153, 158]. Plasmablasts and plasma cells typically do not express BAFFR, but primarily rely on BCMA for survival and proliferation[153, 159, 160]. Previous studies

reported that although the induction of BAFFR on immature B-cells seems to depend on the expression of functional BCRs, BAFFR expression could be maintained in mice after the ablation of spleen tyrosine kinase (SYK), a key element in BCR signalling, as well as in cells which were depleted of CD79A, an essential BCR component. This finding suggests the survival of B-cells with impaired BCR functions could be supported by BAFFR signalling[134, 161].

In addition to B-cells, previous research has identified a small subset of resting T-cells with surface BAFFR, and the expression of BAFFR increases following stimulation *in vitro*. Similar to other TIM-containing receptors in the TNFRSF, upon ligand binding activation, BAFFR signalling is dependent on TRAF binding in the cytoplasmic tail of the receptor, which uniquely binds to TRAF3[132].

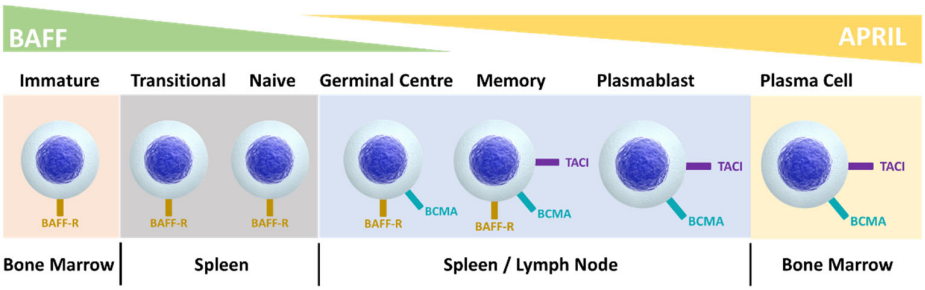

Figure 1.3. Expressions of BAFFR, BCMA, and TACI along B-cell development process
B-cell development process from immature B-cells to plasma cells and the expressions of receptors BAFFR, BCMA and TACI during different stages along the development cycle.

1.4.4.2 Biological significance of BAFFR signalling

As described earlier, BAFF is the only cognate ligand for BAFFR (Figure 1.2). The BAFF-BAFFR signalling axis plays a vital role in the survival, maturation, and differentiation of B-cells through the development process. As briefly mentioned in the previous section, BAFFR signalling does not impact central B-cell selection in the bone marrow since the expression level of BAFFR on immature B-cells is typically extremely low. Upon exiting the bone marrow, naïve B-cells encounter self-antigens, experience the transitional stage, and then compete for survival signals mediated by BCR and BAFFR cooperatively[132, 162]. During the early transitional stage, BCR signalling regulates the deletion and anergy of B-cells. However, at the late transitional stage, when BAFFR expression gains importance, BCR and BAFFR form a positive feedback loop to facilitate B-cell survival. BCR initially triggers the expression of BAFFR through the PI3K signalling pathway[163]. In addition, BCR signalling leads to the expression of p100, which serves as a substrate for the alternative NF-κB pathway, which is the key survival pathway mediated via BAFFR / BAFF signalling. On the other hand, BAFFR signalling up-regulates CD19, which enhances BCR signalling. Therefore, BAFFR and BCR signalling feedback loop during the B-cell maturation process plays an important role in mediating B-cell survival by regulating key pro-survival and anti-apoptotic proteins[132, 164].

As the unique cognate ligand to BAFFR, trimeric BAFF binds to BAFFR at an affinity measured at K_D of 16 nM with the surface plasmon resonance method[165]. The binding of BAFF to BAFFR activates downstream survival pathways that regulate important functions including protein synthesis and energy metabolism required to extend the half-life of B-cells during development[9, 132, 134]. It has been reported that BAFF / BAFFR signalling is capable of activating both the canonical and alternative NF-κB pathways[166]. However, the alternative pathway appears to be the

primary and most reported mechanism via which BAFFR signalling facilitates B-cell survival and development. In the alternative NF-κB activation, upon BAFF binding, BAFFRs aggregate, and recruit TRAF3 to their intracellular domains, thus reducing the concentration of available TRAF3 in B-cells. As a result, newly synthesized NIK can accumulate and phosphorylate IKK1 which leads to the phosphorylation of NF-κB p100, and the subsequent processing of p100 to p52 in a NIK and IKK-dependent manner, producing the p52 found in resting B-cells. The p52 then dimerizes with RelB to form the p52/RelB heterodimer which translocate into the nucleus to regulate the expression of target genes. Apoptotic proteins including Bim, Bak, and p53 are typically downregulated as a result. On the other hand, pro-survival proteins such as Bcl-2, Bcl-xl, c-Myc and Bcl-6 are up-regulated[167]. In addition to NF-κB activation, BAFFR / BAFF signalling has been reported to activate the PI3K-dependent signalling cascade, resulting in the phosphorylation of AKT and mTOR[132]. The AKT / mTOR axis initiates the metabolic reprogramming of B-cells, resulting in increased cellular fitness and lifespan[134, 168].

Previous studies with various mouse models showed that BAFF / BAFFR signalling is essential for B-cell survival. Inhibition of the signalling axis typically result in a reduction of mature B-cells and leads to immune-deficiency characterized by B-lymphopenia, agammaglobulinemia, and impaired humoral immune responses. However, neither BCMA nor TACI knockout (KO) mice show any B-cell deficiency[134, 169], suggesting the BAFF-BAFFR axis could be the primary pathway regulating B-cell development and growth prior to maturation into plasma cells when BCMA becomes the critical regulator[9, 134].

Interestingly, certain subsets of B-cells appear to be less dependent on the BAFF / BAFFR axis. For example, studies showed that BAFFR deficient or BAFF and BAFFR KO mice had much lower levels of follicular and marginal zone B-cells (B2 B-cells),

but the population of B1 B-cells in the peritoneal seemed to be less affected in the mouse models[170-172]. Studies with antibodies to inhibit BAFF and BAFFR showed similar impact on B2 B-cells, but spared immature and transitional 1 B-cells. In addition, plasma cells and memory B-cell also appeared to be much less dependent on the BAFF / BAFFR axis for survival[134].

In human, only two cases of BAFFR deficiency resulting from complete inactivation of the gene TNFRSF13C have been reported[173]. The cases showed that the lack of BAFFR resulted in an arrest of B-cell differentiation from transitional 1 B-cells to transitional 2 / naïve and marginal zone B-cells. Common symptoms reported include severe lymphopenia, low IgM and IgG antibody titres, but increased levels of serum IgA[134]. This is consistent with the functions of BAFF / BAFFR signalling and with observations from mouse studies. The increase in IgA levels, however, may indicate that the severe inhibition of B2 B-cells due to BAFFR ablation may contribute to the expansion of B1 B-cells which could develop into IgA-secreting plasma cells independent of BAFFR signalling.

1.4.4.3 Characterization of BCMA

BCMA, also known as TNFRSF17 or CD269, is a closely related family member to BAFFR and TACI. BCMA was initially discovered in 1992 as a translocation event t(4:16) in a human T-cell lymphoma, yet its expression is mostly limited to mature B-cells[137]. Similar to BAFFR, BCMA is also a single-pass, Type III transmembrane protein lacking a signal peptide, and as an atypical TNF receptor, contains only one extracellular CRD for ligand binding[4, 165]. The BCMA gene is located on chromosome 16 in humans. Specifically, it is located on the long arm of chromosome 16 at position 16p13.13. Exon 1 encodes the CRD, exon 2 the transmembrane domain and exon 3 the intracellular domain. Studies have reported that the BCMA protein consists of 184 amino acids. The extracellular domain of BCMA consists of 54 amino acids, while the transmembrane domain consists of 23 amino acids, and the intracellular domain consists of 107 amino acids. The intracellular domain of BCMA is highly similar to BAFFR over a short sequence of 18 amino acids[105, 140]. Unlike BAFFR, BCMA's intracellular domain contains a TRAF binding consensus site that engages with several TRAFS, while the BAFFR domain is highly specific toward TRAF3[174, 175]. BCMA is synthesized in the endoplasmic reticulum (ER) and is then transported to the cell surface via the Golgi apparatus. Therefore, earlier research reported BCMA expressions both in the Golgi and on cell surface[165]. BCMA is expressed exclusively in B-cell lineage cells, and in particular, is selectively induced and expressed from late-stage B-cell maturation to terminal differentiation to plasma cells during B-cell development, concurrent to the loss of BAFFR[5, 137, 165, 176]. More importantly, BCMA is almost exclusively expressed on plasma cells, but not in earlier-phase and memory B-cells. This suggests that BCMA is not critical to B-cell selection and development but is essential for the survival of plasmablasts and long-lived plasma cells in the bone marrow[4, 9, 132, 160, 177, 178]. Previous research showed that

BCMA-knockout mice exhibited normal B-cell development and humoral responses to T-cell dependent and independent antigens in the short-term as well as memory B-cell responses. However, there was a sharp reduction of plasma cells in the bone marrow, indicating the vital role BCMA plays in plasma cell physiology[9]. In addition to its full-length, membrane-bound form, BCMA can be cleaved at the N-terminus to form soluble BCMA.

1.4.4.4 Biological significance of BCMA signalling

APRIL and BAFF are the cognate ligands for BCMA. However, APRIL, due to its significantly stronger binding affinity toward BCMA, is commonly accepted as the primary ligand for BCMA. Previous studies utilising flow cytometry have reported a binding affinity between APRIL and BCMA measured at 25 – 48 pM[179, 180], while the interaction between BAFF and BCMA was found to be undetectable using the same technique[181]. Upon binding with APRIL or BAFF, BCMA activates key pro-survival and anti-apoptosis pathways including the canonical NF-κB and MAPK, via recruitment of TRAF proteins at its intracellular domain. Previous research reported BCMA interaction with TRAF1, 2 and 3, or with TRAF5 and 6, but not with TRAF2[140, 182, 183]. The activation of the canonical NF-κB signalling by BCMA is one mechanism by which BCMA promotes the survival of plasma cells. Canonical NF-κB is a signalling pathway that leads to the activation of the p50/RelA complex, which translocates into the nucleus and activates the expression of target genes involved in cell survival and proliferation. Studies have shown that BCMA activation of canonical NF-κB signalling pathway in plasma cells leads to the upregulation of anti-apoptotic proteins, such as Bcl-2 and Bcl-xL, and downregulation of pro-apoptotic proteins, such as Bim and Bad[168].

Furthermore, the canonical NF-κB activation via BCMA results in enhanced production of IL-6, which promotes plasma cell survival via the JAK-STAT pathway[61]. IL-6 is a cytokine that plays an important role in regulating immune responses and promoting cellular survival and proliferation. IL-6 signals through a receptor complex that consists of two subunits: a ligand-binding subunit (IL-6R) and a signal transducing subunit (gp130)[184]. Upon binding of IL-6 to IL-6R, the receptor complex undergoes conformational changes that promote the recruitment and

activation of JAKs, which then phosphorylate the cytoplasmic domain of gp130, leading to the recruitment and activation of signal transducer and activator of STAT proteins. Once activated, STATs form homodimers or heterodimers and translocate into the nucleus, where they bind to specific DNA sequences and regulate the expression of target genes[185]. Alternatively, the IL6 receptor complex can also activate the JAK/STAT pathway via TRAF recruitment. In the context of plasma cells, IL-6 activation of JAK/STAT upregulates anti-apoptotic proteins such as BCL-2 and BCL-X, which facilitate the survival and proliferation of plasma cells[186].

In addition to activating the canonical NF-κB pathway, ligand-mediated BCMA signalling has been shown to activate the MAPK pathway, specifically the ERK pathway, in plasma cells. The precise molecular mechanism by which BCMA activates the MAPK signalling pathway in plasma cells is not fully understood. However, it is believed that BCMA activates the MAPK pathway through recruitment of TRAF proteins at its intracellular domain upon binding with APRIL or BAFF. TRAF proteins then activate downstream molecules such as MAP3K and MAP2K, leading to the activation of the MAPK pathway. Previous studies have shown BCMA-mediated activation of the MAPK pathway in plasma cells specifically involves the MAPK subtype ERK pathway, which is considered critical for plasma cell survival and for the maintenance of long-lived plasma cells[183].

Overall, although not essential for earlier-phase B-cell development and survival, BCMA is almost exclusively expressed on plasma cells which rely critically on the receptor for maturation, survival and proliferation via ligand mediated activation of key downstream survival pathways such as NF-κB, MAPK, and JAK/STAT.

1.4.4.5 Characterization of TACI

The transmembrane activator and CAML interactor (TACI), also designated as TNFRSF13B, is a closely related family member of BAFFR and BCMA. TACI was initial discovered as a binding partner of calcium-modulator and cyclophilin ligand (CAML) protein in Jurkat T-cells and induces the transcription factor NF-AT (nuclear factor of activated T-cells)[143]. Similar to BAFFR and BCMA, TACI is also a single-pass, Type III transmembrane protein. However, unlike BCMA and BAFFR, TACI has two extracellular CRDs for ligand binding. The first ligand-binding CRD has a much weaker binding affinity than the second CRD[140, 179]. The TACI gene is located on human chromosome 17p11.2 and consists of six exons. Exons 1 to 3 encode the extracellular CRDs, exon 4 encodes the transmembrane domain, and exons 5 and 6 encode the cytoplasmic domain of TACI, which contains several conserved motifs that mediate downstream signalling pathways, including the TRAF-binding motif and the proline-rich motif[140, 143, 155, 187].

Interestingly, the human TACI gene undergoes alternative splicing to produce short and long isoforms (TACI-S and TACI-L), serving different but important biological functions. The longest TACI isoform (Isoform 1) in humans has a total of 293 amino acids, while other TACI isoforms have slightly shorter sequences due to the exclusion of certain exons[188]. For instance, one short isoform has been shown to lack the first CRD due to the skipping of exon 2[140]. Studies have shown that the expression of different isoforms in humans provide unique controls on B-cell maturation. For example, transduction of the TACI-S isoform into human pre-B-cells or murine B-cells lacking TACI resulted in the maturation of the B-cells into plasma cells. Furthermore, TACI-S appears to bind with BAFF and APRIL with substantially higher affinity and promotes canonical NF-κB activation. TACI-L has been shown to be predominantly on cell surface, while substantially more TACI-S was found in the intracellular

compartment. TACI-L was more predominant as a surface receptor for transitional, marginal zone-like, switched memory B-cells and plasmablasts; while TACI-S was significantly more abundant intracellularly with especially increased expression in marginal zone and isotype switched B-cells, and plasmablasts[188].

As a much larger molecule compared to BCMA and BAFFR, the two extracellular CRDs of TACI consists of approximately 90 amino acids, the transmembrane domain approximately 25 amino acids, and the intracellular domain about 60 amino acids. Similar to BCMA, TACI's intracellular domain binds with TRAFs upon ligand-mediated activation by BAFF and APRIL, and subsequently activates the NF-κB and MAPK pathways downstream[140].

As discussed, TACI is predominantly expressed on B-cells, and is especially upregulated in activated B-cells. To a lesser extent, TACI was found on a subset of T-cells and macrophages, which may explain why TACI expression was also observed in tissues where the number of B-cells are typically low[168, 189]. Previous research has shown that intracellular TACI is present in human macrophages and migrates to the cell surface upon incubation with BAFF *in vitro*[135, 138]. Specifically, through the B-cell development process, TACI expressions are primarily observed in marginal zone B-cells, short-lived plasma cells in the spleen; and in memory B-cells and long-lived plasma cells in the lymph node and bone marrow[134]. Similar to BCMA but unlike BAFFR, TACI has two cognate ligands, both BAFF and APRIL, and binds to both at high affinity[144, 154, 189, 190]. Although TACI can bind with BAFF and APRIL in soluble trimer form, research has shown that TACI preferentially binds both ligands in oligomeric forms – BAFF 60-mer, HSPG-bound APRILs, or cross-linked trimers of APRIL or BAFF. HSPG exists in both the extracellular matrix and on the surface of cells such as plasma cells (such as syndecan-1), and triggers APRIL multimerization[143, 189]. BAFF 60-mer has been reported to function as a TACI

activator with a long range of action. In addition, TACI can also interact with membrane-bound BAFF[189]. Previous studies utilising the surface plasmon resonance method have demonstrated that TACI exhibits a binding affinity to APRIL measured at 6.4 nM and to BAFF measured at 0.16 nM, respectively[190].

1.4.4.6 Biological significance of TACI signalling

Receptor-mediated activation of TACI signalling has been shown to play an important role in normal B-cell homeostasis, functioning both as a positive and negative regulator of B-cell activities in a context-dependent manner. For example, TACI-deficient mice accumulate an increased number of mature B-cells, have elevated serum immunoglobulin levels, and display signs of systemic lupus erythematosus (SLE)-like autoimmunity. In other reports, the loss of TACI function is associated with immune-deficiency disorders and IgA deficiency[9, 132, 191].

Typically considered a negative regulator of B-cell survival and proliferation, both in surface-bound and soluble form, TACI is able to sequester soluble BAFF, thereby inhibiting the critical pro-survival BAFF / BAFFR signalling axis. This has been shown in mouse studies where TACI knockout mice exhibited elevated levels of circulation BAFF in serum, and developed splenomegaly with increased mature B-cells[140, 143].

As a positive regulator of B-cell activities, TACI has been showed to play a role in the differentiation and survival of plasmablasts and plasma cells. Previous studies have shown that TACI signalling is able to promote CD40-stimulated B-cells to differentiate into plasmablasts; and TACI signalling is important for LPS-induced plasmablast formation. Canonical NF-κB activation via TACI has also been shown to result in sustained Blimp-1 expression in B-cells, supporting differentiation to long-lived plasma cells[168]. TACI knockout mice appeared to be activated normally in response to TI-2 antigens, but showed delayed differentiation into plasmablasts[153]. Furthermore, TACI has been shown to be the more important facilitator of the survival of plasmablasts, compared to BCMA, possibly via the canonical NF-κB pathway and the target Bcl-2 family proteins[132, 143, 168]. Similar to BCMA, TACI has been

shown to facilitate the survival of plasma cells via the canonical NF-κB and MAPK pathways, although not considered as significant as BCMA[153].

Although dispensable for B-cell maturation and survival, APRIL mediated activation of TACI is considered an important regulator of Ig isotype class switching[140]. Ig class switch recombination requires at least two signals, either via cytokines, or by CD40 via T-dependent antigens. Although CD40 knockout mice displayed severely reduced levels of IgG1 and no IgE, IgA levels were only slightly changed. In human B-cells, APRIL and BAFF have been identified to be able to induce Ig class switch independently of CD40, via TACI and BAFFR. Studies showed that TACI can mediate class switch to IgA, IgG and IgE, while BAFFR can mediate switch to IgG and IgE[192] [ref:24].

Ligand binding results in the recruitment of MyD88 at the cytoplasmic tail of TACI, which then leads to the activation of NF-κB, Ig germline gene transcription, and activation-induced cytidine deaminase expression, which eventually results in Ig class switch recombination. TACI activation via MyD88 has been reported as an important regulator of class switch to IgA[139]. In human patient cases of CVID, TACI mutations have been shown to cause low levels of serum immunoglobulins, or selective IgA deficiency, but normal or increased B-cell numbers[140]. Although both APRIL and BAFF have been reported to contribute to induce Ig class switch recombination, only APRIL knockout mice showed decreased level of IgA production while BAFF knockout mice showed normal levels of IgA[193, 194]. Furthermore, since B1 B-cells are thought to produce IgA contributing to basal IgA levels in the serum, and B1 B-cells can develop normally without BAFF, inhibition of BAFF / BAFFR alone may not affect B1 B-cell's IgA production capabilities[189].

Although TACI is expressed primarily on B-cells, recent study has identified that regulatory T-cells (Treg), marked by CD4+ / CD8+ / CD25+ / FOXP3+, have significantly elevated levels of TACI expression compared to conventional T-cells. APRIL-mediated TACI signalling significantly upregulates the survival and proliferation, as well as immune suppressive capabilities of Tregs. TACI activation via APRIL induces expressions of pro-survival genes including CCND1/2, BCL2, BCL2L1/BCLxL in Tregs; and augments the production of immune inhibitory factors in Tregs including FOXP3, IL-10, TGF-β, and PD-L1, which are typically expressed at low levels in conventional T-cells. In particular, APRIL-mediated TACI signalling in Tregs can induce the expression of FOXP3, a key marker of Treg, and a master transcription factor critical for the development, function, and lineage of Tregs. TACI neutralization resulted in the inhibition of the aforementioned immune-suppressive genes. Thus, TACI signalling in Tregs appears to function as a potent regulator of Treg's immune inhibitory effects[191].

In summary, unlike BCMA which positively regulates the survival of plasma cells, the role of TACI in normal B-cell physiology appears to be complex and context-dependent. In addition, TACI's contribution to immune regulation via regulatory T-cells is worthy of further investigation.

1.5 BAFF and APRIL are critical drivers of B-cell malignancies

The tumour microenvironment involves critical components contributing to tumour survival, proliferation and resistance to treatments. Stromal cells, immune cells, blood vessels, and the extracellular matrix are of particular importance, and have been shown to interact with tumour cells and secret soluble factors to facilitate tumour progression[35, 195]. As described in previous sections, cytokines BAFF and APRIL are primarily produced by cells in the microenvironment in a paracrine manner to regulate the survival, differentiation, and maturation of normal B-cells. Recently, April and BAFF have garnered increased research interest regarding their roles in the pathogenesis of B-cell malignancies. Studies have consistently shown that BAFF mediated receptor signalling via BAFFR plays an important role in the development of B-cell lymphomas such as NHL; and APRIL, via activation of BCMA and TACI, facilitates the progression of MM in a more dominant manner compared to BAFF.

Clinically, BAFF expression in malignant B-cells from NHL patients is up-regulated. In addition, elevated levels of soluble BAFF in serum of NHL patients are correlated with aggressive disease and poor response to therapy. In the microenvironment, BAFF levels were found to be much higher in bone marrow stromal cells compared to lymphoma cells, indicating a predominant paracrine contribution of the cytokine. Although in DLBCL, malignant B-cells efface normal lymphoid tissue structure and thus the tumour microenvironment is relatively sparse, studies have shown that adhesion of DLBCL cell lines to BM stromal cells promoted survival via activation of the NF-κB pathway, even upon treatment of cytotoxic agents. This could be explained by the observation that direct contact with DLBCL cells induced elevated expression of BAFF by BM stromal cells, which in turn activates survival pathways such as NF-κB in DLBCL cells. In addition, lymphoma cells' adhesion to BM stromal cells is increased when BAFF level is elevated, further reinforcing the pro-tumour functions

of BAFF via a positive feedback loop[35, 196, 197]. In addition to secretion by cells in the microenvironment, research has found elevated expressions of BAFF and APRIL in malignant B-cells, indicating autocrine secretion. As shown earlier, BAFF-mediated signalling of BAFFR activates downstream alternative NF-κB pathway that facilitates B-cell growth and survival. Elevated BAFF and BAFFR expressions in B-cell lymphomas result in the aberrant activation of the alternative NF-κB signalling pathway, supporting tumour proliferation and survival[198]. In MM, BAFF expression is elevated, and the cytokine supports MM cell adhesion and survival via a paracrine mechanism in the BM microenvironment[4, 5, 9]. When cultured with BAFF, MM cells showed enhanced proliferation, long-term survival, and resistance to dexamethasone and lenalidomide[9]. Furthermore, tumour-associated macrophages, via elevated secretion of BAFF in the TME, were implicated in the protection of MM cells from bortezomib-induced apoptosis[135].

Similarly, in MM, APRIL expression is significantly elevated[177]. Produced by tumour-supporting BM accessory cells, APRIL signalling promotes MM cell growth, survival, drug-resistance, and contributes to the development of an immune-suppressive BM microenvironment[5, 177]. Unlike BAFF, APRIL does not appear to be as significant a pro-tumour cytokine in B-cell lymphomas, most likely due to the limited expression of BCMA on B-cells other than plasma cells, and the unique interaction between BAFFR and BAFF.

In other B-cell cancers, BAFF and APRIL have also been shown to play a similar and important role. In chronic lymphocytic leukaemia (CLL), the production of BAFF and APRIL within the microenvironment can enhance the survival of cancer cells through paracrine signalling. For instance, BAFF and APRIL were shown to protect cancer cells from apoptosis within the stromal niches, contributing to their persistence and growth[132, 199]. In mantle cell lymphoma, *in vitro*, BAFF was able to maintain the

survival of cancer cells for at least 7 months[132]. In primary central nervous system lymphoma, extensive expression of BAFF was discovered in all specimens[200].

BAFF and APRIL effect their biological functions via activation of cognate receptors BAFFR, BCMA and TACI. BCMA is widely and almost exclusively expressed on plasma cells but not so on earlier-phase B-cells and other normal tissues. The receptor is significantly up-regulated on MM cells compared to normal plasma cells, and the level of expression is increasingly elevated as MM progresses[4, 5]. As discussed previously, activated BCMA signalling upregulates key pro-tumour pathways such as the canonical NF-κB, MAPK and PI3K-AKT pathways, which in turn upregulates pro-survival and anti-apoptotic proteins such as IL-6. Interestingly, elevated BCMA expression increases osteoclast activation, cell adhesion, angiogenesis, tumour metastasis, and immune suppression, suggesting that the development of MM is heavily dependent on BCMA signalling in the BM microenvironment[5]. For instance, in the context of the BM TME, BCMA signalling upregulates adhesion molecule CD44 and osteoclast-promoting factor CCL3/4. Furthermore, BCMA signalling can induce immune-suppressive genes including IL-10, PD-L1, VEGF, and TGF-β[177, 201, 202]. Studies have shown that APRIL / BCMA signalling was able to rescue IL-6 dependent MM cell lines from apoptosis following IL-6 deprivation[177].

As a result, BCMA is a critical regulator of the growth, survival, and drug-resistance of MM cells, while playing an important role in the immune-suppressive and tumour-promoting BM microenvironment[73, 177, 203]. Due to its high specificity and vital role in MM, BCMA is an effective target with minimal off-target toxicity for MM therapy, and has thus emerged as a key target for novel MM therapeutics such as BCMA-targeting CAR T-cell therapies and ADCs.

Similarly, BAFFR is a pro-survival receptor significantly upregulated on most malignant B-cells, including DLBCL and CLL, which is the most prevalent form of adult leukaemia[133, 199]. In MM, however, BAFFR expression is variable and limited on malignant plasma cells[9]. The BAFF-BAFFR signalling axis plays an important role in malignant B-cells' resistance to spontaneous and drug-induced apoptosis[169, 199], as BAFF-BAFFR engagement up-regulates pro-survival and anti-apoptotic proteins via the alternative NF-κB pathway[199].

In contrast to BCMA and BAFFR, in the context of B-cell malignancies, TACI plays a role in promoting an immune-suppressive TME in MM. As discussed earlier, TACI was found to be highly expressed on Tregs. TACI activation by APRIL significantly promotes the proliferation and survival of Tregs (CD4+/CD8+, CD25+ and FOXP3+)[204]. Furthermore, TACI signalling enhances the immune inhibitory functions of Tregs via upregulation of immune suppressive proteins including FOXP10, IL-10, TGF-β and PD-L1, resulting in increased inhibition of conventional T-cell proliferation and functions. Similarly, previous study showed TACI expressions are elevated in iTregs (CD4+, CD25+ and FOXP3+), which resulted from MM tumour cell-induced conversion from conventional T-cells. iTregs in turn inhibit the proliferation of anti-tumour conventional T-cells[205, 206]. In addition to Tregs, TACI, but not BCMA, signalling also upregulates IL10+ Bregs derived from MM BM microenvironment. Since Bregs can facilitate the conversion from conventional T-cells to Tregs, TACI signalling can indirectly inhibit anti-tumour effector T-cells via Bregs[191, 207].

In DLBCL, a study with immunophenotypic profiling of sample from 405 patients with previously untreated DLBCL found impaired immune functionality in the tumour microenvironment, characterized by deficiency in tumour infiltrating T-cells and/or natural killer cells, high PD-1 expression on CD8+ T-cells, PD-L1 expression on T-

cells and macrophages. This immune suppressive TME was shown to be correlated with significantly poorer OS after R-CHOP treatment. Although the investigators of the study did not specifically analyse the levels of Tregs, Bregs, and TACI, the study demonstrated the importance of immune suppressive microenvironment in DLBCL. Taken together, research and clinical data suggest an important potential role TACI plays in the immune suppressive TME[35, 208].

Finally, although not as widely expressed as BAFFR, research has shown that TACI and BCMA are constitutively signalling in NHL B-cells thus activating NF-κB, contributing to the survival of malignant B-cells[198], indicating a direct role TACI plays in promoting NHL development.

1.6 Study Aims

Recognizing the importance of BAFF and APRIL in normal B-cell physiology and malignancy pathogenesis, we hypothesized that pharmacologically targeting BAFF and APRIL could be a viable therapeutic modality for the treatment of DLBCL and MM. In this study we aimed to identify and validate potential BAFF and APRIL inhibitors that are translatable into the clinic. To strategically achieve this dual-targeting objective, we adopted a ligand trap approach and developed a soluble BCMA-Fc decoy receptor, initially using the wild-type extracellular CRD of the BCMA receptor. Subsequently, to enhance the inhibitor's efficacy, we developed a second-generation, engineered mutant sBCMA-Fc fusion protein that traps APRIL and BAFF with significantly enhanced binding affinities. *In vitro* and *in vivo* experiments with MM and DLBCL models were conducted to characterise the pharmacokinetic and pharmacodynamic profiles, validate the anti-tumour efficacy, and assess drug-related normal tissue toxicities of the first and second generation sBCMA-Fc fusion proteins. In doing so, we have deepened our understanding of the BAFF and APRIL-mediated signalling pathways in the context of MM and DLBCL, and have gained insight into the biological consequences of the sequestration of BAFF and APRIL with our molecules.

CHAPTER 2 MATERIALS AND METHODS

2.1 Cell lines

2.1.1 Cell lines

For MM studies, human MM cell lines U266, MM1.R, and INA6 were used. All MM cell lines were obtained from Dr. A. C. Koon and Dr. D. Jiang at the Department of Radiation Oncology, University of Texas MD Anderson Cancer Centre at Houston, Texas, USA.

For DLBCL studies, human DLBCL cell lines SU-DHL-6 (Cat. No. CRL-2959; ATCC) and Daudi (Cat. No. CCL-213; ATCC) were purchased from American Type Culture Collection (ATCC).

Isolation of B-cells from healthy donors and MM patients was performed using EasySep Human B-Cell Isolation Kit per manufacturers protocol (Cat. No. 17954; Stemcell Technologies).

2.1.2 Cell culture

Cells were cultured in RPMI-1640 medium supplemented with 10% FBS and 1% Penicillin-Streptomycin solution in standing flasks. Human IL-6 at a concentration of 2 ng/mL was used to supplement MM and DLBCL cells used for the experiments to maintain growth. Cells were stored in mycoplasma-free, humidified 37°C, 5% CO_2 incubator. Cells were subcultured and split by 1:5 ratio. Cells with less than 10 passages were used for the studies.

2.1.3 Mycoplasma testing

Cells were tested for mycoplasma upon arrival with the Lonza MycoAlert Mycoplasma Detection Kit and were re-tested regularly.

2.1.4 Cryostorage and thawing conditions

Cells were stored in cryovials for long-term storage. Typically, each cryovial contains 3 million cells in freezing medium with 100% FBS and 10% DMSO in a volume of 1,000 μL; and cryovials were stored at -80°C. Cells were thawed at 37°C and re-suspended in culture medium in standing culture flasks and maintained in cell culture condition described earlier.

2.2 Cell count and viability assays

Cells were counted with a haemocytometer or Beckman Coulter counter, depending on the study.

To determine the impact of the wild-type sBCMA-Fc and engineered sBCMA-Fc V3 on cell viability, MM and DLBCL cells were cultured in reduced 3% FBS RPMI-1640 overnight followed by one-hour stimulation by incubation with 100 ng of recombinant human APRIL or BAFF. For the MM study, MM1.R and INA-6 MM cells were plated in 96-well plates at a density of 3,000 cells per well in 100 μL of medium. For the DLBCL study, U266, SU-DHL-6, and Daudi DLBCL cells were plated in 96-well plates at a density of 2,500 cells per well in 100 μL of medium.

Increasing doses of treatment (wild-type sBCMA-Fc or sBCMA-Fc V3) were added to designated wells. APRIL, BAFF and treatment were replenished every 48 hours until the completion of study on day 7.

2.3 Protein analysis

2.3.1 Protein extraction and sample preparation

Suspended MM or DLBCL cells were collected in a tube and centrifuged for 5 minutes at 300 G at 4 °C. Supernatant was aspirated and cell pellets were washed with PBS. The steps were repeated 2 to 3 times followed by addition of ice-cold 1X RIPA buffer, protease inhibitor and phosphatase inhibitor mix. The samples were then sonicated and centrifuged to collect pellet cell debris, and supernatant was transferred to a fresh microfuge tube without disturbing the pellet. The concentrations of total proteins in the samples were measured using a BCA assay (Cat No. 23225; ThermoFisher Scientific). We established a standard curve via BSA dilutions to serve as a reference for quantifying the total proteins in the samples. The samples underwent a 1:10 dilution. BSA standards and samples were both brought to a final volume of 500 µL with deionized water. A further 500 µL of the BCA working reagent (at a 1:50 dilution) was introduced to both the standards and samples, bringing the overall volume to 1 mL. Every standard and sample were then incubated at 37°C for half an hour. The Nanodrop 2000c (Cat No. ND-2000c; ThermoFisher Scientific) reader was utilized to conduct all tests using cuvettes, with the absorbance wavelength set at 562 nm.

Each mixture was 40 µL in volume, consisting of 4 µL of Sample Reducing Agent (10X), 10 µL of Sample Buffer (4X), and 26 µL of the protein sample. The sample mixture was heated to 95 °C for 5 minutes for de-naturing before loading onto SDS-PAGE gel.

2.3.2 SDS PAGE and protein transfer

Electrophoresis apparatus was setup and immersed in 1X runner buffer. Samples prepared above and protein markers were loaded on to the gel for protein separation by electrophoresis. Typically the power of the electrophoresis was set to 120V. Upon

completion of the SDS PAGE process, proteins were transferred from the gel to PVDF membranes with semi-dry transfer system.

2.3.3 Immunoblotting

Upon completion of the transfer, membrane was blocked with TBST containing 5% non-fat dry milk with constant rocking for 1 to 1.5 hours. Primary antibody was diluted in blocking solution with a typical starting dilution ratio of 1:1,000, followed by incubation with membrane overnight at 4°C. Membrane was then incubated for 1 to 1.5 hours with constant rocking with diluted secondary HRP-conjugated anti-goat or anti-rabbit antibody as appropriate in blocking solution. Membrane was then washed 3 times with TBST for 10 minutes each.

Upon completion of immunoblotting, membrane was incubated with substrate for 1-5 minutes. Membrane was then exposed to chemiluminescence detection reagent followed by reading with a chemiluminescence imaging system to detect target protein signals.

Primary antibodies used for the study include the following: BCMA (Cat. No. 27724-1-AP; Proteintech), Pan-Akt (Cat. No. 4691; Cell Signalling Technology), pAkt (Cat. No. 4060; Cell Signalling Technology), phospho-p38 MAPK (Cat. No 4511; Cell Signalling Technology), p38 MAPK (Cat. No. 8690; Cell Signalling Technology), phospo-p44/42 MAPK (Cat No. 4370, Cell Signalling Technology), phospho-mTOR ser2448 (Cat. No. 5536; Cell Signalling Technology), total mTOR (Cat. No. 2983; Cell Signalling Technology), NF-κB (Cat No. 8242; Cell Signalling Technology), phosphor-NF-κB (Cat No. 3039, Cell Signalling Technology), and β-actin (Cat. No. sc-47778 HRP; Santa Cruz Biotechnology) at 4°C overnight.

Secondary antibodies were HRP-conjugated anti-goat (Cat. No. sc-2020; Santa Cruz Biotechnology) or HRP-conjugated anti-rabbit (Cat. No. A16110; Thermo Fisher Scientific) as depending on the type of primary antibody used for the experiment.

2.4 ELISA

Commercial ELISA kits were used per manufacturers' protocols to determine levels of the following proteins in serum or cell lysates: human APRIL (Cat. No. DY884B; R&D Systems), human BAFF (Cat. No. DBLYS0B; R&D Systems), mouse APRIL (Cat. No. MBS738004; My BioSource), mouse BAFF (Cat. No. MBLYS0; R&D Systems), human total IgG (Cat. No. BMS2091; ThermoFisher Scientific), human IgGκ (Cat No. MBS265641, My BioSource); human IgG1 (Cat No. BMS2092, ThermoFischer Scientific), mouse IgG (Cat. No. 88-50400-88; Thermo Fisher Scientific), mouse IgM (Cat No. MBS564075, My BioSource), and mouse IgA (Cat No. MBS564073, My BioSource).

In brief, samples were diluted first. HRP-conjugated detection antibody was diluted with assay buffer. Microwells pre-coated with capture antibody were washed with wash buffer, followed by standard dilution on microwell plate. Assay buffer and prediluted samples were then added to the microwells. Diluted HRP-conjugated detection antibody was added to all wells. Microwell plate was covered and then incubated for 1 hour at room temperature on a microplate shaker. Microwells were emptied and washed with wash buffer, and substrate solution were added to each well. Microwells were incubated at room temperature and stop solution was added to all wells. Microwell plate was then read with a reader at typical color intensity of 450 nm; and the absorbance of both the samples and the standards were determined. Standard curve was then plotted, and concentrations of the target protein in sample determined.

2.5 Immunohistochemistry

Tissue samples were fixed in 10% neutral buffered formalin overnight and subsequently transferred to 70% ethanol. Samples were then further processed and embedded in paraffin blocks sliced and mounted on glass slides.

Ki67 proliferation assay was conducted with the indirect method. Wash buffer was prepared with PBS and 0.05% Tween 20. Tissue sample sections were deparaffined and rehydrated by washing with Xylene and ethanol of decreasing concentrations. Antigen retrieval was completed with 10 mM citric acid and 0.05% Tween 20 in deionized water, adjusted to pH value of 6. Samples were washed 3 times with wash buffer.

Samples were then cooled to room temperature and submerged for 15 minutes in endogenous peroxidase blocking solution of 1:10 dilution of hydrogen peroxide (34%) and water, followed by wash of 3 times with wash buffer. Samples were then incubated with biotin and avidin blocking buffers for 15 minutes each, then followed by incubation with protein blocking buffer of 2% FCS for 20 minutes. After completion, samples were washed 4 times with buffer.

Mouse serum and antibodies were diluted in PBT (1xPBS, 0.1% BSA, 0.2% and 0.01% Tween 20). Samples were incubated with primary anti-human Ki67 antibody (Cat. No. sc-23900; Santa Cruz Biotechnologies) overnight at 4°C. Samples were then incubated with biotinylated secondary anti-mouse IgG secondary antibody 1:2,500 (Cat. No. BA92001; Vector Laboratories) for 30 minutes at 37°C. Subsequently, samples were incubated with STREP-HRP for 30 minutes at 37°C. Signals were developed using the Pierce DAB Substrate Kit (Cat. No. 34002; Thermo Fisher Scientific).

TUNEL apoptosis assay was conducted with ApopTag Peroxidase In Situ Apoptosis Detection Kit (Cat. No. S7100; EMD Millipore Corporation) per manufacturer's

protocol. In brief, with the indirect method, tissue samples were deparaffined and rehydrated, and pre-treated with Proteinase K (Cat. No. 21627; EMD Millipore Corporation) of 1:10 dilution in PBS. Samples were then submerged in 3.0% hydrogen peroxide in PBS for 5 minutes at room temperature to block endogenous peroxidase. Equilibration Buffer was then immediately applied, followed by Working Strength TdT Enzyme Mixture of 70% Reaction Buffer and 30% TdT Enzyme. Samples were then incubated for 1 hour at 37°C for one hour. Anti-digoxigenin Conjugate was applied to the samples followed by incubation for 30 minutes at room temperature. Peroxidase substrate (0.05% DAB in staining buffer) was then applied to the for 5 minutes for staining. After wash, samples were then counter-stained with methyl green (0.5% methyl green in 0.1 M sodium acetate, pH = 4.0) for 10 minutes at room temperature.

All samples were scanned at 40X magnification using the Leica Aperio AT2 Digital Pathology Scanner (Leica Biosystem). NDP.view2 (Hamamatsu Japa) software was used to analyse images.

2.6 Real-time PCR analysis

2.6.1 RNA extraction and purification

RNA was isolated using Invitrogen TRIzol Reagent (Thermo Fisher Scientific) according to manufacturer's instructions. In brief, cells cultured in suspension were collected by centrifuge and supernatant discarded. TRIzol was then added to the pellet at the ratio of 0.75 mL of TRIzol / 0.25 mL of sample, and the lysate mixture was homogenized by pipetting. The sample mixture was incubated for 5 minutes followed by addition of chloroform at the ratio of 0.2 mL of chloroform per 1.0 mL of TRIzol. After shaking and incubation for 2 to 3 minutes, the aqueous sample mix was transferred to a new tube and centrifuged at 12,000 G at 4°C, resulting in a lower red phenol-chloroform, an interphase, and a colourless upper aqueous phase. The colourless upper aqueous phase was then carefully extracted and transferred to a new tube. 0.5 mL of isopropanol per 1 mL of TRIzol was then added to the aqueous phase, followed by incubation for 10 minutes at 4°C. The mixture was centrifuged for 10 minutes at 12,000 G at 4°C to allow total RNA to precipitate, forming a white gel-like pellet, and supernatant discarded. RNA pellet was then washed with TRIzol and solubilized in solution with RNase-free water and SDS solution, followed by incubation in water at 60°C for 10 to 15 minutes.

2.6.2 Primer sequences

Primer sequences were as follows:

BCMA forward: 5'-TGTTCTTCTAATACTCCTCCTCT-3'

BCMA reverse: 3'-AACTCGTCCTTTAATGGTTC-5'

GAPDH forward: 5'-TGCACCACCAACTGCTTAGC-3'

GAPDH reverse: 3'-GGCATGGACTGTGGTCATGAG-5'

2.6.3 Reverse transcription

RNA extracted from the process described above was then reverse-transcribed using cDNA synthesis kit (Bio-Rad). In brief, primer was annealed to the target (template) RNA. The annealed RNA template was then combined with manufacturer's reaction mix, reverse transcriptase enzyme, and nuclease-free water per manufacturer's instructions for incubation. The combined reaction mixture was first incubated at 46°C for 20 minutes, followed by incubation at 95°C for 1 minute to inactivate the reverse transcription reaction. Upon completion of reactions, the cDNA product was used for the PCR amplification that immediately followed.

2.6.4 Real-time qPCR reactions

The protocol applied was optimized for 10uL reactions in 384 well plate format (plates: Applied Biosystems, Cat No. 4309849; covers: Applied Biosystems, Cat No. 4311971).

Reaction mix consisting of 5 μL of 2x SYBR Green PCR Master Mix, primers designed for the target gene of interest, with 0.05 μL of 10 μM forward primer and 0.05 μL of 10 μM reverse primer, 2 μL of 1:10 diluted template cDNA, and 2.9 μL of RNase-free water.

Reactions were carried out in ABI qPCR machine (Applied Biosystems) per the following steps.

The reaction mix was loaded into a thermal cycle and the follow program was run:

- Initial denaturation at 95°C for 15 seconds;
- 40 cycles of:
    - Denaturation at 95°C for 15 seconds;
    - Annealing at 60 – 65°C for 30 seconds, depending on the primer annealing temperature;

- Extension at 72°C for 30 seconds;
- Final extension at 72°C for 5 minutes;
- Hold at 4°C.

For mRNA expression level analysis of target genes, target gene expression levels were normalized against GAPDH expression levels. Fold difference of relative mRNA expressions was determined using the comparative threshold count (Ct) method, as $2^{Ct(GAPDH\ RNA - Gene\ of\ Interest)}$.

2.7 Genetic knockdown studies

2.7.1 Transient BCMA knockdown studies with siRNA

BCMA siRNA construct was purchased from GE Dharmacon Horizon (Cat. No. L-011217-00-0005; SMARTPool).

2.7.1.1 BCMA siRNA transfection

Transfection was completed with a Lonza 4D-Nucleofector System and kit per manufacturer's instructions. In brief, MM cells were subcultured 1 – 2 days before transfection and were at logarithmic growth phase immediately prior to experiment. 4D-Nucleofector System parameters and appropriate programs were set and cell culture plates with culture medium were prepared and pre-incubated at 37°C in a humidified CO_2 incubator. BCMA siRNA was prepared in advance.

Aliquots containing approximately 1.6 x 10^7 MM cells were centrifuged at 90 G for 10 minutes at room temperature. Cells were then re-suspended in room temperature 320 μL of 4D Nucleofector Solution provided by the manufacturer. 6.4 μg of BCMA siRNA were added to the aliquot to create one aliquot of the master mix. Three master mix aliquots were prepared.

20 μL of each of the master mix aliquots were transferred into the wells of the three 16-well strips provided. Strips were then placed in the 4D-Nucleofector System and transfection process was run. After run completion, strips were carefully removed from the device and then incubated for 10 minutes at room temperature. MM cells were resuspended with pre-warmed medium and plated in humidified 37°C CO_2 incubator for 4 – 8 hours for target gene down regulation and related analyses.

2.7.2 Stable dox-inducible BCMA knockdown with shRNA

2.7.2.1 shRNA sequences

shRNA sequences were designed using software supplied by the vendor. Three shRNA sequences listed as follows were tested per transfection protocols provided by manufacturer. Sequences 1 and 2 demonstrated successful knockdown of BCMA and Sh2 was used for subsequent *in vivo* studies.

1) 5'-CAGTCCTGCTCTTTTCCAG-3' (Sh1)
2) 5'-CTTGATGCAGTCTTCACAG-3' (Sh2)
3) 5'-AGCCATGCCCAGGAGACCT-3' (Sh3)

2.7.2.2 shRNA transfection

The following two solutions were prepared per manufacturer's protocol:

Solution A: For each transfection reaction, 10 μL of resuspended shRNA plasmid (i.e., 1 μg of shRNA) were diluted into 90 μL of shRNA Plasmid Transfection Medium (Cat. No. 108062; Santa Cruz Biotechnology, Inc.).

Solution B: For each transfection reaction, 1 – 6 μL of shRNA Plasmid Transfection Reagent (Cat. No. 108061; Santa Cruz Biotechnology, Inc.) was diluted into shRNA Plasmid Transfection Medium (Cat. No. 108062; Santa Cruz Biotechnology, Inc.) such that the final volume of the solution was 100 μL.

Solution A was added to Solution B at a ratio of 1:1, and the mixture was incubated for 15 to 45 minutes at room temperature. HEK293 producer cells for lentiviral particles were washed twice with 2 mL of shRNA Plasmid Transfection Medium (Cat. No. 108062; Santa Cruz Biotechnology, Inc.) and medium was then aspirated. For each transfection reaction, 0.8 mL of shRNA Plasmid Transfection Medium was added per well. 200 μL of the mixture of Solutions A and B were then added. The plate was then

incubated for 5 to 7 hours at 37°C in a CO^2 incubator. Following incubation, 1 mL of 2X normal growth medium without antibiotics was added. HEK293 Producer cells were incubated for an additional 18 – 24 hours under normal culture conditions. 48 hours post transfection, medium was aspirated and replaced with fresh medium containing selection antibiotic puromycin at a concentration of 1 – 3 μg/mL. Subsequently supernatant with viral particles was harvested and titter determined. MM cells were then incubated with medium containing viral supernatant and stably transduced MM cells were selected with antibiotics. Successfully transduced MM cells were maintained for subsequent *in vivo* studies under normal conditions and culture medium was replaced every 2 – 3 days.

2.8 Development of engineered mutant sBCMA-Fc fusion proteins

2.8.1 Synthesis of a mutant soluble BCMA library with yeast surface display

2.8.1.1 Generation of an error-prone library of DNA sequences

The ECD of the human BCMA receptor, or sBCMA, with amino acids Met1 to Ala54 was selected as the starting template for the mutant library synthesis. Corresponding DNA sequence of the sBCMA was incorporated into the pCT yeast display plasmid using NheI and BamHI restriction sites. Random and unbiased mutations were introduced into the sBCMA DNA sequence using low-fidelity Taq polymerase (Invitrogen, Thermo Fisher Scientific) and the nucleotide analogues 8-oxo-dGTP and dPTP (TriLink Biotech), to create an error-prone library of mutant DNA sequences.

2.8.1.2 PCR and generation of cDNA library

For PCR reactions, concentrations of cDNA and cycle number combinations were different for each PRC reaction to obtain a range of mutation frequencies, as follows:

1) 5 cycles, concentration of 200 μM;
2) 10 cycles, concentration of 2, 20, or 200 μM;
3) 20 cycles, concentration of 2 or 20 μM.

Mutant DNA sequences from the library were amplified by 6 PCR reactions using forward and reverse primers associated with the pCT yeast display plasmid. Each product had a 50 base pair homology to the pCT yeast display plasmid in the absence of nucleotide analogues.

Amplified resulting cDNA was purified using gel electrophoresis followed by removal of the pCT plasmid with NheI and BamHI. Subsequently, purified mutant cDNA and linearized mutant DNA were subject to electroporation in a 5:1 ratio by weight into EBY100 yeast, where they were assembled in yeast via homologous recombination

into double-stranded DNA and the resulting mutant sBCMA proteins were displayed by on yeast surface.

2.8.2 Mutant sBCMA library screening

Yeast displaying desired high-affinity mutant sBCMA were selected from the library with FACS through 6 successive rounds, as follows.

During the first round of FACS sorting (equilibrium binding sort), yeast was incubated at room temperature in PBS of 0.1% BSA (PBSA) with 2 nM of human APRIL (Pepro Tech) for 24 hours. Upon completion, yeast was pelleted, washed, and then incubated in PBSA with a mixture of anti-c-Myc FITC antibody (Abcam) and anti-HA (AF647) antibody (Invitrogen) at a ratio of 1:100 for 1 hour at 4°C. Yeasts were then pelleted, washed, and suspended in PBSA, followed by FACS analysis.

For FACS sorting rounds 2 to 6, kinetic off-rate sorts were completed. Yeast was initially incubated with 2 nM of APRIL for 3 hours at room temperature, followed by wash to remove unbound APRIL. Yeast was then resuspended at room temperature in PBSA containing approximately 50-fold molar excess of BCMA compared to the concentration of APRIL to render unbinding events irreversible (dissociation reaction). Incubation with excess BCMA followed different time lengths as follows: sort 2, 48 hours; sort 3, 4, and 5, 72 hours; sort 6, 84 hours. During the final hour of incubation, yeast was mixed with a 1:100 mixture of anti-c-Myc FITC antibody - yeast (Abcam) and anti-HA (AF647) - ligand antibody (Invitrogen), similar to the first sorting round. Yeasts were then pelleted, washed and suspended in PBSA, followed by FACS analysis. Vantage SE Flow Cytometer (Stanford FACS Core Facility) and CellQuest software (Becton Dickinson) were used.

FACS sorting were conducted such that 1 – 3% of clones with the highest APRIL binding / c-Myc expression ratio were selected, enriching the library for clones with

the highest binding affinity to target ligand. In round 1, 10^8 yeast cells were screened, and selected clones were propagated at least 10X to ensure sampling diversity of the library. Selected clones were then subjected to subsequent sorting rounds. After 6 rounds of sorting, plasmid DNA was recovered using Zymoprep kit (Zymo Research Corporation), transformed into DH5α supercompetent cells, and isolated using the Plasmid Miniprep Kit (Qiagen). Sequencing was conducted by MCLAB. Yeast-displayed sort products were analysed with BD FACSCalibur Flow Cytometer (BD Biosciences), and FlowJo software (TreeStar Inc.).

2.8.3 Binding affinity assay

Yeast expressing individual clones were incubated with varying concentrations of APRIL and BAFF, from 1 pM to 1 μM. Immunofluorescent labelling for FACS analysis was performed as described above and FACS Calibur (BD Biosciences) was used to analyse samples. Data were analysed using FlowJo software (TreeStar Inc.) and full binding titrations were fit as a four-parameter sigmoidal curve using Kaleida Graph (Synergy Software) to calculate equilibrium binding constants. Experiments were performed on different days in triplicate.

2.8.4 Computational structural simulation

Structural simulation was conducted with several software programs. sBCMA-Fc V3 in co-complex with human APRIL and human BAFF was modelled with Prime (Schrodinger), AlphaFold2, RoseTTAFold, trRosetta, and RosettaRemodel, based on data retrieved from Protein Data Bank 1XU2 (crystal structure of APRIL bound to wild-type BCMA). Changes in binding between sBCMA-Fc V3 and human APRIL / human BAFF due to mutation in the engineered fusion protein were calculated with Residue Scanning Calculation Module from Bioluminate (Schrodinger). Protein Interaction Analysis module from Bioluminate was used to analyse surface complementarity and protein-protein interactions between sBCMA-Fc V3 and human APRIL / BAFF.

2.9 *In vivo* studies

2.9.1 Study approval

The aim of the study was to characterize the therapeutic efficacy and safety profile of soluble BCMA, as a decoy receptor ligand trap targeting APRIL and BAFF, for the treatment of MM and DLBCL.

MM and DLBCL patient samples were collected from patients at the Stanford Cancer Centre under the approval of Stanford Institutional Review Board (Protocol No. 13535). Blood specimens from healthy donors were obtained from the Stanford Blood Centre (Protocol No. 13535).

In vivo studies were reviewed and approved by the Institutional Animal Care and Use Committee of Stanford University under Protocol AAAPLAC. Mice were housed in a pathogen-free facility under a controlled environment with 12-hour light-dark cycles.

Study endpoints were defined in advance. Sample sizes were determined based on power calculations. Animals were randomly assigned to control and treatment groups. Only animals that required early termination due to illness unrelated to the studies were excluded. For study results, tumour growth curves were presented when tumour growth was measurable. Kaplan-Meier analysis was used to determine survival advantages between control and treatment groups. Biomarkers were measured when applicable and feasible to determine disease progression. Appropriate statistical analysis was used to determine the statistical significance of study results.

2.9.2 *In vivo* safety study

Non-tumour bearing nude mice were treated with sBCMA-Fc at 10 mg/kg every 48 hours for 28 days. Organ tissues samples of spleen, bone marrow, kidney and liver were collected and prepared for histology. Stained sections were analysed by a board-certified veterinary pathologist. Blood sample was collected from each animal at termination and analysed for complete blood count (CBC) and chemistry.

2.9.3 Subcutaneous tumour models

2.9.3.1 MM *in vivo* studies

MM1.R and INA-6 tumour studies were conducted under the following conditions: dox-inducible stable knockdown of BCMA with shRNA, treatment with wild-type sBCMA-FC, and treatment with engineered sBCMA-Fc V3. For each study, 1 x 10^7 MM cells were injected into mice subcutaneously with 50% growth factor-reduced Matrigel (Cat. No. 356230; Corning Inc.). Body weight of mice and tumour growth were measured using callipers three times a week until study termination. Animals were terminated when subcutaneous tumour growth reached ethical termination point size of 2,000 mm^3. Female NOD-scid γ (NSG) mice aged 6 – 8 weeks were purchased from The Jackson Laboratory (Stock No. 005557) and used for MM *in vivo* studies.

2.9.3.2 DLBCL *in vivo* studies

SU-DHL-6 and Daudi tumour studies were conducted under the following conditions: treatment with wild-type sBCMA-Fc, and treatment with engineered sBCMA-Fc V3 mutant. 5 x 10^6 DLBCL cells were injected into mice subcutaneously with 50% growth factor-reduced Matrigel (Cat. No. 356230; Corning Inc.). Body weight and tumour growth were measured once a week until study termination. Animals were terminated when subcutaneous tumour reached ethical terminational point. Female NOD-scid γ

(NSG) mice aged 6 – 8 weeks were purchased from The Jackson Laboratory (Stock No. 005557) and used for DLBCL *in vivo* studies.

2.9.4 Patient-derived xenograft (PDX) model

Mononuclear cells were isolated from the aspirate drawn from MM patient bone marrow. Cells were then inoculated into the left tibias of 5- to 6-week-old NSG mice (Stock No. 005557, Jackson Laboratory) with the following procedure. X-ray was used to guide the injection path into the tibias of an empty needle for the inoculation of patient cells. Upon completion, the needle was removed, and the X-ray was turned off to avoid patient cell exposure to radiation. Patient cells were then inoculated using a fresh needle and syringe. 15 days post tumour inoculation, MM tumour growth in mice was monitored by the level of human M protein levels in mouse serum with ELISA. When the host mouse showed an increase of human M protein levels in serum, indication successful engraftment, CT scans were conducted on day 90 to confirm macroscopic osteolytic lesions that are consistent with osteopenia observed clinically in MM patients. Upon confirmation, the animal was sacrificed, and mono-nuclear cells were collected from the bone marrow for intratibial injection into two new host mice. The process was repeated until reaching the target sample size. In summary, MM samples were collected from 11 patients. Samples from two patients were successfully propagated for the study.

During the study, non-terminal bleeding was performed on animals every 14 days for evaluating serum M protein as a marker of tumour progression. Animals were terminated at signs of physical distress.

2.9.5 Treatment materials

Wild-type sBCMA-Fc and engineered sBCMA-Fc V3 were manufactured by Shanghai ChemPartner using the HEK-293 transient expression system. Proteins produced where then purified with protein G purification method. Purified materials were assessed by size exclusion chromatography HPLC and SDS-PAGE for quality control. Anti-CD38 antibody (Cat. No. A2027) was purchased from Selleck Chemicals, recombinant mouse soluble TACI-Fc (Cat. No. 577708) was purchased from BioLegend Inc., and anti-BAFF antibody (Cat. No. MA1-822774; Invitrogen) was purchased from Thermo Fisher Scientific.

2.10 Mouse CT scans

Mouse CT scans were conducted to confirm MM induced bone degradation in mouse MM PDX models. SkyScan 1276 (Bruker Corporation) *in vivo* micro-CT scanner was used to capture high-resolution micro-CT images under isoflurane anaesthesia. Scanning mode was set to 360 degrees step-and-shoot without average framing. Images were reconstructed using NRecon software (Bruker Corporation) after scan, and subsequently converted to DICOM files with DICOM Converter (Bruker Corporation).

2.11 Statistical analysis

Prism (GraphPad Software) was used for cell number, tumour volume, survival and quantification analyses for *in vitro* and *in vivo* studies. For *in vivo* studies, ANOVA with Tukey-Kramer test was used for treatment group comparisons. For comparing treatment groups over time, repeated-measure ANOVA was used. The P-value of $P<0.05$ is considered statistically significant. For survival studies, statistical analysis of survival curves was conducted. Mantel-Cox test was used to compare mean survival across groups and the P-value of $P<=0.05$ was considered statistically significant.

CHAPTER 3 INHIBITION OF APRIL-MEDIATED SIGNALLING EFFECTIVELY REDUCES MM TUMOUR GROWTH

3.1 Introduction

MM is a cancer of plasma cells that is characterized by the excessive growth and accumulation of clonal, malignant plasma cells in the BM, resulting in the excessive production of M proteins and the consequent range of clinical manifestations such as bone degradation, renal dysfunctions, and anaemia. Despite advancements in diagnostics and novel therapeutics which have resulted in better MM patient outcomes, almost all patients ultimately experience relapse and become unresponsive to treatment. The average five-year survival rate for MM patients is only about 50%. Recent development of CAR T-cell therapies, ADCs, and bispecific antibodies have achieved considerable success in the clinic with a subset of patients reported complete remission post treatment[209, 210]. However, due to dose-limiting normal tissue toxicities, only a small fraction of MM patients is suitable for treatment. Thus, novel efficacious and safe therapeutics are urgently needed for patients who are ineligible for front line, and new investigational therapies associated with severe potential treatment-related adverse effects.

BCMA has been considered a high value target in MM because of the restricted expression pattern[160, 211] and functional role in plasma cell survival[212-214]. As such, recent BCMA-directed novel therapeutics have leveraged BCMA as a homing target to deliver T-cell therapies or anti-tumour toxins. Ligand-mediated activation of BCMA signalling promotes important downstream signalling pathways such as NF-κB and MAPK, which in addition to promote tumour cell survival and proliferation, also facilitate the transcriptional increase of pro-tumour cytokines that lead to increased bone degradation, cell adhesion and angiogenesis within the tumour niche, which

together promote tumour progression and relapse[73, 177]. BCMA binds with primary cognate ligand APRIL at a significantly higher affinity compared to that to BAFF. Interestingly previous studies have reported higher serum levels of BAFF in MM patients, suggesting a potential compensatory effect for its weaker binding affinity toward BCMA. Although the pro-tumour functional role of the BCMA signalling pathway in MM is well-researched, attempts to exploit the pathway for the development of novel MM treatments have been largely unsuccessful. Previous efforts to use mABs against BCMA or APRIL, as well as soluble TACI-Fc fusion proteins to sequester APRIL and BAFF, have had limited success in clinical trials.

In this chapter, we examined the potential of inhibiting BCMA signalling as a therapeutic approach for the treatment of MM. We began by confirming elevated levels of BCMA, APRIL and BAFF expressions in MM patient samples; followed by initial *in vitro* and *in vivo* genetic knockdown studies to demonstrate the impact of BCMA signalling inhibition on tumour cell survival and proliferation. Next, we developed a Fc fusion protein comprised of the Extracellular Cysteine Rich Domain (ECD) of the wild-type BCMA receptor fused to an IgG1 Fc domain to trap ligands APRIL and BAFF, to inhibit ligand-mediated BCMA signalling. We showed that the sBCMA-Fc was effective at suppressing serum levels of APRIL and BAFF *in vivo*, while resulting in minimal normal tissue toxicities. In mouse xenograft models with INA-6 and MM1.R MM tumour cells, sBCMA-Fc was able to significantly reduce tumour growth. To further validate the sBCMA-Fc's therapeutic potential in patient MM, we developed a patient-derived xenograft (PDX) mouse model with fresh biopsy samples from MM patients. sBCMA-Fc treatment demonstrated effective tumour growth inhibition, M protein reduction, and prolonged overall survival *in vivo*. Finally, in a combination *in vivo* study with anti-CD38 mAB, we showed that the sBCMA-Fc can be safely

combined with SOC without additional normal tissue toxicities while enhancing therapeutic efficacy.

Together, our results in this chapter validated the pro-tumour functional roles that BCMA signalling plays in MM. Inhibition of ligand-mediated BCMA signalling with the sBCMA-Fc decoy receptor ligand trap could be a viable treatment for MM patients in urgent need of novel efficacious and safe therapeutic options.

3.2 Results

3.2.1 BCMA mRNA level is elevated in MM and other B-cell malignancies

To test the hypothesis that APRIL-mediated BCMA signalling is an important driver of disease progression and poor patient outcomes in MM, we first examined the level of BCMA mRNA in MM patient samples.

PBMC samples of 11 MM patients and 6 normal healthy donors were collected, and primary myeloma and plasma cells were isolated for PCR analysis to quantify mRNA levels. Consistent with previous findings, RT-qPCR results indicated significantly elevated levels of BCMA mRNA in patient myeloma cells compared to the level in normal healthy donors' plasma cells (Figure 3.1).

To further determine the uniqueness and levels of expression of BCMA in B-cell malignancies in comparison with other tumour types, a panel of tumour cell lines covering a diverse range of 18 solid and hematologic tumour types were queried through the ONCOMINE database (Figure 3.2). As expected, BCMA mRNA levels were found to be elevated in tumour cell lines of B-cell lineage, including lymphoma, MM, and leukaemia.

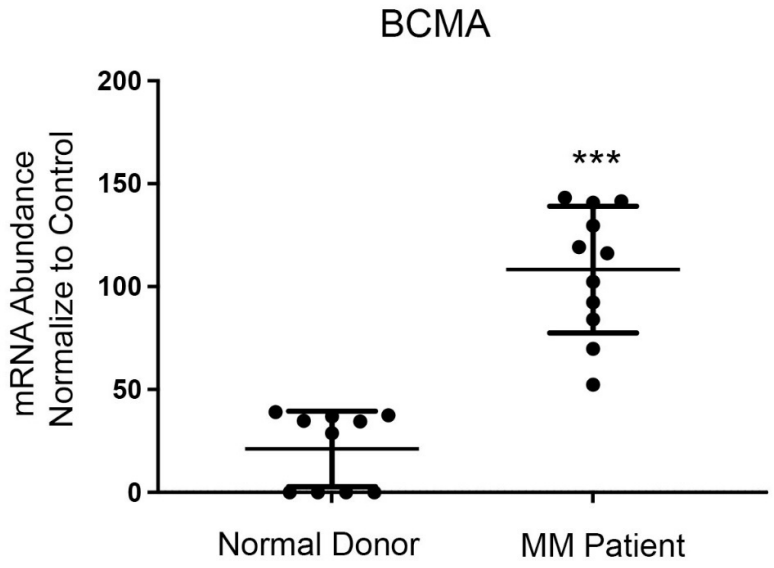

Figure 3.1. BCMA mRNA level in MM patient samples
BCMA mRNA level in patient myeloma cells (N = 11) compared to plasma cells from healthy individual donors (N = 10); P = 0.0001 compared to Normal Donor.

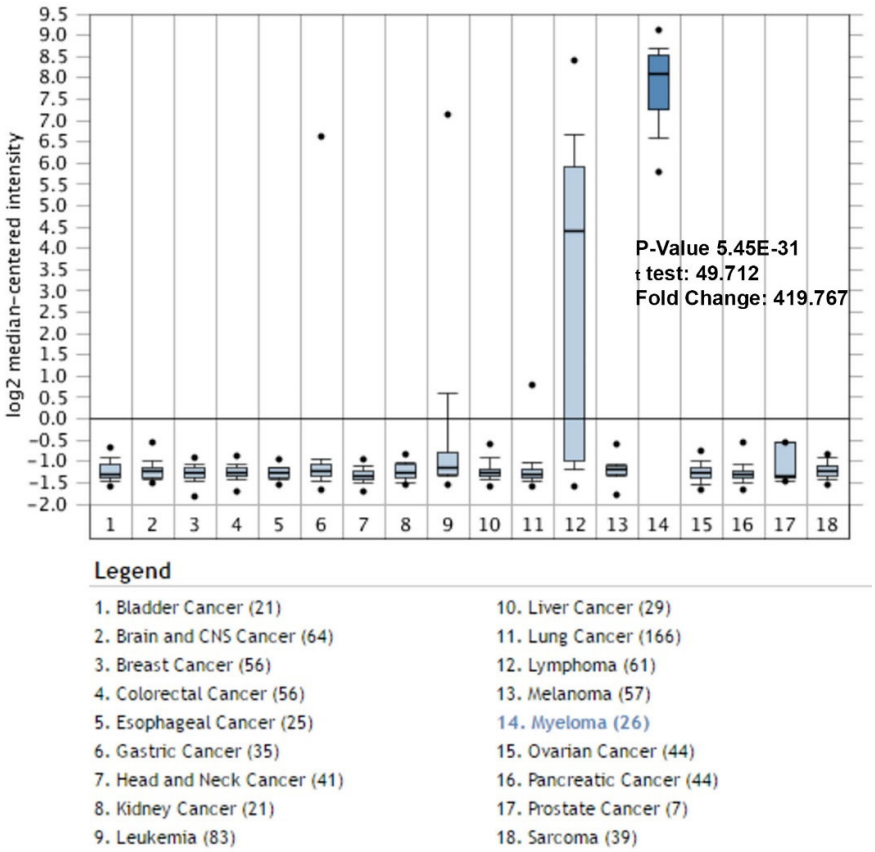

Figure 3.2. ONCOMINE database query on BCMA expression across cancer types
BCMA mRNA levels in a panel of 18 tumour types queried through ONCOMINE database. Number next to tumour type indicates the number of cell lines tested from each tumour type. BCMA expression is significantly elevated myeloma; $P = 5.45 \times 10^{-31}$ compared to normal cell expression level.

3.2.2 APRIL and BAFF levels are elevated in MM patient serum samples

With serum samples from the same 11 MM patients and 4 of the normal donors as the previous section, we examined the levels of APRIL and BAFF in serum with ELISA. Results indicated significantly elevated levels of both APRIL and BAFF in MM patient serum samples compared to that of normal health donors. In MM patient samples, the mean level of APRIL was 345.6 ng/mL while that in normal donor samples was 22.5 ng/mL (Figure 3.3). The mean level of BAFF in MM patient samples was 735.7 ng/mL while that in normal donor samples was 101.3 ng/mL (Figure 3.4).

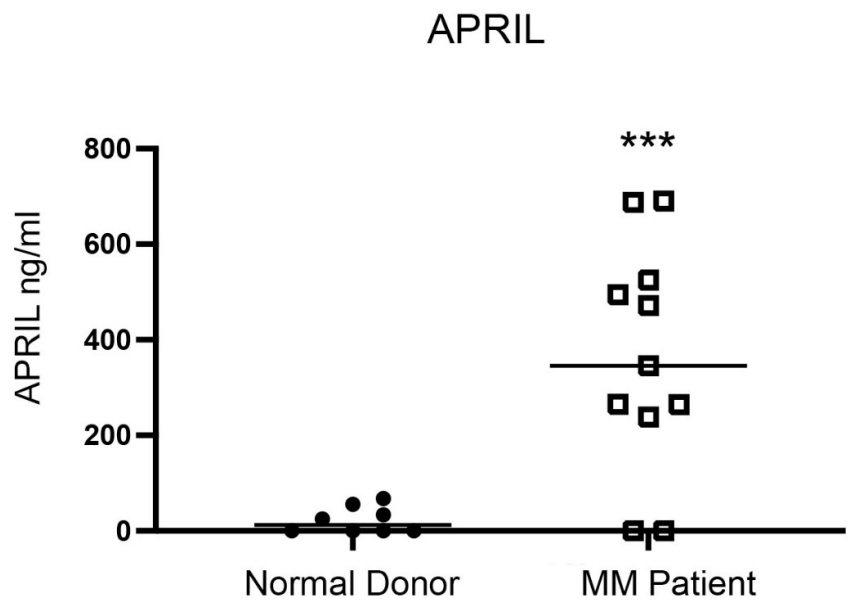

Figure 3.3. APRIL level is elevated in MM patient samples
Serum APRIL levels in MM patients (N = 11) compared to healthy individual donors (N = 8) measured by ELISA; P = 0.001 compared to Normal Donor.

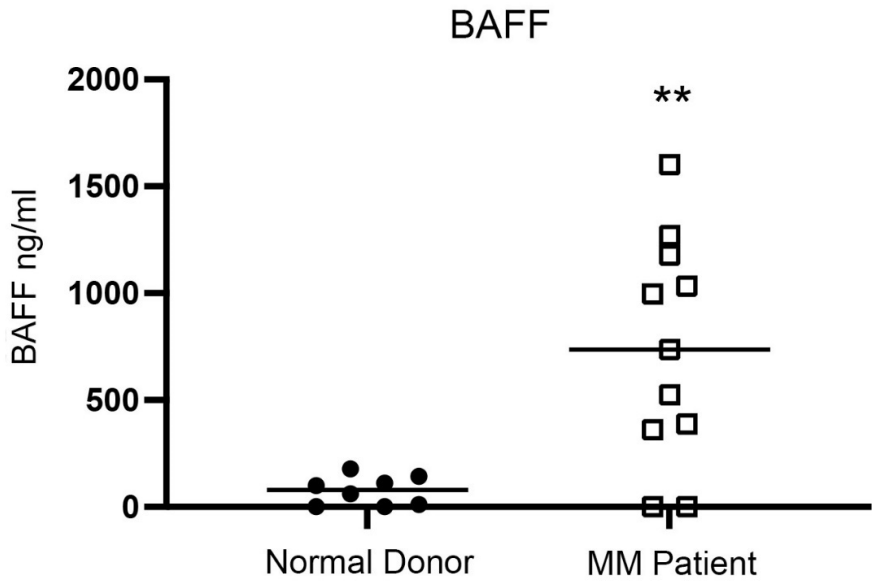

Figure 3.4. BAFF level is elevated in MM patient samples
Serum BAFF levels in MM patients (N = 11) compared to healthy individual donors (N = 8) by measured by ELISA; P = 0.0028 compared to Normal Donor.

3.2.3 Transient knockdown of BCMA inhibits signalling pathways critical to MM cell survival and proliferation *in vitro*

To validate the functional significance of BCMA signalling, we conducted genetic knockdown studies by introducing siRNA to transiently inhibit the expression of BCMA in MM cell line U266. Western blot analysis was conducted on successfully transfected MM U266 cells to assess the impact of transient BCMA knockdown on critical downstream effectors of BCMA signalling, including MAPK and mTOR, which regulate cellular proliferation and survival. Consistent with previous reports, western blot results showed robust inhibition of MAPK and mTOR signalling in BCMA-knockdown U266 cells, as demonstrated by the reduced levels of phosphorylated p44/42 MAPK and mTOR, compared to control (Figure 3.5).

We next observed U266 MM tumour cell growth *in vitro* 72 hours post siBCMA transfection, to determine whether BCMA knockdown affects tumour cell growth and survival as indicated by western blot analysis above. U266 MM cells transfected with siBCMA showed no proliferation and started to decline in approximately 60 hours post transfection. Control group MM cells however showed normal and steady growth (Figure 3.6). Initial transient BCMA knockdown results therefore indicated the important role BCMA signalling plays in MM cell survival and proliferation.

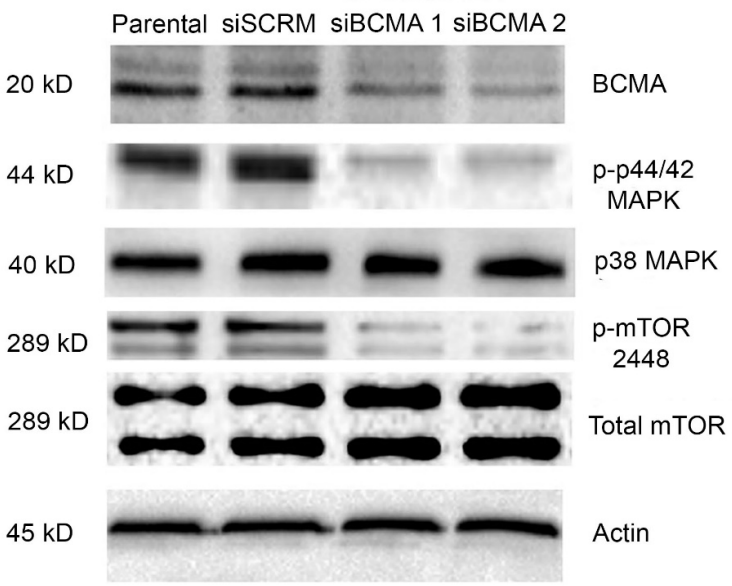

Figure 3.5. BCMA regulates important downstream signalling pathways in MM
Western blot analysis of changes in the expression of key proteins involved in cell survival and proliferation upon transient knockdown of BCMA with siRNA in U266 MM cells. siBCMA samples in duplicate.

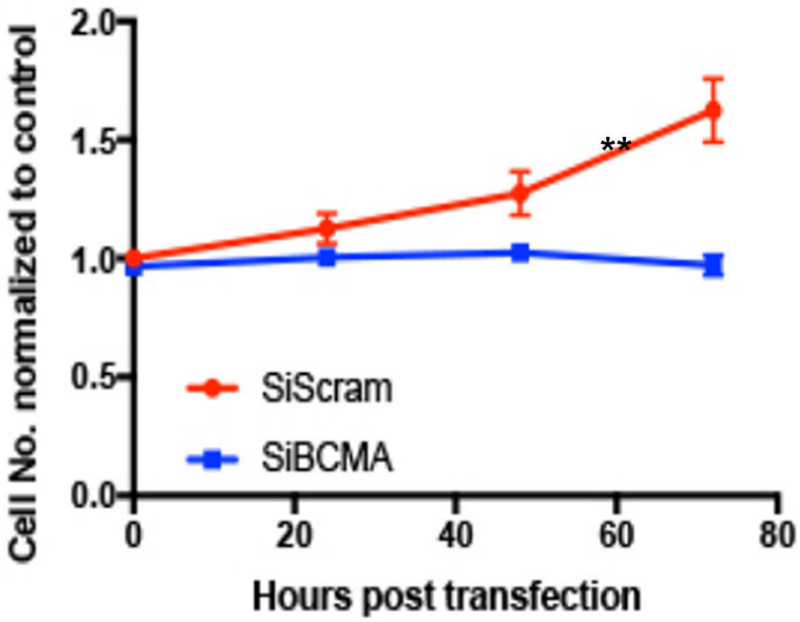

Figure 3.6. BCMA transient knockdown reduces MM cell proliferation
In vitro growth of U266 MM cells 72 hours post siRNA transfection compared to control; P <= 0.01 compared to control (SiScram).

3.2.4 Development of dox-inducible BCMA stable knockdown MM cell lines

We next examined the dependence of MM cell proliferation and survival on BCMA signalling by introducing a doxycycline (dox)-inducible BCMA stable knockdown system (Tet-on) with shRNA into two MM cell lines, MM1.R and INA-6.

INA-6 is a human MM cell line that has been used extensively as a model for studying MM. INA-6 cells have been genetically altered to enhance their growth and survival *in vitro*. Specifically, INA-6 cells are dependent on IL-6 for their growth and survival, and thus they have been genetically engineered to overexpress IL-6 and its receptor. This alteration results in the constitutive activation of signalling pathways downstream of IL-6, leading to enhanced growth and survival of the INA-6 cells. Additionally, INA-6 cells have been found to carry several genetic abnormalities that are commonly observed in MM, such as t(4;14) which is observed in High Risk MM Patients according to the Mayo Clinic Risk Stratification System. Also, INA-6 MM cells have NRAS and TP53 mutations, which are commonly observed in MM patients associated with poor prognosis.

MM1.R is a human MM cell line that was derived from the bone marrow of a patient with relapsed MM. MM1.R cells are widely used as a model for studying MM and for testing new therapies. MM1.R cells carry a number of genetic alterations that are commonly observed in MM, including t(14;16) which is observed in High Risk MM Patients according to the Mayo Clinic Risk Stratification System; and KRAS and TRAF3 mutations which are typically associated with aggressive MM disease. In addition, MM1.R cells exhibit aberrant expression of the oncogene c-myc, which is associated with a poor prognosis in MM patients.

The dox-inducible gene expression system is a widely used method for regulating gene expression in a variety of organisms. The system consists of three key elements, the target gene of interest, a tetracycline-controlled transcriptional activator called tTA or

rtTA, and a tetracycline-responsive element (TetR) or a minimal promoter containing tetracycline-responsive operator sequences (tetO) which the transcriptional activator binds to. In the Tet-On dox-inducible system, in the absence of dox, the rtTA protein does not bind to the tetO element and thus is unable to activate the expression of the target gene – in the case of our study, the shBCMA. However, in the presence of dox, binding with dox triggers a conformational change in the rtTA, allowing the rtTA protein to bind to the tetO element, and the expression of the shBCMA is turned on, leading to the inhibition of BCMA expression. This system provides a high level of control over gene expression, as the addition or removal of dox can be used to turn gene expression on or off in a precise and reversible manner[215].

INA-6 and MM1.R MM cell lines were tested for successful inducible BCMA knockdown with dox *in vitro* prior to the *in vivo* experiments that followed. We tested 2 BCMA shRNA vector sequences and selected shBCMA2 based on the success of BCMA knockdown confirmed with western blot (Figure 3.7 and Figure 3.8).

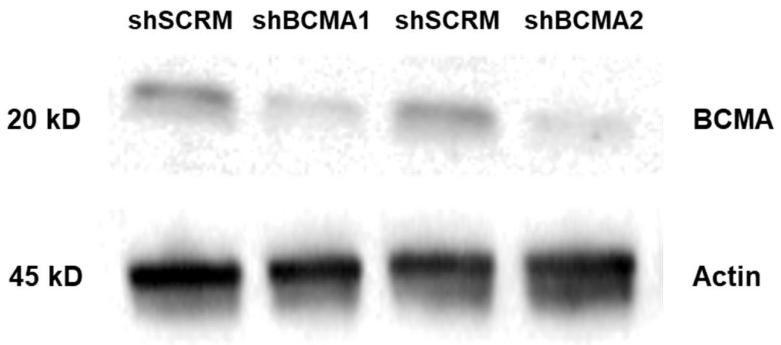

Figure 3.7. Stable knockdown of BCMA with shRNA in MM1.R MM cells
Western blot analysis of changes in the expression of BCMA upon dox-induced stable knockdown with shBCMA1 and shBCMA2, compared to control shCRM, in MM1.R MM cells.

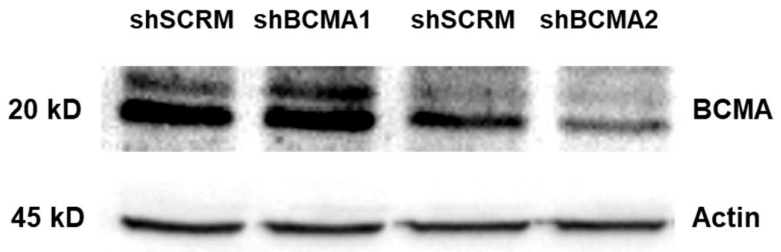

Figure 3.8. Stable knockdown of BCMA with shRNA in INA-6 MM cells
Western blot analysis of changes in the expression of BCMA upon dox-induced stable knockdown with shBCMA1 and shBCMA2, compared to control shCRM, in INA-6 MM cells.

3.2.5 Dox-induced stable knockdown of BCMA inhibits tumour initiation *in vivo* in INA-6 MM xenograft model

Successfully transfected INA-6 MM tumour cells were inoculated subcutaneously into NSG immune deficient mice to examine MM tumour growth and progression upon dox-induced BCMA knockdown *in vivo* compared to vehicle control. Mice were divided into experimental and control groups. Mice in experimental group were subcutaneously injected with MM tumour cells transfected with the shBCMA2 vector, while the control group mice received shSCRM which does not respond to dox. $1x10^7$ INA-6 MM cells in RPMI with 50% Matrigel were injected. Matrigel was used as an initial scaffold to support the growth of cells, and to provide a three-dimensional matrix that mimics the structure and function of native tissue. Matrigel contains various extracellular matrix components, including collagen and growth factors which facilitate initial cell growth post inoculation. Animals were fed with drinking water containing 5 mg/mL of dox for the study duration of 28 days. On day 28, animals were terminated, and tumours harvested for histology analysis.

Throughout the study duration we gathered time series measurements of subcutaneous tumour volume upon tumour cell inoculation to assess the impact of BCMA knockdown on tumour growth *in vivo*. Results indicated significant inhibition of tumour initiation in the BCMA knockdown group compared to vehicle control.

Tumours were harvested at the termination of study and measured by weight. Mean tumour weight of the dox-induced BCMA knockdown group was 0.09 g; and the mean tumour weight of the control group was 0.43 g. Consistent with tumour volume measurement data, terminally-harvested tumour weight data indicated significantly inhibited tumour initiation in the dox-induced BCMA knockdown group (Figure 3.9).

A

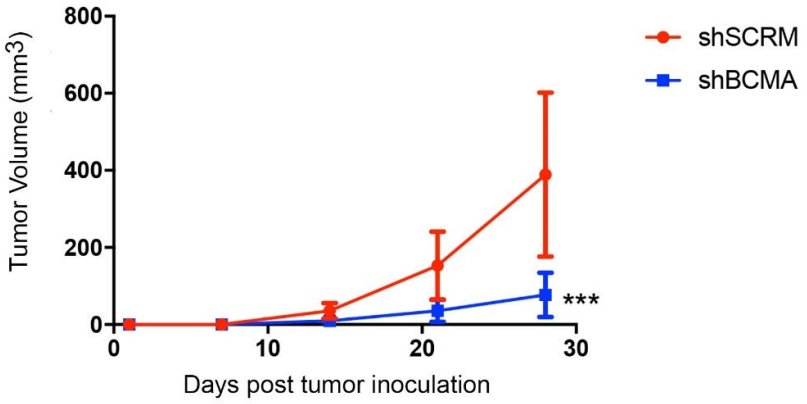

B

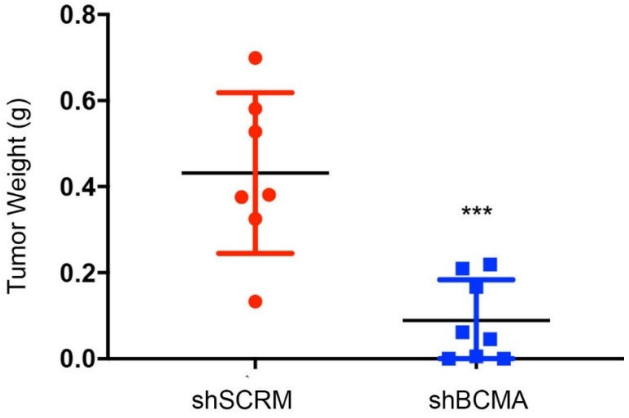

Figure 3.9. INA-6 MM *in vivo* tumour growth analysis with dox-induced stable BCMA knockdown
(A) Subcutaneous *in vivo* growth of INA-6 MM tumour cells transfected with dox-inducible BCMA knockdown shRNA (shBCMA2) (N = 8), or transfected with scramble shRNA (shSCRM) (N = 7), in 6-week-old female NSG mice; P = 0.0005 compared to control (shSCRM).
(B) Weights of terminally-harvested tumours from mice inoculated with dox-inducible shBCMA2 (N = 8) or shSCRM (N = 7) transfected INA-6 MM tumour cells; P = 0.0005 compared to control (shSCRM).

This study was performed in collaboration with Dr. Yu Rebecca Miao and Dr. Kazue Mizuno at Stanford University Department of Radiation Oncology.

Upon tumour harvesting at the termination of the study on day 28, we prepared tumour samples, and conducted Ki67 and TUNEL assays to observe and quantify cellular proliferation and apoptosis for the dox-induced BCMA knockdown group and the vehicle control group.

ICH staining results for Ki67 analysis indicated decreased tumour cell proliferation in tumour samples from the BCMA knockdown group compared to that of the control group, as shown by a higher number of Ki67-positive cells. To quantify the staining results, we measured average numbers of Ki67-positive cells per image field for each group, and observed a marked reduction of Ki67 positive cells in the BCMA knockdown group (Figure 3.10).

A

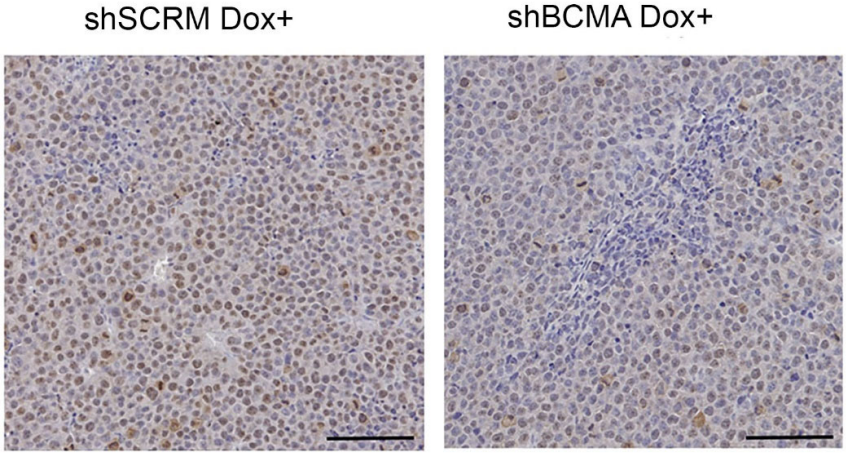

B

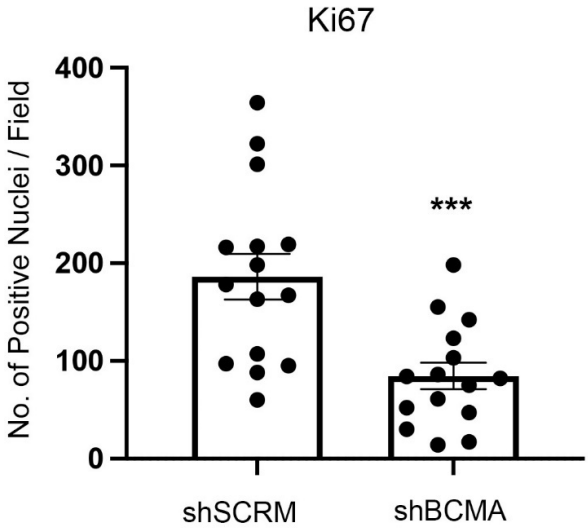

Figure 3.10. Ki-67 assay results analysing the impact of stable BCMA knockdown with shRNA on the proliferation of INA-6 MM tumours *in vivo*
(A) Representative ICH staining images of Ki67-positive cells in the harvested INA-6 MM tumours with dox-inducible shBCMA or shSCRM; scale bar: 50 μm.
(B) Quantification of Ki67-positive cells in the harvested INA-6 MM tumours with dox-inducible shBCMA or shSCRM, represented as the average number of positive nuclei per image field; P = 0.008 compared to control (shSCRM).

TUNEL assay was conducted on harvested tumour samples to assess changes in cellular apoptosis upon dox-induced BCMA knockdown. ICH staining images showed increased TUNEL-positive cells in samples from the experimental group compared to the control group. To quantify the staining results, we measured average numbers of TUNEL-positive cells per image field for each group, and observed a marked increase of TUNEL-positive cells in the dox-induced BCMA knockdown group (Figure 3.11).

A

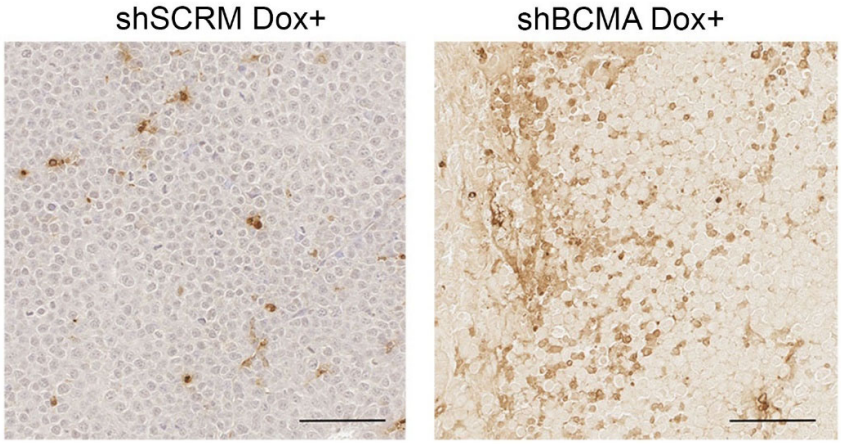

B

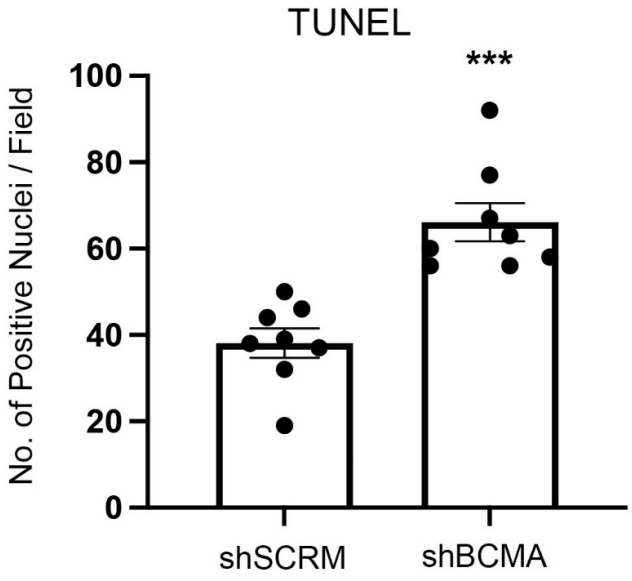

Figure 3.11. TUNEL assay results analysing the impact of stable BCMA knockdown with shRNA on the apoptosis of INA-6 MM tumours *in vivo*
(A) Representative ICH staining images of TUNEL-positive cells in the harvested INA-6 MM tumours with dox-inducible shBCMA or shSCRM; scale bar: 50 μm.
(B) Quantification of TUNEL-positive cells in the harvested INA-6 MM tumours with dox-inducible shBCMA or shSCRM, represented as the average number of positive nuclei per image field; P = 0.0002 compared to control (shSCRM).

To conclude the experiment, we measured mouse serum levels of total human M protein secreted by MM cells at the termination of the study. Elevated level of M protein is typically considered the hallmark of MM. M protein level is used to assess MM tumour burden and patient prognosis, as elevated secretion and build-up of M proteins in the blood eventually result in end organ dysfunctions for MM patients.

ELISA results showed a marked decrease in M protein levels in the dox-induced BCMA knockdown group compared to vehicle control. The mean level of M protein in the dox-induced BCMA knockdown group was lower at 1.53 ng/mL, compared to that of the control group at 7.03 ng/mL (Figure 3.12).

Taken together, results of the INA-6 dox-inducible BCMA knockdown model showed BCMA signalling inhibition resulted in reduced *in vivo* tumour initiation, increased tumour cell apoptosis and reduced human M protein secretion which indicates reduced MM disease burden.

Statistical analysis for this experiment was conducted using one-way ANOVA for comparing between treatment groups and repeated ANOVA for changes occurring over time. *, $P < 0.05$; **, $P < 0.01$; ***, $P < 0.001$.

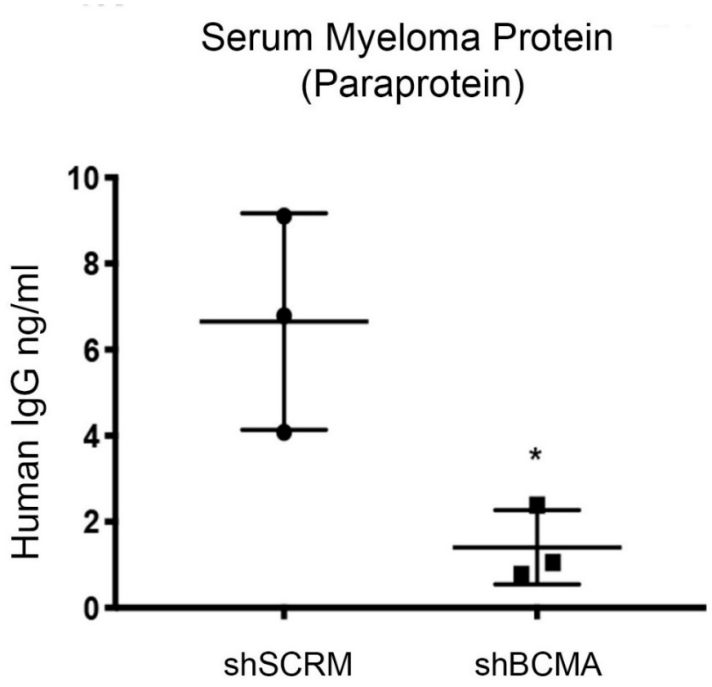

Figure 3.12. Human M protein levels in serum of INA-6 MM mouse model
Total human M protein in the serum of NSG immune-deficient mice inoculated with dox-inducible shBCMA or shSCRM transfected human INA-6 MM tumour cells at harvest (N = 3); P = 0.0268 compared to control (shSCRM).

This study was performed in collaboration with Dr. Yu Rebecca Miao and Dr. Kazue Mizuno at Stanford University Department of Radiation Oncology.

3.2.6 Dox-induced stable knockdown of BCMA inhibits tumour initiation *in vivo* in MM1.R MM xenograft model

Considering the genetic heterogeneity of MM, we hypothesized that BCMA signalling functions as a master regulator of cellular survival and proliferation independent of the heterogeneous genetic mutations present in MM. To test this hypothesis, we conducted the same dox-inducible BCMA knockdown *in vivo* study with the MM1.R MM tumour cell line.

Following the same protocol as the INA-6 study in the previous section, successfully transfected MM1.R MM tumour cells were inoculated subcutaneously into NSG mice to examine MM tumour survival and proliferation upon BCMA knockdown with dox compared to vehicle control. Subcutaneous tumour volume was measured over time upon tumour cell inoculation until the termination of the study. Similar to the INA-6 study, results indicated a significant delay in tumour growth in the BCMA knockdown group compared to vehicle control. Tumours were harvested at the termination of study and measured by weight. Mean tumour weight of the dox-induced BCMA knockdown group was 0.12 g; and the mean tumour weight of the control group was 0.47 g. Consistent with tumour volume measurements, terminally harvest tumour weight data indicated a significantly inhibited tumour initiation in the dox-induced BCMA knockdown group (Figure 3.13).

A

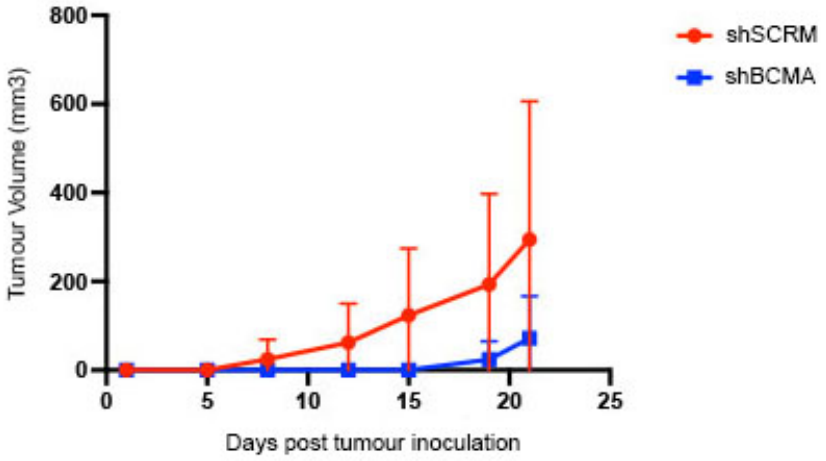

B

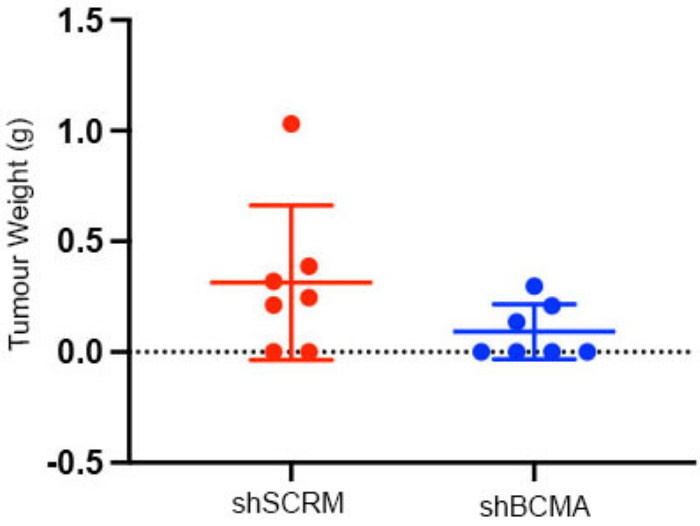

Figure 3.13. MM1.R MM *in vivo* tumour growth analysis with dox-induced stable BCMA knockdown
(A) Subcutaneous *in vivo* growth of MM1.R MM tumour cells transfected with dox-inducible BCMA knockdown shRNA (shBCMA2) (N = 7), or transfected with scramble shRNA (shSCRM) (N = 7), in 6-week-old female NSG mice.
(B) Weights of terminally harvested tumours from mice inoculated with dox-inducible shBCMA2 (N = 7) or shSCRM (N = 7) transfected MM1.R MM tumour cells.

This study was performed in collaboration with Dr. Yu Rebecca Miao and Dr. Kazue Mizuno at Stanford University Department of Radiation Oncology.

Upon termination of the study, we examined samples from harvested tumours with Ki67 and TUNEL assays to assess the impact of BCMA knockdown on tumour cell proliferation and apoptosis.

Consistent with the INA-6 study, ICH staining results from Ki67 analysis indicated decreased tumour cell proliferation in the BCMA knockdown group compared to the control group, as shown by a higher number of Ki67-positive cells. To quantify the results, we measured average numbers of Ki67-positive cells per image field for each group and observed a marked reduction of Ki67 positive cells in the BCMA knockdown group (Figure 3.14).

A

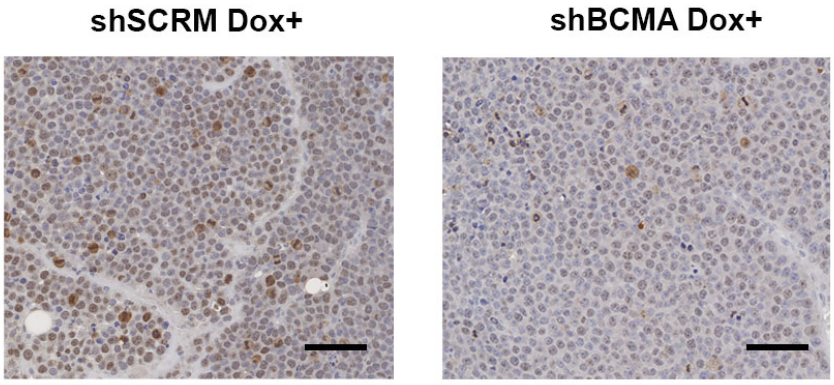

B

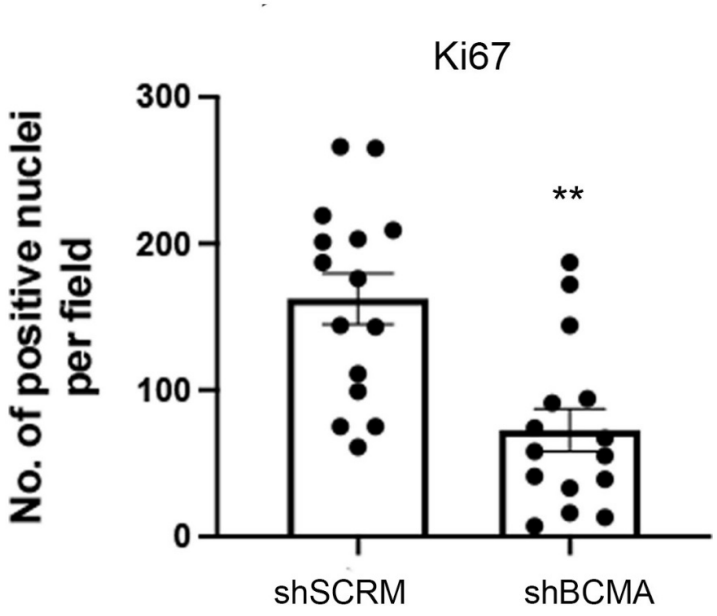

Figure 3.14. Ki-67 assay results analysing the impact of stable BCMA knockdown with shRNA on the proliferation of MM1.R MM tumours *in vivo*
(A) Representative ICH staining images of Ki67-positive cells in the harvested MM1.R MM tumours with dox-inducible shBCMA or shSCRM; scale bar: 50 μm.
(B) Quantification of Ki67-positive cells in the harvested MM1.R MM tumours with dox-inducible shBCMA or shSCRM, represented as the average number of positive nuclei per image field; P = 0.0055 compared to control (shSCRM).

We next conducted TUNEL assay on harvested tumour samples to assess changes in cellular apoptosis upon dox-induced BCMA knockdown. ICH stain image showed increased TUNEL-positive cells in samples from the experimental group compared to the control group. To quantify the results, we measured average numbers of TUNEL-positive cells per image field for each group and observed a marked increase of TUNEL-positive cells in the dox-induced BCMA knockdown group (Figure 3.15).

Statistical analysis for this study was conducted using one-way ANOVA for comparing between treatment groups and repeated ANOVA for changes occurring over time. *, P <= 0.05; **, P <= 0.01; ***, P <= 0.001.

A

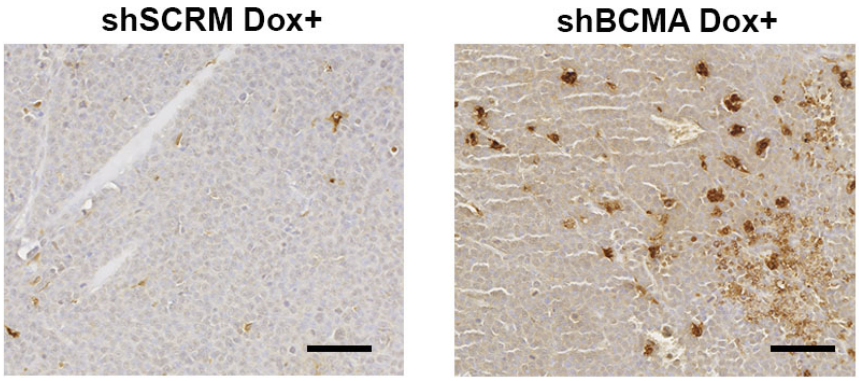

B

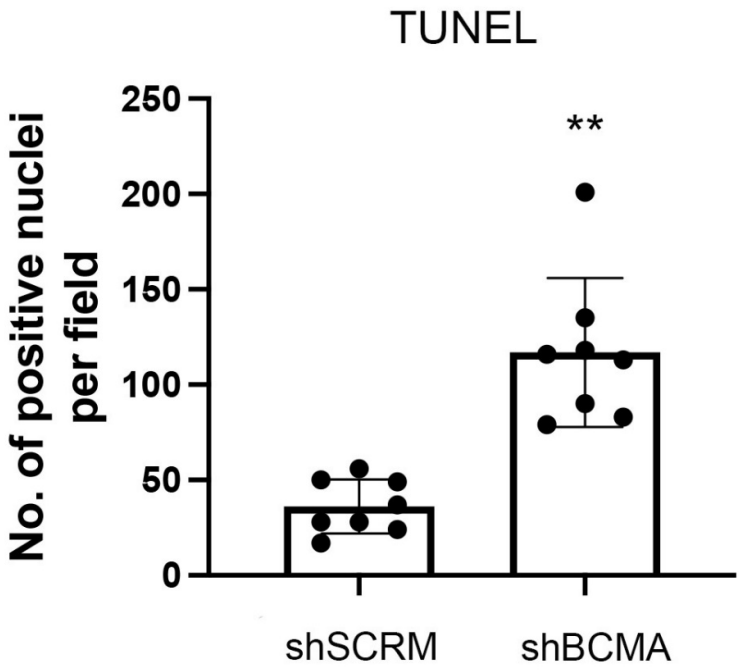

Figure 3.15. TUNEL assay results analysing the impact of stable BCMA knockdown with shRNA on the apoptosis of MM1.R MM tumours *in vivo*
(A) Representative ICH staining images of TUNEL-positive cells in the harvested MM1.R MM tumours with dox-inducible shBCMA or shSCRM; scale bar: 50 μm.
(B) Quantification of TUNEL-positive cells in the harvested MM1.R MM tumours with dox-inducible shBCMA or shSCRM, represented as the average number of positive nuclei per image field; P = 0.0026 compared to control (shSCRM).

3.2.7 Development of a wild-type soluble BCMA-Fc fusion protein

Since gain of function mutations in BCMA is uncommon, BCMA signalling in myeloma cells is almost entirely mediated by APRIL and BAFF. As reported previously, while the binding affinity as measured by K_D between BCMA and APRIL has been reported to be between 25-48 pM [179, 180], the K_D between BCMA and BAFF was not detected with flow cytometry[181]. We therefore hypothesized that a decoy receptor with the ECD of the wild-type BCMA receptor could be an effective approach to inhibit BCMA signalling by trapping ligands APRIL and BAFF (Figure 3.16).

The yeast surface display system is used here to express the BCMA ECD. The process involves the genetic fusion of a BCMA ECD with an anchor protein aga2p that is displayed on the surface of yeast cells. The BCMA ECD gene was cloned downstream of the aga2p gene, and the plasmid was transformed into the yeast host. Subsequently, the expression of the BCMA ECD protein was induced on the surface of the yeast cell. The yeast surface display system has several advantages over other protein expression systems, such as the ability to express and engineer proteins with complex folding and post-translational modifications.

To enhance the *in vivo* pharmacokinetic and pharmacodynamic characteristics of the wild-type BCMA ECD, we fused the ECD to a human IgG1 Fc domain to create an Fc fusion protein, sBCMA-Fc. The addition of an IgG1 Fc domain to biologic therapeutics can improve their pharmacokinetics and bioavailability by protecting them from degradation and slowing down their clearance from the body, which result in a longer half-life and improved therapeutic effect. The IgG1 Fc domain can bind to FcRn, a receptor present in various tissues, and be taken up into cells, after which the therapeutic is released back into the bloodstream. This mechanism is known as Fc-mediated recycling and helps extend the therapeutic effect of biologic therapeutics.

The sBCMA-Fc fusion protein effectively binds to APRIL / BAFF in trimer form and forms a stable receptor-ligand co-complex. The trimeric form of APRIL and BAFF is stabilized by the intermolecular disulphide bonds that form between the cysteine residues on adjacent individual APRIL / BAFF monomers. This allows the trimeric ligands to interact with their receptors on the surface of B-cells and plasma cells with high affinity and specificity.

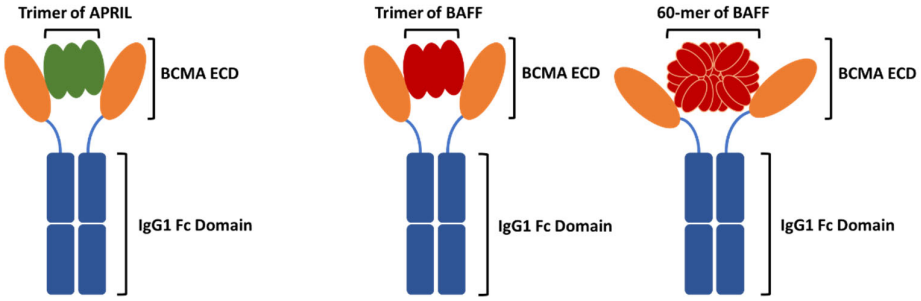

Figure 3.16. Design of the wild-type sBCMA-Fc fusion protein
Schematic illustration of recombinant human wild-type sBCMA-Fc fusion protein binding to human APRIL trimer / BAFF trimer and 60-mer.

This study was performed in collaboration with Dr. Kaushik Thakkar at Stanford University Department of Radiation Oncology.

3.2.8 sBCMA-Fc demonstrates effective anti-tumour activity *in vitro*

To assess the effect of the wild-type sBCMA-Fc on the viability of MM cells *in vitro*, we performed cytotoxicity assays with U266 and MM1.R MM cell lines. To control for the stimulus effects of APRIL and other growth factors that exist in the culture medium, we incubated MM cells with 100 ng/mL of recombinant human APRIL to activate BCMA signalling, and cultured MM cells in reduced serum conditions to minimize the effects of other growth factors in the medium. MM tumour cells in the three experimental groups were treated with increasing doses of the sBCMA-Fc every 48 hours for a duration of 7 days. MM tumour cells in the control groups were treated with vehicle control alone, human recombinant APRIL alone, IgG1-Fc alone without the presence of human recombinant APRIL, and sBCMA-Fc alone without the presence of human recombinant APRIL.

Results of the cytotoxicity assay showed a marked decrease of the viability of MM cells dependent on APRIL-mediated BCMA signalling as treatment dose increased, demonstrating the inhibitory effect of sBCMA-Fc and a treatment dose-response relationship. Transmission Electron Microscopy imaging further confirmed U266 MM cell apoptosis upon sBCMA-Fc treatment; and apoptosis occurred in a dose-dependent manner (Figure 3.17).

A

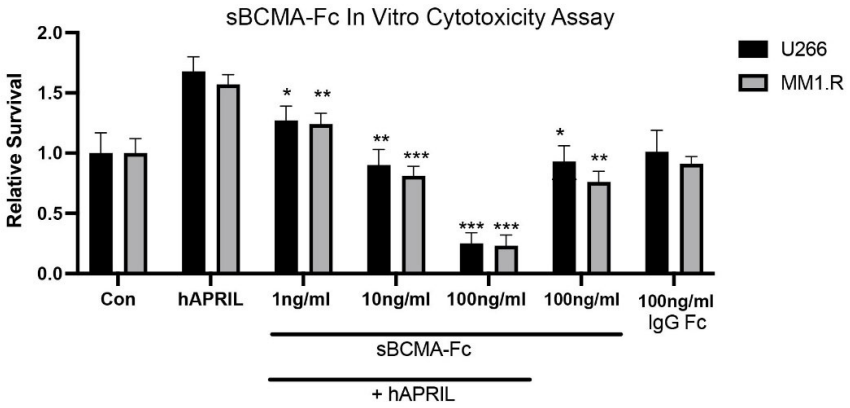

B

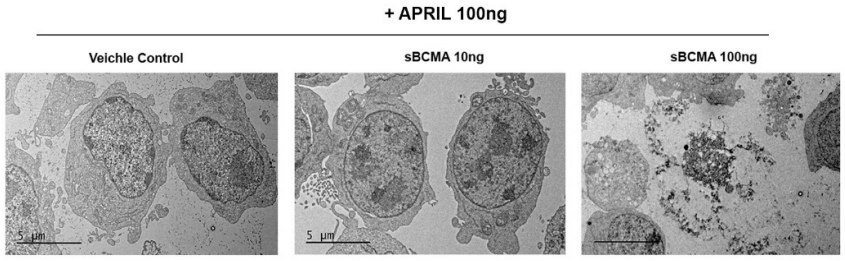

Figure 3.17. *In vitro* cytotoxicity assay examining the impact of sBCMA-Fc treatment on MM cells

(A) Cytotoxicity assay examining *in vitro* tumour cell survival with U266 and MM1.R MM tumours in the presence of increasing doses of sBCMA-Fc and human APRIL at 100 ng/mL. *, $P < 0.05$; **, $P < 0.01$; ***, $P < 0.001$, compared to APRIL-stimulated control (hAPRIL). Cells were maintained in low (3%) FBS to reduce possible growth stimulation mediated through other growth factors present in FBS. Each sample was performed in triplicate.

(B) Representative Transmission Electron Microscopy images of U266 MM cells treated with wild-type sBCMA-Fc and vehicle control in the presences of human APRIL recombinant protein at 100 ng/mL; scale bar = 5 μM.

3.2.9 sBCMA-Fc demonstrates effective suppression of APRIL and BAFF in serum *in vivo*

To determine the pharmacological effect of the sBCMA-Fc *in vivo*, we administered a single dose of sBCMA-Fc at 10 mg/kg into non-tumour bearing mice. We then collected mouse serum samples at different time points post dosing and measured levels of mouse APRIL and BAFF with ELISA as a proxy of the sBCMA-Fc's *in vivo* pharmacodynamic profile, since mouse APRIL and BAFF share a high degree with homology with their human counterparts per assessment with UniProt.

Results showed almost complete inhibition of APRIL for nearly 4 hours, and that of BAFF for nearly 20 hours. Overall, we observed a half-life of the inhibitory effect of sBCMA-Fc on APRIL of approximately 20 hours, and that on BAFF of approximately 72 hours (Figure 3.18). It is interesting to note that the basal levels of APRIL and BAFF were measured to be 7.1 ng/mL and 31.5 ng/mL, respectively. However, our results showed a longer inhibition of BAFF considering the wild-type BCMA's binding affinity toward BAFF is much weaker than that toward APRIL. One potential explanation could be that our results were obtained with commercial ELISA kits for a preliminary assessment of ligand suppression. Thus, the ELISA assays were not optimized for sensitivity and capture efficiency, resulting in such observed results.

The preliminary pharmacodynamic study results confirmed that sBCMA-Fc was able to effectively sequester mouse APRIL and BAFF in circulation, and the sBCMA-Fc can be used for further *in vivo* studies.

A

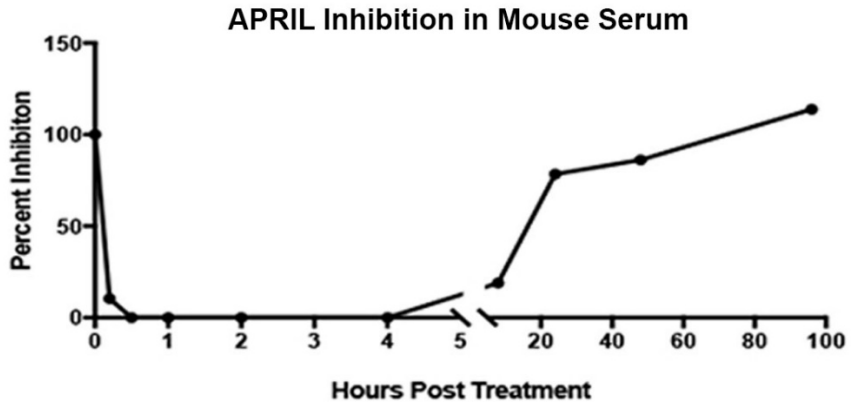

B

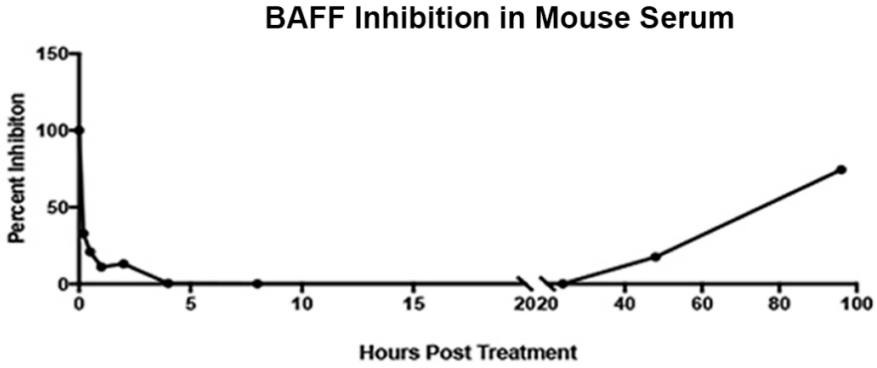

Figure 3.18. sBCMA-Fc demonstrates effective suppression of free APRIL and BAFF in serum
(A) Free mouse APRIL level in mouse serum over time after a single dose of sBCMA-Fc at 10 mg/kg given intraperitoneally.
(B) Free mouse BAFF level in mouse serum over time after a single dose of sBCMA-Fc at 10 mg/kg given intraperitoneally.

This study was performed in collaboration with Dr. Yu Rebecca Miao at Stanford University Department of Radiation Oncology.

3.2.10 sBCMA-Fc demonstrates impressive safety profile *in vivo*

We next proceeded to assess the safety profile of the sBCMA-Fc *in vivo*. Normal non-tumour bearing nude mice (N=6) were treated with sBCMA-Fc at 10 mg/kg every 48 hours for a duration of 28 days.

Body weight of mice in both control and treatment groups were measured three times per week till study termination. At the termination of the study, normal tissue samples of spleen, bone marrow, kidney and liver were collected and prepared for histology and pathology analyses. Stained sections were analysed by a board-certified veterinary pathologist. Staining images showed no significant normal tissue toxicity for the treatment group. Furthermore, we observed no significant changes in mouse body weight and haematological profiles for the treatment group compared to vehicle control (Figure 3.19 and Table 3.1).

A

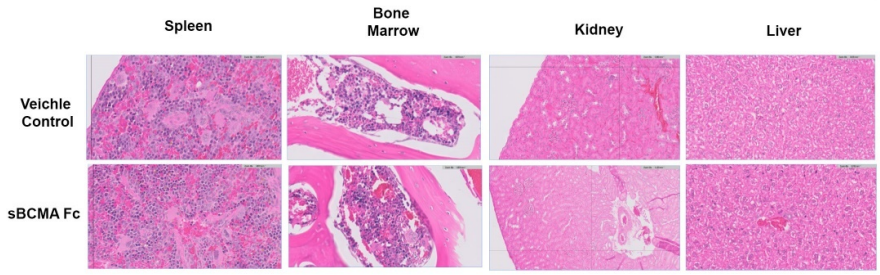

B

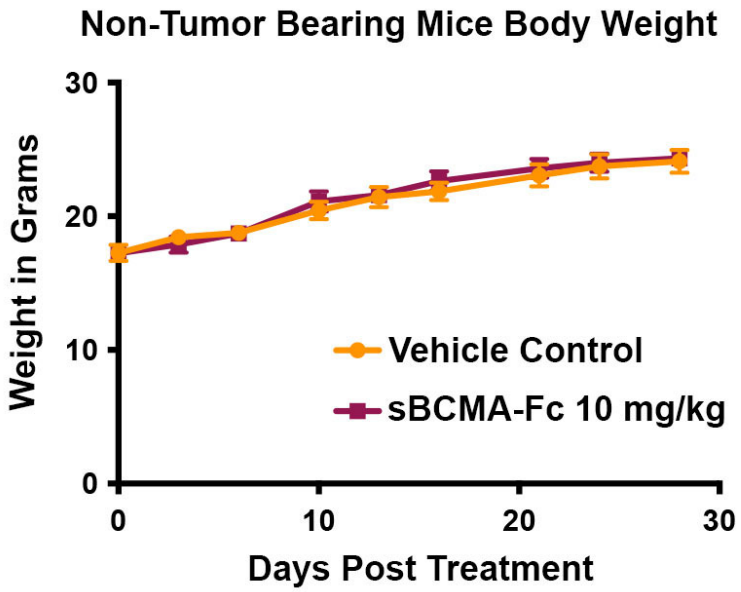

Figure 3.19. sBCMA-Fc showed minimal normal tissue toxicity in naïve mice
(A) Representative Haematoxylin and Eosin (H&E) staining images of organ tissues harvested from naïve mice treated with sBCMA-Fc at 10 mg/kg every 48 hours for 28 days. (B) Changes in body weight of naïve mice treated with sBCMA-Fc at 10 mg/kg every 48 hours for 28 days.

This study was performed in collaboration with Dr. Yu Rebecca Miao and Dr. Anh Diep at Stanford University Department of Radiation Oncology.

	Control		Treated		Standard Range	
CBC						
RBC	9.3	± 0.63	9.7	± 0.82	7.0 – 8.8	M/μL
HGB	14.6	± 1.34	14.8	± 1.88	13.7 – 16.4	gm/dL
HCT	53.4	± 29.9	54.2	± 3.90	39.0 – 47.0	%
MCV	57.4	± 0.9	56.0	± 0.79	52.0 – 68.7	fL
MCH	15.8	± 0.21	15.9	± 0.23	18.4 – 19.6	pg
MCHC	27.4	± 0.56	28.4	± 0.15	34.0 – 36.0	g/dL
Platelet Count	1,477.0	± 266.34	1138.8	± 263.72	675 – 1,338	K/u
PCT	1.0	± 0.20	0.8	± 0.19		
Neutrophils	71.0	± 7.10	73.0	± 8.12	15 – 32	%
Lymphocytes	18.0	± 5.22	15.6	± 5.73	65 – 83	%
Monocytes	10.0	± 3.75	10.8	± 5.07	0 – 3	%
Chemistry						
AST	140.5	± 89.44	150.0	± 117.75	192 – 388	U/L
ALT	28.3	± 7.60	34.0	± 9.67	76 – 160	U/L
Alkaline Phosphorus	172.3	± 21.70	176.6	± 26.33	171 – 183	U/L
Cholesterol	69.0	± 6.50	80.3	± 3.79	N/A	mg/dL
BUN	27.3	± 5.50	18.2	± 1.30	20.3 – 24.7	mg/dL
Creatine	0.2	± 0.08	0.1	± 0.08	0.1 – 1.1	mg/dL

Table 3.1. Hematological profile analyses at termination for naïve mice treated with sBCMA-Fc

3.2.11 sBCMA-Fc demonstrates effective anti-tumour activity *in vivo* in INA-6 MM xenograft model

To assess the *in vivo* therapeutic efficacy of the wild-type sBCMA-Fc fusion protein, we conducted similar experiments as the dox-inducible BCMA knockdown study, but with normal INA-6 and MM1.R MM tumour cells, and observed consistent results as follows.

INA-6 MM cells were inoculated subcutaneously into NSG immune deficient mice to examine MM tumour survival and proliferation upon treatment with sBCMA-Fc compared to vehicle control. Mice were divided into experimental (N=10) and control (N=10) groups. Mice were subcutaneously injected with $1x10^7$ INA-6 MM cells in RPMI with 50% Matrigel. Animals in the treatment group received sBCMA-Fc at 10 mg/kg every 48 hours for a study duration of 28 days, while animals in the control group received vehicle control at the same schedule. On day 28, animals were terminated, and tumours harvested for histology analysis.

Harvested tumours at the termination of study were measured by weight. Mean tumour weight of sBCMA-Fc treated group was 0.04 g and the mean tumour weight of the control group was 0.23 g, indicating significantly reduced tumour growth in the treatment group (Figure 3.20).

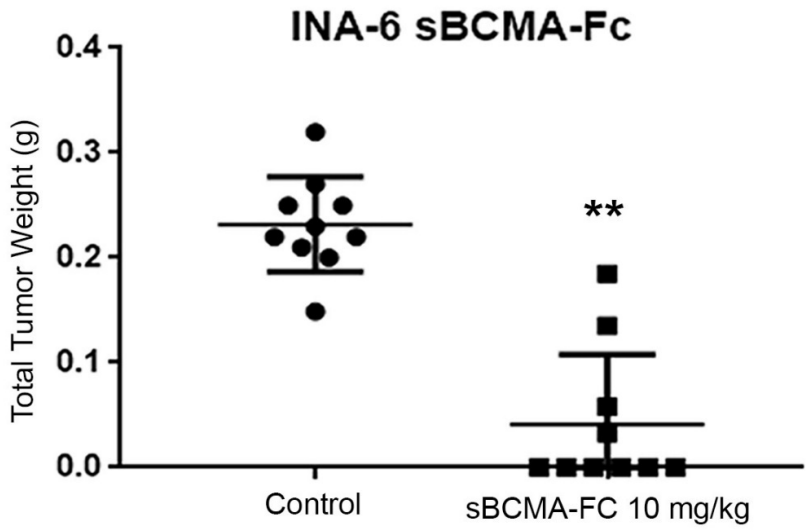

Figure 3.20. INA-6 MM *in vivo* tumour growth analysis with sBCMA-Fc treatment
Measurement of terminally harvested tumour weight of mice inoculated with INA-6 MM tumour and treated with sBCMA-Fc at 10 mg/kg or vehicle control every 48 hours for a duration of 28 days (N = 10); P = 0.0082 compared to Control.

This study was performed in collaboration with Dr. Yu Rebecca Miao at Stanford University Department of Radiation Oncology.

Upon tumour harvesting at the termination of the study on day 28, we prepared tumour samples, and conducted Ki67 and TUNEL assays to observe and quantify cellular proliferation and apoptosis for the sBCMA-Fc treated group and vehicle control group.

ICH staining results for Ki67 analysis indicated decreased tumour cell proliferation in tumour samples from the treatment group compared to that from the control group, as shown by higher number of Ki67-positive cells. To quantify the staining results, we measured average numbers of Ki67-positive cells per image field for each group and observed marked reduction of Ki67 positive cells in the treatment group (Figure 3.21).

A

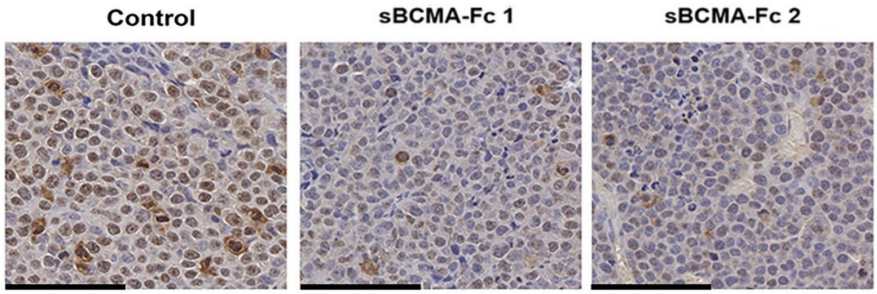

B

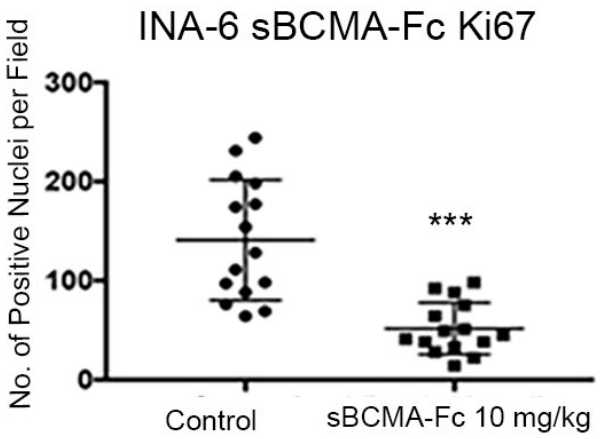

Figure 3.21. Ki-67 assay results analysing the impact of sBCMA-Fc treatment on the proliferation of INA-6 MM tumours *in vivo*

(A) Representative ICH staining images of Ki67-positive cells in the terminally harvested INA-6 MM tumours from two sBCMA-Fc treated mice (sBCMA-Fc 1 and 2) from the treatment group, and vehicle control; scale bar = 50 µm.

(B) Quantification of Ki67-positive cells in the terminally harvested INA-6 MM tumours from sBCMA-Fc treated mice in the treatment group, and vehicle control, represented as the average number of positive nuclei per image field; $P < 0.0001$ compared to Control.

TUNEL assay was conducted on harvested tumour samples to assess changes in cellular apoptosis upon sBCMA-Fc treatment. ICH staining images showed increased TUNEL-positive cells in samples from the experimental group compared to vehicle control. To quantify the staining results, we measured average numbers of TUNEL-positive cells per image field for each group and observed a marked increase of TUNEL-positive cells in the treatment group (Figure 3.22).

A

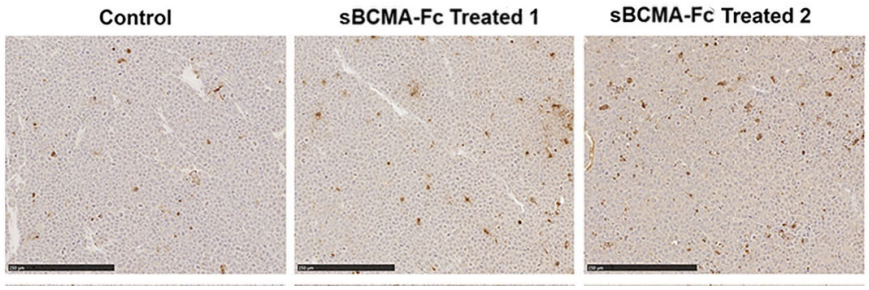

B

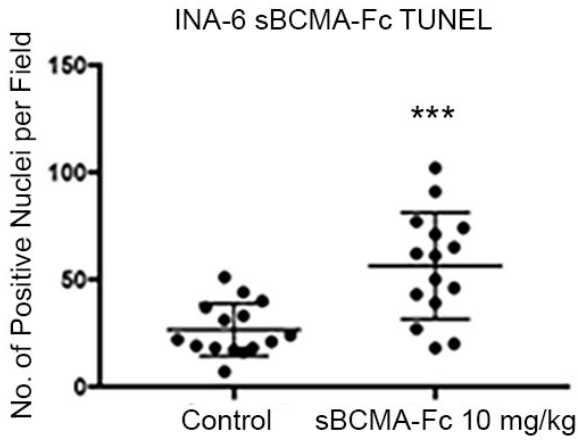

Figure 3.22. TUNEL assay results analysing the impact of sBCMA-Fc treatment on the apoptosis of INA-6 MM tumours *in vivo*
(A) Representative ICH staining images of TUNEL-positive cells in the terminally harvested INA-6 MM tumours from two sBCMA-Fc treated mice (sBCMA-Fc 1 and 2) from the treatment group, and vehicle control; scale bar = 50 μm.
(B) Quantification of TUNEL-positive cells in the terminally harvested INA-6 MM tumours from sBCMA-Fc treated mice in the treatment group, and vehicle control, represented as the average number of positive nuclei per image field; P = 0.0001 compared to Control.

3.2.12 sBCMA-Fc demonstrates effective anti-tumour activity *in vivo* in MM1.R MM xenograft model

We next repeated the same study as in the previous section with MM1.R MM cells to further validate the sBCMA-Fc's *in vivo* therapeutic efficacy. MM1.R MM cells were inoculated subcutaneously into NSG immune deficient mice to examine MM tumour survival and proliferation upon treatment with sBCMA-Fc compared to vehicle control. Mice were divided into experimental (N=9) and control (N=6) groups. Mice were subcutaneously injected with $1x10^7$ MM1.R MM cells in RPMI with 50% Matrigel. Animals in the treatment group received sBCMA-Fc at 10 mg/kg every 48 hours for a study duration of 28 days, while animals in the control group received vehicle control at the same schedule. On day 28, animals were terminated, and tumours harvested for histology analysis.

Harvested tumours at the termination of study were measured by weight. Mean tumour weight of sBCMA-Fc treated group was 0.24 g; and the mean tumour weight of the control group was 0.85 g, indicating significantly reduced tumour growth in the treatment group (Figure 3.23).

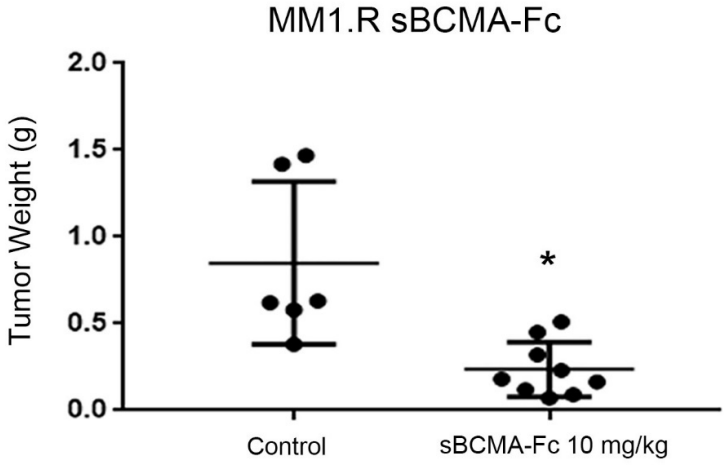

Figure 3.23. MM1.R MM *in vivo* tumour growth analysis with sBCMA-Fc treatment
Measurement of terminally harvested tumour weight of mice inoculated with MM1.R MM tumour and treated with sBCMA-Fc at 10 mg/kg or vehicle control every 48 hours for a duration of 28 days; P = 0.0217 compared to Control.

This study was performed in collaboration with Dr. Yu Rebecca Miao at Stanford University Department of Radiation Oncology.

Upon tumour harvesting at the termination of the study on day 28, we prepared tumour samples, and conducted Ki67 and TUNEL assays to observe and quantify cellular proliferation and apoptosis for the sBCMA-Fc treated group and vehicle control group.

ICH staining results for Ki67 analysis indicated decreased tumour cell proliferation in tumour samples from the treatment group compared to that from the control group, as shown by a higher number of Ki67-positive cells. To quantify the staining results, we measured average numbers of Ki67-positive cells per image field for each group, and observed a marked reduction of Ki67 positive cells in the treatment group (Figure 3.24).

A

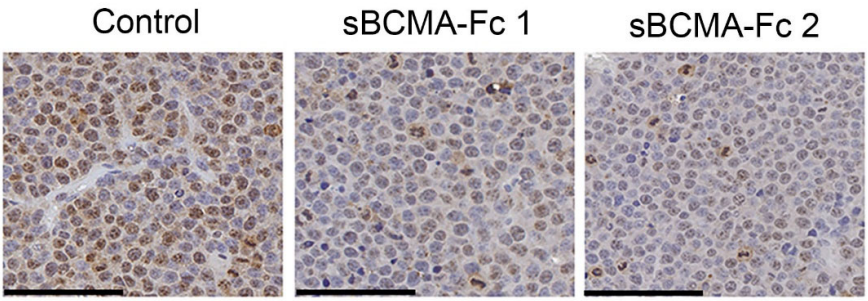

B

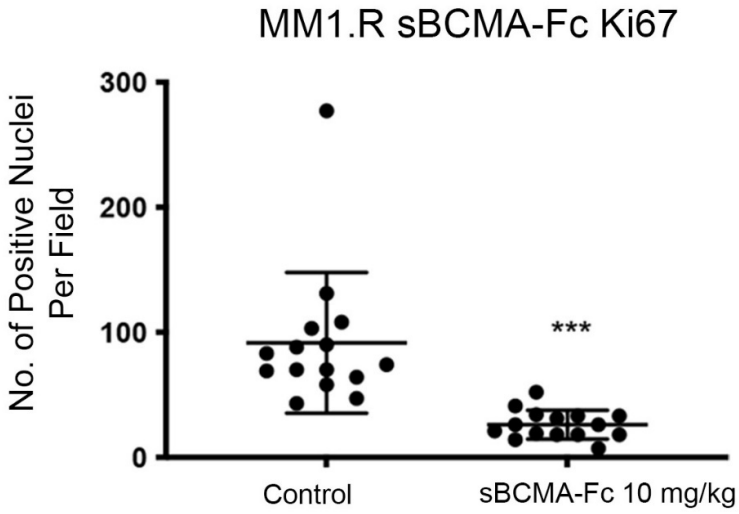

Figure 3.24. Ki-67 assay results analysing the impact of sBCMA-Fc treatment on the proliferation of MM1.R MM tumours *in vivo*
(A) Representative ICH staining images of Ki67-positive cells in the terminally harvested MM1.R MM tumours from two sBCMA-Fc treated mice (sBCMA-Fc 1 and 2) from the treatment group, and vehicle control; scale bar = 50 µm.
(B) Quantification of Ki67-positive cells in the terminally harvested MM1.R MM tumours from sBCMA-Fc treated mice in the treatment group, and vehicle control, represented as the average number of positive nuclei per image field; P = 0.0001 compared to Control.

TUNEL assay was conducted on harvested tumour samples to assess changes in cell apoptosis upon sBCMA-Fc treatment. ICH staining images showed increased TUNEL-positive cells in samples from the experimental group compared to control. To quantify the staining results, we measured average numbers of TUNEL-positive cells per image field for each group, and observed a marked increase of TUNEL-positive cells in the treatment group (Figure 3.25).

A

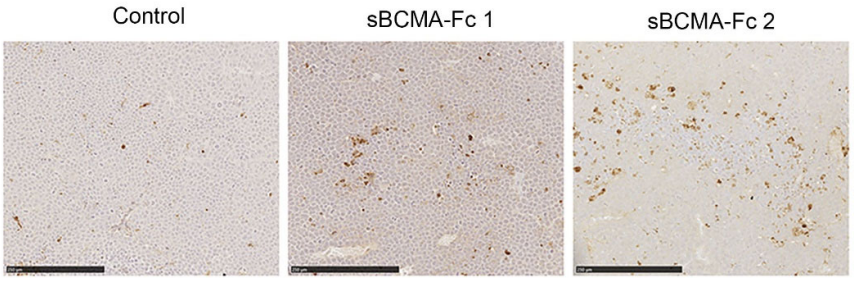

B

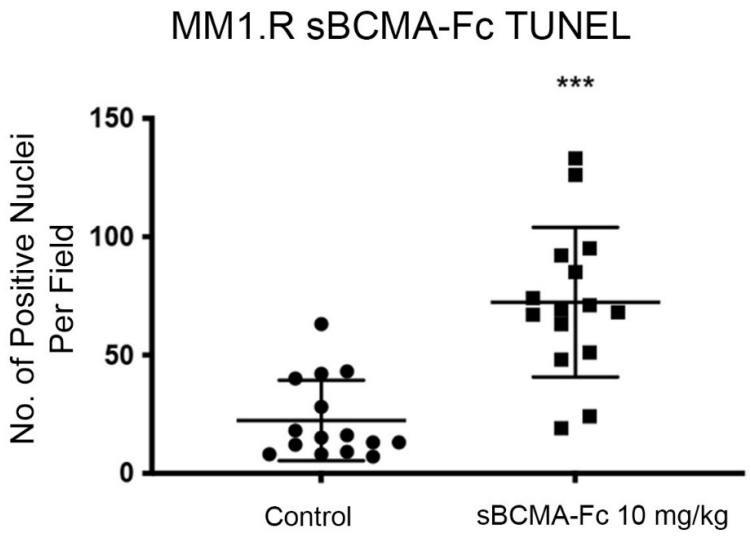

Figure 3.25. TUNEL assay results analysing the impact of sBCMA-Fc treatment on the apoptosis of MM1.R MM tumours *in vivo*

(A) Representative ICH staining images of TUNEL-positive cells in the terminally harvested MM1.R MM tumours from two sBCMA-Fc treated mice (sBCMA-Fc 1 and 2) from the treatment group, and vehicle control; scale bar = 50 µm.

(B) Quantification of TUNEL-positive cells in the terminally harvested MM1.R MM tumours from sBCMA-Fc treated mice in the treatment group, and vehicle control, represented as the average number of positive nuclei per image field; P = 0.0001 compared to Control.

3.2.13 sBCMA-Fc demonstrates specificity to target ligands *in vivo*

To ensure the sBCMA-Fc delivers target mediated therapeutic efficacy, we compared sBCMA-Fc treatment (N=5) with three different groups in an MM1.R MM subcutaneous model: vehicle control (N=5), IgG1-Fc (N=5), and a randomly selected Fc fusion protein (Non-binding-Fc) without binding to APRIL or BAFF (N=5).

Animals were treated with test articles at a dose of 10 mg/kg every 48 hours for a treatment duration of 28 days. Subcutaneous tumour volume was measured at different time points to assess tumour growth *in vivo*.

Results confirmed the therapeutic specificity of the sBCMA-Fc as mice treated with the sBCMA-FC showed significant tumour growth reduction, while the IgG-Fc and Non-binding-Fc treated groups did not differ significantly from vehicle control (Figure 3.26).

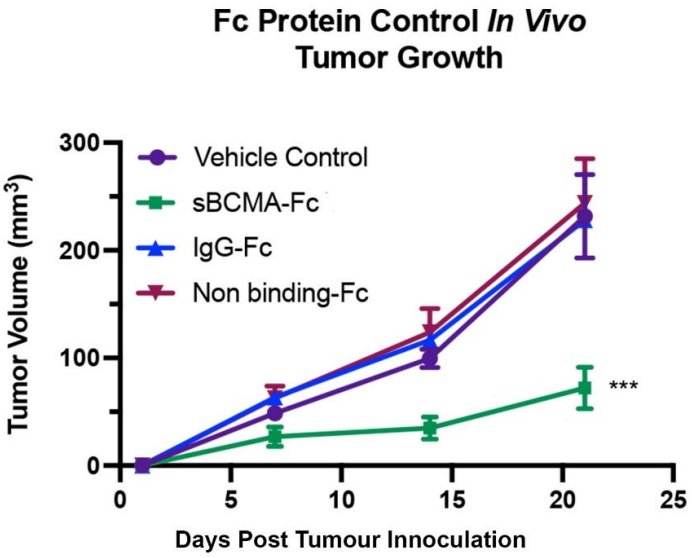

Figure 3.26. MM1.R MM *in vivo* study demonstrates sBCMA-Fc's target specificity
In vivo tumour growth analysis with MM1.R MM tumour. Animals were treated with sBCMA-Fc (10 mg/kg; $P < 0.0001$ compared to Vehicle Control), vehicle control, IgG1-Fc control (10 mg/kg), and Non binding-Fc control (10 mg/kg); $N = 5$ for each of the groups.

This study was performed in collaboration with Dr. Yu Rebecca Miao at Stanford University Department of Radiation Oncology.

3.2.14 sBCMA-Fc demonstrates therapeutic efficacy in patient-derived xenograft MM mouse model

To assess the therapeutic potential of the sBCMA-Fc *in vivo* with human MM patient specimens, we developed a patient-derived xenograft (PDX) mouse model of MM by engrafting freshly isolated MM tumour cells from patient biopsies into the tibias of immune-deficient NSG mice.

We collected fresh samples from 11 MM patients of various age and treatment status. The myeloma types of patients were also identified to the extent possible (Table 3.2).

Patient No.	Gender	Collection Date	Age	Treatment Status	Myeloma Type
1	M	6/1/18	53	Untreated	Unknown
2	F	6/11/18	59	Previously Treated	IgGκ
3	M	7/25/18	53	Untreated	IgGκ
4	M	7/25/18	56	Previously Treated	IgGλ
5	M	8/2/18	60	Untreated	IgGκ
6	M	8/3/18	55	Previously Treated	Unknown
7	M	9/18/18	66	Untreated	IgGκ
8	F	10/23/18	64	Untreated	IgGλ
9	M	10/23/18	71	Relapse / Refractory	IgGκ
10	F	2/13/19	49	Untreated	Unknown
11	M	7/9/19	52	Previously Treated	IgGκ

Table 3.2. Demographic details and treatment status of MM patients from whom samples were collected.

To control for quality, mononuclear cells were isolated from MM patient bone marrow biopsies, and then inoculated into the left tibias of NSG mice using X-ray guided procedure. We measured serum levels of human M protein 15 days post tumour cell injection to confirm initial successful engraftment. Upon confirmation, on day 90, we conducted CT scans to confirm macroscopic osteolytic lesions that are consistent with osteopenia observed clinically in MM patients. We then sacrificed the mouse, collected bone marrow mononuclear cells, and continued to propagate with the same protocol until the sufficient sample size for the experiment was reached (Figure 3.27).

A

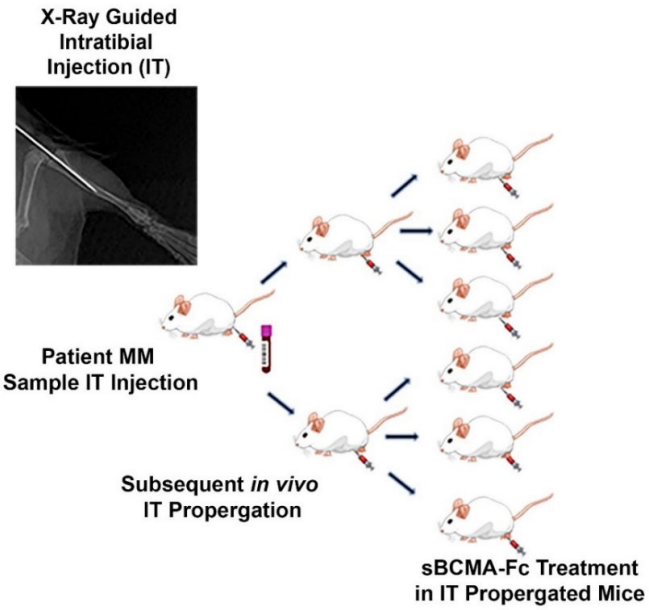

B

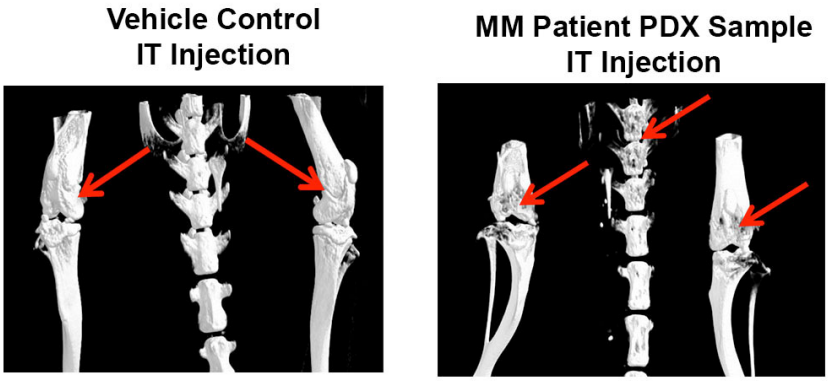

Figure 3.27. Illustration of MM PDX model development process
(A) Schematic illustration of *in vivo* MM PDX propagation. Patient MM tumour cells were isolated from bone marrow samples and injected into the tibia of NSG mice. Upon successful engraftment as indicated by an increase in serum level of M protein, MM cells were collected from bone marrow and propagated until the target sample size number was reached.
(B) Representative CT scans of mice tibias, femurs and vertebrates for the vehicle control and PDX-engrafted experimental groups. Osteolytic bone degradation was observed in the experimental group only.

This study was performed in collaboration with Dr. Yu Rebecca Miao at Stanford University Department of Radiation Oncology.

Upon confirmation of successful patient MM cell engraftment for the treatment group mice, we initiated treatment with sBCMA-Fc at 10 mg/kg every 48 hours for 28 days. MM tumour growth was evaluated by measuring levels of human IgGκ in serum until mice reached terminal disease burden.

A

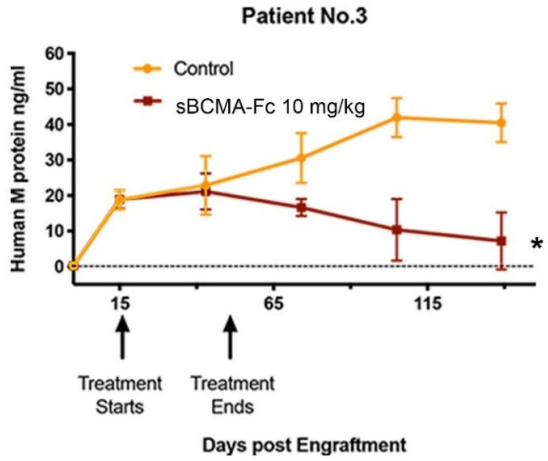

B

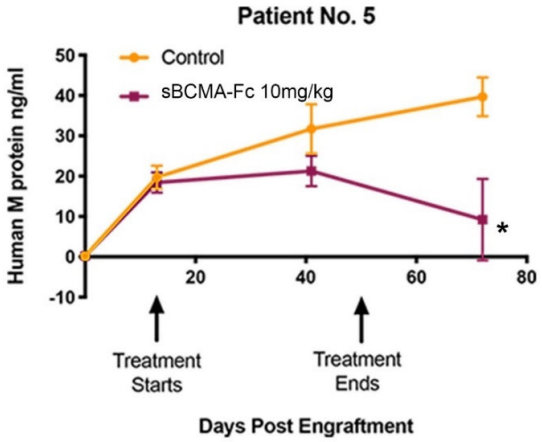

Figure 3.28. sBCMA-Fc is effective at controlling MM tumour growth in PDX model
(A) Serum human M protein levels in animals engrafted with MM samples from Patient No.3. Animals were divided into treatment and control groups. Treatment group (N=8) showed a reduction in human M protein level post sBCMA-Fc treatment compared to control group that received placebo (N=7); P = 0.012 compared to Control.
(B) Serum human M protein levels in animals engrafted with MM samples from Patient No.5. Animals were divided into treatment and control groups. Treatment group (N=10) showed a reduction in human M protein level post sBCMA-Fc treatment compared to control group that received placebo (N=10); P = 0.0026 compared to Control.

This study was performed in collaboration with Dr. Yu Rebecca Miao at Stanford University Department of Radiation Oncology.

A

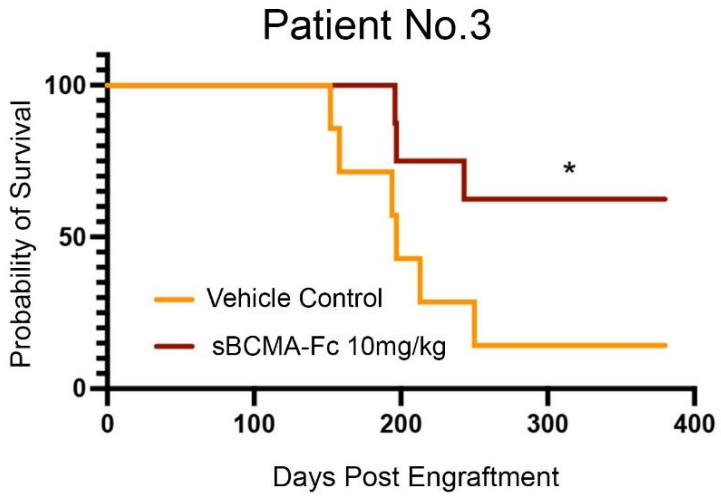

B

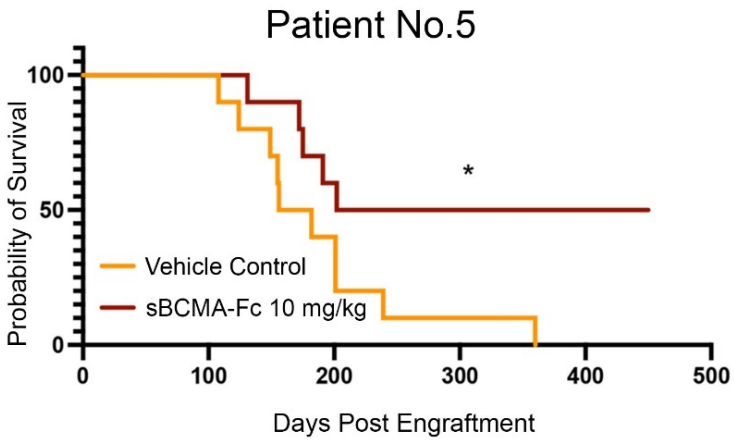

Figure 3.29. Treatment with sBCMA-Fc results in prolonged survival in PDX model
(A) Kaplan Meier survival curves of animals engrafted with MM cells from Patient No. 3. Animals were divided into treatment and control groups. Analysis shows prolonged overall survival in the sBCMA-Fc treated group (N = 8) compared to the control group (N = 7); P = 0.027 compared to Vehicle Control.
(B) Kaplan Meier survival curves of animals engrafted with MM cells from Patient No. 5. Animals were divided into treatment and control groups. Analysis shows prolonged overall survival in the sBCMA-Fc treated group (N = 10) compared to the control group (N = 10); P = 0.0362 compared to Vehicle Control.

This study was performed in collaboration with Dr. Yu Rebecca Miao at Stanford University Department of Radiation Oncology.

Study results demonstrated that treatment with sBCMA-Fc significantly reduced MM tumour growth as measured by reduced serum levels of human IgGκ compared to vehicle control. Furthermore, mice in the treatment group had prolonged overall survival compared to the control group, supporting our hypothesis that BCMA signalling plays an important role in the development of MM and patient outcome (Figure 3.28 and Figure 3.29).

3.2.15 sBCMA-Fc demonstrates superior anti-tumour efficacy in combination with anti-CD38 mAB in MM1.R MM xenograft model

In recent years, anti-CD38 mAB emerged as a promising therapeutic delivering an unprecedented percentage of minimal residual disease (MRD) negativity in MM patients who received treatment[6, 216], and had thus been approved by the FDA for MM patients after one or more lines of therapy. To evaluate the relevance of the sBCMA-Fc fusion protein in combination with SOC therapeutics, we tested the combination of sBCMA-Fc and anti-CD38 mAB in a MM1.R MM xenograft mouse model.

$1x10^7$ MM1.R MM cells in RPMI with 50% Matrigel were inoculated subcutaneously into 6-week-old female NSG mice, followed by treatment initiation on the next day. For the study duration of 28 days, mice in the experimental group (N=8) received sBCMA (10 mg/kg; every 48 hours) and anti-CD38 mAB (10 mg/kg; weekly) combination. For the comparison single-agent treatment groups, mice received sBCMA-Fc alone at 10 mg/kg every 48 hours (N=7), or anti-CD38 mAB alone at 10 mg/kg every week (N=7), while the vehicle control group (N=8) received placebo every 48 hours.

Throughout the study duration, we collected time series measurements of tumour volume and mouse body weight. At study termination, tumours were harvested, and tumour weights were measured. As expected, the sBCMA-Fc+anti-CD38 mAB combination treatment group achieved superior tumour growth control compared to the rest of the groups (Figure 3.30). Furthermore, the combination treatment resulted in no additional normal tissue toxicity as indicated by comparable body weights to the vehicle control group (Figure 3.31).

A

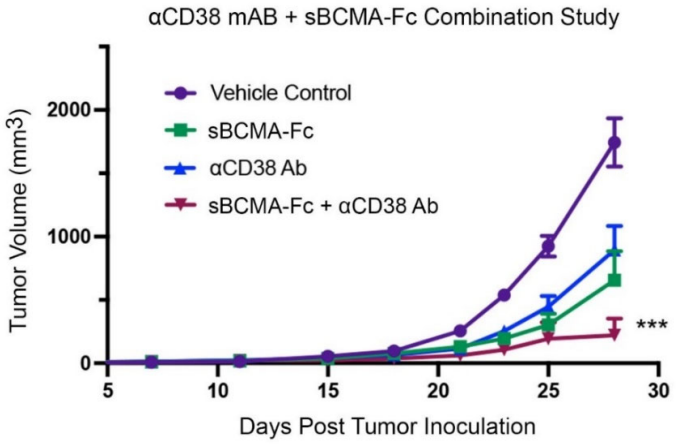

B

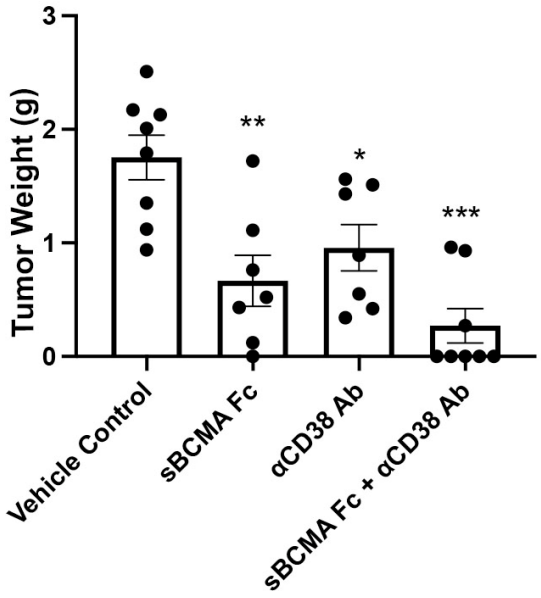

Figure 3.30. Combination treatment of sBCMA-Fc and anti-CD38 mAB shows superior anti-tumour activity compared to single agents
(A) Subcutaneous *in vivo* MM1.R MM tumour growth in 6-week-old NSG female mice treated with sBCMA-Fc (N = 7; P = 0.0195 compared to Vehicle Control), anti-CD38 mAB (N = 7; P = 0.0238 compared to Vehicle Control), combination treatment with sBCMA-FC + anti-CD38 mAB (N = 8; P < 0.01 compared to Vehicle Control), and vehicle control (N = 8).
(B) Terminal tumour weight measurements from the sBCMA-FC + anti-CD38 mAB combination study described above; P-values: * <= 0.05, ** <= 0.01; *** <= 0.001 compared to Vehicle Control.

This study was performed in collaboration with Dr. Yu Rebecca Miao at Stanford University Department of Radiation Oncology.

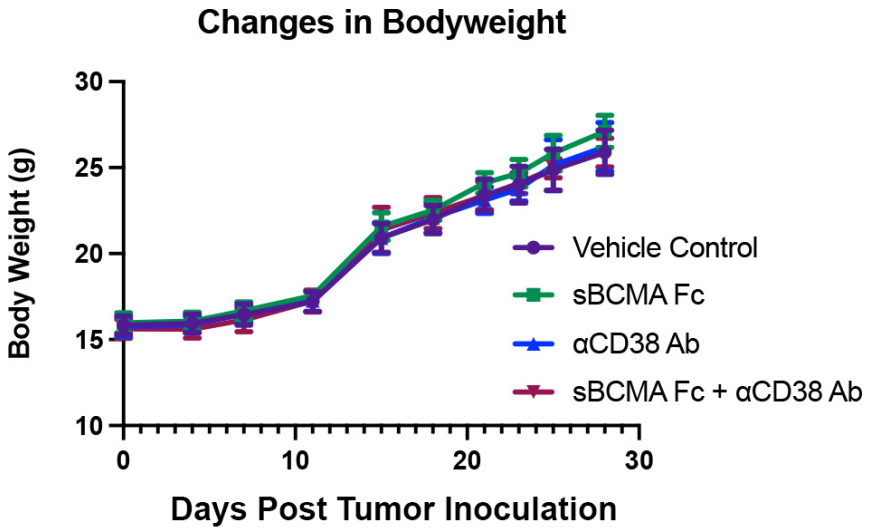

Figure 3.31. Combination treatment of sBCMA-Fc and anti-CD38 mAB shows negligible additional normal tissue toxicity
Time series measurements of body weight for mice in treatment and vehicle control groups in the study described above.

This study was performed in collaboration with Dr. Yu Rebecca Miao at Stanford University Department of Radiation Oncology.

3.3 Discussion

Aberrant ligand-mediated activation of the BCMA signalling pathway has been reported to facilitate the progression of MM and attributed to poor patient outcomes[73, 217]. Here we observed significantly elevated levels of BCMA mRNA in MM patient samples compared to normal healthy donors. ONCOMINE database results at a broader scale showed abnormal BCMA expressions in B-cell related malignancies amongst a variety of tumour types, thus further supporting our initial finding. Similarly, we observed significantly elevated levels of APRIL and BAFF in MM patient serum samples. We therefore hypothesized that inhibition of BCMA signalling would inhibit MM tumour survival and proliferation.

We began testing our hypothesis by transiently knockdown BCMA with siRNA and observed reduced U266 MM tumour growth *in vitro*. Study results also confirmed suppressed pro-survival signalling activation downstream of BCMA signalling upon transient BCMA knockdown.

We next conducted a similar study with dox-inducible stable knockdown of BCMA with shRNA and obtained consistent results. To mitigate for the heterogenetic nature of MM, we used two different MM cell lines for this study, INA-6 and MM1.R. Results with both cell lines showed significant inhibition of tumour initiation *in vivo* in the BCMA knockdown experimental group as indicated by tumour volume, tumour weight measurements, as well as proliferation and apoptosis assay results. Furthermore, we observed a reduction in serum M protein level in the BCMA knockdown group.

Supported by initial results and existing literature, we hypothesized that inhibition of ligand-mediated BCMA signalling via neutralizing APRIL and BAFF with a wild-type sBCMA-Fc fusion protein could be an effective approach to treating MM.

Previous attempts to therapeutically inhibit ligand-mediated BCMA signalling followed two approaches. The first approach with mABs against BCMA or its primary ligand APRIL had achieved limited success in the clinic. For example, Aduro Biotech developed an anti-APRIL mAB, BION-1301, with a K_D in the nanomolar range. Phase 1/2 clinical trial results demonstrated that BION-1301 was well tolerated in patients with relapsed or refractory MM across a wide dose range, and no dose limited toxicities were observed at any dose level. Aduro reported 95% target engagement at peak exposure levels by BION-1301, and free APRIL levels decreased dose-dependently. However, BION-1301 failed to achieve meaningful objective responses. We believe this could be due to the strong native binding, at picomolar levels, between BCMA and APRIL, since therapeutic antibodies typically have nanomolar binding affinities toward targets. Furthermore, targeting APRIL alone is insufficient since BAFF also binds to BCMA. In addition, Aduro did not elaborate on the approach used to calculate the 95% target engagement, which warrants further investigation. However, it would be valuable to investigate the physiological relevance of BAFF binding to BCMA if the affinity is indeed in the low micromolar range, 100 times lower than APRIL, as previous studies reported. If not relevant, then the failure of BIO-1301 could indicate that BCMA could be a specific recognition element, but functional modulation may not be as useful.

The second approach with a sTACI-Fc fusion protein also has proven to be challenging. Atacicept, a wild-type sTACI-Fc fusion protein, only showed modest efficacy in MM clinical studies[218]. This could be explained by the difference in binding affinities between APRIL/BCMA and APRIL/TACI, where the former was reported to be stronger[219]. Also, previous research reported the expression of TACI on MM cells appears to be bimodal, which may indicate a less important function of the receptor for MM cells. Therefore, further receptor knockout / knockdown studies on

BCMA/TACI/BAFFR with different permutations could be conducted, to gain a deeper understanding on the impacts of their functional roles on MM cell survival and growth.

Our sBCMA-Fc fusion protein demonstrated effective suppression of APRIL and BAFF *in vivo* in naïve mice. Furthermore, results showed minimal normal tissue toxicities related to treatment. To test the molecule's therapeutic efficacy, we conducted *in vivo* studies with INA-6 and MM1.R MM tumour cell lines. Consistent with our BCMA knockdown study results, treatment with sBCMA-Fc significantly reduced MM tumour growth *in vivo*. To confirm the target specificity of the sBCMA-Fc, we conducted a controlled study with IgG1-Fc and a non-target-binding Fc fusion protein, and showed that sBCMA-Fc's efficacy resulted from specific APRIL and BAFF engagements. Encouraged by the results, we developed a MM PDX model with fresh MM patient biopsy samples. Results demonstrated effective *in vivo* tumour growth inhibition and the suppression of human M proteins. In the final study for this chapter, we combined sBCMA-Fc with a anti-CD38 mAB to assess whether our fusion protein could enhance the current SOC therapy. We observed superior anti-tumour effect for the combination treatment group compared to the rest of the groups while did not observe any additional treatment-related normal tissue toxicities.

In conclusion, results from studies in this chapter provided sound rationale supporting ligand neutralization with sBCMA-Fc as a feasible approach to inhibit BCMA signalling-promoted MM tumour growth. Mechanistically, we confirmed BCMA signalling as a critical pro-survival factor that promotes activities of NF-κB and MAPK cascades, consistent with previous reports. Furthermore, we reported previously BCMA's role in regulating the translation of a subset of proteins, such as ATMIN, which recent reports indicated to be involved in the dysregulated B-cell development in lymphomas[181]. *In vitro* and *in vivo* studies have shown satisfactory anti-tumour activities of the sBCMA-Fc while resulting in minimal normal tissue toxicities.

In the immediate future, additional confirmatory studies are warranted to further validate the sBCMA-Fc's therapeutic efficacy against MM. For example, BCMA is normally shed in a gamma secretase-dependent fashion that leads to high patient serum levels of wild-type soluble BCMA, which is considered a barrier to BCMA-targeting therapeutics, and led to trials where GS inhibitors are added to prevent the shedding of BCMA. As such, future investigations are warranted to assess the impact of shed soluble BCMA on the efficacy of the sBCMA-Fc for late-stage, r/r MM patients who typically have high circulating shed soluble BCMA[220]. This question becomes more critical considering late-stage, r/r MM patients will most likely be evaluated in the early clinical trials that will determine the success of the sBCMA-Fc. For example, it would be helpful to conduct a confirmatory *in vivo* study with one of our MM tumour cell lines but with prior measurement of serum level shed BCMA, which could be a cause of the apparent long median survival for the untreated mice in our studies.

It would be interesting to also investigate the therapeutic efficacy of sBCMA-Fc in combination with BCMA-targeting novel therapeutics which are gaining approvals by regulatory agencies recently, such as BCMA-targeting CAR T-cell therapies or ADCs. Since BCMA-targeting agents bind to wild-type BCMA receptors, thus will also bind to the sBCMA-FC, we could see a drop in efficacy for either the sBCMA-Fc or the BCMA-targeting agent due to the binding between the two therapeutics.

To prepare the sBCMA-Fc for future clinical studies, further studies to investigate the pharmacokinetic, pharmacodynamic, and toxicology profiles of the sBCMA-Fc in more advanced species such as non-human primates are warranted to fully characterize the molecule. For instance, it would be interesting to determine if the sBCMA-Fc could reach and scavenge APRIL and BAFF in the bone marrow where MM develops. In addition, assessing the safety profile of the molecule, and whether anti-drug antibodies develop, in a repeat and escalating dose setting is critical to prepare for clinical studies.

Finally, manufacturing characteristics such as stability, purity, and yield, will need to be optimized to fully develop the sBCMA-Fc into a viable therapeutic for the clinic.

CHAPTER 4 INHIBITION OF BAFF-MEDIATED SIGNALLING WITH ENGINEERED sBCMA-FC EFFECTIVELY REDUCES DLBCL TUMOUR GROWTH

4.1 Introduction

DLBCL, the most common type of NHL, develops when B-cells become abnormal and grow uncontrollably. The malignant B-cells can form tumours in lymph nodes, bone marrow, and other organs of the body. First-line SOC with R-CHOP typically achieves a high response rate of 70% to 80%, although the exact response may vary between patients. In addition, novel CD19-targeting CAR T-cell therapy has recently been approved by the US FDA as a treatment for adult DLBCL patients who are refractory to, or relapsed within 12 months of completing first-line SOC treatments. Despite impressive objective response rates, approximately 40% of DLBCL patients will relapse after front-line R-CHOP treatment[39, 40], and only a limited sub-population of patients are eligible for CAR T-cell therapy depending on health condition. Furthermore, more than half of patients who received CAR T treatment did not have a sustained response to treatment[37, 40]. The overall five-year survival rate of DLBCL is about 60% – 70%, and current SOCs are not curative[2, 3].

BAFFR is expressed on most types of B-cells except for bone marrow plasma cells. Ligand-mediated activation of BAFFR by BAFF facilitates normal B-cell growth and differentiation into plasma cells, at which stage BCMA becomes the dominant receptor, as described earlier[138]. Previous studies have shown that BAFF expression levels are elevated in DLBCL cells compared to normal B-cells. In addition, serum level of BAFF is positively associated with a poorer prognosis and a higher likelihood of disease progression for NHL patients. Thus, serum BAFF level is often used as a biomarker to assess disease progression. Similarly, BAFFR, the primary receptor of BAFF, has been reported to be significantly up-regulated on malignant B-cells, including DLBCL[133,

199]. Activation of BAFFR results in downstream alternative NF-κB signalling, which promotes the survival and growth of malignant B-cells. BAFFR signalling can also lead to the activation of the AKT – mTOR pathway, which is involved in the regulation of cellular growth and survival[153]. Thus, aberrant activation of BAFFR signalling has been implicated in the development and progression of DLBCL and other B-cell malignancies[199]. Furthermore, BAFF/BAFFR signalling plays an important role in malignant B-cell's resistance to spontaneous and drug-induced apoptosis[35, 169, 221]. Given the critical pro-survival and drug resistance functions BAFF/BAFFR signalling plays in B-cell malignancies, we hypothesized that our sBCMA-Fc, by sequestering BAFF and APRIL, could effectively inhibit the BAFF/BAFFR signalling axis in DLBCL tumour cells, thereby inhibiting tumour growth.

In this chapter, we began our studies by initially testing the anti-tumour activities of the sBCMA-Fc *in vitro* and *in vivo* with BAFF-driven DLBCL cell lines SU-DHL-6 and Daudi. We observed that the wild-type-based sBCMA-Fc was ineffective against these BAFF-driven DLBCL tumour models; and we hypothesized that this result could be due to the wild-type sBCMA-Fc's weak binding affinity toward BAFF, measured at 1.6 μM by surface plasmon resonance, compared to the stronger wild-type BAFF / BAFFR binding affinity measured at 16 nM by surface plasmon resonance[165].

To overcome the affinity barrier, we developed mutant clones of the wild-type soluble BCMA using a yeast surface display-based system. The resulting mutant clone library was screened based on enhanced binding affinities toward ligands APRIL and BAFF. After six rounds of sorting, we identified sBCMA-Fc V3 as the top clone based on improved binding affinities toward BAFF and APRIL and minimized mutations in the clone's sequence to avoid potential immunogenicity issues.

We next proceeded to test our hypothesis that sBCMA-Fc V3, with its significantly enhanced binding affinity toward BAFF measured at 9 pM, and toward APRIL measured at 8 pM, would result in improved anti-tumour efficacy compared to the wild-type sBCMA-Fc. Initial studies with normal immune-deficient mice showed that sBCMA-Fc V3 was effective at suppressing BAFF and APRIL in serum, and has an improved half-life compared to the wild-type sBCMA-Fc. As an assessment for the molecule's pharmacodynamic characteristics, we observed transient and reversible reduction of immunoglobulin levels in mouse serum, and a reduction of bone marrow plasma cells. In xenograft models with SU-DHL-6 and Daudi DLBCL cell lines, sBCMA-Fc V3 demonstrated significant anti-tumour activity in a dose-dependent manner. Furthermore, in a head-to-head comparison study, sBCMA-Fc V3 performed better compared to a sTACI-Fc fusion protein and our wild-type sBCMA-Fc, potentially due to sBCMA-Fc V3's enhanced binding toward BAFF.

Overall, results in this chapter support the sBCMA-Fc V3 as a clinically viable therapeutic for the treatment DLBCL, and potentially other B-cell malignancies in general. Furthermore, as shown in the previous chapter with the wild-type sBCMA-Fc, given the molecule's expected favourable safety profile, we believe the sBCMA-Fc V3 could be a desirable agent for use in combination with first-line SOC or novel T-cell therapies, as well as a single agent for r/r patients and patients who are ineligible for T-cell therapies due to health conditions.

4.2 Results

4.2.1 Wild-type sBCMA-Fc lacks potency in BAFF-driven DLBCL studies

Previous literature reported the dependence of B-cell lymphomas on BAFF-mediated signalling for survival and proliferation[153, 159, 222]. Since the BCMA receptor also binds to BAFF, albeit at a lower affinity compared to that with primary ligand APRIL as previously reported[140], we investigated the therapeutic potential of the wild-type sBCMA-Fc fusion protein in DLBCL, which is BAFF-dependent, using models with BAFF-sensitive DLBCL cell lines of SU-DHL-6 and Daudi, both of which express BAFF and BAFFR[223-225].

Initially to assess the effect of the sBCMA-Fc on the viability of DLBCL cells *in vitro*, we performed cytotoxicity assay with SU-DHL-6 and Daudi cell lines. To control for the stimulus effects of BAFF and other growth factors that exist in the culture medium, we incubated DLBCL cells with 100 ng/mL of recombinant human BAFF to activate BAFF-mediated signalling, and cultured DLBCL cells in reduced serum conditions to minimize the effects of other growth factors in the medium. DLBCL cells in the three experimental groups were treated with increasing doses of sBCMA-Fc every 48 hours for a duration of 7 days. DLBCL cell lines in the control groups were treated with vehicle control without BAFF, and human recombinant BAFF alone.

Results of cytotoxicity assay (Figure 4.1) showed a gradual decrease of DLBCL cell viability as treatment dose increased, indicating a potential inhibitory effect of the sBCMA-Fc and a treatment dose-response relationship. However, compared to the MM cell lines in the previous chapter, the SU-DHL-6 and Daudi DLBCL cells seemed to be less responsive to the wild-type sBCMA-Fc treatment.

A

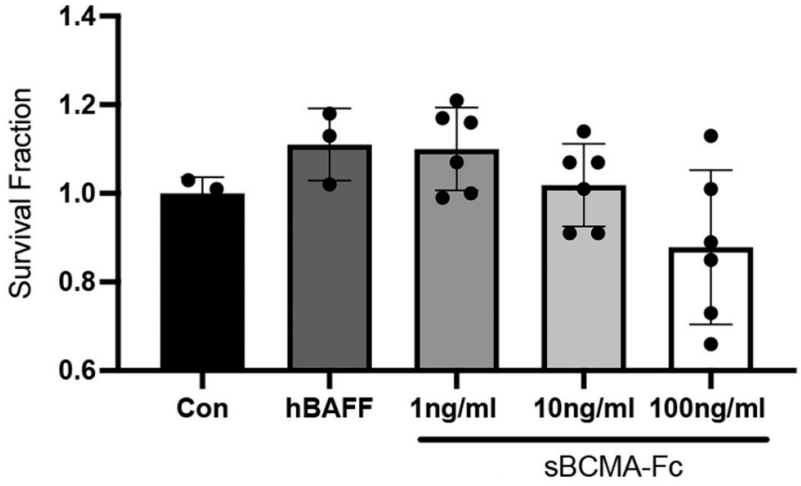

B

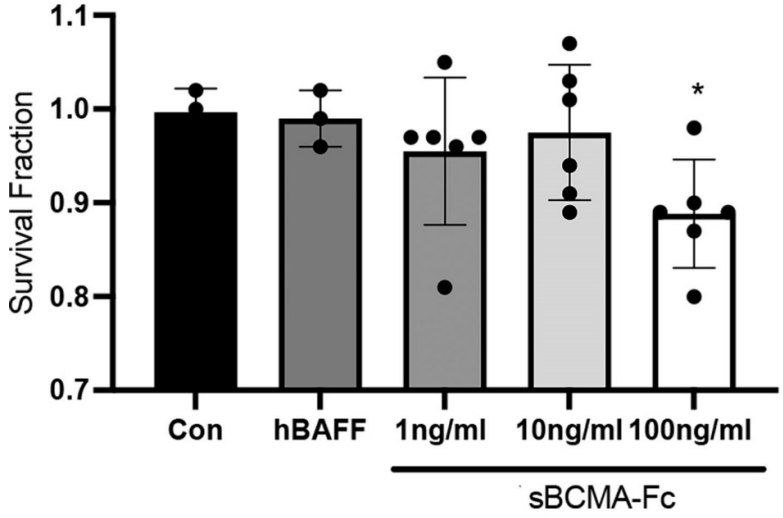

Figure 4.1. sBCMA-Fc was not effective at inhibiting BAFF-driven DLBCL tumour growth *in vitro*

(A) Cytotoxicity assay examining *in vitro* cell survival of SU-DHL-6 DLBCL cells in the presence of human BAFF (100 ng/mL), and increasing doses of sBCMA-Fc.

(B) Cytotoxicity assay examining *in vitro* cell survival of Daudi DLBCL cells in the presence of human BAFF (100 ng/mL), and increasing doses of sBCMA-Fc. At the highest concentration of 100 ng/mL, sBCMA-Fc treatment led to a statistically significant reduction in cell number; P = 0.045 compared to BAFF-stimulated control (hBAFF).

We next investigated the therapeutic efficacy of the wild-type sBCMA-Fc *in vivo* in a xenograft mouse model. SU-DHL-6 DLBCL tumour cells were inoculated subcutaneously into NSG immune deficient mice to examine tumour survival and proliferation upon treatment with the sBCMA-Fc compared to vehicle control. Mice were subcutaneously injected with $5x10^6$ SU-DHL-6 DLBCL cells in RPMI with 50% Matrigel. Mice in the treatment group (N=5) were dosed with the sBCMA-Fc at 10 mg/kg every 48 hours for the treatment duration of 28 days. Mice in the control group (N=5) were dosed with vehicle control at the same schedule. At study termination, tumours were harvested and measured by weight to assess *in vivo* tumour growth. Results showed marginal and insignificant tumour growth reduction for the sBCMA-Fc treated experimental group, consistent with results from *in vitro* cytotoxicity assays (Figure 4.2).

Statistical analysis for this study was conducted using t test and one-way ANOVA for comparing between treatment groups. Repeated ANOVA used for changes in tumour growth over time. *, $P < 0.05$; **, $P < 0.01$; ***, $P < 0.001$.

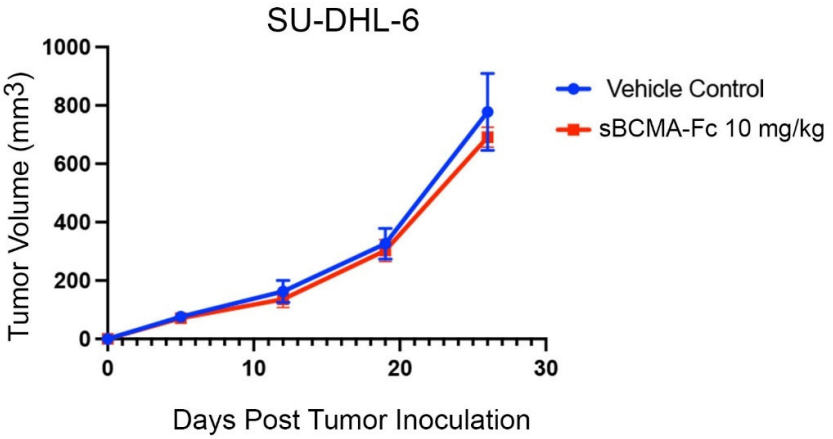

Figure 4.2. sBCMA-Fc was not effective at inhibiting BAFF-driven SU-DHL-6 DLBCL tumour growth *in vivo*
In vivo growth of SU-DHL-6 DLBCL tumours in mice dosed with sBCMA-Fc at 10 mg/kg, or vehicle control, every 48 hours for 28 days; N = 5 for each group.

This study was performed in collaboration with Dr. Yu Rebecca Miao at Stanford University Department of Radiation Oncology.

4.2.2 Developing a high-affinity soluble BCMA-Fc ligand trap against BAFF and APRIL

As indicated by results from the previous *in vitro* and *in vivo* studies, BAFF-sensitive SU-DHL-6 and Daudi DLBCL cells did not respond to treatment with the wild-type sBCMA-Fc fusion protein. As reported previously, the binding affinity between human BAFF and BCMA was not detected with flow cytometry, and that between human APRIL and BCMA was estimated to be 25 – 48 pM as measured by K_D [179-181]. Our binding analysis using the flow cytometry method on wild-type interactions between BCMA and its ligands reported similar findings (Figure 4.3). Using the surface plasmon resonance method, a previous study reported a binding affinity between BAFF and BAFFR measured at 16 nM, and that between BAFF and wild-type BCMA measured at 1.6 μM[165]. Since DLBCL is driven more by BAFF compared to APRIL, and the wild-type sBCMA-Fc has a weaker binding affinity toward BAFF compared to the wild-type BAFF / BAFFR binding, we hypothesized that the sBCMA-Fc lacks sufficient potency to sequester BAFF and inhibit BAFF-mediated signalling, resulting in the apparently weak therapeutic efficacy.

A

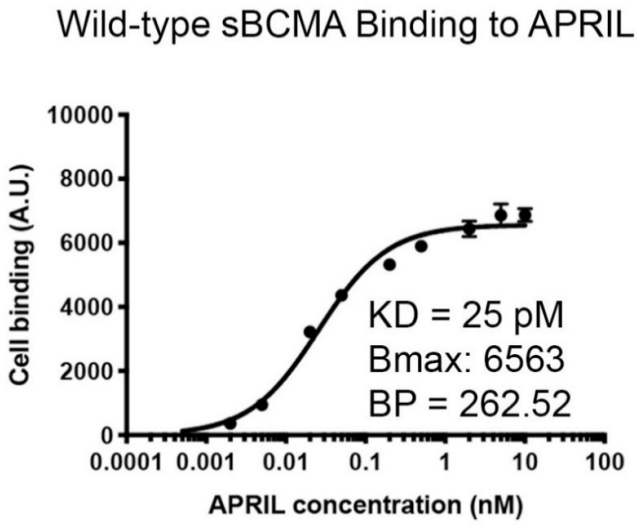

B

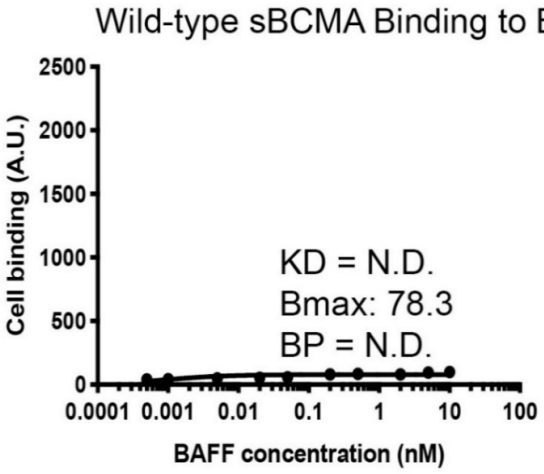

Figure 4.3. Binding affinities between wild-type BCMA and its ligands APRIL and BAFF

(A) Binding affinity measured with flow cytometry showing the binding of wild-type sBCMA generated with yeast surface display to increasing concentrations of APRIL. A.U., arbitrary units.

(B) Binding affinity measured with flow cytometry showing the binding of wild-type sBCMA generated with yeast surface display to increasing concentrations of BAFF. A.U., arbitrary units.

This study was performed in collaboration with Dr. Kaushik Thakkar at Stanford University Department of Radiation Oncology.

To address the weak binding affinity between the wild-type sBCMA-Fc fusion protein and human BAFF, we engineered a mutant BCMA ECD and fused it with a human IgG1 Fc domain as summarized next. Random nucleotide mutations were introduced into the ECD of the human wild-type BCMA gene without bias, from amino acid 1 (methionine) to 54 (alanine), using low-fidelity Taq polymerase-based error prone PCR[226]. The resulting library of mutant sequences were displayed on the yeast surface and sorted by FACS to select mutant clones with the highest binding affinities. We used human APRIL for initial affinity screening because, as previously reported, human APRIL and human BAFF share a high homology. Thus, we hypothesized that clones selected with this process will have high binding affinities toward BAFF as well[227].

We performed six rounds of sorting sequentially and isolated 1 – 3% of mutants from the library. The top 118 clones were then sequenced and analysed for consensus mutations compared to the wild-type BCMA ECD. Overall, seven consensus mutations were identified. As expected, selected mutants had dramatically improved binding affinities toward APRIL and, especially, BAFF. To avoid potential immunogenicity and the resulting anti-drug antibody (ADA) issues, we focused on mutant clones with high binding affinities while possessing fewer mutations. Ultimately, Clone V3 was selected, and we proceeded to developing a Fc fusion protein, sBCMA-Fc V3, by fusing Clone V3 with a human IgG1 Fc domain for improved stability and bioavailability *in vivo*. The sBCMA-Fc V3 has a binding affinity toward BAFF measured at 9 pM, and a binding affinity toward APRIL measured at 8 pM (Figure 4.4).

To characterize the selected sBCMA-Fc V3, we analysed the structural and biophysical properties of the mutant sBCMA V3 ECD domain, assisted by computational modelling. In summary as previously reported[181], of the four mutations in the sequence of the sBCMA V3 ECD, S16G and H19Y are located within the sBCMA

binding motif while T36A and N53D are outside of the binding motif. Results indicated that mutation H19Y is likely to be the most important contributor to the improvement in binding affinities toward APRIL and BAFF, since the mutation improved the receptor-ligand co-complex's stability, thermodynamic interactions and surface complementarity. Also, mutations S16G and T36A were also found to be positive contributors although to a lesser extent than H19Y (Table 4.1; Figure 4.4).

% in Library	24%	24%	41%	66%	76%	17%	14%	BAFF (K_D, BP)	APRIL (K_D, BP)
Mutation: Clone No.:	**S9P**	**N11D**	**S16G**	**H19Y**	**T36A**	**N47S**	**N53D**		
WT	--	--	--	--	--	--	--	~4,900 pM N.D.	~25 – 48 pM 262
Clone V5	√	√	√	√	√	√	√	9 pM, 186	7 pM, 1313
Clone V3			√	√	√		√	9 pM, 136	8 pM, 1034
Clone V2			√	√	√			8 pM, 121	18 pM, 325
Clone V8			√		√			N.D.	54 pM, 102

Table 4.1. sBCMA-Fc V3 exhibits the highest binding affinities with fewest mutations Binding affinities between wild-type sBCMA and APRIL / BAFF; and binding affinities between selected mutant sBCMA clones and APRIL / BAFF. Conserved amino acid mutations were identified in mutant clones, and the frequency of occurring mutations is also listed.

This study was performed in collaboration with Dr. Kaushik Thakkar at Stanford University Department of Radiation Oncology.

A

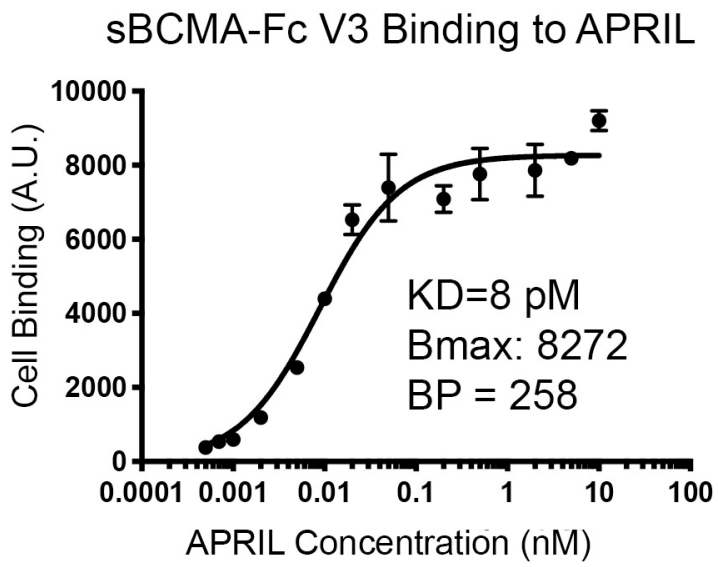

B

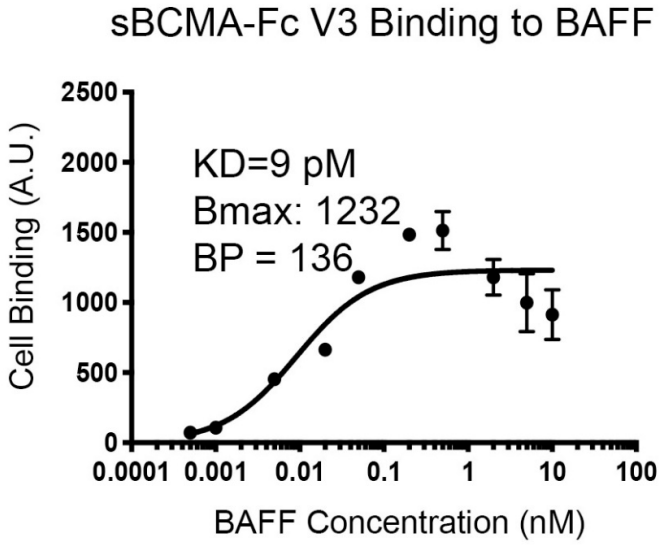

Figure 4.4. Binding affinities between sBCMA-Fc V3 and human APRIL and BAFF
(A) Binding affinity measured with flow cytometry showing the binding of sBCMA-Fc V3 to increasing concentrations of APRIL. A.U., arbitrary units.
(B) Binding affinity measured with flow cytometry showing the binding of sBCMA-Fc V3 to increasing concentrations of BAFF. A.U., arbitrary units.

This study was performed in collaboration with Dr. Kaushik Thakkar at Stanford University Department of Radiation Oncology.

4.2.3 sBCMA-Fc V3 demonstrates improved anti-tumour efficacy *in vitro*

To compare the *in vitro* anti-tumour efficacy of the sBCMA-Fc V3 with the wild-type sBCMA-Fc, we performed cytotoxicity assays with SU-DHL-2 and Daudi DLBCL cell lines. To control for the stimulus effects of BAFF and other growth factors that exist in the culture medium, we incubated DLBCL cells with 100 ng/mL of recombinant human BAFF to activate BAFF mediated signalling, and cultured DLBCL cells in reduced serum conditions to minimize the effects of other growth factors in the medium.

DLBCL tumour cells in the three experimental groups were treated with increasing doses of sBCMA-Fc V3 every 48 hours for a duration of 7 days. DLBCL tumour cells in the control groups were treated with vehicle control alone, human recombinant BAFF alone, IgG1-Fc alone without the presence of human recombinant BAFF, and sBCMA-Fc V3 alone without the presence of human recombinant BAFF.

Results of cytotoxicity assay showed a marked decrease of the viability of DLBCL cells dependent on BAFF-mediated signalling as treatment dose increases, demonstrating the inhibitory effect of sBCMA-Fc V3 and a treatment dose-response relationship (Figure 4.5). Compared to the similar study completed with the wild-type sBCMA-Fc, results from this experiment indicated significantly enhanced anti-tumour efficacy of the engineered sBCMA-Fc V3 *in vitro*.

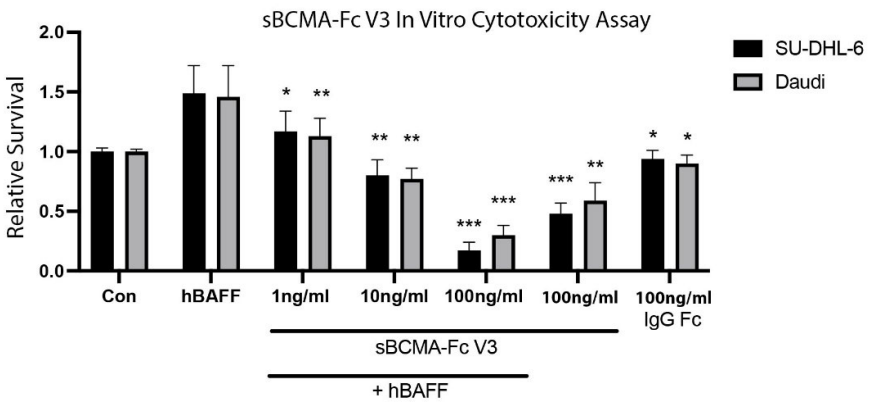

Figure 4.5. ***In vitro*** **cytotoxicity assay examining the impact of sBCMA-Fc V3 treatment on DLBCL cells**

Cytotoxicity assay examining *in vitro* tumour cell survival with SU-DHL-6 and Daudi DLBCL tumours in the presence of increasing doses of sBCMA-Fc V3 and human BAFF at 100 ng/mL. *, $P < 0.05$; **, $P < 0.01$; ***, $P < 0.001$, compared to BAFF-stimulated control (hBAFF). Cells were maintained in low (3%) FBS to reduce possible growth stimulation mediated through other growth factors present in FBS. Each sample was performed in triplicate.

We next analysed changes in protein expressions downstream to BAFF-mediated signalling. Western blot at different time points post treatment indicated that treatment with the sBCMA-Fc V3 resulted in decreased expressions of phosphorylated-AKT, phosphorylated-mTOR, phosphorylated-p38 MAPK and phosphorylated-NF-κB, which are critical regulators of cellular survival and proliferation (Figure 4.6).

Taken together, results from this *in vitro* study suggest that further *in vivo* studies were warranted to assess the therapeutic potential of the sBCMA-Fc V3 in DLBCL mouse models.

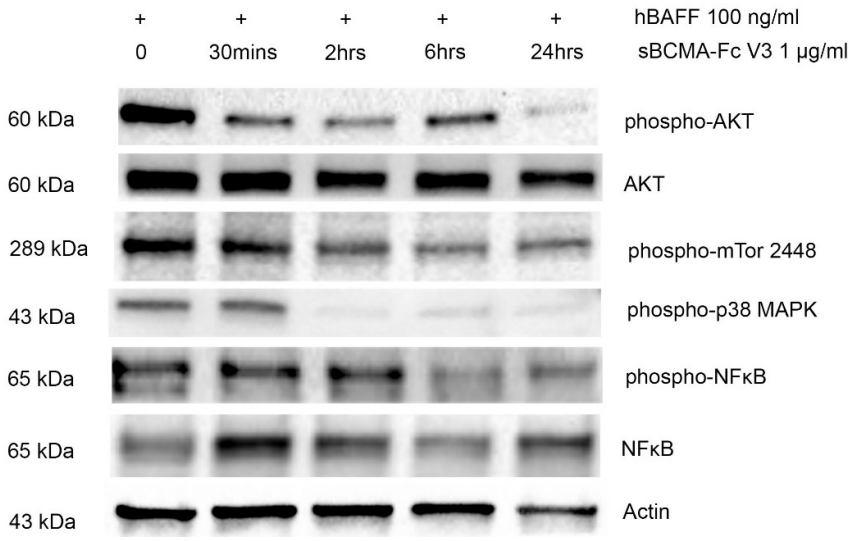

Figure 4.6. BCMA regulates important downstream signalling pathways in DLBCL
Analysis of downstream protein expressions in SU-DHL-6 DLBCL cells upon sBCMA-Fc V3 treatment at multiple time points.

4.2.4 sBCMA-Fc V3 demonstrates potent suppression of APRIL and BAFF in serum *in vivo*

To assess the pharmacodynamic characteristics of the sBCMA-Fc V3 *in vivo*, we measured serum levels of APRIL and BAFF with ELISA upon a single dose of sBCMA-Fc V3 at 10 mg/kg, injected into NOD-scid immunocompromised non-tumour bearing mice (N=2).

Results indicated a near-complete suppression of APRIL for almost five hours, with an overall half-life of APRIL inhibition of approximately 20 hours. In addition, sBCMA-Fc V3 effectively sequestered BAFF almost completely for over 20 hours and achieved an overall BAFF inhibition half-life of approximately 60 hours (Figure 4.7).

Compared to the similar preliminary pharmacodynamic study completed with the wild-type sBCMA-Fc in the previous chapter, sBCMA-Fc V3 demonstrates a higher potency in BAFF inhibition as shown by the longer complete-suppression time and overall half-life.

A

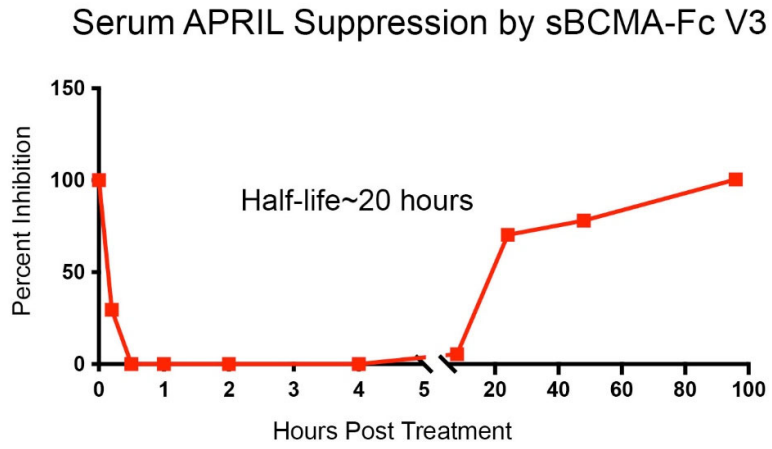

B

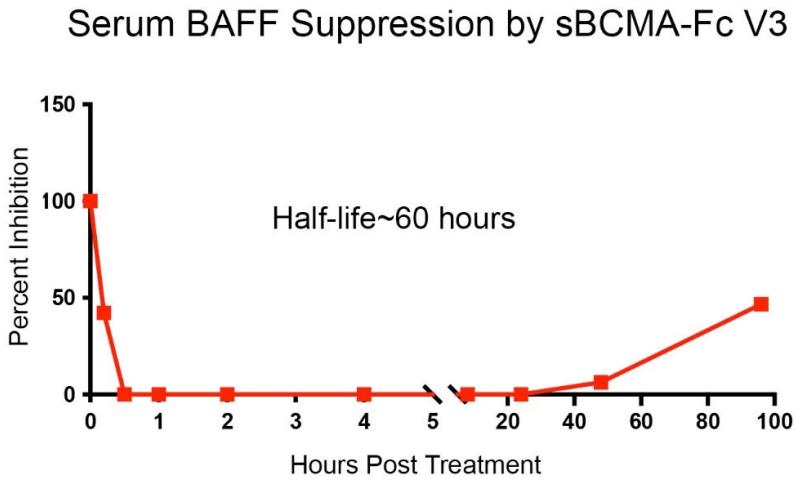

Figure 4.7. sBCMA-Fc V3 demonstrates effective suppression of free APRIL and BAFF in serum *in vivo*
(A) APRIL level in mouse serum measured by ELISA after a single dose of sBCMA-Fc V3 at a concentration of 10 mg/kg. Each data point represents duplicated repeats collected at each time point.
(B) BAFF level in mouse serum measured by ELISA after a single dose of sBCMA-Fc V3 at a concentration of 10 mg/kg. Each data point represents duplicated repeats collected at each time point.

This study was performed in collaboration with Dr. Yu Rebecca Miao at Stanford University Department of Radiation Oncology.

4.2.5 sBCMA-Fc V3 effectively suppresses B-cell-mediated immunoglobulin class switching

Previous literature reported the impact of APRIL and BAFF inhibition on B-cell-mediated immunoglobulin (Ig) class switching[192, 193, 228]. Therefore, we hypothesized that investigating changes in Ig levels *in vivo* upon sBCMA-Fc V3 treatment could further provide an approximate measure of the fusion protein's pharmacodynamic property. Here we assessed the levels of IgM, IgA and IgG in mouse serum after a single dose of sBCMA-Fc V3 at 10 mg/kg into naïve mice (N=2). Mouse IgM, IgA and IgG levels in serum were measured at different time points post initial dosing throughout the study.

Results showed a transient decrease of IgM, IgA and IgG within 48 hours after dosing, consistent with previous reports and our hypothesis. Furthermore, we observed that levels of IgM, IgA and IgG returned to normal levels within 7 days, suggesting the treatment effect of sBCMA-Fc V3 is reversible (Figure 4.8).

A

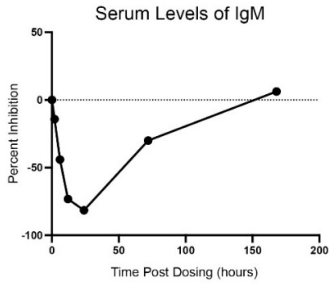

B

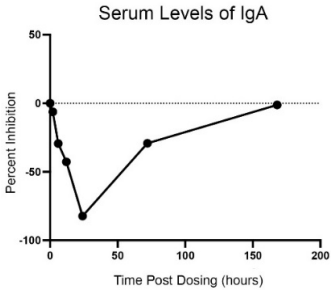

C

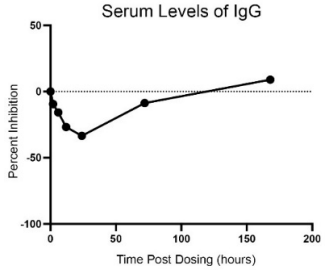

Figure 4.8. sBCMA-Fc V3 treatment suppresses Ig class switching
(A) Levels of IgM in mouse serum after a single dose of sBCMA-Fc V3 at 10 mg/kg.
(B) Levels of IgA in mouse serum after a single dose of sBCMA-Fc V3 at 10 mg/kg.
(C) Levels of IgG in mouse serum after a single dose of sBCMA-Fc V3 at 10 mg/kg.

This study was performed in collaboration with Dr. Yu Rebecca Miao at Stanford University Department of Radiation Oncology.

4.2.6 Preliminary pharmacokinetic analysis for the sBCMA-Fc V3

To assess the pharmacokinetic profile of the sBCMA-Fc V3, we administered a single dose of the molecule to two experimental groups of naïve mice (N=2) at two different concentrations, 1 mg/kg and 10 mg/kg, respectively. Mouse serum levels of IgG1 were measured using ELISA over time post initial dosing. This method was effective because antibodies for IgG1 are commercially available, which enabled us to detect the IgG1 domain of the sBCMA-Fc V3 in serum.

Results showed that at the lower dose of 1 mg/kg, sBCMA-Fc V3 had a half-life of approximately 43 hours while at the higher dose of 10 mg/kg, the half-life was approximately 94 hours (Figure 4.9). This could be explained with the pharmacokinetic phenomenon of target-mediated drug disposition (TMDD), in which the high-affinity specific binding of a drug to its target (such as a receptor or enzyme) affects the drug's pharmacokinetic behaviour, including absorption, distribution, metabolism, and elimination. In TMDD, the drug-target binding results in the formation of drug-target complexes, which may alter the pharmacokinetics of the drug by affecting its clearance, distribution, or bioavailability. At the lower concentration, sBCMA-Fc V3 binds specifically with targets APRIL and BAFF at high affinities. Consequently, only a small fraction of the unbound drug is available in the systemic circulation. At the higher concentration, however, there is an excess of the sBCMA-Fc V3 over target ligands. As a result, a larger amount of the unbound protein (IgG1 domain) was detected by ELISA. TMDD can have important clinical implications in drug development, as it may result in nonlinear pharmacokinetics, dose-limiting toxicity, and reduced efficacy of the drug. Therefore, it is important to consider TMDD in the design of drug development programs, especially for drugs that target high-affinity receptors or enzymes.

A

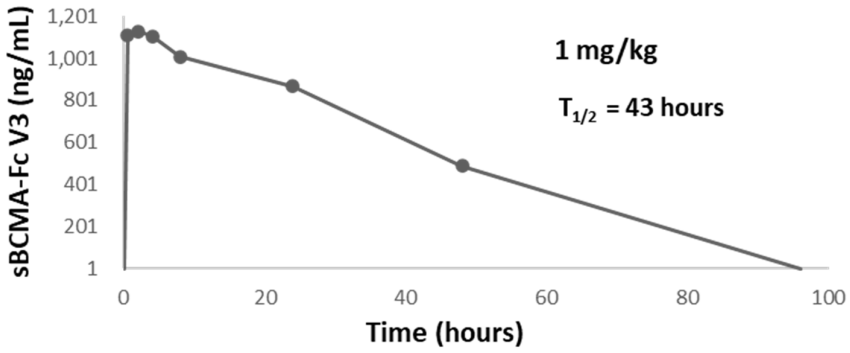

B

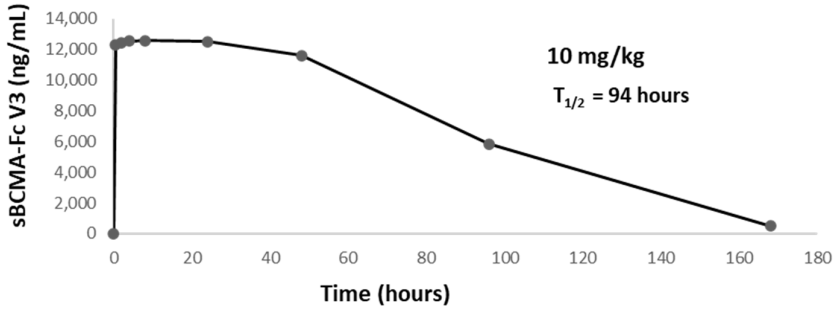

Figure 4.9. Preliminary pharmacokinetic analysis on sBCMA-Fc V3
(A) A single dose of sBCMA-Fc V3 at 1 mg/kg was injected into naïve mice. Pharmacokinetic profile of the sBCMA-Fc V3 was assessed by detecting the human IgG1 domain of the molecule over time by ELISA in serum of mouse.
(B) A single dose of sBCMA-Fc V3 at 10 mg/kg was injected into naïve mice. Pharmacokinetic profile of the sBCMA-Fc V3 was assessed by detecting the human IgG1 domain of the molecule over time by ELISA in serum of mouse.

This study was performed in collaboration with Dr. Yu Rebecca Miao at Stanford University Department of Radiation Oncology.

To conclude this study, as a preliminary pharmacodynamic assessment, we harvested bone marrow samples from mice at study termination and examined normal plasma cell counts 48 hours after treatment. As expected, we observed a marked decrease of normal plasma cells in the two treatment groups, and a dose-response relationship as treatment dose increases (Figure 4.10). This is consistent with previous literature reports and our hypothesis that inhibition of APRIL and BAFF leads to reduced transition from immature B-cells into plasma cells; and inhibits the survival of existing plasma cells.

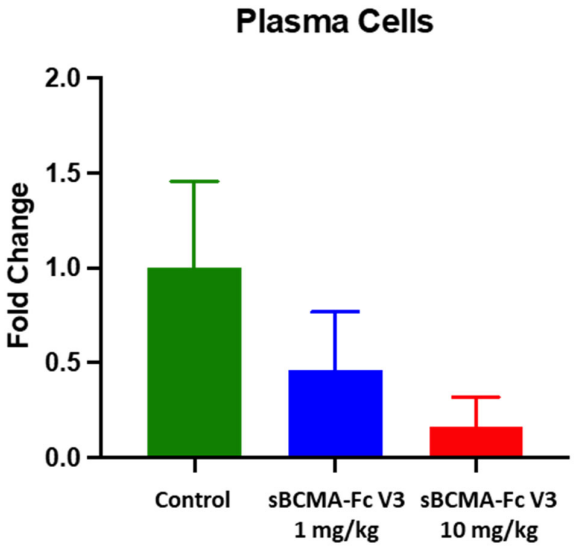

Figure 4.10. sBCMA-Fc V3 treatment reduces normal plasma cells *in vivo*
Bone marrow derived plasma cells quantified by histology 48 hours after treatment with sBCMA-Fc V3 at two different concentrations compared to vehicle control. N = 2 per group; 10 fields for cell count for each mouse.

This study was performed in collaboration with Dr. Yu Rebecca Miao at Stanford University Department of Radiation Oncology.

4.2.7 sBCMA-Fc V3 effectively inhibits DLBCL tumour initiation *in vivo*

To determine the therapeutic efficacy of the engineered sBCMA-Fc V3 fusion protein, we conducted subcutaneous xenograft studies with SU-DHL-6 and Daudi DLBCL cell lines.

SU-DHL-6 DLBCL cells were inoculated subcutaneously into NSG immune deficient mice to examine DLBCL tumour growth upon treatment with sBCMA-Fc V3 compared to control. $5x10^6$ SU-DHL-6 tumour cells in RPMI with 50% Matrigel were injected into mice, which were then divided into experimental and control groups.

Animals in the treatment groups (N=5 each) received two constant doses of sBCMA-Fc V3, at 5 mg/kg or 10 mg/kg, every 48 hours for a study duration of 28 days; while animals in the control group (N=5) received vehicle control at the same schedule. Subcutaneous tumour volume measurements were collected at different time points throughout the study to assess *in vivo* tumour growth.

In the SU-DHL-6 DLBCL model, results showed a significant inhibition of tumour initiation for mice in the treatment group. Furthermore, we observed a dose-response relationship indicated by the superior therapeutic efficacy achieved by the higher dose of sBCMA-Fc V3 at 10 mg/kg compared to the lower dose at 5 mg/kg (Figure 4.11 A).

A

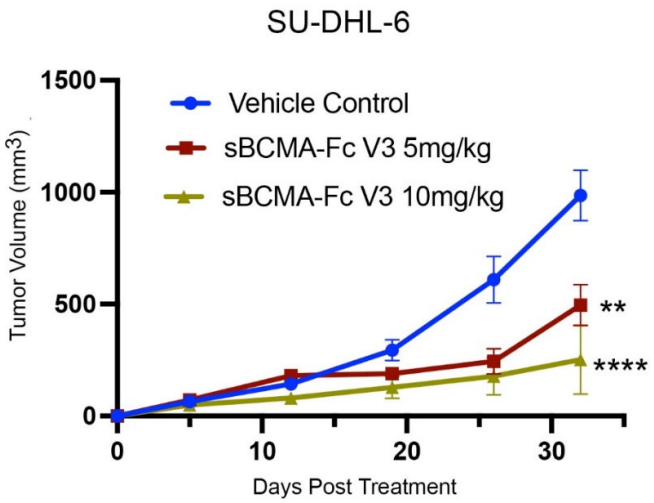

B

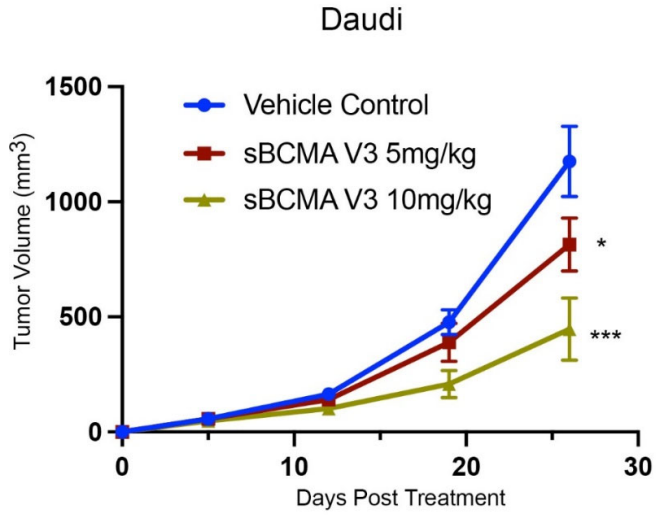

Figure 4.11. sBCMA-Fc V3 treatment effectively inhibits DLBCL tumour growth *in vivo* in a dose-dependent manner

(A) *In vivo* growth of SU-DHL-6 DLBCL tumours in 6-week-old female NSG mice dosed with sBCMA-Fc V3 at 5 or 10 mg/kg, or vehicle control, every 48 hours for 28 days; N = 5 for each group, $P < 0.0001$ compared to Vehicle Control.
(B) *In vivo* growth of Daudi DLBCL tumours in 6-week-old female NSG mice dosed with sBCMA-Fc V3 at 5 or 10 mg/kg, or vehicle control, every 48 hours for 28 days; N = 5 for each group, $P = 0.001$ compared to Vehicle Control.

This study was performed in collaboration with Dr. Yu Rebecca Miao at Stanford University Department of Radiation Oncology.

We next repeated the study with the Daudi DLBCL cell line. As expected, in the Daudi DLBCL model, results also showed a significant inhibition of tumour growth for mice in the treatment group. Again, we observed a dose-response relationship indicated by the superior therapeutic efficacy achieved by the higher dose of sBCMA-Fc V3 at 10 mg/kg compared to the lower dose at 5 mg/kg (Figure 4.11 B).

4.2.8 sBCMA-Fc V3 out-performs sTACI-Fc and anti-BAFF mAB *in vivo*

To determine whether enhanced binding affinities would result in improved therapeutic efficacy *in vivo*, we compared the sBCMA-Fc V3 against alternative inhibitors of BAFF, including a wild-type soluble TACI-Fc fusion protein that binds to APRIL at an affinity of ~6.4 nM and BAFF at an affinity of ~160 pM[190], and an anti-BAFF mAB that binds to BAFF at an affinity of ~0.995 nM and no reported binding to APRIL[229].

In a head-to-head comparison study, we established four experimental groups, treated with the wild-type sBCMA-Fc, engineered sBCMA-Fc V3, wild-type sTACI-Fc, and anti-BAFF mAB, respectively. We applied the same dose of 10 mg/kg for all treatment groups; and treatment schedule of 3 times per week for Fc fusion proteins, and 2 times per week for the anti-BAFF mAB, since mABs typically have a longer half-life based on published half-life data, for a treatment duration of 28 days. Subcutaneous tumour volume was measured at different time points throughout the study to assess *in vivo* tumour growth for all groups.

Results showed that sBCMA-Fc V3 treatment delivered superior therapeutic benefit compared to control and the rest of the treatment groups, as demonstrated by significant tumour initiation inhibition. Consistent with our previous experimental results, treatment with the wild-type sBCMA did not result in visible tumour growth differences compared to vehicle control. Similarly, treatment with the sTACI-Fc resulted in only marginal and insignificant tumour growth delay compared to control, this could be due to wild-type TACI's stronger binding toward BAFF, reported at approximately 0.16 nM, compared to that between wild-type BCMA and BAFF. Mice treated with the anti-BAFF mAB exhibited a statistically significant delay in tumour growth, which was superior to the other treatment groups, except for the sBCMA-Fc V3 treated group. This outcome is consistent with our hypothesis that effective

inhibition of BAFF is crucial for tumour inhibition in BAFF-dependent DLBCL, as the anti-BAFF mAB demonstrated a stronger binding affinity toward BAFF, surpassed only by the sBCMA-Fc V3 (Figure 4.12).

Statistical analysis throughout the study was conducted using t test and one-way ANOVA for comparing between treatment groups. Repeated ANOVA used for changes in tumour growth over time. *, $P < 0.05$; **, $P < 0.01$; ***, $P < 0.001$, ****, $P<0.0001$.

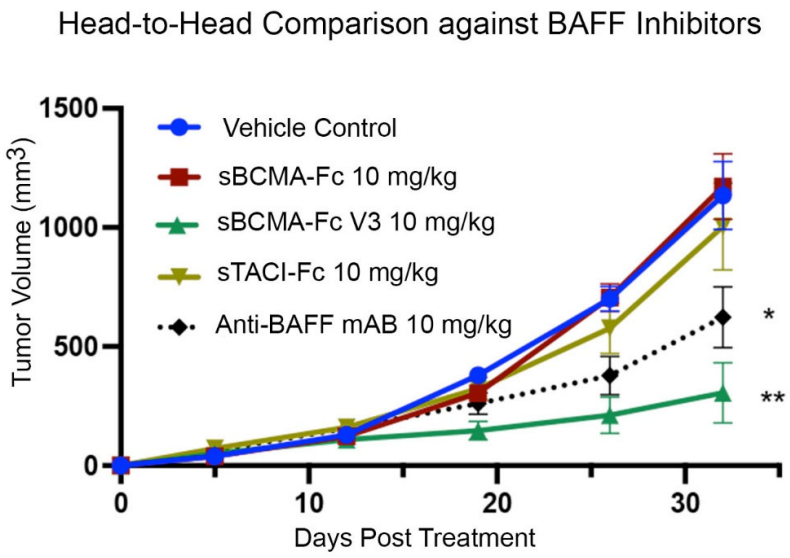

Figure 4.12. sBCMA-Fc V3 out-performs sTACI-Fc and anti-BAFF mAB in SU-DHL-6 DLBCL model
In vivo efficacy comparison study using subcutaneous SU-DHL-6 DLBCL mouse model treated with 10 mg/kg of wild-type sBCMA-Fc every 48 hours (N = 5), 10 mg/kg of sBCMA-Fc V3 every 48 hours (N = 5; $P < 0.0001$ compared to Vehicle Control), 10 mg/kg of sTACI-Fc every 48 hours (N = 5), and 10 mg/kg of αBAFF antibody twice a week (N = 5; $P = 0.01$ compared to Vehicle Control), for 28 days.

This study was performed in collaboration with Dr. Yu Rebecca Miao at Stanford University Department of Radiation Oncology.

4.3 Discussion

Based on previous literature, the wild-type BCMA receptor also binds to BAFF albeit at a much lower binding affinity compared to that toward APRIL[140]. As such, we tested the wild-type sBCMA-Fc fusion protein *in vitro* and *in vivo*, with BAFF-driven DLBCL cell lines of SU-DHL-6 and Daudi. *In vitro* cytotoxicity assay results indicated a hint of inhibitory effect on DLBCL tumour initiation; and a high dose of 100 ng/mL was needed to show a clearer albeit insignificant inhibitory effect. Similarly in the SU-DHL-6 xenograft *in vivo* model, the wild-type sBCMA-Fc did not show significantly differentiated tumour inhibition therapeutic effect. We believed that the apparent lack of efficacy was due to the weak binding affinity between BAFF and the wild-type sBCMA-Fc fusion protein, which is considerably weaker than the binding affinity between wild-type BAFFR and BAFF.

To overcome the affinity barrier between BAFF and the wild-type sBCMA-Fc, we developed an engineered fusion protein, sBCMA-Fc V3. The development process involved the use of a yeast surface display-based engineering technology, where random mutations were introduced into the ECD of the wild-type BCMA receptor in an unbiased manner. The resulting library of over 10 million mutant clones were selected based on binding affinities with target ligands. Subsequent analyses and characterization of the selected mutant sBCMA-Fc V3 indicated that a key mutation at H19Y contributed to the significantly enhanced binding affinities toward BAFF and APRIL. Previous study also reported H19Y as an important residue for binding between BAFF and BCMA[140]. However, our sBCMA-Fc V3 also showed improved binding toward APRIL. To further study the binding interactions, crystal structures of binding co-complexes will provide detailed biophysical evidence to explain the observed affinity enhancements.

In vitro DLBCL cell line studies with the engineered sBCMA-Fc V3 treatment showed significantly enhanced tumour growth reduction and inhibition of key pro-survival downstream pathways. Subsequent preliminary pharmacokinetic and pharmacodynamic investigations demonstrated that sBCMA-Fc V3 was capable of effectively suppressing target ligands BAFF and APRIL, and treatment resulted in the reduction of immunoglobulins and normal plasma cells. Furthermore, we analysed the pharmacokinetic profile of the sBCMA-Fc V3 by measuring serum drug levels over time to assess the molecule's half-life *in vivo*.

We next tested the sBCMA-Fc V3 in xenograft mouse models with SU-DHL-6 and Daudi DLBCL cell lines. Results were in line with our expectation that enhanced binding affinity toward BAFF significantly improved the molecule's therapeutic efficacy compared to the earlier study with the wild-type sBCMA-Fc. To conclude the study, we tested the sBCMA-Fc V3 in a head-to-head study against alternative treatment options targeting BAFF, including a wild-type sTACI-Fc fusion protein, and an anti-BAFF mAB. Results were consistent with our hypothesis that sBCMA-Fc V3's superior binding affinity toward BAFF led to superior efficacy compared to the rest of the groups.

Although the sBCMA-Fc V3 demonstrated sufficient safety in mouse and non-human primate models[181], we have not yet investigated the safety profile of the molecule in repeat-dosing experiments with primates. Previous clinical trials with sTACI and anti-BAFF mAB reported lymphopenia as a common treatment-related adverse effect. As evidenced by the reduction of normal plasma cells in our mouse study, we expect that repeated treatment with the sBCMA-Fc V3 will result in lymphopenia although reversible. Furthermore, additional investigations are warranted to determine the potential development of treatment resistance in a repeat dosing-setting. To prepare the molecule for clinical investigations, further studies to investigate the pharmacokinetic,

pharmacodynamic, and toxicology profiles of the sBCMA-Fc V3 in primates will be needed to fully characterize the molecule for clinical studies. Also, the sBCMA-Fc V3 will need to be further optimized for enhanced yield and purity to be used in clinical trials.

CHAPTER 5 GENERAL DISCUSSION

5.1 BAFF and APRIL play a critical role in B-cell malignancies

Cytokines BAFF and APRIL are important regulators of B-cell survival, differentiation, and maturation. The aberrant up-regulation of BAFF and APRIL leads to dysregulated B-cell proliferation and is thus considered a potential driving factor of B-cell malignancies[211, 230, 231]. BAFF and APRIL effect their biological functions via activation of cognate receptors BAFFR, BCMA and TACI. Previous research has consistently demonstrated that aberrant BAFF and APRIL-mediated receptor activation facilitates the progression and treatment resistance of NHL and MM. In MM, upregulation of BCMA signalling via primary ligand APRIL activates key pro-tumour pathways such as the canonical NF-κB and MAPK, which facilitate tumour progression and up-regulate important pro-tumour molecules in the microenvironment. In addition, BCMA signalling induces immune suppressive genes, such as IL-10, PD-L1 and TGF-β[177, 202]. Similarly, BAFF / BAFFR signalling plays a critical role in the progression of DLBCL. Aberrant BAFF-mediated BAFFR signalling up-regulates the alternative NF-κB pathway and leads to malignant B-cells' abnormal growth and resistance to treatment[199]. TACI, in the context of B-cell malignancies, were found to contribute to an immune-suppressive microenvironment via the regulation of Tregs and Bregs[191].

Given the important roles APRIL and BAFF play in B-cell malignancies, both ligands have garnered significant research interests recently and have become attractive therapeutic targets. However, the multifaceted interactions involving BAFF, APRIL, and their receptors represent a significant challenge for the development of therapeutic inhibitors. As a result, there is an urgent unmet clinical need for a safe and efficacious

approach targeting BAFF and APRIL for the treatment of B-cell malignancies such as MM and DLBCL.

5.2 Urgent need for safe and efficacious therapeutics for MM and DLBCL patients

B-cell malignancies, in particular MM and DLBCL, represent one of the most common types of cancers globally. Despite recent therapeutic advancements, both MM and DLBCL remain incurable, as 100% of MM patients experience treatment relapse and eventually succumb to the disease, and nearly half of DLBCL patients relapse after initial treatment. Current SOC therapeutic regimens for both diseases primarily involve the use of chemo-cytotoxic drugs in combination with certain recently approved targeted therapies. For MM patients, regimens containing proteasome inhibitors and immune modulatory agents, such as bortezomib and lenalidomide, in combination with anti-CD38 mABs are typically used as a front-line therapy. For DLBCL patients, R-CHOP, which consists of rituximab, an anti-CD20 mAB, and chemotherapy agents, are typically used as first-line treatment. Recent approvals of novel agents, most notably CAR T-cell therapies, such as Abecma, a BCMA-targeting CAR T for MM, and Kymirah, a CD-19-targeting CAR T for DLBCL, have meaningfully improved overall patient outcomes. However, due to the drug-related toxicities of CAR T-cell therapies such as cytokine release syndrome, a significant portion of patients in poor health conditions are ineligible for CAR T treatments. Therefore, safe and effective novel therapeutics are needed for patients who have exhausted currently approved and investigational agents.

Recognizing the importance of BAFF and APRIL as a driver of B-cell malignancies, we hypothesized that pharmacologically targeting BAFF and APRIL could be a viable strategy for the treatment of MM and DLBCL. In this study we adopted a ligand trap approach and developed two generations of Fc fusion proteins based on the ECD of the receptor BCMA, initially with the wild-type soluble BCMA and subsequently with an engineered soluble BCMA mutant with enhanced binding affinities toward APRIL and

BAFF to overcome wild-type affinity barriers. Our results showed that such strategy could be a safe and efficacious approach for the treatment of MM and DLBCL.

5.3 Wild-type sBCMA-Fc effectively inhibits MM development with minimal normal tissue toxicities

To test our hypothesis that inhibition of APRIL-mediated activation of BCMA would inhibit MM tumour growth, we began with genetic knockdown studies targeting BCMA. In both transient siRNA and stable dox-induced shRNA BCMA knockdown studies, we demonstrated inhibition of downstream pro-tumour survival signalling as well as *in vitro* and *in vivo* inhibition of tumour development upon BCMA signalling inhibition. We next proceeded to develop a Fc fusion protein with the wild-type sBCMA ECD and demonstrated the molecule's potency at suppressing APRIL and BAFF while resulting in minimal toxicities *in vivo*. Furthermore, our results showed that the sBCMA-Fc was effective at inhibiting tumour growth *in vivo*, most notably in a PDX MM model that we developed.

Overall, our study results with the wild-type sBCMA-Fc fusion protein demonstrated that ligand neutralization targeting APRIL and BAFF is a feasible approach to treat MM. Previous attempts to therapeutically inhibit BCMA signalling utilized monoclonal antibodies against BCMA or APRIL; or wild-type soluble TACI to trap APRIL and BAFF. However, due to the strong wild-type binding affinity between APRIL and BCMA, neither approach showed promising results in the clinic.

Although our initial results showed therapeutic promises of the sBCMA-Fc in MM, further studies are warranted to validate the mechanism of action of the molecule. For example, pre-treatment shed soluble BCMA in serum should be measured to determine its impact on the efficacy of the sBCMA-Fc, since late-stage r/r MM patients tend to have high levels of shed soluble BCMA in circulation. Furthermore, given the recent regulatory approvals of BCMA-targeting CAR T-cell therapies, it would be interesting to study the effect of combining such CAR T-cell therapies with the sBCMA-Fc since

the fusion protein may bind to the BCMA-targeting CAR T-cells and result in a drop of efficacy for both agents.

5.4 Inhibition of APRIL and BAFF with engineered mutant sBCMA-Fc V3 reduces DLBCL tumour growth

In BAFF-driven DLBCL tumour models, the wild-type sBCMA-Fc fusion protein failed to show significant anti-tumour activities. To test the hypothesis that this lack of efficacy was caused by the weak binding affinity between wild-type BCMA and BAFF compared to the stronger binding between wild-type BAFFR and BAFF, we developed an engineered sBCMA-Fc V3 fusion protein with significantly enhanced binding affinities toward BAFF and APRIL. The sBCMA-Fc V3 showed potent suppression of BAFF and APRIL, and reduced immunoglobulins and normal plasma cells *in vivo*. In DLBCL mouse models, the sBCMA-Fc V3 showed significantly enhanced therapeutic efficacy compared to the wild-type sBCMA-Fc, supporting our hypothesis that enhanced binding toward BAFF would lead to an improvement in efficacy. Furthermore, in a head-to-head comparison study, the sBCMA-Fc V3 outperformed a sTACI-Fc fusion protein and an anti-BAFF mAB.

In summary, the sBCMA-Fc V3 fusion protein overcame the weakness in binding affinity between wild-type BCMA and BAFF and showed improved efficacy results in DLBCL mouse models. Although the molecule showed satisfactory safety profile in mouse and non-human primate models, repeat-dose studies should be conducted to further assess the molecule's safety as our results showed a reduction of normal plasma cells and previous clinical studies with sTACI fusion proteins reported lymphopenia as a side effect. Similarly, it would be interesting to assess if treatment resistance develops in DLBCL or MM models in a repeat-dose setting.

5.5 Future direction for the translational development of the sBCMA-Fc V3

The sBCMA-Fc V3, with enhanced targeting toward ligands BAFF and APRIL, represents a novel, safe and efficacious approach for the treatment of B-cell malignancies. Although novel treatments such as CAR T-cell therapy have achieved impressive success, treatment-related toxicities remain a significant barrier for patients in poor health conditions. As such, the sBCMA-Fc V3 is well-positioned to address this unmet patient need.

Results of our study showed the impact of the sBCMA-Fc V3 on immunoglobulin class switch, leading to a reduction of IgA levels in serum. Furthermore, the sBCMA-Fc V3 was found to be effective at reducing the level of normal plasma cells *in vivo*. Taken together, these data indicate that in addition to B-cell malignancies, the sBCMA-Fc V3 could be a novel candidate for the treatment of autoimmune diseases such as systemic lupus erythematosus (SLE), and rare autoimmune diseases such as IgA nephropathy – both of which are driven by pathological B-cells.

To prepare the sBCMA-Fc V3 for clinical studies, additional investigations focusing on the molecule's pharmacokinetic, pharmacodynamic and toxicology profiles in non-human primates are warranted. In addition, repeat-dosing studies with primates will help us determine the optimal dose and formulation (subcutaneous or intravenous) for human trials in the clinic. Finally, the sBCMA-Fc V3 will need to be further optimized for important parameters including production yield, purity and formulation stability to prepare for patient trials.

REFERENCES

1. Thandra, K.C., et al., *Epidemiology of Non-Hodgkin's Lymphoma.* Med Sci (Basel), 2021. **9**(1).
2. Li, S., K.H. Young, and L.J. Medeiros, *Diffuse large B-cell lymphoma.* Pathology, 2018. **50**(1): p. 74-87.
3. Chavez, J.C., C. Bachmeier, and M.A. Kharfan-Dabaja, *CAR T-cell therapy for B-cell lymphomas: clinical trial results of available products.* Ther Adv Hematol, 2019. **10**: p. 2040620719841581.
4. Tai, Y.T. and K.C. Anderson, *Targeting B-cell maturation antigen in multiple myeloma.* Immunotherapy, 2015. **7**(11): p. 1187-99.
5. Cho, S.F., et al., *BCMA-Targeting Therapy: Driving a New Era of Immunotherapy in Multiple Myeloma.* Cancers (Basel), 2020. **12**(6).
6. Petrucci, M.T. and F. Vozella, *The Anti-CD38 Antibody Therapy in Multiple Myeloma.* Cells, 2019. **8**(12).
7. Cerrato, C., R. Mina, and A. Palumbo, *Optimal management of elderly patients with myeloma.* Expert Rev Anticancer Ther, 2014. **14**(2): p. 217-28.
8. Kazandjian, D., *Multiple myeloma epidemiology and survival: A unique malignancy.* Semin Oncol, 2016. **43**(6): p. 676-681.
9. Hengeveld, P.J. and M.J. Kersten, *B-cell activating factor in the pathophysiology of multiple myeloma: a target for therapy?* Blood Cancer J, 2015. **5**: p. e282.
10. Sidana, S. and N. Shah, *CAR T-cell therapy: is it prime time in myeloma?* Blood Adv, 2019. **3**(21): p. 3473-3480.
11. Varga, C., et al., *Investigational agents in immunotherapy: a new horizon for the treatment of multiple myeloma.* British Journal of Haematology, 2018. **181**(4): p. 433-446.
12. Joshua, D.E., et al., *Biology and therapy of multiple myeloma.* Med J Aust, 2019. **210**(8): p. 375-380.
13. Landgren, O., et al., *Monoclonal gammopathy of undetermined significance (MGUS) consistently precedes multiple myeloma: a prospective study.* Blood, 2009. **113**(22): p. 5412-7.
14. Weiss, B.M., et al., *A monoclonal gammopathy precedes multiple myeloma in most patients.* Blood, 2009. **113**(22): p. 5418-22.
15. Kyle, R.A., et al., *Clinical course and prognosis of smoldering (asymptomatic) multiple myeloma.* N Engl J Med, 2007. **356**(25): p. 2582-90.
16. Rajkumar, S.V., *Multiple myeloma: 2022 update on diagnosis, risk stratification, and management.* Am J Hematol, 2022. **97**(8): p. 1086-1107.
17. Kyle, R.A., et al., *A long-term study of prognosis in monoclonal gammopathy of undetermined significance.* N Engl J Med, 2002. **346**(8): p. 564-9.
18. Rajkumar, S.V., et al., *Impact of primary molecular cytogenetic abnormalities and risk of progression in smoldering multiple myeloma.* Leukemia, 2013. **27**(8): p. 1738-44.
19. Neben, K., et al., *Progression in smoldering myeloma is independently determined by the chromosomal abnormalities del(17p), t(4;14), gain 1q, hyperdiploidy, and tumor load.* J Clin Oncol, 2013. **31**(34): p. 4325-32.
20. Rajkumar, S.V., *Multiple myeloma: Every year a new standard?* Hematol Oncol, 2019. **37 Suppl 1**(Suppl 1): p. 62-65.
21. Gulla, A. and K.C. Anderson, *Multiple myeloma: the (r)evolution of current therapy and a glance into future.* Haematologica, 2020. **105**(10): p. 2358-2367.
22. Medical Masterclass, c. and J. Firth, *Haematology: multiple myeloma.* Clin Med (Lond), 2019. **19**(1): p. 58-60.

23. Hillengass, J., et al., *International myeloma working group consensus recommendations on imaging in monoclonal plasma cell disorders.* Lancet Oncol, 2019. **20**(6): p. e302-e312.
24. Kumar, S.K. and S.V. Rajkumar, *The multiple myelomas - current concepts in cytogenetic classification and therapy.* Nat Rev Clin Oncol, 2018. **15**(7): p. 409-421.
25. Kuehl, W.M. and P.L. Bergsagel, *Multiple myeloma: evolving genetic events and host interactions.* Nat Rev Cancer, 2002. **2**(3): p. 175-87.
26. Bergsagel, P.L. and W.M. Kuehl, *Chromosome translocations in multiple myeloma.* Oncogene, 2001. **20**(40): p. 5611-22.
27. Fonseca, R., et al., *Genomic abnormalities in monoclonal gammopathy of undetermined significance.* Blood, 2002. **100**(4): p. 1417-24.
28. Seidl, S., H. Kaufmann, and J. Drach, *New insights into the pathophysiology of multiple myeloma.* Lancet Oncol, 2003. **4**(9): p. 557-64.
29. Miller, A., et al., *High somatic mutation and neoantigen burden are correlated with decreased progression-free survival in multiple myeloma.* Blood Cancer J, 2017. **7**(9): p. e612.
30. Russell, S.J. and S.V. Rajkumar, *Multiple myeloma and the road to personalised medicine.* Lancet Oncol, 2011. **12**(7): p. 617-9.
31. Kumar, S.K., et al., *Management of newly diagnosed symptomatic multiple myeloma: updated Mayo Stratification of Myeloma and Risk-Adapted Therapy (mSMART) consensus guidelines.* Mayo Clin Proc, 2009. **84**(12): p. 1095-110.
32. Kumar, S., et al., *Trisomies in multiple myeloma: impact on survival in patients with high-risk cytogenetics.* Blood, 2012. **119**(9): p. 2100-5.
33. Wang, L., L.R. Li, and K.H. Young, *New agents and regimens for diffuse large B cell lymphoma.* J Hematol Oncol, 2020. **13**(1): p. 175.
34. Kanas, G., et al., *Epidemiology of diffuse large B-cell lymphoma (DLBCL) and follicular lymphoma (FL) in the United States and Western Europe: population-level projections for 2020-2025.* Leuk Lymphoma, 2022. **63**(1): p. 54-63.
35. He, M.Y. and R. Kridel, *Treatment resistance in diffuse large B-cell lymphoma.* Leukemia, 2021. **35**(8): p. 2151-2165.
36. Caimi, P.F., et al., *Clinical approach to diffuse large B cell lymphoma.* Blood Rev, 2016. **30**(6): p. 477-491.
37. Harris, L.J., K. Patel, and M. Martin, *Novel Therapies for Relapsed or Refractory Diffuse Large B-Cell Lymphoma.* Int J Mol Sci, 2020. **21**(22).
38. Crombie, J.L. and P. Armand, *Diffuse Large B-Cell Lymphoma's New Genomics: The Bridge and the Chasm.* J Clin Oncol, 2020. **38**(30): p. 3565-3574.
39. Ennishi, D., et al., *Toward a New Molecular Taxonomy of Diffuse Large B-cell Lymphoma.* Cancer Discov, 2020. **10**(9): p. 1267-1281.
40. Crombie, J.L. and P. Armand, *Diffuse Large B-Cell Lymphoma and High-Grade B-Cell Lymphoma: Genetic Classification and Its Implications for Prognosis and Treatment.* Hematol Oncol Clin North Am, 2019. **33**(4): p. 575-585.
41. Mondello, P. and M. Mian, *Frontline treatment of diffuse large B-cell lymphoma: Beyond R-CHOP.* Hematol Oncol, 2019. **37**(4): p. 333-344.
42. MacLennan, I.C., *Germinal centers.* Annu Rev Immunol, 1994. **12**: p. 117-39.
43. Alizadeh, A.A., et al., *Distinct types of diffuse large B-cell lymphoma identified by gene expression profiling.* Nature, 2000. **403**(6769): p. 503-11.

44. Victora, G.D., et al., *Identification of human germinal center light and dark zone cells and their relationship to human B-cell lymphomas.* Blood, 2012. **120**(11): p. 2240-8.
45. Lenz, G., et al., *Molecular subtypes of diffuse large B-cell lymphoma arise by distinct genetic pathways.* Proc Natl Acad Sci U S A, 2008. **105**(36): p. 13520-5.
46. Young, R.M., et al., *B-cell receptor signaling in diffuse large B-cell lymphoma.* Semin Hematol, 2015. **52**(2): p. 77-85.
47. Shaffer, A.L., 3rd, R.M. Young, and L.M. Staudt, *Pathogenesis of human B cell lymphomas.* Annu Rev Immunol, 2012. **30**: p. 565-610.
48. Scott, D.W., et al., *High-grade B-cell lymphoma with MYC and BCL2 and/or BCL6 rearrangements with diffuse large B-cell lymphoma morphology.* Blood, 2018. **131**(18): p. 2060-2064.
49. Ennishi, D., et al., *Genetic profiling of MYC and BCL2 in diffuse large B-cell lymphoma determines cell-of-origin-specific clinical impact.* Blood, 2017. **129**(20): p. 2760-2770.
50. Iqbal, J., et al., *BCL2 predicts survival in germinal center B-cell-like diffuse large B-cell lymphoma treated with CHOP-like therapy and rituximab.* Clin Cancer Res, 2011. **17**(24): p. 7785-95.
51. Visco, C., et al., *Patients with diffuse large B-cell lymphoma of germinal center origin with BCL2 translocations have poor outcome, irrespective of MYC status: a report from an International DLBCL rituximab-CHOP Consortium Program Study.* Haematologica, 2013. **98**(2): p. 255-63.
52. Chapuy, B., et al., *Molecular subtypes of diffuse large B cell lymphoma are associated with distinct pathogenic mechanisms and outcomes.* Nat Med, 2018. **24**(5): p. 679-690.
53. Schmitz, R., et al., *Genetics and Pathogenesis of Diffuse Large B-Cell Lymphoma.* N Engl J Med, 2018. **378**(15): p. 1396-1407.
54. Lacy, S.E., et al., *Targeted sequencing in DLBCL, molecular subtypes, and outcomes: a Haematological Malignancy Research Network report.* Blood, 2020. **135**(20): p. 1759-1771.
55. Sarkozy, C., A. Traverse-Glehen, and B. Coiffier, *Double-hit and double-protein-expression lymphomas: aggressive and refractory lymphomas.* Lancet Oncol, 2015. **16**(15): p. e555-e567.
56. Johnson, N.A., et al., *Concurrent expression of MYC and BCL2 in diffuse large B-cell lymphoma treated with rituximab plus cyclophosphamide, doxorubicin, vincristine, and prednisone.* J Clin Oncol, 2012. **30**(28): p. 3452-9.
57. Horn, H., et al., *MYC status in concert with BCL2 and BCL6 expression predicts outcome in diffuse large B-cell lymphoma.* Blood, 2013. **121**(12): p. 2253-63.
58. Hu, S., et al., *MYC/BCL2 protein coexpression contributes to the inferior survival of activated B-cell subtype of diffuse large B-cell lymphoma and demonstrates high-risk gene expression signatures: a report from The International DLBCL Rituximab-CHOP Consortium Program.* Blood, 2013. **121**(20): p. 4021-31; quiz 4250.
59. Herrera, A.F., et al., *Relapsed or Refractory Double-Expressor and Double-Hit Lymphomas Have Inferior Progression-Free Survival After Autologous Stem-Cell Transplantation.* J Clin Oncol, 2017. **35**(1): p. 24-31.
60. Miura, K., et al., *Clinical significance of co-expression of MYC and BCL2 protein in aggressive B-cell lymphomas treated with a second line immunochemotherapy.* Leuk Lymphoma, 2016. **57**(6): p. 1335-41.

61. Vrabel, D., L. Pour, and S. Sevcikova, *The impact of NF-kappaB signaling on pathogenesis and current treatment strategies in multiple myeloma.* Blood Rev, 2019. **34**: p. 56-66.
62. Myung, J., K.B. Kim, and C.M. Crews, *The ubiquitin-proteasome pathway and proteasome inhibitors.* Med Res Rev, 2001. **21**(4): p. 245-73.
63. Kubiczkova, L., et al., *Proteasome inhibitors - molecular basis and current perspectives in multiple myeloma.* J Cell Mol Med, 2014. **18**(6): p. 947-61.
64. Finley, D., *Recognition and processing of ubiquitin-protein conjugates by the proteasome.* Annu Rev Biochem, 2009. **78**: p. 477-513.
65. Glickman, M.H. and A. Ciechanover, *The ubiquitin-proteasome proteolytic pathway: destruction for the sake of construction.* Physiol Rev, 2002. **82**(2): p. 373-428.
66. Vigneron, N. and B.J. Van den Eynde, *Proteasome subtypes and regulators in the processing of antigenic peptides presented by class I molecules of the major histocompatibility complex.* Biomolecules, 2014. **4**(4): p. 994-1025.
67. Obeng, E.A., et al., *Proteasome inhibitors induce a terminal unfolded protein response in multiple myeloma cells.* Blood, 2006. **107**(12): p. 4907-16.
68. Rastogi, N. and D.P. Mishra, *Therapeutic targeting of cancer cell cycle using proteasome inhibitors.* Cell Div, 2012. **7**(1): p. 26.
69. Ri, M., *Endoplasmic-reticulum stress pathway-associated mechanisms of action of proteasome inhibitors in multiple myeloma.* Int J Hematol, 2016. **104**(3): p. 273-80.
70. Meister, S., et al., *Extensive immunoglobulin production sensitizes myeloma cells for proteasome inhibition.* Cancer Res, 2007. **67**(4): p. 1783-92.
71. Kumar, S., et al., *Expression of VEGF and its receptors by myeloma cells.* Leukemia, 2003. **17**(10): p. 2025-31.
72. Li, Z.W., et al., *NF-kappaB in the pathogenesis and treatment of multiple myeloma.* Curr Opin Hematol, 2008. **15**(4): p. 391-9.
73. Moreaux, J., et al., *BAFF and APRIL protect myeloma cells from apoptosis induced by interleukin 6 deprivation and dexamethasone.* Blood, 2004. **103**(8): p. 3148-57.
74. Terpos, E., et al., *Mechanisms of bone destruction in multiple myeloma.* Eur J Cancer Care (Engl), 2017. **26**(6).
75. Bergsagel, P.L., et al., *Cyclin D dysregulation: an early and unifying pathogenic event in multiple myeloma.* Blood, 2005. **106**(1): p. 296-303.
76. Sewify, E.M., et al., *Cyclin D1 amplification in multiple myeloma is associated with multidrug resistance expression.* Clin Lymphoma Myeloma Leuk, 2014. **14**(3): p. 215-22.
77. Giuliani, N., et al., *Proangiogenic properties of human myeloma cells: production of angiopoietin-1 and its potential relationship to myeloma-induced angiogenesis.* Blood, 2003. **102**(2): p. 638-45.
78. Hideshima, T., et al., *NF-kappa B as a therapeutic target in multiple myeloma.* J Biol Chem, 2002. **277**(19): p. 16639-47.
79. van de Donk, N. and S.Z. Usmani, *CD38 Antibodies in Multiple Myeloma: Mechanisms of Action and Modes of Resistance.* Front Immunol, 2018. **9**: p. 2134.
80. van de Donk, N.W., et al., *Monoclonal antibodies targeting CD38 in hematological malignancies and beyond.* Immunol Rev, 2016. **270**(1): p. 95-112.
81. Cho, S.F., et al., *Promising Antigens for the New Frontier of Targeted Immunotherapy in Multiple Myeloma.* Cancers (Basel), 2021. **13**(23).

82. Karakasheva, T.A., et al., *CD38-Expressing Myeloid-Derived Suppressor Cells Promote Tumor Growth in a Murine Model of Esophageal Cancer.* Cancer Res, 2015. **75**(19): p. 4074-85.
83. Deaglio, S., K. Mehta, and F. Malavasi, *Human CD38: a (r)evolutionary story of enzymes and receptors.* Leuk Res, 2001. **25**(1): p. 1-12.
84. Mellor, J.D., et al., *A critical review of the role of Fc gamma receptor polymorphisms in the response to monoclonal antibodies in cancer.* J Hematol Oncol, 2013. **6**: p. 1.
85. Taylor, R.P. and M.A. Lindorfer, *Cytotoxic mechanisms of immunotherapy: Harnessing complement in the action of anti-tumor monoclonal antibodies.* Semin Immunol, 2016. **28**(3): p. 309-16.
86. Overdijk, M.B., et al., *Antibody-mediated phagocytosis contributes to the anti-tumor activity of the therapeutic antibody daratumumab in lymphoma and multiple myeloma.* MAbs, 2015. **7**(2): p. 311-21.
87. Jiang, H., et al., *SAR650984 directly induces multiple myeloma cell death via lysosomal-associated and apoptotic pathways, which is further enhanced by pomalidomide.* Leukemia, 2016. **30**(2): p. 399-408.
88. Kumar, S.K., et al., *Risk of progression and survival in multiple myeloma relapsing after therapy with IMiDs and bortezomib: a multicenter international myeloma working group study.* Leukemia, 2012. **26**(1): p. 149-57.
89. Pineda-Roman, M., et al., *VTD combination therapy with bortezomib-thalidomide-dexamethasone is highly effective in advanced and refractory multiple myeloma.* Leukemia, 2008. **22**(7): p. 1419-27.
90. Richardson, P.G., et al., *Multicenter, phase I, dose-escalation trial of lenalidomide plus bortezomib for relapsed and relapsed/refractory multiple myeloma.* J Clin Oncol, 2009. **27**(34): p. 5713-9.
91. Rajkumar, S.V. and R.A. Kyle, *Progress in Myeloma - A Monoclonal Breakthrough.* N Engl J Med, 2016. **375**(14): p. 1390-1392.
92. Kumar, S.K., et al., *Clinical course of patients with relapsed multiple myeloma.* Mayo Clin Proc, 2004. **79**(7): p. 867-74.
93. Dimopoulos, M.A., et al., *Carfilzomib and dexamethasone versus bortezomib and dexamethasone for patients with relapsed or refractory multiple myeloma (ENDEAVOR): a randomised, phase 3, open-label, multicentre study.* Lancet Oncol, 2016. **17**(1): p. 27-38.
94. Kumar, S.K., et al., *Safety and tolerability of ixazomib, an oral proteasome inhibitor, in combination with lenalidomide and dexamethasone in patients with previously untreated multiple myeloma: an open-label phase 1/2 study.* Lancet Oncol, 2014. **15**(13): p. 1503-1512.
95. Moreau, P., et al., *Oral Ixazomib, Lenalidomide, and Dexamethasone for Multiple Myeloma.* N Engl J Med, 2016. **374**(17): p. 1621-34.
96. Lonial, S., et al., *Elotuzumab Therapy for Relapsed or Refractory Multiple Myeloma.* N Engl J Med, 2015. **373**(7): p. 621-31.
97. Moreau, P., et al., *Isatuximab, carfilzomib, and dexamethasone in relapsed multiple myeloma (IKEMA): a multicentre, open-label, randomised phase 3 trial.* Lancet, 2021. **397**(10292): p. 2361-2371.
98. Lin, Q., et al., *Recent updates on CAR T clinical trials for multiple myeloma.* Mol Cancer, 2019. **18**(1): p. 154.
99. Berdeja, J.G., et al., *Ciltacabtagene autoleucel, a B-cell maturation antigen-directed chimeric antigen receptor T-cell therapy in patients with relapsed or refractory multiple myeloma (CARTITUDE-1): a phase 1b/2 open-label study.* Lancet, 2021. **398**(10297): p. 314-324.

100. Neelapu, S.S., et al., *Chimeric antigen receptor T-cell therapy - assessment and management of toxicities.* Nat Rev Clin Oncol, 2018. **15**(1): p. 47-62.
101. Brudno, J.N. and J.N. Kochenderfer, *Toxicities of chimeric antigen receptor T cells: recognition and management.* Blood, 2016. **127**(26): p. 3321-30.
102. Lee, D.W., et al., *Current concepts in the diagnosis and management of cytokine release syndrome.* Blood, 2014. **124**(2): p. 188-95.
103. Munshi, N.C., et al., *Idecabtagene Vicleucel in Relapsed and Refractory Multiple Myeloma.* N Engl J Med, 2021. **384**(8): p. 705-716.
104. Chari, A., et al., *Oral Selinexor-Dexamethasone for Triple-Class Refractory Multiple Myeloma.* N Engl J Med, 2019. **381**(8): p. 727-738.
105. Bera, T.K., *Anti-BCMA Immunotoxins: Design, Production, and Preclinical Evaluation.* Biomolecules, 2020. **10**(10).
106. Salles, G., et al., *Rituximab in B-Cell Hematologic Malignancies: A Review of 20 Years of Clinical Experience.* Adv Ther, 2017. **34**(10): p. 2232-2273.
107. Coiffier, B., et al., *Long-term outcome of patients in the LNH-98.5 trial, the first randomized study comparing rituximab-CHOP to standard CHOP chemotherapy in DLBCL patients: a study by the Groupe d'Etudes des Lymphomes de l'Adulte.* Blood, 2010. **116**(12): p. 2040-5.
108. Crump, M., et al., *Outcomes in refractory diffuse large B-cell lymphoma: results from the international SCHOLAR-1 study.* Blood, 2017. **130**(16): p. 1800-1808.
109. Van Den Neste, E., et al., *Outcome of patients with relapsed diffuse large B-cell lymphoma who fail second-line salvage regimens in the International CORAL study.* Bone Marrow Transplant, 2016. **51**(1): p. 51-7.
110. Gisselbrecht, C., et al., *Salvage regimens with autologous transplantation for relapsed large B-cell lymphoma in the rituximab era.* J Clin Oncol, 2010. **28**(27): p. 4184-90.
111. Crump, M., et al., *Randomized comparison of gemcitabine, dexamethasone, and cisplatin versus dexamethasone, cytarabine, and cisplatin chemotherapy before autologous stem-cell transplantation for relapsed and refractory aggressive lymphomas: NCIC-CTG LY.12.* J Clin Oncol, 2014. **32**(31): p. 3490-6.
112. Gehlert, C.L., et al., *Dual Fc optimization to increase the cytotoxic activity of a CD19-targeting antibody.* Front Immunol, 2022. **13**: p. 957874.
113. Zinzani, P.L. and G. Minotti, *Anti-CD19 monoclonal antibodies for the treatment of relapsed or refractory B-cell malignancies: a narrative review with focus on diffuse large B-cell lymphoma.* J Cancer Res Clin Oncol, 2022. **148**(1): p. 177-190.
114. Katz, B.Z. and Y. Herishanu, *Therapeutic targeting of CD19 in hematological malignancies: past, present, future and beyond.* Leuk Lymphoma, 2014. **55**(5): p. 999-1006.
115. Poe, J.C., et al., *A c-Myc and surface CD19 signaling amplification loop promotes B cell lymphoma development and progression in mice.* J Immunol, 2012. **189**(5): p. 2318-25.
116. Uckun, F.M., et al., *Detailed studies on expression and function of CD19 surface determinant by using B43 monoclonal antibody and the clinical potential of anti-CD19 immunotoxins.* Blood, 1988. **71**(1): p. 13-29.
117. Anderson, K.C., et al., *Expression of human B cell-associated antigens on leukemias and lymphomas: a model of human B cell differentiation.* Blood, 1984. **63**(6): p. 1424-33.

118. Nadler, L.M., et al., *B4, a human B lymphocyte-associated antigen expressed on normal, mitogen-activated, and malignant B lymphocytes.* J Immunol, 1983. **131**(1): p. 244-50.
119. Zalevsky, J., et al., *The impact of Fc engineering on an anti-CD19 antibody: increased Fcgamma receptor affinity enhances B-cell clearing in nonhuman primates.* Blood, 2009. **113**(16): p. 3735-43.
120. Fujimoto, M., et al., *CD19 regulates B lymphocyte responses to transmembrane signals.* Semin Immunol, 1998. **10**(4): p. 267-77.
121. Bradbury, L.E., et al., *The CD19/CD21 signal transducing complex of human B lymphocytes includes the target of antiproliferative antibody-1 and Leu-13 molecules.* J Immunol, 1992. **149**(9): p. 2841-50.
122. Bradbury, L.E., V.S. Goldmacher, and T.F. Tedder, *The CD19 signal transduction complex of B lymphocytes. Deletion of the CD19 cytoplasmic domain alters signal transduction but not complex formation with TAPA-1 and Leu 13.* J Immunol, 1993. **151**(6): p. 2915-27.
123. Sato, S., et al., *Regulation of B lymphocyte development and activation by the CD19/CD21/CD81/Leu 13 complex requires the cytoplasmic domain of CD19.* J Immunol, 1997. **159**(7): p. 3278-87.
124. Engel, P., et al., *Abnormal B lymphocyte development, activation, and differentiation in mice that lack or overexpress the CD19 signal transduction molecule.* Immunity, 1995. **3**(1): p. 39-50.
125. Rickert, R.C., K. Rajewsky, and J. Roes, *Impairment of T-cell-dependent B-cell responses and B-1 cell development in CD19-deficient mice.* Nature, 1995. **376**(6538): p. 352-5.
126. Turtle, C.J., et al., *CD19 CAR-T cells of defined CD4+:CD8+ composition in adult B cell ALL patients.* J Clin Invest, 2016. **126**(6): p. 2123-38.
127. Neelapu, S.S., et al., *Axicabtagene Ciloleucel CAR T-Cell Therapy in Refractory Large B-Cell Lymphoma.* N Engl J Med, 2017. **377**(26): p. 2531-2544.
128. Sotillo, E., et al., *Convergence of Acquired Mutations and Alternative Splicing of CD19 Enables Resistance to CART-19 Immunotherapy.* Cancer Discov, 2015. **5**(12): p. 1282-95.
129. Orlando, E.J., et al., *Genetic mechanisms of target antigen loss in CAR19 therapy of acute lymphoblastic leukemia.* Nat Med, 2018. **24**(10): p. 1504-1506.
130. Hernandez, I., V. Prasad, and W.F. Gellad, *Accounting for All Costs in the Total Cost of Chimeric Antigen Receptor T-Cell Immunotherapy-Reply.* JAMA Oncol, 2018. **4**(12): p. 1785-1786.
131. Coyle, L., et al., *Open-Label, phase 2 study of blinatumomab as second salvage therapy in adults with relapsed/refractory aggressive B-cell non-Hodgkin lymphoma.* Leuk Lymphoma, 2020. **61**(9): p. 2103-2112.
132. Yang, S., J.Y. Li, and W. Xu, *Role of BAFF/BAFF-R axis in B-cell non-Hodgkin lymphoma.* Crit Rev Oncol Hematol, 2014. **91**(2): p. 113-22.
133. Qin, H., et al., *Novel BAFF-Receptor Antibody to Natively Folded Recombinant Protein Eliminates Drug-Resistant Human B-cell Malignancies In Vivo.* Clin Cancer Res, 2018. **24**(5): p. 1114-1123.
134. Smulski, C.R. and H. Eibel, *BAFF and BAFF-Receptor in B Cell Selection and Survival.* Front Immunol, 2018. **9**: p. 2285.
135. Chen, J., et al., *BAFF is involved in macrophage-induced bortezomib resistance in myeloma.* Cell Death Dis, 2017. **8**(11): p. e3161.
136. Kalled, S.L., C. Ambrose, and Y.M. Hsu, *The biochemistry and biology of BAFF, APRIL and their receptors.* Curr Dir Autoimmun, 2005. **8**: p. 206-42.

137. Mackay, F., et al., *BAFF AND APRIL: a tutorial on B cell survival.* Annu Rev Immunol, 2003. **21**: p. 231-64.
138. Mackay, F., P.A. Silveira, and R. Brink, *B cells and the BAFF/APRIL axis: fast-forward on autoimmunity and signaling.* Curr Opin Immunol, 2007. **19**(3): p. 327-36.
139. Mackay, F., et al., *The BAFF/APRIL system: an important player in systemic rheumatic diseases.* Curr Dir Autoimmun, 2005. **8**: p. 243-65.
140. Bossen, C. and P. Schneider, *BAFF, APRIL and their receptors: structure, function and signaling.* Semin Immunol, 2006. **18**(5): p. 263-75.
141. Gross, J.A., et al., *TACI-Ig neutralizes molecules critical for B cell development and autoimmune disease. impaired B cell maturation in mice lacking BLyS.* Immunity, 2001. **15**(2): p. 289-302.
142. Roschke, V., et al., *BLyS and APRIL form biologically active heterotrimers that are expressed in patients with systemic immune-based rheumatic diseases.* J Immunol, 2002. **169**(8): p. 4314-21.
143. Xu, S. and K.P. Lam, *Transmembrane Activator and CAML Interactor (TACI): Another Potential Target for Immunotherapy of Multiple Myeloma?* Cancers (Basel), 2020. **12**(4).
144. Gross, J.A., et al., *TACI and BCMA are receptors for a TNF homologue implicated in B-cell autoimmune disease.* Nature, 2000. **404**(6781): p. 995-9.
145. Liu, Y., et al., *Crystal structure of sTALL-1 reveals a virus-like assembly of TNF family ligands.* Cell, 2002. **108**(3): p. 383-94.
146. Zhukovsky, E.A., et al., *TNF ligands: is TALL-1 a trimer or a virus-like cluster?* Nature, 2004. **427**(6973): p. 413-4; discussion 414.
147. Bossen, C., et al., *Mutation of the BAFF furin cleavage site impairs B-cell homeostasis and antibody responses.* Eur J Immunol, 2011. **41**(3): p. 787-97.
148. Gavin, A.L., et al., *DeltaBAFF, an alternate splice isoform that regulates receptor binding and biopresentation of the B cell survival cytokine, BAFF.* J Biol Chem, 2003. **278**(40): p. 38220-8.
149. Gavin, A.L., et al., *deltaBAFF, a splice isoform of BAFF, opposes full-length BAFF activity in vivo in transgenic mouse models.* J Immunol, 2005. **175**(1): p. 319-28.
150. Dou, H., et al., *APRIL promotes non-small cell lung cancer growth and metastasis by targeting ERK1/2 signaling.* Oncotarget, 2017. **8**(65): p. 109289-109300.
151. Guadagnoli, M., et al., *Development and characterization of APRIL antagonistic monoclonal antibodies for treatment of B-cell lymphomas.* Blood, 2011. **117**(25): p. 6856-6865.
152. Pradet-Balade, B., et al., *An endogenous hybrid mRNA encodes TWE-PRIL, a functional cell surface TWEAK-APRIL fusion protein.* EMBO J, 2002. **21**(21): p. 5711-20.
153. Rickert, R.C., J. Jellusova, and A.V. Miletic, *Signaling by the tumor necrosis factor receptor superfamily in B-cell biology and disease.* Immunol Rev, 2011. **244**(1): p. 115-33.
154. Bossen, C., et al., *TACI, unlike BAFF-R, is solely activated by oligomeric BAFF and APRIL to support survival of activated B cells and plasmablasts.* Blood, 2008. **111**(3): p. 1004-12.
155. Zhang, Y., et al., *Effect of TACI signaling on humoral immunity and autoimmune diseases.* J Immunol Res, 2015. **2015**: p. 247426.
156. Thompson, J.S., et al., *BAFF-R, a newly identified TNF receptor that specifically interacts with BAFF.* Science, 2001. **293**(5537): p. 2108-11.

157. Pieper, K., et al., *A common single nucleotide polymorphism impairs B-cell activating factor receptor's multimerization, contributing to common variable immunodeficiency.* J Allergy Clin Immunol, 2014. **133**(4): p. 1222-5.
158. Meyer-Bahlburg, A., et al., *Characterization of a late transitional B cell population highly sensitive to BAFF-mediated homeostatic proliferation.* J Exp Med, 2008. **205**(1): p. 155-68.
159. Vincent, F.B., et al., *The BAFF/APRIL system: emerging functions beyond B cell biology and autoimmunity.* Cytokine Growth Factor Rev, 2013. **24**(3): p. 203-15.
160. O'Connor, B.P., et al., *BCMA is essential for the survival of long-lived bone marrow plasma cells.* J Exp Med, 2004. **199**(1): p. 91-8.
161. Muller-Winkler, J., et al., *Critical requirement for BCR, BAFF, and BAFFR in memory B cell survival.* J Exp Med, 2021. **218**(2).
162. Liu, Z. and A. Davidson, *BAFF and selection of autoreactive B cells.* Trends Immunol, 2011. **32**(8): p. 388-94.
163. Carrillo-Ballesteros, F.J., et al., *B-cell activating factor receptor expression is associated with germinal center B-cell maintenance.* Exp Ther Med, 2019. **17**(3): p. 2053-2060.
164. Mackay, F., et al., *B-cell stage and context-dependent requirements for survival signals from BAFF and the B-cell receptor.* Immunol Rev, 2010. **237**(1): p. 205-25.
165. Day, E.S., et al., *Selectivity of BAFF/BLyS and APRIL for binding to the TNF family receptors BAFFR/BR3 and BCMA.* Biochemistry, 2005. **44**(6): p. 1919-31.
166. Jost, P.J. and J. Ruland, *Aberrant NF-kappaB signaling in lymphoma: mechanisms, consequences, and therapeutic implications.* Blood, 2007. **109**(7): p. 2700-7.
167. Claudio, E., et al., *BAFF-induced NEMO-independent processing of NF-kappa B2 in maturing B cells.* Nat Immunol, 2002. **3**(10): p. 958-65.
168. Kampa, M., et al., *The TNFSF Members APRIL and BAFF and Their Receptors TACI, BCMA, and BAFFR in Oncology, With a Special Focus in Breast Cancer.* Front Oncol, 2020. **10**: p. 827.
169. Zhou, X., et al., *The Role of BAFF-R Signaling in the Growth of Primary Central Nervous System Lymphoma.* Front Oncol, 2020. **10**: p. 682.
170. Lentz, V.M., C.E. Hayes, and M.P. Cancro, *Bcmd decreases the life span of B-2 but not B-1 cells in A/WySnJ mice.* J Immunol, 1998. **160**(8): p. 3743-7.
171. Schiemann, B., et al., *An essential role for BAFF in the normal development of B cells through a BCMA-independent pathway.* Science, 2001. **293**(5537): p. 2111-4.
172. Sasaki, Y., et al., *TNF family member B cell-activating factor (BAFF) receptor-dependent and -independent roles for BAFF in B cell physiology.* J Immunol, 2004. **173**(4): p. 2245-52.
173. Warnatz, K., et al., *B-cell activating factor receptor deficiency is associated with an adult-onset antibody deficiency syndrome in humans.* Proc Natl Acad Sci U S A, 2009. **106**(33): p. 13945-50.
174. Xu, L.G. and H.B. Shu, *TNFR-associated factor-3 is associated with BAFF-R and negatively regulates BAFF-R-mediated NF-kappa B activation and IL-10 production.* J Immunol, 2002. **169**(12): p. 6883-9.
175. Ni, C.Z., et al., *Key molecular contacts promote recognition of the BAFF receptor by TNF receptor-associated factor 3: implications for intracellular signaling regulation.* J Immunol, 2004. **173**(12): p. 7394-400.

176. Marsters, S.A., et al., *Interaction of the TNF homologues BLyS and APRIL with the TNF receptor homologues BCMA and TACI.* Curr Biol, 2000. **10**(13): p. 785-8.
177. Tai, Y.T., et al., *APRIL and BCMA promote human multiple myeloma growth and immunosuppression in the bone marrow microenvironment.* Blood, 2016. **127**(25): p. 3225-36.
178. Avery, D.T., et al., *BAFF selectively enhances the survival of plasmablasts generated from human memory B cells.* J Clin Invest, 2003. **112**(2): p. 286-97.
179. Hymowitz, S.G., et al., *Structures of APRIL-receptor complexes: like BCMA, TACI employs only a single cysteine-rich domain for high affinity ligand binding.* J Biol Chem, 2005. **280**(8): p. 7218-27.
180. Yu, G., et al., *APRIL and TALL-I and receptors BCMA and TACI: system for regulating humoral immunity.* Nat Immunol, 2000. **1**(3): p. 252-6.
181. Miao, Y.R., et al., *Developing high-affinity decoy receptors to treat multiple myeloma and diffuse large B cell lymphoma.* J Exp Med, 2022. **219**(9).
182. Shu, H.B. and H. Johnson, *B cell maturation protein is a receptor for the tumor necrosis factor family member TALL-1.* Proc Natl Acad Sci U S A, 2000. **97**(16): p. 9156-61.
183. Hatzoglou, A., et al., *TNF receptor family member BCMA (B cell maturation) associates with TNF receptor-associated factor (TRAF) 1, TRAF2, and TRAF3 and activates NF-kappa B, elk-1, c-Jun N-terminal kinase, and p38 mitogen-activated protein kinase.* J Immunol, 2000. **165**(3): p. 1322-30.
184. Rose-John, S., *IL-6 trans-signaling via the soluble IL-6 receptor: importance for the pro-inflammatory activities of IL-6.* Int J Biol Sci, 2012. **8**(9): p. 1237-47.
185. Heinrich, P.C., et al., *Principles of interleukin (IL)-6-type cytokine signalling and its regulation.* Biochem J, 2003. **374**(Pt 1): p. 1-20.
186. Jego, G., R. Bataille, and C. Pellat-Deceunynck, *Interleukin-6 is a growth factor for nonmalignant human plasmablasts.* Blood, 2001. **97**(6): p. 1817-22.
187. Xia, X.Z., et al., *TACI is a TRAF-interacting receptor for TALL-1, a tumor necrosis factor family member involved in B cell regulation.* J Exp Med, 2000. **192**(1): p. 137-43.
188. Garcia-Carmona, Y., et al., *TACI Isoforms Regulate Ligand Binding and Receptor Function.* Front Immunol, 2018. **9**: p. 2125.
189. Mackay, F. and P. Schneider, *TACI, an enigmatic BAFF/APRIL receptor, with new unappreciated biochemical and biological properties.* Cytokine Growth Factor Rev, 2008. **19**(3-4): p. 263-76.
190. Wu, Y., et al., *Tumor necrosis factor (TNF) receptor superfamily member TACI is a high affinity receptor for TNF family members APRIL and BLyS.* J Biol Chem, 2000. **275**(45): p. 35478-85.
191. Tai, Y.T., et al., *APRIL signaling via TACI mediates immunosuppression by T regulatory cells in multiple myeloma: therapeutic implications.* Leukemia, 2019. **33**(2): p. 426-438.
192. Castigli, E., et al., *TACI and BAFF-R mediate isotype switching in B cells.* J Exp Med, 2005. **201**(1): p. 35-9.
193. Castigli, E., et al., *Impaired IgA class switching in APRIL-deficient mice.* Proc Natl Acad Sci U S A, 2004. **101**(11): p. 3903-8.
194. Varfolomeev, E., et al., *APRIL-deficient mice have normal immune system development.* Mol Cell Biol, 2004. **24**(3): p. 997-1006.
195. Junttila, M.R. and F.J. de Sauvage, *Influence of tumour micro-environment heterogeneity on therapeutic response.* Nature, 2013. **501**(7467): p. 346-54.

196. Lwin, T., et al., *Bone marrow stromal cells prevent apoptosis of lymphoma cells by upregulation of anti-apoptotic proteins associated with activation of NF-kappaB (RelB/p52) in non-Hodgkin's lymphoma cells.* Leukemia, 2007. **21**(7): p. 1521-31.
197. Lwin, T., et al., *Lymphoma cell adhesion-induced expression of B cell-activating factor of the TNF family in bone marrow stromal cells protects non-Hodgkin's B lymphoma cells from apoptosis.* Leukemia, 2009. **23**(1): p. 170-7.
198. He, B., et al., *Lymphoma B cells evade apoptosis through the TNF family members BAFF/BLyS and APRIL.* J Immunol, 2004. **172**(5): p. 3268-79.
199. McWilliams, E.M., et al., *Anti-BAFF-R antibody VAY-736 demonstrates promising preclinical activity in CLL and enhances effectiveness of ibrutinib.* Blood Adv, 2019. **3**(3): p. 447-460.
200. Birnbaum, T., et al., *Expression of B-cell activating factor, a proliferating inducing ligand and its receptors in primary central nervous system lymphoma.* Neurol Int, 2013. **5**(1): p. e4.
201. An, G., et al., *Osteoclasts promote immune suppressive microenvironment in multiple myeloma: therapeutic implication.* Blood, 2016. **128**(12): p. 1590-603.
202. Cho, S.F., K.C. Anderson, and Y.T. Tai, *Targeting B Cell Maturation Antigen (BCMA) in Multiple Myeloma: Potential Uses of BCMA-Based Immunotherapy.* Front Immunol, 2018. **9**: p. 1821.
203. Moreaux, J., et al., *The level of TACI gene expression in myeloma cells is associated with a signature of microenvironment dependence versus a plasmablastic signature.* Blood, 2005. **106**(3): p. 1021-30.
204. Sakaguchi, S., et al., *Regulatory T cells and immune tolerance.* Cell, 2008. **133**(5): p. 775-87.
205. Campbell, J.D., et al., *Suppression of IL-2-induced T cell proliferation and phosphorylation of STAT3 and STAT5 by tumor-derived TGF beta is reversed by IL-15.* J Immunol, 2001. **167**(1): p. 553-61.
206. Knutson, K.L., M.L. Disis, and L.G. Salazar, *CD4 regulatory T cells in human cancer pathogenesis.* Cancer Immunol Immunother, 2007. **56**(3): p. 271-85.
207. Zhang, L., et al., *Regulatory B cell-myeloma cell interaction confers immunosuppression and promotes their survival in the bone marrow milieu.* Blood Cancer J, 2017. **7**(3): p. e547.
208. Xu-Monette, Z.Y., et al., *Immune Profiling and Quantitative Analysis Decipher the Clinical Role of Immune-Checkpoint Expression in the Tumor Immune Microenvironment of DLBCL.* Cancer Immunol Res, 2019. **7**(4): p. 644-657.
209. Raje, N., et al., *Anti-BCMA CAR T-Cell Therapy bb2121 in Relapsed or Refractory Multiple Myeloma.* N Engl J Med, 2019. **380**(18): p. 1726-1737.
210. Gil-Sierra, M.D. and M.D.P. Briceno-Casado, *Belantamab mafodotin for relapsed or refractory multiple myeloma.* J Oncol Pharm Pract, 2022. **28**(6): p. 1375-1380.
211. Chiu, A., et al., *Hodgkin lymphoma cells express TACI and BCMA receptors and generate survival and proliferation signals in response to BAFF and APRIL.* Blood, 2007. **109**(2): p. 729-39.
212. Xu, S. and K.P. Lam, *B-cell maturation protein, which binds the tumor necrosis factor family members BAFF and APRIL, is dispensable for humoral immune responses.* Mol Cell Biol, 2001. **21**(12): p. 4067-74.
213. Lee, L., et al., *Evaluation of B cell maturation antigen as a target for antibody drug conjugate mediated cytotoxicity in multiple myeloma.* Br J Haematol, 2016. **174**(6): p. 911-22.

214. Tai, Y.T., et al., *Novel anti-B-cell maturation antigen antibody-drug conjugate (GSK2857916) selectively induces killing of multiple myeloma.* Blood, 2014. **123**(20): p. 3128-38.
215. Das, A.T., L. Tenenbaum, and B. Berkhout, *Tet-On Systems For Doxycycline-inducible Gene Expression.* Curr Gene Ther, 2016. **16**(3): p. 156-67.
216. Gozzetti, A., et al., *Anti CD38 monoclonal antibodies for multiple myeloma treatment.* Hum Vaccin Immunother, 2022. **18**(5): p. 2052658.
217. Tai, Y.T., et al., *Role of B-cell-activating factor in adhesion and growth of human multiple myeloma cells in the bone marrow microenvironment.* Cancer Res, 2006. **66**(13): p. 6675-82.
218. Rossi, J.F., et al., *Atacicept in relapsed/refractory multiple myeloma or active Waldenstrom's macroglobulinemia: a phase I study.* Br J Cancer, 2009. **101**(7): p. 1051-8.
219. Schuepbach-Mallepell, S., et al., *Stoichiometry of Heteromeric BAFF and APRIL Cytokines Dictates Their Receptor Binding and Signaling Properties.* J Biol Chem, 2015. **290**(26): p. 16330-42.
220. Sanchez, E., et al., *Soluble B-Cell Maturation Antigen Mediates Tumor-Induced Immune Deficiency in Multiple Myeloma.* Clin Cancer Res, 2016. **22**(13): p. 3383-97.
221. Kern, C., et al., *Involvement of BAFF and APRIL in the resistance to apoptosis of B-CLL through an autocrine pathway.* Blood, 2004. **103**(2): p. 679-88.
222. Ullah, M.A. and F. Mackay, *The BAFF-APRIL System in Cancer.* Cancers (Basel), 2023. **15**(6).
223. Fu, J., et al., *BST-2/Tetherin is involved in BAFF-enhanced proliferation and survival via canonical NF-kappaB signaling in neoplastic B-lymphoid cells.* Exp Cell Res, 2021. **398**(1): p. 112399.
224. Lyu, M.A., et al., *The rGel/BLyS fusion toxin inhibits diffuse large B-cell lymphoma growth in vitro and in vivo.* Neoplasia, 2010. **12**(5): p. 366-75.
225. Hase, H., et al., *BAFF/BLyS can potentiate B-cell selection with the B-cell coreceptor complex.* Blood, 2004. **103**(6): p. 2257-65.
226. Miao, Y.R., et al., *Neutralization of PD-L2 is Essential for Overcoming Immune Checkpoint Blockade Resistance in Ovarian Cancer.* Clin Cancer Res, 2021. **27**(15): p. 4435-4448.
227. Liu, Y., et al., *Ligand-receptor binding revealed by the TNF family member TALL-1.* Nature, 2003. **423**(6935): p. 49-56.
228. Grasset, E.K., et al., *Gut T cell-independent IgA responses to commensal bacteria require engagement of the TACI receptor on B cells.* Sci Immunol, 2020. **5**(49).
229. Shin, W., et al., *BAFF-neutralizing interaction of belimumab related to its therapeutic efficacy for treating systemic lupus erythematosus.* Nat Commun, 2018. **9**(1): p. 1200.
230. Bolkun, L., et al., *BAFF and APRIL as TNF superfamily molecules and angiogenesis parallel progression of human multiple myeloma.* Ann Hematol, 2014. **93**(4): p. 635-44.
231. Briones, J., et al., *BLyS and BLyS receptor expression in non-Hodgkin's lymphoma.* Exp Hematol, 2002. **30**(2): p. 135-41.

APPENDICES

Appendix A: Previously published paper

1. Miao, Y.R., et al., Developing high-affinity decoy receptors to treat multiple myeloma and diffuse large B cell lymphoma. J Exp Med, 2022. 219(9). Reprinted with permission from Rockefeller University Press.

JEM Journal of Experimental Medicine

ARTICLE

Developing high-affinity decoy receptors to treat multiple myeloma and diffuse large B cell lymphoma

Yu Rebecca Miao[1*], Kaushik Thakkar[1*], Can Cenik[2], Dadi Jiang[3], Kazue Mizuno[1], Chenjun Jia[4], Caiyun Grace Li[1], Hongjuan Zhao[5], Anh Diep[1], Yu Xu[1], Xin Eric Zhang[7], Teddy Tat Chi Yang[4], Michaela Liedtke[6], Parveen Abidi[6], Wing-sze Leung[1], Albert C. Koong[3], and Amato J. Giaccia[1,7]

Disease relapse and treatment-induced immunotoxicity pose significant clinical challenges for patients with hematological cancers. Here, we reveal distinctive requirements for neutralizing TNF receptor ligands APRIL and BAFF and their receptor activity in MM and DLBCL, impacting protein translation and production in MM cells and modulating the translation efficiency of the ATM interactor (ATMIN/ACSIZ). Therapeutically, we investigated the use of BCMA decoy receptor (sBCMA-Fc) as an inhibitor of APRIL and BAFF. While wild-type sBCMA-Fc effectively blocked APRIL signaling in MM, it lacked activity in DLBCL due to its weak BAFF binding. To expand the therapeutic utility of sBCMA-Fc, we engineered an affinity-enhanced mutant sBCMA-Fc fusion molecule (sBCMA-Fc V3) 4- and 500-fold stronger in binding to APRIL and BAFF, respectively. The mutant sBCMA-Fc V3 clone significantly enhanced antitumor activity against both MM and DLBCL. Importantly, we also demonstrated an adequate toxicity profile and on-target mechanism of action in nonhuman primate studies.

Introduction

B cell malignancies, in particular multiple myeloma (MM) and diffuse large B cell lymphoma (DLBCL), represent some of the most common hematological cancers worldwide (Chim et al., 2018; Durer et al., 2020; Swerdlow et al., 2016; Weber and Schmitz, 2022). While the use of treatment regimens combining chemo-cytotoxic drugs and targeted therapies has significantly improved overall survival, patients suffering from relapse/refractory diseases after standard-of-care treatment still face poor outcomes (Caimi et al., 2021; Lonial et al., 2020; Raje et al., 2019). The recent approval of chimeric antigen receptor (CAR) T cells has provided a more effective treatment for patients who failed to respond to conventional therapies, with some patients able to achieve complete remission. However, restrictive patient eligibility, immune-related adverse toxicities, and treatment relapse are challenges remain to overcome. Therefore, safe and effective targeted therapies for patients who exhaust currently available treatment options is still needed.

Two ligands of the TNF superfamily, known as a proliferation-inducing ligand (APRIL) and B cell activating factor (BAFF), are well documented as critical regulators of B cell maturation and differentiation (Bolkun et al., 2014; Chiu et al., 2007). APRIL and BAFF facilitate their diverse functions on B lymphocytes through binding to three TNF receptors, TACI (transmembrane activator and Ca^{2+} modulator interactor), B cell maturation antigen (BCMA), and BAFF receptor (BAFF-R), with various affinities (Wu et al., 2000; Yu et al., 2000). TACI and BAFF-R are present on mature B cells, whereas BCMA is almost exclusively confined to plasma cells (O'Connor et al., 2004). Differences in binding affinities between APRIL and BAFF toward TACI, BCMA, and BAFF-R in part result in highly differentiated receptor–ligand interactions to promote unique biological outcomes. For example, APRIL possesses a 1,000-fold stronger binding affinity to BCMA than BAFF, whereas the reverse is reported for BAFF–TACI and BAFF–BAFF-R interactions (Marsters et al., 2000; Schuepbach-Mallepell et al., 2015; Yu et al., 2000). This distinctive receptor–ligand binding relationship further supports the differentiated roles of APRIL and BAFF in B cell biology: APRIL-BCMA signaling is an exclusive regulator of plasma cells, and BAFF-TACI/BAFF-R activation is required for the maturation of B lymphocytes (Moreaux et al., 2007; Pelletier et al., 2003). In oncology, aberrant expression of APRIL and BAFF supports disease progression and is associated with a poor treatment outcome in MM and DLBCL. Persistent APRIL and BAFF activation promotes survival advantages in MM and DLBCL, facilitating

[1]Department of Radiation Oncology, Stanford University, Stanford, CA; [2]Department of Molecular Biosciences, University of Texas at Austin, Austin, TX; [3]Department of Radiation Oncology, MD Anderson Cancer Center, Houston, TX; [4]ChemPartner Shanghai, Shanghai, China; [5]Department of Urology, Stanford University, Stanford, CA; [6]Department of Medicine (Hematology), Stanford University, Stanford, CA; [7]Department of Oncology, Oxford Institute for Radiation Oncology, University of Oxford, Oxford, UK.

*Y.R. Miao and K. Thakkar contributed equally to this paper. Correspondence to Yu Rebecca Miao: ymiao@stanford.edu; Amato J. Giaccia: giaccia@stanford.edu or amato.giaccia@oncology.ox.ac.uk.

disease progression and treatment resistance (Kuo et al., 2008; Moreaux et al., 2004). Similar to the dichotomous relationship between APRIL and BAFF in normal B cell development, APRIL-BCMA signaling is critical in MM progression, where persistent activation of BAFF-TACI/BAFF-R is critical for promoting malignant B cell growth and survival (Pham et al., 2011). Therefore, neutralizing APRIL and BAFF in B cell malignancies may offer a new treatment option for MM and DLBCL.

In this study, we investigated the therapeutic strategy of using soluble BCMA as a ligand trap for blocking APRIL-mediated signaling in MM. We also discovered a new function of BCMA signaling as a regulator of the translation of a subset of proteins, including ATMIN, a protein critical for the development of both normal and malignant B cells (Jurado et al., 2012b). Therapeutically, we developed an affinity-enhanced, soluble BCMA-based mutant Fc fusion protein, trapping both APRIL and BAFF with stronger binding affinities. This high-affinity fusion protein showed superior blockade of both APRIL/BCMA signaling and BAFF-TACI/BAFF-R signaling in MM and DLBCL models, while demonstrating little toxicity and an on-target mechanism of action in nonhuman primate studies.

Results

BCMA signaling activation is required for MM progression

We began our study by validating the functional significance of BCMA signaling in MM using genetic and biochemical approaches. Consistent with previous reports, BCMA mRNA expression was uniquely elevated on MM and B cell lymphoma and was not detectable in cancer cells other than those of a B cell lineage (Figs. 1 A and S1 A). High levels of APRIL (Fig. 1 B) and BAFF (Fig. 1 C) were detected in MM patients, also consistent with previous reports that both ligands serve as biomarkers of various B cell malignancies (Bolkun et al., 2014; Fragioudaki et al., 2012).

The dependence of MM proliferation on BCMA signaling was tested by introducing a Tet-off doxycycline (dox)-controlled BCMA stable knockdown system (dox shBCMA) into MM cell lines INA-6 and MM1.R (Fig. S1 B). INA-6 MM cells have a chromosomal translocation at t(11;14) and *NRAS* and *TP53* mutations and are dependent on IL-6 for growth and survival (Burger et al., 2001; Keats et al., 2007). MM1.R has chromosomal translocations at t(14;16) and t(8;14) and *KRAS* and *TRAF3* mutations (Greenstein et al., 2003). Genetic inhibition of BCMA with dox-inducible shBCMA led to a significant decrease in established MM tumor size in both models (Fig. 1, D and E; and Fig. S1 C), further demonstrating that BCMA signaling can act as a master regulator of MM survival and is independent of heterogeneous genetic mutations. Smaller tumor size is associated with decreased proliferation (Fig. 1, F and G; and Fig. S1 D) and increased apoptosis (Fig. 1, H and I; and Fig. S1 E) upon genetic inhibition of BCMA. Furthermore, the level of human myeloma immunoglobulin protein (paraprotein) secreted by MM tumor cells was significantly reduced in mice bearing shBCMA MM tumors, indicating decreased tumor burden (Fig. 1 J; Collier and Jackson, 1953).

Ribosome profiling reveals distinct changes in protein translation regulated by BCMA signaling

Upon analyzing downstream biological changes associated with BCMA signaling, we found robust changes in key regulators of protein translation and synthesis such as mTOR and the EIF family member eIF4E, suggesting a potential link between BCMA signaling and protein translation that has not been described previously (Figs. 2 A and S2 A). To investigate whether BCMA acts as a regulator of protein translation, we performed ribosome profiling on U266 MM cells with siRNA BCMA knockdown. U266 harbors some of the most frequently found genetic alternations in MM patients and is a reasonable representative of MM tumor cells (Keats et al., 2007). Ribosome profiling is a specialized analysis method that provides a quantitative measure of gene-specific translation efficiency. Technically, mRNA fragments protected by ribosomes were isolated and sequenced, and in the same population of cells, total RNA abundance was quantified by RNA sequencing (RNA-seq) for normalization (Fig. 2 B; Ingolia et al., 2011). Quality control analysis of the ribosome profiling data was performed to ensure accurate ribosome-bound RNA readouts (Fig. S2, B and C). Total mRNA obtained from RNA-seq data served as a reference for quantitating ribosome-bound mRNA–associated changes in translation efficiency (Fig. S2, D and E), and translation efficiency was analyzed from ribosome-bound mRNA normalized against total mRNA (Cenik et al., 2015). Ingenuity pathway analysis of total mRNA and GSEA reactome analysis of ribosome sequencing (Ribo-seq) data both showed enrichment of pathways and gene signatures associated with protein translation (Fig. 2, C and D). Ribo-seq data are also presented in the format of volcano plot (Fig. S2 F). Furthermore, pathways that are responsible for the synthesis of both large and small ribosome subunits were affected in BCMA-inhibited MM cells (Fig. S2 H). This finding was further confirmed by reverse-phase protein array (RPPA), which showed a decreased protein translation signature upon loss of BCMA (Fig. S2 G). Collectively, these data suggest a previously unreported role of BCMA signaling as a regulator of protein translation machinery in MM growth.

Upon further investigation, we found that the translation efficiency of ATMIN (ASCIZ) to be significantly downregulated upon loss of BCMA, while its mRNA transcription level remained unchanged (Fig. 2 E). ATMIN and its binding partner Dynein light chain have been reported to regulate the development of B cell malignancies (Jurado et al., 2012a; Jurado et al., 2012b; Leszczynska et al., 2016; Rapali et al., 2011). Initially discovered as an ATM interacting protein, ATMIN is often associated with ATM-mediated signaling and recruitment of 53BP1 upon DNA damage (Becker et al., 2018; Jurado et al., 2010; McNees et al., 2005). Because RPPA showed no significant changes in DNA damage response upon BCMA loss (Fig. S2 G), we hypothesized that altered ATMIN expression may not be a result of DNA damage response but instead modulation by BCMA. To validate our Ribo-seq findings, we performed polysome fractionation to demonstrate BCMA-mediated translational changes in ATMIN expression. Ribosomes captured from MM cell lysates were separated into pooled fractions of heavy polysomes, lighter ribosomes, and monosomes to determine

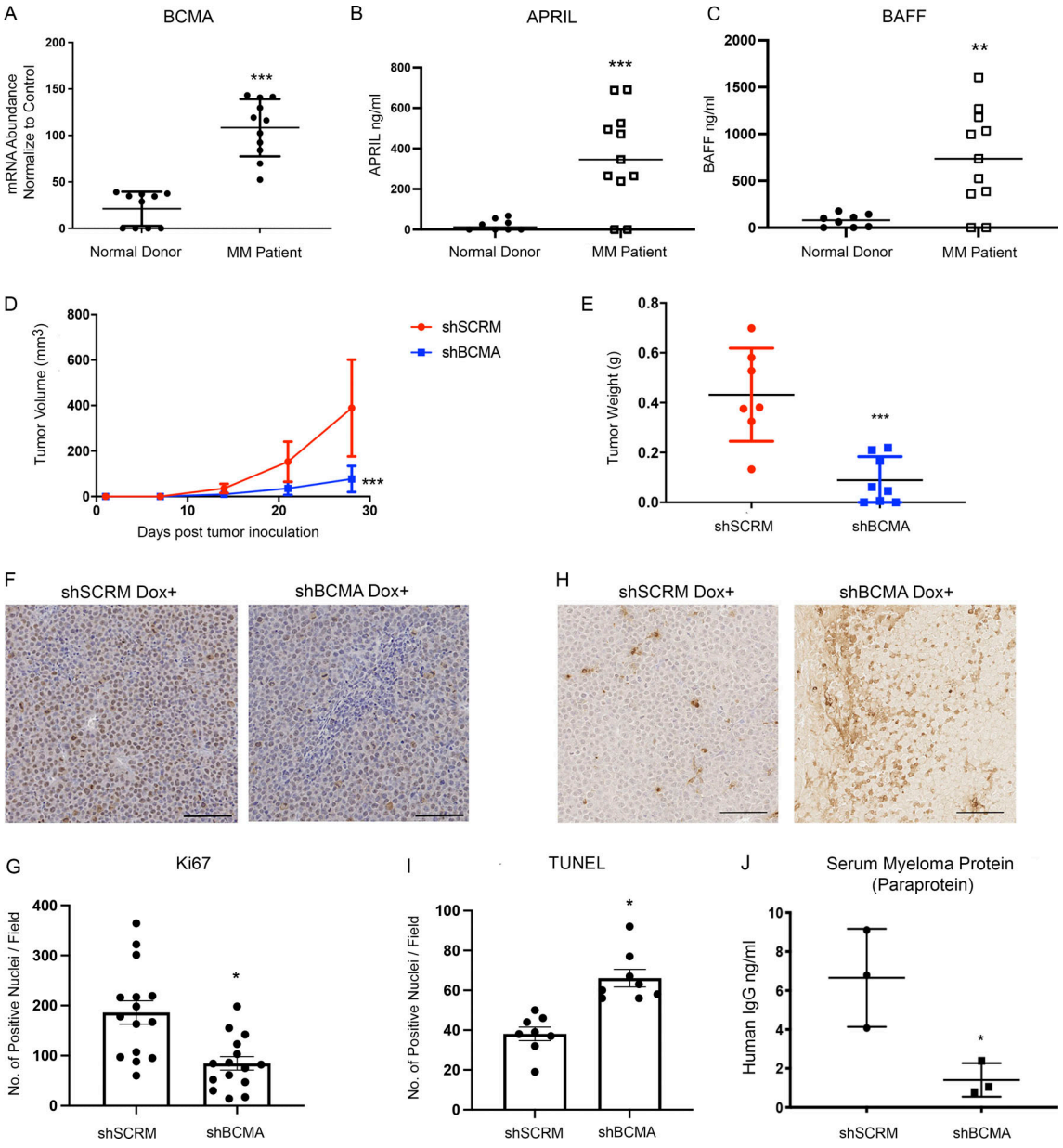

Figure 1. **BCMA and its ligands APRIL and BAFF are upregulated in MM and support the growth and survival of MM in vivo. (A)** BCMA mRNA transcript validated in patient myeloma cells (n = 11) and plasma cells harvested from healthy donors (n = 6); P = 0.0001. **(B)** Serum APRIL level detected in MM patients (n = 11) compared with healthy donors (n = 8) through ELISA; P = 0.001. **(C)** Serum BAFF level detected in MM patients (n = 11) compared with healthy donors (n = 8) through ELISA; P = 0.0028. **(D)** Subcutaneous tumor growth of INA-6 MM cells with stably transfected dox-inducible BCMA KO shRNA (n = 8) or scramble shRNA (n = 7) in 6-wk-old female NSG mice; P = 0.0005. **(E)** Comparing tumor weights of terminally harvested mice inoculated with dox-inducible shSCRM (n = 7) and shBCMA (n = 8) in INA-6 MM tumor cells; P = 0.0005. **(F)** Representative images of Ki67-positive cells in the harvested tumors of dox-inducible shSCRM and shBCMA, analyzed by immunohistochemical (IHC) staining. Scale bar, 50 µm. **(G)** Quantitative analysis of Ki67-positive cells in the harvested tumors of dox-inducible shSCRM and shBCMA, represented as the average number of positive nuclei per image field; P = 0.0008. **(H)** Representative images of TUNEL-positive cells in the harvested tumors of dox-inducible shSCRM and shBCMA, analyzed by IHC staining. Scale bar, 50 µm. **(I)** Quantitative analysis of TUNEL-positive cells in the harvested tumors of dox-inducible shSCRM and shBCMA, represented as the average number of positive nuclei per image field; P = 0.0002. **(J)** Total human M protein (paraprotein) detected in the serum of NSG mice inoculated with dox-inducible shSCRM and shBCMA human INA-6 MM tumor cells harvested terminally (n = 3); P = 0.0268. Statistical analysis was conducted using one-way ANOVA for comparing between treatment groups and repeated ANOVA for changes occurring over time. *, P < 0.05; **, P < 0.01; ***, P < 0.001.

which fractions bound ATMIN upon the loss of BCMA expression (Fig. 2 F). Compared with the control, siBCMA-expressing MM cells showed significantly decreased ATMIN transcript binding to heavy polysomes, indicating reduced ATMIN translation efficiency (Fig. 2 G). In addition, ATMIN is exclusively regulated at the translational level by BCMA, since total ATMIN mRNA transcripts remain unchanged upon the loss of BCMA expression (Fig. 2 H).

To directly access changes in ATMIN after BCMA inhibition, we compared ATMIN protein levels in MM cells treated with

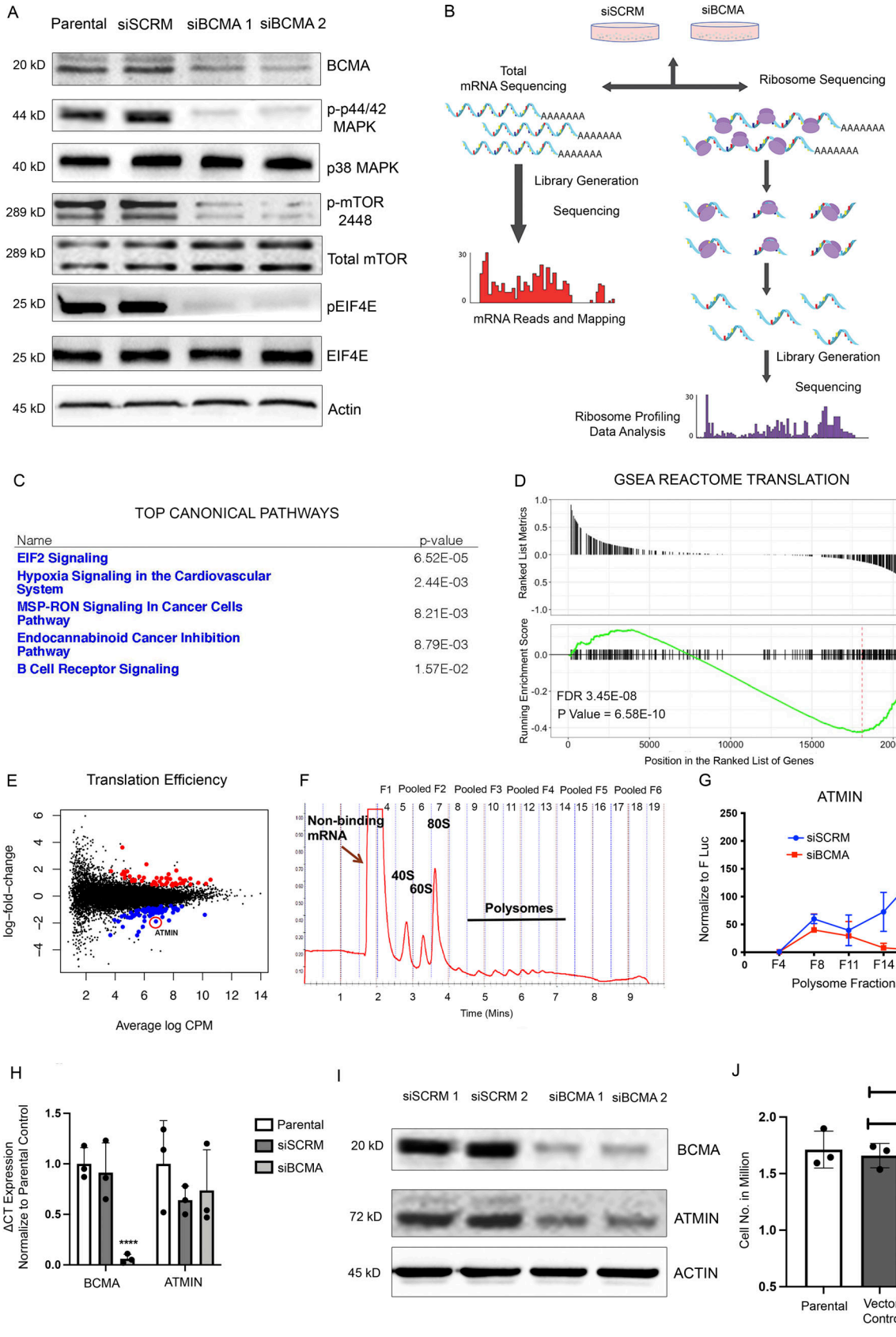

Figure 2. **Ribosome profiling identifies BCMA as a master regulator of protein translation machinery in MM. (A)** Western blotting analysis of changes in protein expression associated with protein translation upon genetic knockdown using siBCMA. **(B)** Schematic illustration of ribosome profiling workflow. **(C)** Ingenuity pathway analysis of RNA-seq data showing top five significantly changed canonical pathways. **(D)** GSEA REACTOME enrichment analysis showing

enriched signatures in associated with protein translation. FDR, false discovery rate. **(E)** Translation efficiency analysis of MM cells upon loss of BCMA expression in MM. Significant events are colored in blue (downregulated) and red (upregulated). ATMIN highlighted with red circle. **(F)** Representative polysome profile of MM cells fractionated by ultracentrifugation through a 10–50% sucrose gradient. Fractions were pooled for mRNA analysis. **(G)** Relative abundance of ATMIN mRNA expression analyzed in each of the pooled polysome fractions comparing siSCRM with siBCMA MM cells. Each biological sample were performed in triplicate. P = 0.0228. **(H)** Total mRNA expression of BCMA (P = 0.0078) and ATMIN (NS) examined in parental, siSCRM, and siBCMA U266 cells. Each biological sample was performed in triplicate. **(I)** Western blotting analysis of ATMIN expression in siSCRM and two clones of siBCMA MM cells. **(J)** Cell growth analysis comparing ATMIN vector control with ATMIN CRISPR KO clone #1 (P = 0.0129) and with ATMIN CRISPR KO clone #2 (P = 0.0055) in U266 MM cells. Statistical analysis was conducted using *t* test and one-way ANOVA for comparing between treatment groups. *, P < 0.05; **, P < 0.01; ***, P < 0.001. Source data are available for this figure: SourceData F2.

siSCRM controls or two different siBCMA clones. We found strong inhibition of ATMIN protein by siBCMA compared with siSCRM (Fig. 2 I). To determine the effect of ATMIN on cell viability, we generated two independent ATMIN CRISPR knockout pools in U266 cells and observed a 30–40% reduction in cell viability. This result suggests that, like BCMA, ATMIN is also required for the viability of MM cells (Fig. 2 J).

Wild-type soluble BCMA decoy receptor inhibits MM growth through APRIL/BCMA signaling but lacks efficacy in BAFF-driven DLBCL models

Because gain-of-function mutations in BCMA are rarely reported, BCMA signaling activity is almost exclusively regulated by its ligands APRIL and BAFF. Therefore, we investigated a ligand blocking approach, using a soluble decoy receptor comprising the BCMA extracellular domain (sBCMA) fused to the human IgG1 Fc domain (sBCMA-Fc) to trap and neutralize APRIL and BAFF (Fig. 3 A).

Treatment with sBCMA-Fc decreased downstream protein expression of similar canonical signaling regulated by the BCMA that we found through genetic inhibition of BCMA (Fig. 3 B). To determine the inhibitory effect of sBCMA-Fc on the viability of MM cells, we performed in vitro cytotoxicity assays using U266 and MM1.R cells. A concentration-dependent decrease in MM cell viability was observed when cells were treated with sBCMA-Fc and cultured in exogenous APRIL under reduced serum conditions, supporting the importance of APRIL as a growth stimulus in MM cells (Fig. 3 C). Thus, sBCMA-Fc effectively neutralized ligand-mediated activation of BCMA signaling pathways in vitro, resulting in decreased MM cell growth.

We next examined the efficacy of sBCMA-Fc in vivo. Treatment with sBCMA-Fc resulted in a significant tumor reduction in both MM1.R (Fig. 3 D) and INA-6 MM (Fig. S3 A) tumors and was associated with decreased tumor cell proliferation (Figs. 3 E and S3 B) and increased apoptosis (Figs. 3 F and S3 C). A separate study was conducted using IgG Fc and a decoy receptor without binding to APRIL and BAFF to show the therapeutic specificity of the sBCMA-Fc molecule (Fig. S3 D). Collectively, these findings provide supporting evidence that sBCMA-Fc is efficacious as a monotherapy in xenograft models of MM. To further validate the therapeutic potential of sBCMA-Fc in human MM specimens, we established patient-derived xenografts (PDX) by engrafting freshly isolated human MM cells into the tibia of an immunodeficient murine host (Fig. S4 A). We screened eight male and three female patients, of whom six were untreated and five were treated; most had IgGκ or IgGλ myeloma type (Table S1). MM cells from patients 3 and 5 (both IgGκ myeloma type) were successfully engrafted and propagated for in vivo tumor study. After inoculation of PDX-derived MM cells, we confirmed engraftment upon the presence of human M protein (IgGκ) and proceeded with sBCMA-Fc treatment (Fig. S4, B and C). Computed tomography (CT) scans of animals with successful engraftment showed macroscopic osteolytic lesions consistent with osteopenia found in MM patients (Fig. 3 G). Engrafted mice were treated with sBCMA-Fc at 10 mg/kg every 48 h for 28 d, and tumor growth was monitored with systemic level of human IgGκ in blood serum until mice reached an ethical endpoint. In both PDX lines that were successfully propagated, treatment with sBCMA-Fc led to significant reduction in tumor expansion, decreased IgGκ signal, and prolonged overall survival, which demonstrates the ligand dependence of BCMA signaling in human MM (Fig. 3, H and I; and Fig. S4, B and C). We also evaluated the therapeutic relevance of sBCMA-Fc in combination with other MM-targeted therapies such as αCD38 antibodies. The combination of sBCMA-Fc with a CD38 therapeutic antibody (αCD38) showed superior antitumor activity compared with either monotherapy alone (Figs. 3 J and S4 D). There were no differences in body weight among the treatment groups (Fig. S4 D).

Based on published studies, BAFF is also capable of binding to BCMA receptor at a lower affinity (Bossen and Schneider, 2006). Therefore, we investigated the therapeutic efficacy of sBCMA-Fc in B cell malignancy models such as DLBCL, which is BAFF dependent (Fu et al., 2021; Lyu et al., 2010). BAFF-sensitive SU-DHL-6 and Daudi DLBCL cells were treated with ascending concentrations of sBCMA-Fc to assess in vitro cytotoxicity. Interestingly, compared with MM, DLBCL cells were less sensitive toward sBCMA-Fc treatment (Fig. S4, F and G). To determine the efficacy of sBCMA-Fc in DLBCL tumor models, mice bearing subcutaneous SU-DHL-6 tumors were treated with sBCMA-Fc at 10 mg/kg every 48 h, which is the efficacious dose in MM tumors. However, treatment with sBCMA-Fc at 10 mg/kg did not provide significant antitumor benefit in BAFF-sensitive SU-DHL-6 lymphomas (Fig. 3 K). Knowing that MM is primarily APRIL driven, while DLBCL is BAFF dependent, we hypothesized that the sBCMA-Fc molecule lacks sufficient binding affinity toward BAFF and hence failed to inhibit BAFF-mediated signaling.

Engineering a high-affinity decoy receptor fusion protein against APRIL and BAFF

To validate whether the lack of antitumor activity demonstrated by sBCMA-Fc against DLBCL is due to weak binding affinity toward BAFF, we evaluated the binding kinetics of sBCMA to

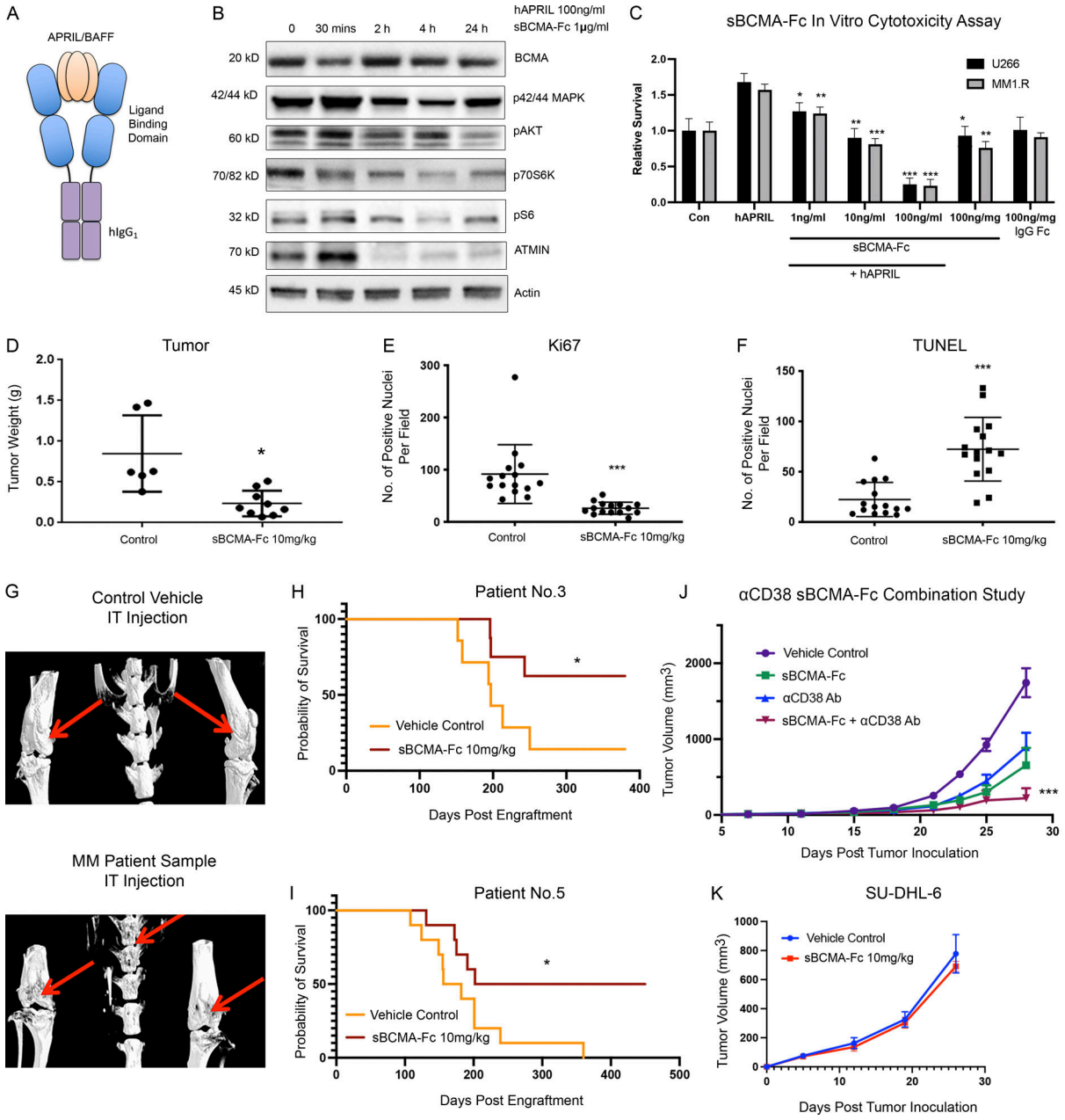

Figure 3. **Wild-type sBCMA decoy receptor inhibits MM growth through APRIL/BCMA signaling but lacks efficacy in BAFF-driven DLBCL model.** **(A)** Schematic illustrations of recombinant human sBCMA-Fc binding to human APRIL. **(B)** Analysis of BCMA downstream protein expression in U266 MM cells upon sBCMA-Fc treatment at multiple time points. **(C)** sBCMA-Fc dose-dependent cytotoxicity assay validating in vitro cell survival in the presence of increasing doses of sBCMA-Fc (P = 0.0095, 1 ng/ml; P = 0.0024, 10 ng/ml; and P = 0.0001, 100 ng/ml) and hAPRIL (100 ng/ml) in U266 and MM1.R MM cells. Cells were maintained in low (3%) FCS to reduce possible growth stimulation mediated through other growth factors present in FCS. Each sample was performed in triplicate. **(D)** Terminal tumor weight of mice inoculated with MM1.R MM tumors and treated with vehicle control or 10 mg/kg of sBCMA-Fc; P = 0.0217. **(E)** Quantification of Ki67 staining in MM1.R MM tumors and treated with vehicle control or 10 mg/kg of sBCMA-Fc; P = 0.0001. **(F)** Quantification of TUNEL staining in MM1.R MM tumors and treated with vehicle control or 10 mg/kg of sBCMA-Fc; P = 0.0001. **(G)** Representative CT scans of mice tibias, femurs, and vertebrae inoculated with control (top) or MM PDX tumor cells (bottom). Osteolytic bone degradation was observed in MM PDX injected animal (bottom image) but not in the control injected animals (top image). **(H)** Kaplan–Meier survival analysis of animals engrafted with MM cells from patient 3 showing prolonged overall survival in the sBCMA-Fc–treated group (n = 8) compared with the vehicle control (n = 7); P = 0.027. **(I)** Kaplan–Meier survival analysis of animals engrafted with MM cells from patient 5 showing prolonged overall survival in the sBCMA-Fc–treated group (n = 10) compared with vehicle control (n = 10); P = 0.0362. **(J)** Subcutaneous tumor growth of MM1.R MM tumors in 6-wk-old female NSG mice dosed with sBCMA-Fc 10 mg/kg every 48 h (n = 7); P = 0.0195. αCD38 10 mg/kg weekly (n = 7; P = 0.0238) and sBCMA-Fc and αCD38 combination (n = 8; P < 0.001) compared with vehicle control (n = 8). **(K)** Subcutaneous tumor growth of SU-DHL-6 DLBCL tumors in mice dosed with vehicle control or sBCMA-Fc 10 mg/kg every 48 h (n = 5). Statistical analysis was conducted using t test and one-way ANOVA for comparing between treatment groups. Repeated ANOVA used for changes in tumor growth over time. *, P < 0.05; **, P < 0.01; ***, P < 0.001. Source data are available for this figure: SourceData F3.

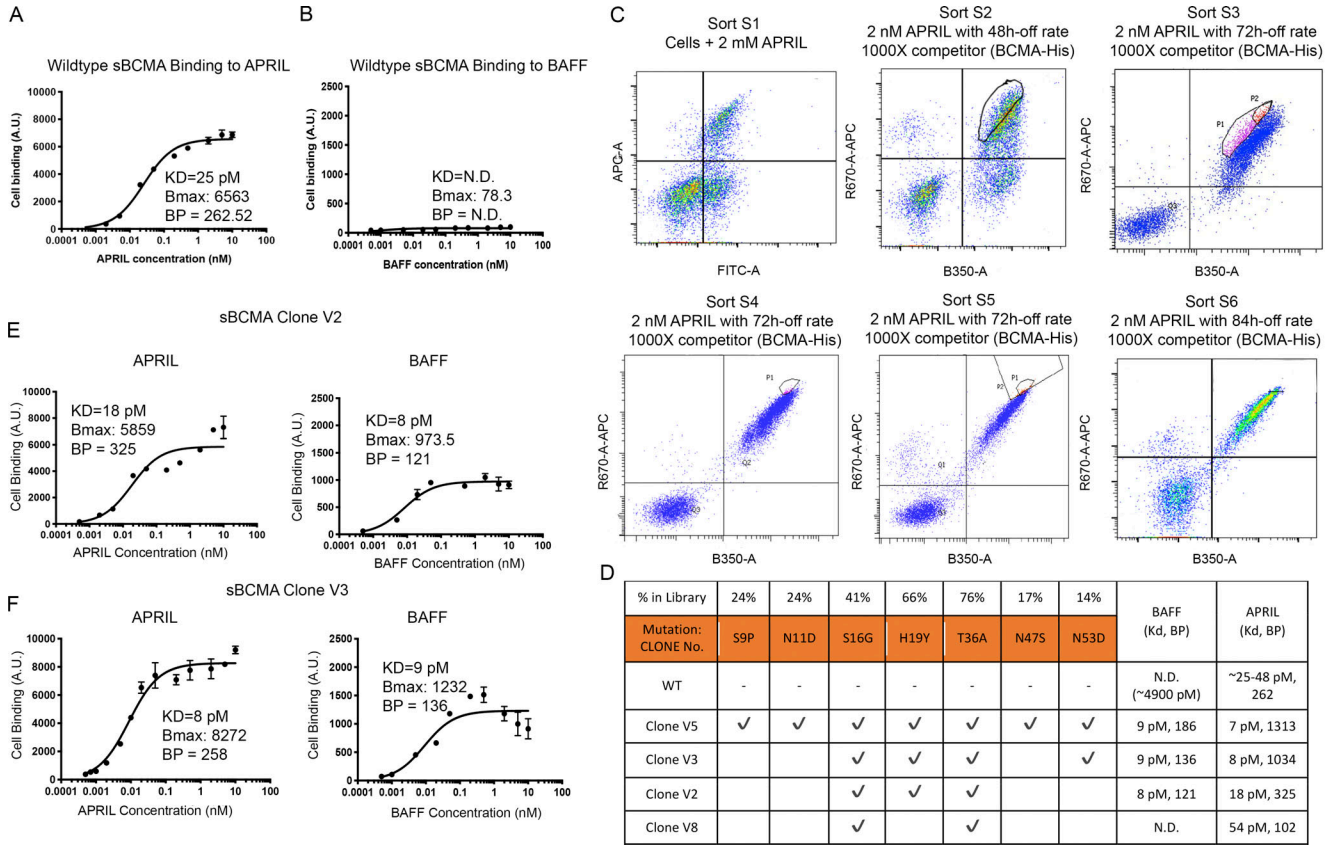

% in Library	24%	24%	41%	66%	76%	17%	14%	BAFF (Kd, BP)	APRIL (Kd, BP)
Mutation: CLONE No.	S9P	N11D	S16G	H19Y	T36A	N47S	N53D		
WT	-	-	-	-	-	-	-	N.D. (~4900 pM)	~25-48 pM, 262
Clone V5	✓	✓	✓	✓	✓	✓	✓	9 pM, 186	7 pM, 1313
Clone V3			✓	✓	✓		✓	9 pM, 136	8 pM, 1034
Clone V2			✓	✓	✓			8 pM, 121	18 pM, 325
Clone V8			✓		✓			N.D.	54 pM, 102

Figure 4. **Engineering high-affinity decoy receptor fusion protein against APRIL and BAFF. (A)** Flow cytometry–based binding curve showing yeast-displayed wild-type sBCMA binding to increasing concentrations of APRIL. Calculated K_D, B_{max}, and binding potential (BP) is also shown. A.U., arbitrary units. **(B)** Flow cytometry–based binding curve showing yeast-displayed wild-type sBCMA binding to increasing concentrations of BAFF. Calculated K_D, B_{max}, and BP is shown. **(C)** Overlaid flow cytometry dot plots representing sorting strategies of yeast-displayed sBCMA library binding to 2 nM APRIL in six consecutive sorts with 48–84 h off-rate binding and 1,000× competitor. Gated populations are collected from each sort and propagated for the next sorting round. **(D)** Binding affinities to APRIL and BAFF of wild-type sBCMA and selected mutant sBCMA clones. Conserved amino acid mutations were identified in mutant clones, and the frequency of occurring mutations is also listed. **(E)** Binding curve of high-affinity mutant sBCMA clone V2 binding to increasing concentrations of APRIL (left) and BAFF (right). Calculated K_D, B_{max}, and BP is shown. **(F)** Binding curve of high-affinity mutant sBCMA clone V3 binding to increasing concentration of APRIL (left) and BAFF (right). Calculated K_D, B_{max}, and BP is shown.

hAPRIL and hBAFF. While the K_D between sBCMA and hAPRIL has been reported to be 25–48 pM (Hymowitz et al., 2005; Yu et al., 2000), the K_D between sBCMA and hBAFF was weak and was experimentally estimated to be ∼4,900 pM (Fig. 4, A and B). This finding supported our hypothesis that weak binding between sBCMA-Fc and BAFF is likely to be a contributing factor toward poor therapeutic efficacy in BAFF-driven DLBCL models.

To address this shortcoming, we engineered a sBCMA mutant with the capability of neutralizing both APRIL and BAFF at high affinity. Using low-fidelity Taq polymerase-based error-prone PCR as previously described (Miao et al., 2021), nucleotide mutations were randomly generated into the extracellular domain of BCMA gene from amino acid 1 (methionine) to 54 (alanine). The resulting library displayed on the yeast surface was analyzed by FACS to isolate clones with desired binding characteristics. We carried out initial affinity screening using hAPRIL, because it was previously reported that the BCMA binding site to APRIL and BAFF shares high homology (Fig. S5 A). Therefore, we hypothesized that clones identified in this screening process will likely have high binding affinity to both APRIL and BAFF (Liu et al., 2003). Six rounds of FACS sorting were performed sequentially, and 1–3% clones with the highest binding to APRIL were enriched from each sort and propagated for the subsequent sorting round (Fig. 4 C).

The top 118 clones selected from sort rounds 3–6 were sequenced and analyzed for consensus mutations (Tables S2, S3, S4, and S5). Overall, seven consensus mutations were identified (Fig. 4 D). As hypothesized, we observed a dramatic improvement in the binding affinities of candidate mutant clones toward both APRIL and BAFF. Ultimately, the mutant sBCMA V3 carrying mutations S16G, H19Y, T36A, and N53D was selected as our top candidate because it possessed fewer mutations while still retaining high binding affinity toward APRIL and BAFF. The sBCMA V2 without N53D mutation resulted in a slightly weaker binding to APRIL (Fig. 3, E and F).

Structural and biological characterization of affinity-enhanced sBCMA-Fc V3

To characterize the structural, biophysical, and biological properties of our affinity-enhanced clone sBCMA V3, we

performed computational model simulations of sBCMA-Fc V3 in cocomplex with APRIL and BAFF. The sequence alignment and subsequent modeling based on the wild-type hBCMA and mAPRIL complex structures were obtained from PDB 1XU2; Fig. S5 A; Hymowitz et al., 2005; Schuepbach-Mallepell et al., 2015). Structural alignment between hAPRIL and mAPRIL revealed high structural homology with a root mean square deviation (RMSD) of 0.893 Å. While hBAFF and mAPRIL were not highly conserved in their primary sequence (Fig. S5 B), they shared high similarity on tertiary structure, with RMSD of 1.248 Å (Fig. S5 C). This is consistent with a previous report that hAPRIL and hBAFF share a similar binding site at the DxL motif of BCMA (Gordon et al., 2010). We found that residues 44–54 are likely to be a highly flexible. Of the four mutations we identified, mutations S16G and H19Y are located within the BCMA binding motif, and T36A and N53D are located outside of the binding motif. Mutations S16G, H19Y, and T36A both individually and collectively led to an improvement in the binding affinity, stability, and thermodynamic interaction of sBCMA V3/hAPRIL and sBCMA V3/hBAFF cocomplexes (Fig. 5 A and Table 1; Fig. 5 B and Table 2). Based on protein interaction modeling, the H19Y mutation is likely to be the most important contributor responsible for improved binding affinity to both hAPRIL and hBAFF. While residue 19 was reported as a critical residue within the sBCMA/BAFF cocomplex (Bossen and Schneider, 2006), no such analysis has been done with sBCMA/APRIL cocomplex. Furthermore, we found that amino acid substitution of H19Y on sBCMA is the critical mutation responsible for enhanced binding toward both APRIL and BAFF (Tables 1 and 2). Surface complementarity analysis between wild-type sBCMA, sBCMA V3, hAPRIL, and hBAFF was performed. We found that the H19Y mutation improved surface complementarity of sBCMA V3 toward both hAPRIL and hBAFF (Table 3). In its cocomplex form, the H19Y mutation shortened the intramolecular distance between sBCMA and hAPRIL. Similarly, the intramolecular distance between sBCMA V3 and hBAFF was also reduced, corresponding to a tighter binding cocomplex structure (Table 3).

To establish the therapeutic potency of affinity-enhanced mutant clone sBCMA V3 in models of MM and B cell malignancies, we first generated a sBCMA V3 + hIgG1 fusion protein (sBCMA-Fc V3) for improved stability and bioavailability. The pharmacokinetics of sBCMA-Fc V3 was validated in *NOD-scid* immunocompromised non–tumor-bearing mice. A single dose of 10 mg/kg sBCMA-Fc V3 injected into non–tumor-bearing animals completely suppressed the level of APRIL and BAFF within 30 min. Over time, sBCMA-Fc V3 showed an inhibitory half-life of ∼20 h with APRIL suppression (Fig. 5 C) and 60 h with BAFF inhibition (Fig. 5 D). This finding is consistent with the half-life of human decoy receptors in mice reported previously (Kariolis et al., 2017; Miao et al., 2021). Inhibition of APRIL and BAFF is known to suppress B cell–mediated immunoglobulin class switching, leading to decreased Ig levels (Castigli et al., 2004; Castigli et al., 2005; Grasset et al., 2020). Here, we examined the expression of IgM, IgA, and IgG in mouse serum after a single 10-mg/kg dose of sBCMA-Fc V3. A transient reduction of IgM, IgA, and IgG was observed within 48 h after treatment and returned to predosing level within 7 d, suggesting this treatment effect is reversible (Fig. 5, E–G).

To investigate whether sBCMA-Fc V3 can improve antitumor activity in MM models compared with wild-type sBCMA-Fc, we tested various doses of wild-type sBCMA-Fc or sBCMA-Fc V3 on MM tumor growth. A significant improvement in antitumor activity was observed in sBCMA-Fc V3–treated groups but not in wild-type treated with sBCMA-Fc at lower doses (Fig. 5 H). Interestingly, the antitumor affects were comparable when animals were treated with both molecules at a higher dose of 10 mg/kg, suggesting that both treatments reached a plateau in achieving ligand/receptor inhibition (Fig. S5 E). Because MM progression is primarily APRIL driven, sBCMA-Fc V3 with enhanced APRIL binding resulted in more efficient APRIL neutralization at lower concentration.

Next, we investigated whether sBCMA-Fc V3 with a 500-fold improvement in its binding affinity to BAFF (9 pM) would increase antitumor activity in BAFF-driven DLBCL models. sBCMA-V3 Fc–mediated inhibition of BAFF signaling pathway was evaluated in vitro in BAFF-dependent SU-DHL-6 and Daudi DLBCL cell lines. sBCMA-Fc V3 treatment effectively reduced DLBCL cell growth in a dose-dependent manner, suggesting these cells rely on BAFF for growth and survival (Fig. 5 I). Treatment with sBCMA-Fc V3 also led to decreased expression of pAKT, p38-MAPK, and pNF-κB p65, all of which are critical molecular components of the BCMA/TACI/BAFF-R canonical signaling pathway that governs malignant B cell growth (Hatzoglou et al., 2000; Fig. S5 G). To determine the therapeutic efficacy of sBCMA-V3 Fc in vivo, SU-DHL-6 and Daudi tumor models were established by subcutaneous engraftment in *NOD-scid* mice. Animals were treated with 5 or 10 mg/kg of sBCMA-Fc V3 and compared with the vehicle control. In both DLBCL tumor models, sBCMA-Fc V3 treatment resulted in significant dose-dependent reduction in tumor size (Fig. 5, J and K). To further study the therapeutic potential of wild-type sBCMA-Fc compared with sBCMA-Fc V3 in DLBCL treatment, we evaluated the growth kinetics of SU-DHL-6 tumors treated with higher doses of wild-type sBCMA-Fc, at 10 and 20 mg/kg. Similar to what we observed in previous studies (Fig. 3 K), 10 mg/kg wild-type sBCMA-Fc had little effect on tumor growth, but tumor reduction was observed in the 20 mg/kg treatment group (Fig. S5 F). These data provide further evidence that wild-type sBCMA-Fc has suboptimal BAFF neutralizing capabilities and requires significantly higher concentrations to inhibit BAFF and DLBCL tumor growth.

To further investigate the therapeutic efficacy of sBCMA-Fc V3, we compared it to other therapeutic agents known to inhibit BAFF in a head-to-head study. These other agents were a recombinant soluble TACI-Fc (sTACI-Fc) decoy receptor that binds APRIL and BAFF at 6.4 nM and 160 pM, respectively (Wu et al., 2000), as well as an antibody against BAFF (αBAFF Ab) with a K_D of 0.995 nM and no reported binding to APRIL (Shin et al., 2018). The clinical versions of both molecules are currently used for the treatment of various B cell–related autoimmune diseases (Bag-Ozbek and Hui-Yuen, 2021; Barratt et al., 2020; Lee and Amengual, 2020). In this study, we compared the antitumor efficacy of sBCMA-Fc V3, sTACI-Fc, αBAFF Ab, and wild-type

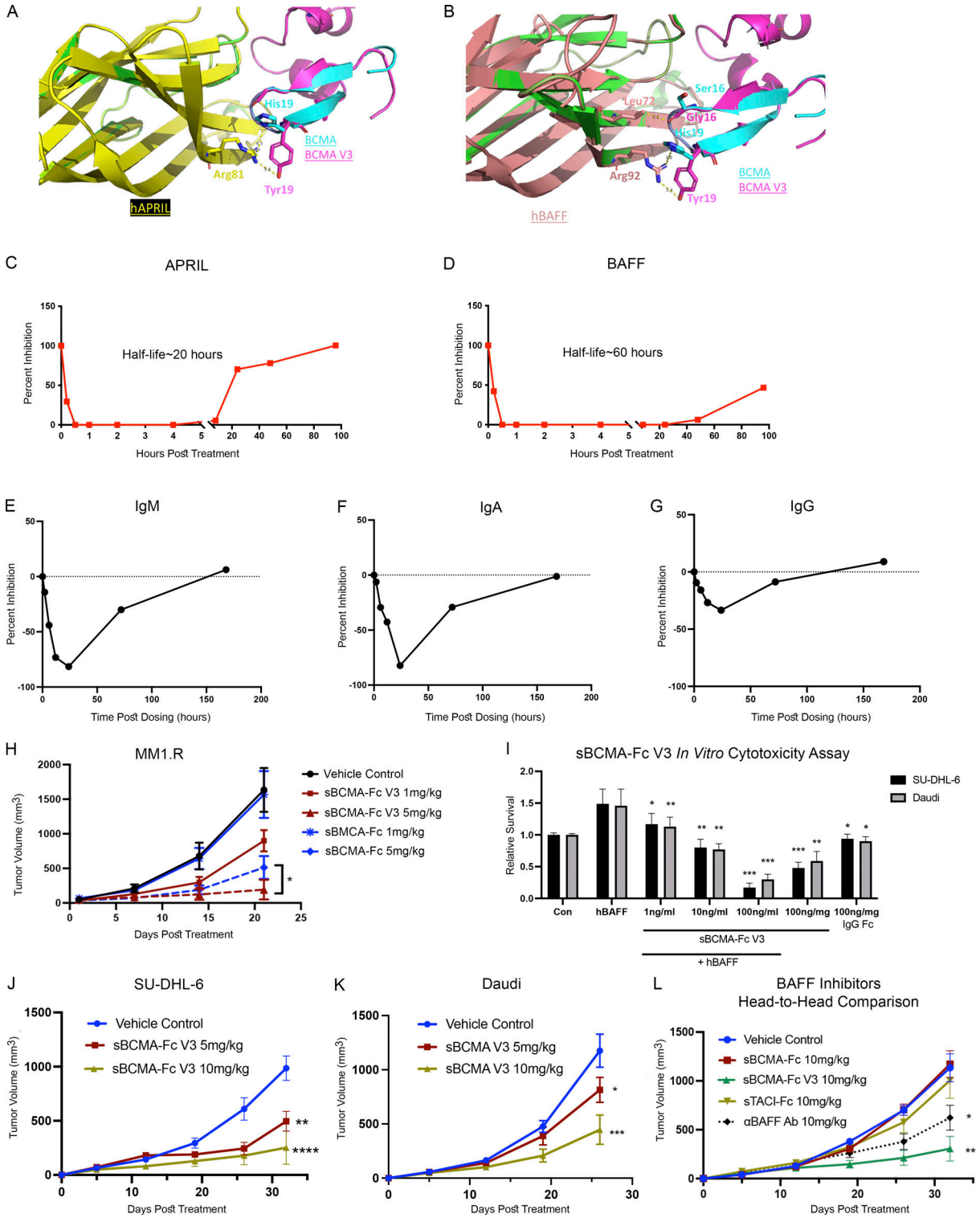

Figure 5. **Structural and biological characterization of affinity-enhanced sBCMA-Fc V3. (A)** Computational modeling of sBCMA V3 mutant clone (magenta) in cocomplex with hAPRIL (yellow) overlaying on PDB structure 1XU2 consisting of hBCMA (cyan) in cocomplex with mAPRIL (green). Predicted binding interaction between hAPRIL (yellow) and sBCMA V3 (cyan) showing Arg81 on hAPRIL interacting with H19Y on sBCMA V3. **(B)** Computational modeling of sBCMA V3 mutant clone (magenta) in cocomplex with hBAFF (salmon) overlaying on PDB structure 1XU2 consisting of human BCMA (cyan) in cocomplex with mAPRIL (green). Predicted binding interaction between hBAFF (salmon) and sBCMA V3 (cyan) showing Arg93 on hBAFF interacting with H19Y on sBCMA V3. **(C)** Serum level of APRIL in mouse serum after a single dose of sBCMA-Fc V3 at 10 mg/kg. Each data point represents duplicate repeats collected at each time point. **(D)** Serum level of BAFF in mouse serum after a single dose of sBCMA-Fc V3 at 10 mg/kg. Each data point represents duplicated repeats collected at each time point. **(E)** Mouse serum IgM levels after sBCMA-Fc V3 treatment. **(F)** Mouse serum IgA levels after sBCMA-Fc V3 treatment. **(G)** Mouse serum IgA levels after sBCMA-Fc V3 treatment. **(H)** Subcutaneous tumor growth of MM1.R MM tumors in 6-wk-old female NSG mice dosed with wild-type sBCMA-Fc at 1 and

5 mg/kg every 48 h (n = 5), sBCMA-Fc V3 at 1 and 5 mg/kg every 48 h (n = 5), and vehicle control (n = 5). MM1.R tumors treated with sBCMA-Fc V3 showed significant reduction in tumor growth compared with sBCMA-Fc treatment at the same concentration; P = 0.0365. **(I)** sBCMA-Fc V3 dose-dependent cytotoxicity assay validating the in vitro cell survival in the presence of increasing doses of sBCMA-Fc V3 and hBAFF (100 ng/ml) in SU-DHL-6 and Daudi DLBCL cells (P = 0.032; 1 ng/ml; P = 0.075, 10 ng/ml; P = 0.0001, 100 ng/ml). Cells were maintained in low (3%) FCS to reduce possible growth stimulation mediated through other growth factors present in FCS. Each sample was performed in triplicate. **(J)** Subcutaneous tumor growth of SU-DHL-6 DLBCL tumors in 6-wk-old female *NOD-scid* mice dosed with 5 or 10 mg/kg sBCMA-Fc V3 every 48 h (n = 5) and vehicle control (n = 5), P < 0.0001. **(K)** Subcutaneous tumor growth of Daudi DLBCL tumors in 6-wk-old female *NOD-scid* mice dosed with 5 or 10 mg/kg sBCMA-Fc V3 every 48 h (n = 5) and vehicle control (n = 5); P = 0.0001. **(L)** In vivo head-to-head comparison of antitumor efficacies in subcutaneous SU-DHL-6 DLBCL tumors treated with 10 mg/kg wild-type sBCMA-Fc every 48 h (n = 5), 10 mg/kg sBCMA-Fc V3 every 48 h (n = 5; P < 0.0001), 10 mg/kg sTACI-Fc every 48 h (n = 5), and 10 mg/kg αBAFF antibody twice a week (n = 5). Subcutaneous tumor growth was monitored throughout the study. Statistical analysis was conducted using t test and one-way ANOVA for comparing between treatment groups. Repeated ANOVA used for changes in tumor growth over time. *, P < 0.05; **, P < 0.01; ***, P < 0.001.

sBCMA-Fc in SU-DHL-6 DLBCL tumors. All therapeutic groups were treated with the same dose of 10 mg/kg, three times per week for decoy receptors and two times per week for antibody. We found that sBCMA-Fc V3 treatment resulted in significant and robust tumor reduction compared with vehicle treatment. In comparison, sTACI-Fc–treated groups showed a trend toward reduced tumor growth that did not reach statistical significance. In contrast, αBAFF Ab–treated animals showed a modest and statistically significant reduction in tumor growth. Consistent with our previous observation, wild-type sBCMA-Fc did not show significant therapeutic benefit, owing to insufficient BAFF binding (Fig. 5 L).

In summary, sBCMA-Fc V3 with enhanced binding affinity to APRIL and BAFF resulted in better antitumor activity in both APRIL-driven MM and BAFF-driven DLBCL models. In particular, compared with wild-type sBCMA-Fc, sTACI-Fc, and αBAFF Ab, sBCMA-Fc V3 treatment resulted in superior antitumor efficacy in a DLBCL model, likely driven by its strong binding toward BAFF. This observation further supports the therapeutic potential of sBCMA-Fc V3 as a treatment for MM and DLBCL.

sBCMA-Fc V3 demonstrates adequate toxicity profile and on-target mechanism of action in nonhuman primates

Nonhuman primate toxicity studies are particularly useful because primates often respond in a physiologic manner similar to humans. To evaluate the translational potential of sBCMA-Fc V3, we conducted a single-dose toxicity study in cynomolgus monkeys to investigate drug-mediated acute toxicity after i.v. infusion of sBCMA-Fc V3.

One animal from each sex was assigned in each of five groups and given a single i.v. infusion of sBCMA-Fc V3 (0.1, 1, 10, and 100 mg/kg) or vehicle (Table 4). Animals were observed for 2 wk before and 6 wk after treatment. Parameters evaluated include body weight, food consumption, hematology, lymphocyte immunophenotype, immunoglobulin production, and gross pathology. Blood samples were collected from each animal on days −13, −6, −3, and 1 before dosing and days 2, 7, 14, and 42 during dosing. Overall, there was no unscheduled deaths in the study, and no drug-related abnormalities of body weight or food consumption were observed for the animals in any group during the observation period (Fig. 6 A). Hematology analysis showed modest declines of RBC, hemoglobin (HGB), and hematocrit (HCT) in female and male monkeys of each group on days 2, 7, and/or 14 (Tables S6, S7, S8, and S9). However, after factoring in the total volume of blood sampled during the experiment, it was likely that the decreases in RBC, HGB, and HCT were related to blood sampling. No other hematological abnormalities were observed. Upon lymphocyte analysis, we observed a dose-dependent, transient reduction in total lymphocyte numbers in female monkeys on day 7 after dose followed by a full recovery by day 14. A similar but less significant trend was observed in male monkeys (Fig. 6 B). We further investigated B lymphocyte subpopulations, including $CD19^+$ pan B cells and $CD20^+$ mature B cells in male (Fig. 6 C) and female (Fig. 6 D) monkeys, with no significant changes observed in any treatment group. No gross abnormal tissue pathology was present in animal tissues examined during necropsy.

A dose-dependent reduction in immunoglobulin pharmacodynamic markers was established in nonhuman primates treated with sBCMA-Fc V3, which led to a reduction in IgA in both male and female monkeys over time. To a lesser extent, a similar result was observed with IgM and IgG (Fig. 6 E). Consistent with our previous observation in mice (Fig. 5, E–G), these observations confirmed the on-target mechanism of sBCMA-Fc V3

Table 1. **Calculated binding affinity and protein stability (in kcal/mol) for each BCMA mutation in cocomplex with APRIL**

Residue	Original	Mutated	Δ Affinity	Δ Stability (solvated)	Total ΔG value (original/mutated)
R:16	SER	ALA	−0.13	−1.78	N/A
R:19	HIS	TYR	−3.95	−3.59	N/A
R:36	THR	ALA	−0.22	4.91	N/A
R:16 R:19 R:36	SER HIS THR	ALA TYR ALA	−5.85	−1.19	−4.333/−33.041

N/A, not applicable.

Table 2. **Calculated binding affinity and protein stability (in kcal/mol) for each BCMA mutation in cocomplex with BAFF**

Residue	Original	Mutated	Δ Affinity	Δ Stability (solvated)	Total ΔG value (original/mutated)
R:36	THR	ALA	−0.14	4.98	N/A
R:19	HIS	TYR	−7.73	−7.52	N/A
R:16	SER	GLY	1.38	1.03	N/A
R:16 R:19 R:36	SER HIS THR	GLY TYR ALA	−3.55	2.8	−17.462/−19.858

N/A, not applicable.

on APRIL- and BAFF-mediated immunoglobulin production and class switching, confirming that the inhibition of APRIL/BAFF-mediated signaling can decreased immunoglobulin production in MM (Fig. 1 J). This finding supports our hypothesis that sBCMA-Fc V3 is a potent APRIL and BAFF inhibitor for the treatment of B cell–driven diseases in oncology and beyond.

Discussion

The aberrant activation of APRIL and BAFF leads to dysregulated B cell growth; therefore, they are attractive therapeutic targets for B cell malignancies and autoimmune diseases (Bolkun et al., 2014; Briones et al., 2002; Carpenter et al., 2013; Chiu et al., 2007). However, the multifaceted ligand/receptor interactions between APRIL and BAFF and their receptors BCMA, BAFF-R, and TACI are particularly challenging to overcome. Past strategies have used ligand neutralization approaches with monoclonal antibodies or decoy receptors for BCMA, BAFF-R, and TACI in a limited number of disease applications (Rossi et al., 2009; Shrestha et al., 2021; Tai and Anderson, 2019). We hypothesized that a soluble BCMA decoy receptor with endogenous, strong affinity to APRIL can successfully target APRIL-driven MM tumors despite the heterogenous cytogenetic profile of MM. However, we found that this same sBCMA-Fc is ineffective against BAFF-driven DLBCL because of its weak binding to BAFF. To overcome the affinity barrier, we used a yeast surface display-based protein engineering approach and generated mutant sBCMA clones with ultra-high binding affinity against both APRIL and BAFF. The resultant therapeutic candidate sBCMA-Fc V3 showed superior antitumor activities for both APRIL-driven MM and BAFF-driven DLBCL, with a desirable safety profile.

The biological dependence of BCMA signaling on MM cell is known, but it is more commonly used as a pan-MM surface marker for targeted delivery of cytotoxic therapeutics (Tai and Anderson, 2019). Here, we provide new insight into the global translational landscape of MM cells upon the loss of BCMA and identify a distinct subgroup of proteins that are translationally controlled, which otherwise would not be detected by measuring changes in total mRNA transcripts (Cenik et al., 2015; Ingolia et al., 2019). Specifically, ATMIN (ATM-interacting protein, ASCIZ) was one of the proteins translationally regulated by BCMA. While ATMIN plays an important role in the DNA damage response (McNees et al., 2005), in B cells, ATMIN can interact with dynein light chain subunit (Dynll1) in an ATM-independent manner (Jurado et al., 2012a; Jurado et al., 2012b). In addition, recent reports indicate that ATMIN and Dynll1 are involved in the development of B cell lymphoma, providing a link between dysregulated B cell development, BCMA, and ATMIN signaling in MM (Jurado et al., 2012b). While our ribosome profiling has identified a subset of cellular proteins regulated by BCMA signaling, we have identified ATMIN as a new target of BCMA that is regulated in a translation-specific manner and is important for MM viability. However, while it is beyond the scope of the study, the causal relationship between BCMA knockdown, altered cell proliferation. and impaired protein translation remain to be fully elucidated and warrants further investigation.

To improve sBCMA binding toward BAFF, we generated a high-affinity mutant sBCMA V3 with low picomolar binding toward both APRIL and BAFF. Computational structural analysis revealed that H19Y on sBCMA V3 contributed toward enhanced binding to both ligands. Although H19 was previously reported

Table 3. **Calculated surface complementarity and molecular distance between BCMA V3 and APRIL/BAFF**

Site in BCMA	Surface complementarity to hAPRIL		Distance to hAPRIL		Surface complementarity to hBAFF		Distance to hBAFF	
	WT	Single mutant	WT	Single mutant	WT	Single mutant	WT	Single mutant
S16G	0.65	0.51	N/A	N/A	0.76	0.76	3.2 Å (to Leu72)	3.2 Å (to Leu72)
H19Y	0.88	0.21	3.8 Å (to Arg81)	2.1 Å (to Arg81)	0.88	0.2	3.7 Å (to Arg92)	2.0 Å (to Arg92)
T36A	0.00	0.00	N/A	N/A	N/A	N/A	N/A	N/A

N/A, not applicable.

Table 4. **sBCMA-Fc V3 single-dose toxicology study design**

Group	Number of animals		Animal number		Treatment	Dose level (mg/kg)	Concentration (mg/ml)	Dose volume (ml/kg)
	Male	Female	Male	Female				
1	1	1	1,101	2,102	Vehicle	0	0	10
2	1	1	1,203	2,204	sBCMA-Fc V3	0.1	0.01	10
3	1	1	1,305	2,306	sBCMA-Fc V3	1	0.1	10
4	1	1	1,407	2,408	sBCMA-Fc V3	10	1	10
5	1	1	1,509	2,510	sBCMA-Fc V3	100	10	10

Body weight recording: predose days −14, −6; after-dose days 1, 2, 7, 14, 21, 28, 35, and 42. Blood sample collection: predose days −13, −16, 1; after-dose days 2, 7, 14, and 42.

as an important residue for binding between BCMA and BAFF, its interaction with APRIL was not described (Bossen and Schneider, 2006). Furthermore, the H19Y mutation was selected from APRIL-driven affinity maturation, indicating that H19Y on BCMA is a highly desirable mutation for achieving stronger binding to both APRIL and BAFF. This finding provides the impetus to solve the crystal structures of sBCMA V3 in co-complex with APRIL and BAFF, which may provide additional biophysical evidence to explain how these mutations provide affinity enhancement. Therapeutically, enhancement in BAFF binding and its associated structural modifications shifted the treatment paradigm of sBCMA-Fc from a treatment selective for

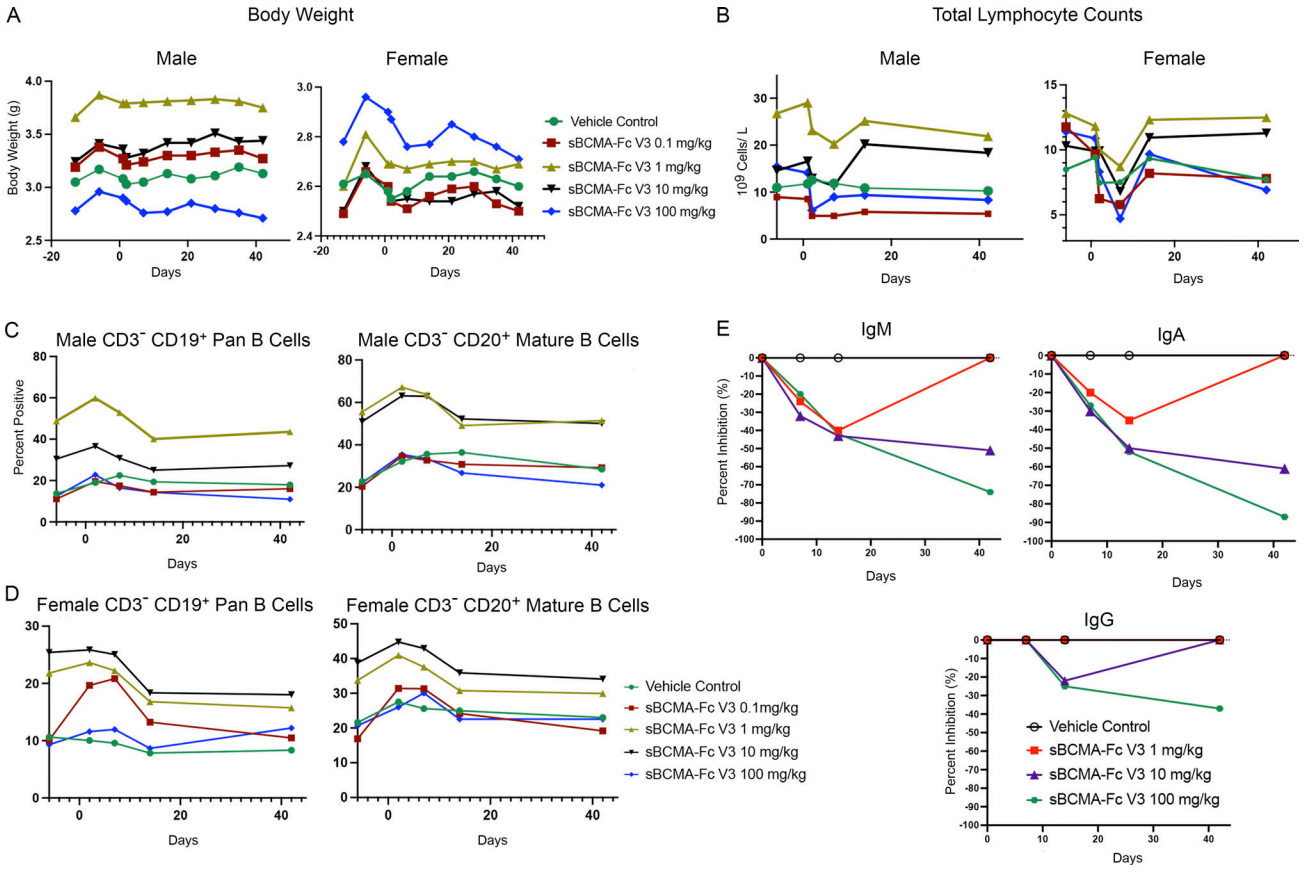

Figure 6. **sBCMA-Fc V3 demonstrates adequate toxicity profile and on-target mechanism of action in nonhuman primates. (A)** Changes in total body weight in kilograms of male (left) and female (right) cynomolgus monkey test subjects throughout the experiment and observation period. **(B)** Total lymphocyte counts expressed as 10^9 cells/liter in the blood of male (left) and female (right) cynomolgus monkey test subjects. **(C)** Counts of $CD3^-CD19^+$ pan B lymphocytes (left) and $CD3^-CD20^+$ mature B lymphocytes in the peripheral blood of male cynomolgus monkey test subjects throughout the experimental period. **(D)** Counts of $CD3^-CD19^+$ pan B lymphocytes (left) and $CD3^-CD20^+$ mature B lymphocytes in the peripheral blood of male cynomolgus monkey test subjects throughout the experimental period. **(E)** Levels of IgM, IgA, and IgG levels in female cynomolgus monkey throughout the experimental period. Statistical analysis not applicable.

MM to a therapeutic candidate suited for targeting multiple B cell–driven diseases. The biological function of BAFF and APRIL is not limited to B cell malignancy but extends to autoimmune disorders and other diseases triggered by pathological B cells, suggesting a much broader clinical indication for sBCMA-Fc V3 (Samy et al., 2017).

Treatment with sBCMA-Fc V3 was found to be well tolerated in a single-dose toxicity study conducted in cynomolgus monkeys. More importantly, a dose-dependent reduction in immunoglobulin production was observed, likely due to inhibition of APRIL- and BAFF-driven Ig class switching. Furthermore, a greater depletion of IgA was observed in animals treated with sBCMA-Fc V3. Considering that a previous study showed the impact of BAFF and APRIL on mouse IgA response in the gut (Grasset et al., 2020), which is the primary site of IgA production, the modulatory effect of sBCMA-Fc V3 on gut-associated IgA production warrants further investigation. Overall, these data provide an explanation for the inhibition of BCMA signaling leading to reduced abnormal immunoglobulin production, a key feature of MM pathogenesis. In summary, sBCMA-Fc V3 was found to be safe and well tolerated in all treated animals for ≤42 d, with no significant clinical or pathological abnormality observed at a dose ≤100 mg/kg. Hence, the maximal tolerated single dose is >100 mg/kg.

The development of BCMA-directed CAR-Ts, antibody–drug conjugates, and bispecific antibodies have enjoyed considerable clinical success with a subset of patients reporting complete remission after treatment. Unfortunately, dose-limiting normal tissue toxicity—including cytokine storm syndrome, peripheral neuropathy, and ocular toxicity—remains a major clinical challenge in this group of treated patients. Additionally, elderly patients are often excluded from both CAR-T and antibody–drug conjugate treatments owing to their poor overall health, representing a critically unmet clinical need within this population (Caimi et al., 2021; Lonial et al., 2020; Raje et al., 2019). Therefore, new efficacious therapeutics with favorable safety and tolerability profiles are needed for treating patients ineligible for both frontline and new investigational MM and DLBCL therapies associated with high drug-related toxicity. The activation of APRIL- and BAFF-mediated signaling through BCMA, TACI, and BAFF-R provides prosurvival signals to sustain MM and DLBCL growth.

In this study, we developed a high-affinity sBCMA-Fc V3 trap for both APRIL and BAFF exhibiting superior antitumor activities in models of MM and DLBCL. More importantly, sBCMA-Fc V3 has a favorable safety profile and on-target mechanism of action in both murine and nonhuman primate models. Collectively, these data support sBCMA-Fc V3 as a clinically viable candidate for the treatment of APRIL- and BAFF-driven B cell malignancies and autoimmune disease.

Materials and methods

Study approval

This study was designed to characterize the therapeutic efficacy and biological functionality of engineered soluble BCMA decoy receptor as a treatment for APRIL- and BAFF-driven MM and DLBCL. MM and DLBCL patient specimens were collected from patients treated at Stanford Cancer Center under the approval of Stanford institutional review board (protocol no. 13535). Healthy blood specimens were obtained from Stanford Blood Center under the same institutional review board protocol. In vivo animal studies were conducted under the approval of AAAPLAC at Stanford University. Sample sizes for animals were determined based on previously conducted in vivo studies for power calculations. All animals were randomly assigned to treatment groups. Samples were not excluded from studies except for animals that required early termination due to unforeseeable illness unrelated to the study. Endpoints of experiments were defined in advance for each experiment. Tumor growth curves were presented for studies where tumor growth was measurable, serum levels of myeloma protein levels were used as a marker of tumor progression in MM orthotopic PDX model, and Kaplan–Meier analysis was used to define survival advantages in the PDX study; all other studies with measurable subcutaneous tumor used final tumor growth as study endpoint. Appropriate statistical analysis was used for each study.

Primate toxicology studies

The purposes of this study were to evaluate acute toxicity after single administration of sBCMA-V3 via i.v. infusion in cynomolgus monkeys, to provide the maximum tolerated dose as reference for the design of subsequent toxicity studies and clinical trials, and to characterize the toxicokinetics and immunogenicity. This study was contracted to the Center for Drug Safety Evaluation and Research, Shanghai Institute of Materia Medica, Chinese Academy of Sciences, Shanghai, PR China. This study was approved by the Center for Drug Safety Evaluation and Research–Shanghai Institute of Materia Medica ethics committee for experimental usage and performed under the guidelines of the National Medical Products Administration: Guideline on Single Dose Toxicity Studies for Pharmaceuticals, May 2014; National Medical Products Administration: General Guideline on Non-clinical Safety Evaluation for Therapeutic Biological Products, January 2007; International Council for Harmonisation (ICH) Guideline M3 (R2): Guideline on Non-clinical Safety Studies for the Conduct of Human Clinical Trials and Marketing Authorization for Pharmaceuticals; CPMP/ICH/286/95, June 2009; and ICH S6 (R1): Guideline on Preclinical Safety Evaluation of Biotechnology-Derived Pharmaceuticals, June 2011. Justification for selection of animal species, number of animals and route of administration is as follows: (1) the cynomolgus monkey is considered an appropriate nonrodent species for safety evaluation of sBCMA-Fc V3; (2) the minimum number of animals used in this study meets the requirements of scientific evaluation of the toxicity of the test article; and (3) sBCMA-Fc V3 was administered via i.v. infusion in this study because i.v. administration is the intended administration route in humans.

Cell lines

Human MM cell lines U266, MM1.R, and INA6 were maintained in RPMI-1640 supplemented with 10% FBS and 1% penicillin/streptomycin in standing flasks and a humidified 37°C, 5% CO_2 incubator. INA6 cells were supplemented with 2 ng/ml human

IL-6 to maintain growth. All cell lines were generously given by A.C. Koong and D. Jiang at the Department of Radiation Oncology, MD Anderson Cancer Center (Houston, TX). Isolation of B cells from healthy donors and MM patients was performed using EasySep Human B-Cell Isolation Kit according to the manufacturer's protocol (cat. no. 17954; Stemcell Technologies). DLBCL cells SU-DHL-6 and Daudi were purchased from ATCC (cat. no. CRL-2959 and CCL-213; ATCC).

Establishing MM PDX models using MM patient specimens

Mononuclear cells were isolated from bone marrow aspirate of MM patients and inoculated into the left tibias of 5–6-wk-old NSG mice. The injection path into the tibia was established using an empty needle penetrating through the tibia bone, guided by x ray. The empty needle was removed, and the x ray was turned off to avoid MM cell exposure to radiation. Patient cells were inoculated using a fresh needle and syringe. MM tumor growth was monitored by serum level of human IgG (M) protein. Once the host mice showed successful engraftment, marked by an increase of serum human IgG levels, the animal was sacrificed, bone marrow was flushed, and mononuclear cells were collected for intratibial injection into two host mice. This process was repeated until sufficient numbers were reached for each study. 11 patient samples were inoculated, and 2 patient samples were successfully propagated for in vivo studies.

In vivo studies

All animal experiments were reviewed and approved by the Institutional Animal Care and Use Committee at Stanford University. Female NOD-*scid* γ mice aged 6–8 wk were purchased from the Jackson Laboratory (stock no. 005557) and used for all in vivo analysis throughout the study. Mice were housed in a pathogen-free animal facility, kept under a controlled environment with 12-h light–dark cycles. For INA6 and MM1.R tumor studies (dox-inducible BCMA KO, WT sBCMA-Fc, and sBCMA-Fc V3), 1×10^7 cells were injected s.c. with 50% growth factor–reduced Matrigel (cat. no. 356230; Corning). Body weight and tumor growth were measured three times a week until study termination. Animals were terminated when the subcutaneous tumor reached the ethical termination point. For PDX studies, nonterminal bleeding was performed on animals every 14 d for evaluating serum M protein as a marker of tumor progression. Animals were terminated at signs of physical distress. For DLBCL tumor studies, female NOD-*scid* γ mice aged 6–8 wk were purchased from the Jackson Laboratory (stock no. 001303). Mice were housed in the same pathogen-free animal facility as mice for MM studies. For SU-DHL-6 and Daudi tumor studies, 5×10^6 cells were injected subcutaneously with 50% growth factor–reduced Matrigel. Body weight and tumor growth were measured once a week until study termination. Wild-type sBCMA-Fc and sBCMA-Fc V3 were manufactured by ChemPartner Shanghai using HEK293 transient expression and a protein G purification system. Purified material was assessed by size exclusion chromatography HPLC and SDS-PAGE for quality control. αCD38 antibody (cat. no. A2027) was purchased from SelleckChem, recombinant mouse soluble TACI-Fc (cat. no. 577708) from BioLegend, and αBAFF antibody from Invitrogen (cat. no. MA1-822774; Thermo Fisher Scientific).

Ribo-seq RNA library preparation

Briefly, snap-frozen cell pellets (100 million cells per sample) were lysed in polysome lysis buffer (20 mM Tris-HCl, pH 7.5, 250 mM NaCl, 15 mM $MgCl_2$, 1 mM dithiothreitol, 0.5% Triton X-100, 0.024 U/ml TurboDNase, 0.48 U/ml RNasin, and 0.1 mg/ml cycloheximide [CHX]). Lysates were centrifuged for 10 min at 4°C, 14,000 *g*. The supernatant was used for isolation of ribosome-bound mRNA and total mRNA-seq. SUPERase-In (0.24 U/ml) was added to the lysate used for polysome fractionation to prevent RNA degradation. Library preparation was performed using SMARTer smRNA-Seq Kit for Illumina (cat. no. 635029; Takara Bio).

Ribo-seq analysis

The sequencing files for ribosome profiling and RNA-seq data were processed using RiboFlow (Ozadam et al., 2020). All source code is freely available at https://github.com/ribosomeprofiling. Briefly, the 3′ adapter sequence (AAAAAAAAAA) was removed from all reads using cutadapt. The 5′ end of each read includes three bases from the template switching reaction and was also removed before alignment. We used a sequential alignment strategy to first filter out rRNA and tRNA mapping reads, followed by mapping to representative isoforms for each as defined in the APPRIS database (Rodriguez et al., 2018). Next, PCR duplicates were removed from the ribosome profiling data using the 5′ end of the sequence alignment coordinates. Finally, the resulting information was compiled into a ribo file (Ozadam et al., 2020) for downstream analyses. Data obtained from Ribo-seq analysis can be accessed through the GEO repository with accession number GSE206045.

Bioinformatic analysis

All statistical analyses were carried out using RiboR (Ozadam et al., 2020). For quantification of ribosome occupancy, footprints of length 26 to 30 nucleotides inclusive were used. Metagene plots were generated using the 5′ end of each ribosome footprint. Ribosome occupancy and RNA-seq data were jointly analyzed, and transcript specific dispersion estimates were calculated after trimmed mean of the M-value (TMM) normalization (Robinson and Oshlack, 2010). To identify genes with differential translation efficiency, we used a generalized linear model that treats RNA expression and ribosome occupancy as two experimental manipulations of the RNA pool of the cells as previously described (Cenik et al., 2015). The model was fitted using edgeR (Robinson and Oshlack, 2010), and P values were adjusted for multiple hypothesis testing using Benjamini–Hochberg correction.

We used an adjusted P value threshold of 0.05 to define significant differences. R packages cowplot, pheatmap, EnhancedVolcano, ggpubr, ggplot2, and reshape2 were used for analyses and plotting (Kassambara and Moreaux, 2018).

Polysome analysis

U266 cells were transfected with siScramble and siBCMA as described. Cells were pelleted and lysed in buffer (20 mM Tris-HCl,

pH 7.4, 100 mM NaCl, 5 mM $MgCl_2$, 1 mM dithiothreitol, 1% Triton X-100, 0.1% NP-40, 100 µg/ml CHX, 20 U/ml TurboDNase I, and complete protease inhibitor EDTA-free) in nuclease-free water. After lysis, RNA concentrations were measured using a Nanodorop UV spectrophotometer, and normalized amounts of RNA were layered onto a sucrose gradient (25–50% sucrose [wt/vol], 20 mM Tris-HCl, pH 7.4, 100 mM NaCl, 15 mM $MgCl_2$, and 100 µg/ml CHX) in nuclease-free water and centrifuged in a SW41Ti rotor (Beckman) for 2.5 h at 40,000 rpm at 4°C. 16 fractions were collected by the Density Gradient Fraction System (Brandel). To each fraction, 0.1 ml of 10% SDS was added and mixed. 0.1 ml of 3 M NaOAc, pH 5.5, and 0.1 ml of water were added to each SDS-containing fraction. For normalization, 500 pg of bicistronic firefly luciferase mRNA was added to each fraction.

Total RNA from each fraction was extracted using acid-phenol:chloroform. Briefly, to each fraction, 900 µl of acid-phenol:chloroform was added and mixed thoroughly. The mixture was heated at 65°C for 5 min and centrifuged at 21,000 *g* for 10 min at room temperature. The aqueous phase (700 µl) was removed and precipitated overnight at −80°C with 700 µl isopropanol and 1.5 µl GlycoBlue Coprecipitate (Invitrogen). The samples were centrifuged at 21,000 *g*, 30 min, 4°C; the supernatant was discarded; and the RNA pellet was washed twice with 500 µl of cold 75% ethanol. Pellets were dried for 15 min at room temperature and resuspended in nuclease-free water. Total RNA from each fraction was treated with 2 U/µl TurboDNase I and incubated at 37°C for 30 min, and the column was purified using RNA Clean and Concentrator-5 (Zymo) according to the manufacturer's instructions. RNA was eluted twice in 6 µl. Except for the first fraction (F1), RNA was pooled from every three subsequent fractions (F2–4, F5–7, F8–10, F11–13, and F14–16) and measured using Nanodorop UV spectrophotometer.

For quantitative RT-PCR, 600 ng of purified RNA was used for reverse transcription with the iScript supermix (Bio-Rad) according to the manufacturer's instructions. See RT-PCR protocol for primer sequences.

Synthesis of yeast-displayed sBCMA library

DNA encoding human BCMA extracellular domain, amino acids Met1–Ala54, was cloned into the pCT yeast display plasmid using NheI and BamHI restriction sites. An error-prone library was created using the BCMA extracellular domain DNA as a template, and mutations were introduced by using low-fidelity Taq polymerase (Invitrogen, Thermo Fisher Scientific) and the nucleotide analogs 8-oxo-dGTP and dPTP (TriLink Biotech). Six separate PCR reactions were performed in which the concentrations of analogs and the numbers of cycles were varied to obtain a range of mutation frequencies: five cycles (200 µM), 10 cycles (2, 20, or 200 µM), and 20 cycles (2 or 20 µM). Products from these reactions were amplified using forward and reverse primers, each with 50-bp homology to the pCT plasmid in the absence of nucleotide analogs. Amplified DNA was purified using gel electrophoresis, and the pCT plasmid was digested with NheI and BamHI. Purified mutant cDNA and linearized plasmids were electroporated in a 5:1 ratio by weight into EBY100 yeast, where they were assembled in vivo through homologous recombination. Library size was estimated to be 2×10^8 by dilution plating.

Library screening

Yeast displaying high-affinity BCMA mutants were isolated from the library using FACS. For FACS round 1, equilibrium binding sorts were performed in which yeast were incubated at room temperature in PBS with 0.1% BSA (PBSA) with 2 nM APRIL (PeproTech) for 24 h. After incubation with APRIL, yeast were pelleted, washed, and resuspended in PBSA with a 1:100 mixture of anti-c-Myc FITC antibody (Abcam) and anti-HA AF647 (Invitrogen) for 1 h at 4°C. Yeast were then washed, pelleted, and resuspended using PBSA followed by FACS analysis. For FACS rounds 2–6, kinetic off-rate sorts were conducted in which yeast were incubated with 2 nM APRIL for 3 h at room temperature, washed twice to remove excess unbound APRIL, and resuspended in PBSA containing an ∼50-fold molar excess of BCMA to render unbinding events irreversible. The length of the unbinding step was as follows: sort 2, 48 h; sorts 3, 4, and 5, 72 h; and sort 6, 84 h, with all unbinding reactions performed at room temperature. During the last hour of the dissociation reaction, cells were mixed with a 1:100 mixture of anti-c-Myc FITC antibody (Abcam) and anti-HA AF647 (Invitrogen) for 1 h at 4°C. Yeast were pelleted, washed, and resuspended in 0.1% BSA. Labeled yeast were sorted by FACS using a Vantage SE flow cytometer (Stanford FACS Core Facility) and CellQuest software (Becton Dickinson). Sorts were conducted such that the 1–3% of clones with the highest APRIL binding/c-Myc expression ratio were selected, enriching the library for clones with the highest binding affinity to APRIL. In sort 1, 10^8 cells were screened, and subsequent rounds analyzed a minimum of 10-fold the number of clones collected in the prior sort round to ensure adequate sampling of the library diversity. Selected clones were propagated and subjected to further rounds of FACS. After sorts 3, 4, 5, and 6, plasmid DNA was recovered using a Zymoprep kit (Zymo Research Corp.), transformed into DH5a supercompetent cells, and isolated using plasmid miniprep kit (Qiagen). Sequencing was performed by MCLAB.

Analysis of yeast-displayed sort products was performed using the same reagents and protocols and described for the library sorts. Samples were analyzed on a FACS Calibur (BD Biosciences), and data were analyzed using FlowJo software (TreeStar).

Binding affinity assay

Cells were cultured in standard tissue culture conditions. Cells were harvested, and the supernatant was discarded then dispensed onto a staining plate at 3×10^5 cells per well. The plate was centrifuged at 300 *g* at 4°C for 5 min. Various concentrations of sBCMA mutants and negative control were diluted in FACS buffer containing 2% FBS, 100 µl/well. Cells were incubated for 1 h at 4°C and washed twice with 200 µl FACS buffer and centrifuged at 300 *g* for 5 min. The supernatant was discarded before and after each wash. Cells were resuspended at 100 µl/well with 1:1,000 diluent with anti-human IgG-Alexa Fluor 488 (cat. no. A28175; Thermo Fisher Scientific). Plates were incubated for 1 h at 4°C. Cells were washed twice with

FACS buffer and centrifuged at 300 *g* for 5 min. Supernatant was discarded, and cells were resuspended in 100 µl cold PBS. The cells were kept in the dark, and FACS analysis was carried out on a FACS CantoII (BD Biosciences). The geometric mean (measure of binding affinity) of the double-positive population was determined by using FlowJo software. To determine the K_D (ligand concentration that binds to half the receptor sites at equilibrium) of the binding reaction, binding affinity was plotted against ligand concentration, and the graph was analyzed using one site–specific binding in GraphPad Prism to get the K_D value.

Computational structural simulation

Computation-based structural simulation was carried out using a number of structural prediction software programs. sBCMA V3 in cocomplex with hAPRIL and hBAFF was modeled using a combination of Prime from Schrödinger Suites 2021–2, Alphafold2, RoseTTAFold, trRosetta, and RosettaRemodel based on sequences and structural alignment mapped to PDB 1XU2. Mutation-mediated changes within sBCMA V3 binding to hAPRIL and BAFF was calculated by Residue Scanning Calculation Module from Bioluminate (Schrödinger). Surface complementarity and protein–protein interaction between sBCMA V3 and hAPRIL/hBAFF was calculated by Protein Interaction Analysis module from Bioluminate.

In vitro cell-based viability assays

Cell viability was determined with a cell counting hemocytometer or Beckman Coulter counter, depending on the study. Cells were plated in 96-well plates at a density of 2,500 cells (U266, SU-DHL-6, and Daudi) or 3,000 cells (MM1.R and INA-6). For wild-type sBCMA-Fc and sBCMA-Fc V3 treatment, cells were cultured in 1% FCS RPMI-1640 overnight followed by 1 h of 100-ng recombinant APRIL or BAFF stimulation, and increasing doses of sBCMA were added to designated wells. Both APRIL and sBCMA-Fc were replenished every 48 h until experiment end on day 7.

Mouse CT scan to confirm MM-induced bone degradation

High-resolution micro-CT images were acquired using an in vivo micro-CT scanner, SkyScan 1276 (Bruker) under isoflurane anesthesia. The scanning mode was set as 360° step-and-shoot scanning without average framing. After each scan, the projection images were reconstructed using software (NRecon with GPU acceleration; Bruker), followed by converting the set of reconstructed slices to DICOM files (DICOM converter; Bruker).

ELISA

Serum and cell lysate expression of human APRIL (cat. no. DY884B; R&D Systems), human BAFF (cat. no. DBLYS0B; R&D Systems), mouse APRIL (cat. no. MBS738004; My BioSource), mouse BAFF (cat. no. MBLYS0; R&D Systems), human total IgG (M) protein (cat. no. BMS2091; Thermo Fisher Scientific), mouse total IgG (M) protein (cat. no. 88-50400-88; Thermo Fisher Scientific), and mouse IgM and IgA (cat. no. MBS564075 and MBS564073; My Biosources) was detected using commercial ELISA kits according to the manufacturers' protocol.

Immunohistochemistry

Tissues were fixed in 10% neutral buffered formalin and embedded in paraffin blocks for cutting and mounting on glass slides. For Ki67 staining, slides were deparaffined, and antigen retrieval was carried out using 10 mM citric acid buffer and 0.05% Tween 20, pH 6 Slides were removed from buffer, cooled at room temperature for 15 min, and quenched in endogenous peroxidase with 1:10 dilution of 34% hydrogen peroxide and water for 15 min. Avidin and biotin blockers were added for 15 min each. Protein block using 2% FCS was added for 20 min. The serum and antibody were diluted in PBT (1× PBS, 0.1% BSA, 0.2%, and 0.01% Tween 20). Anti-human Ki67 antibody (cat. no. sc-23900; Santa Cruz Biotechnologies) incubated overnight at 4°C. Biotinylated anti-mouse secondary antibody 1:2,500 (cat. no. BA92001; Vector Laboratories) was added on each slide and incubated at 37°C for 30 min and then incubated with STREP-HRP for 30 min at 37°C. Signals were developed using DAB substrate kit (#34002; Thermo Fisher Scientific). TUNEL apoptosis assay was carried out using ApopTag Peroxidase In Situ Apoptosis Detection Kit (cat. no. S7100; Millipore Sigma) and performed according to the manufacturer's instructions. All cases were scanned at 40× magnification using the Leica Aperio AT2 Digital Pathology Scanner (Leica Biosystem). Images were analyzed using NDP.view2 image analysis software developed by Hamamatsu Japan.

Immunoblotting

Cell lysates were subjected to SDS-PAGE, followed by transfer to nitrocellulose membrane. The membranes were then probed with primary Abs against total BCMA (cat. no. 27724-1-AP; Proteintech), Pan-Akt (cat. no. 4691; Cell Signaling Technology), pAkt (cat. no. 4060; Cell Signaling Technology), phospho-p38 MAPK (cat. no 4511; Cell Signaling Technology), p38 MAPK (cat. no. 8690; Cell Signaling Technology), phospho-mTOR ser2448 (cat. no. 5536; Cell Signaling Technology), total mTOR (cat. no. 2983; Cell Signaling Technology), Raptor (cat. no. 2280; Cell Signaling Technology), Phospho-Raptor Ser792 (cat. no. 89146; Cell Signaling Technology), phospho-p70 S6K (cat. no. 9204; Cell Signaling Technology), phospho-S6 (cat. no. 9204; Cell Signaling Technology), ATMINASCIZ (cat. no. AB3271-I; Millipore Sigma), and β-actin (cat. no. sc-47778 HRP; Santa Cruz Biotechnology) at 4°C overnight. The blots were then washed and probed with HRP-conjugated anti-goat (cat. no. sc-2020; Santa Cruz Biotechnology) or HRP-conjugated anti-rabbit (cat. no. A16110; Thermo Fisher Scientific) as appropriate. The blots were developed with Bio-Rad Western C Developing Reagent (cat. no. 170-5060; Bio-Rad) and visualized with a Chemidoc digital imager (cat. no. 1708280; Bio-Rad).

In vitro genetic knockdown studies

BCMA siRNA (cat. no. L-011217-00-0005; SMARTPool) and dox-inducible shRNA (cat. no. V3SH7669-230564302; SAMRTvector) constructs were purchased through GE Dharmacon Horizon. ATMIN CRISPR KO (sc-411076) constructs were purchased from Santa Cruz Biotechnology. For siRNA, transfection procedures were carried out using a Lonza 4D-Nucleofactor device and kits in accordance with manufacturer's protocol. For dox-inducible

BCMA knockdown cells, three shRNA sequences were tested according to the transfection protocols provided by the manufacturer. Sequences 1 and 2 showed successful knockdown of BCMA and were used for subsequent in vivo testing.

shRNA sequences

shRNA sequences were as follows: Sh1, 5′-CAGTCCTGCTCTTTTCCAG-3′; Sh2, 5′-CTTGATGCAGTCTTCACAG-3′; and Sh3, 5′-AGCCATGCCCAGGAGACCT-3′.

Real-time PCR analysis

RNA was isolated using TRIzol reagent according to the manufacturer's instructions (Invitrogen). RNA was reverse transcribed using cDNA synthesis kit (Bio-Rad). Real-time PCR was performed as previously described. Relative expression levels of target genes were normalized against the level of GAPDH expression. Fold difference (as relative mRNA expression) was calculated by the comparative threshold count (Ct) method ($2^{Ct(\text{GAPDH RNA–gene of interest})}$).

Primer sequences

Primer sequences were as follows: BCMA forward, 5′-TGTTCTTCTAATACTCCTCCTCT-3′, and reverse, 3′-AACTCGTCCTTTAATGGTTC-5′; ATMIN forward, 5′-AACAGCACTGCAGTCTCACA-3′, and reverse, 3′-CTGGTCTAGGGATTGGTTGGT-5′; and GAPDH forward, 5′-TGCACCACCAACTGCTTAGC-3′, and reverse, 3′-GGCATGGACTGTGGTCATGAG-5′.

RPPA

RPPA was performed by the MD Anderson RPPA core as described in the published protocol.

Statistical analysis

All cell number, tumor volume, survival, and quantification of in vivo and in vitro studies were conducted using Prism software (GraphPad). ANOVA with Tukey–Kramer test was used for comparing multiple treatment groups with each other. $P < 0.05$ was considered significant. Repeated-measures ANOVA was used for comparing multiple treatment groups measured over time. Statistical analysis of survival curves was conducted for the survival studies. A log-rank (Mantel–Cox) test was performed to compare mean survival among groups; $P \le 0.05$ was considered statistically significant.

Online supplemental material

Fig. S1 shows the absolute requirement of BCMA signaling activation during MM progression. Fig. S2 shows both global and specific molecular changes associated with protein translation machinery. Fig. S3 shows the in vivo efficacy of MM models treated with wild-type sBCMA-Fc and appropriate therapeutic controls. Fig. S4 shows the establishment of MM PDX models and human myeloma protein levels in patient 3 and 5 PDX MM models treated with sBCMA-Fc; also, the therapeutic efficacy of sBCMA-Fc in MM was further investigated in combination with current standard-of-care and its therapeutic potential in DLBCL. Fig. S5 shows the computational structural alignment of sBCMA V3/APRIL and sBCMA V3/BAFF cocomplex and the therapeutic efficacy of sBCMA-Fc V3 in MM and DLBCL models. Table S1 shows the demographic information and treatment status of patient samples collected for establishing the MM PDX model. Tables S2, S3, S4, and S5 list the top clones selected from rounds 3–6 of affinity-based flow cytometry sorting. Table S6, S7, S8, and S9 present the hematology analysis of male and female cynomolgus monkeys dosed with sBCMA-Fc V3.

Acknowledgments

We thank Drs. Vignesh Viswanathan, Dhanya Nambiar, and Quynh-Thu Le for sharing experimental reagents. We thank Stanford animal facility for maintaining animal colonies, Chempartner Shanghai for the production of wild-type sBCMA-Fc and sBCMA-Fc V3, TB-seq for isolation and preparation of ribosome mRNA library, and the University of Delaware sequencing facility for performing ribosome sequencing.

This work was supported by grants from the Silicon Valley Foundation (A.J. Giaccia), the Sydney Frank Foundation (A.J. Giaccia), the Kimmelman Fund (A.J. Giaccia), and a Medical Research Council UK Grant (A.J. Giaccia). This work was supported in part by the Cancer Prevention and Research Institute of Texas (RR180042 to C. Cenik) and Welch Foundation (F-2027-20200401 to C. Cenik).

Author contributions: Conceptualization: Y.R. Miao, K. Thakkar, C. Cenik, D. Jiang, K. Mizuno, X.E. Zhang, M. Liedtke, P. Abidi, A.C. Koong, and A.J. Giaccia. Methodology: Y.R. Miao, K. Thakkar, C. Cenik, D. Jiang, K. Mizuno, C.G. Li, H. Zhao, M. Liedtke, and P. Abidi. Investigation: Y.R. Miao, K. Thakkar, C. Cenik, D. Jiang, K. Mizuno, C. Jia, T.T. Chi Yang, C.G. Li, H. Zhao, A. Diep, Y. Xu, and X.E. Zhang. Fund acquisition: A.J. Giaccia and C. Cenik. Project administration: Y.R. Miao and A.J. Giaccia. Supervision: Y.R. Miao, A.C. Koong, and A.J. Giaccia. Writing: Y.R. Miao, K. Thakkar, C. Cenik, C. Jia, D. Jiang, and A.J. Giaccia.

Disclosures: Y.R. Miao reported "other" from AKSO Biopharmaceutical, Inc. outside the submitted work; in addition, Y.R. Miao had a patent to sBCMA variants and Fc fusion proteins thereof pending. K. Mizuno reported a patent to sBCMA variants and FC fusion proteins thereof issued and a patent to biologic inhibitors for therapeutic targeting the B cell maturation antigen (BCMA) licensed (AKSO Biopharmaceutical, Inc.). X.E. Zhang reported "other" from AKSO Biopharmaceutical, Inc. outside the submitted work. M. Liedtke reported personal fees from Celgene/BMS, GSK, Sanofi, Oncopeptides, Karyopharm, Takeda, and Janssen outside the submitted work. A.C. Koong reported holds stock in Aravive, Inc. There is no conflict with the present work but he disclose this in the interest of completeness. A.J. Giaccia reported "other" from AKSO Biopharmaceutical, Inc. outside the submitted work; in addition, A.J. Giaccia had a patent to sBCMA variants and Fc fusion proteins pending. No other disclosures were reported.

Submitted: 4 February 2022
Revised: 5 May 2022
Accepted: 17 June 2022

References

Bag-Ozbek, A., and J.S. Hui-Yuen. 2021. Emerging B-cell therapies in systemic lupus erythematosus. *Ther. Clin. Risk Manag.* 17:39–54. https://doi.org/10.2147/TCRM.S252592

Barratt, J., J.A. Tumlin, Y. Suzuki, A. Kao, A. Aydemir, Y. Zima, and G. Appel. 2020. MO039 the 24-week interim analysis results of a randomized, double-blind, placebo-controlled phase II study of atacicept in patients with IGA nephropathy and persistent proteinuria. *Nephrol. Dial. Transplant.* 35:gfaa140. https://doi.org/10.1093/ndt/gfaa140.mo039

Becker, J.R., R. Cuella-Martin, M. Barazas, R. Liu, C. Oliveira, A.W. Oliver, K. Bilham, A.B. Holt, A.N. Blackford, J. Heierhorst, et al. 2018. The ASCIZ-DYNLL1 axis promotes 53BP1-dependent non-homologous end joining and PARP inhibitor sensitivity. *Nat. Commun.* 9:5406. https://doi.org/10.1038/s41467-018-07855-x

Bolkun, L., D. Lemancewicz, E. Jablonska, A. Kulczynska, U. Bolkun-Skornicka, J. Kloczko, and J. Dzieciol. 2014. BAFF and APRIL as TNF superfamily molecules and angiogenesis parallel progression of human multiple myeloma. *Ann. Hematol.* 93:635–644. https://doi.org/10.1007/s00277-013-1924-9

Bossen, C., and P. Schneider. 2006. BAFF, APRIL and their receptors: Structure, function and signaling. *Semin. Immunol.* 18:263–275. https://doi.org/10.1016/j.smim.2006.04.006

Briones, J., J.M. Timmerman, D.M. Hilbert, and R. Levy. 2002. BLyS and BLyS receptor expression in non-Hodgkin's lymphoma. *Exp. Hematol.* 30:135–141. https://doi.org/10.1016/s0301-472x(01)00774-3

Burger, R., A. Guenther, F. Bakker, M. Schmalzing, S. Bernand, W. Baum, B. Duerr, G.M. Hocke, H. Steininger, E. Gebhart, and M. Gramatzki. 2001. Gp130 and ras mediated signaling in human plasma cell line INA-6: A cytokine-regulated tumor model for plasmacytoma. *Hematol. J.* 2:42–53. https://doi.org/10.1038/sj.thj.6200075

Caimi, P.F., W. Ai, J.P. Alderuccio, K.M. Ardeshna, M. Hamadani, B. Hess, B.S. Kahl, J. Radford, M. Solh, A. Stathis, et al. 2021. Loncastuximab tesirine in relapsed or refractory diffuse large B-cell lymphoma (LOTIS-2): A multicentre, open-label, single-arm, phase 2 trial. *Lancet Oncol.* 22:790–800. https://doi.org/10.1016/S1470-2045(21)00139-X

Carpenter, R.O., M.O. Evbuomwan, S. Pittaluga, J.J. Rose, M. Raffeld, S. Yang, R.E. Gress, F.T. Hakim, and J.N. Kochenderfer. 2013. B-cell maturation antigen is a promising target for adoptive T-cell therapy of multiple myeloma. *Clin. Cancer Res.* 19:2048–2060. https://doi.org/10.1158/1078-0432.CCR-12-2422

Castigli, E., S. Scott, F. Dedeoglu, P. Bryce, H. Jabara, A.K. Bhan, E. Mizoguchi, and R.S. Geha. 2004. Impaired IgA class switching in APRIL-deficient mice. *Proc. Natl. Acad. Sci. USA.* 101:3903–3908. https://doi.org/10.1073/pnas.0307348101

Castigli, E., S.A. Wilson, S. Scott, F. Dedeoglu, S. Xu, K.P. Lam, R.J. Bram, H. Jabara, and R.S. Geha. 2005. TACI and BAFF-R mediate isotype switching in B cells. *J. Exp. Med.* 201:35–39. https://doi.org/10.1084/jem.20032000

Cenik, C., E.S. Cenik, G.W. Byeon, F. Grubert, S.I. Candille, D. Spacek, B. Alsallakh, H. Tilgner, C.L. Araya, H. Tang, et al. 2015. Integrative analysis of RNA, translation, and protein levels reveals distinct regulatory variation across humans. *Genome Res.* 25:1610–1621. https://doi.org/10.1101/gr.193342.115

Chim, C.S., S.K. Kumar, R.Z. Orlowski, G. Cook, P.G. Richardson, M.A. Gertz, S. Giralt, M.V. Mateos, X. Leleu, and K.C. Anderson. 2018. Management of relapsed and refractory multiple myeloma: Novel agents, antibodies, immunotherapies and beyond. *Leukemia.* 32:252–262. https://doi.org/10.1038/leu.2017.329

Chiu, A., W. Xu, B. He, S.R. Dillon, J.A. Gross, E. Sievers, X. Qiao, P. Santini, E. Hyjek, J.W. Lee, et al. 2007. Hodgkin lymphoma cells express TACI and BCMA receptors and generate survival and proliferation signals in response to BAFF and APRIL. *Blood.* 109:729–739. https://doi.org/10.1182/blood-2006-04-015958

Collier, F.C., and P. Jackson. 1953. The precipitin test for Bence-Jones protein. *N. Engl. J. Med.* 248:409–414. https://doi.org/10.1056/NEJM195303052481003

Durer, C., S. Durer, S. Lee, R. Chakraborty, M.N. Malik, A. Rafae, M.A. Zar, A. Kamal, N. Rosko, C. Samaras, et al. 2020. Treatment of relapsed multiple myeloma: Evidence-based recommendations. *Blood Rev.* 39:100616. https://doi.org/10.1016/j.blre.2019.100616

Fragioudaki, M., G. Tsirakis, C.A. Pappa, I. Aristeidou, C. Tsioutis, A. Alegakis, D.S. Kyriakou, E.N. Stathopoulos, and M.G. Alexandrakis. 2012. Serum BAFF levels are related to angiogenesis and prognosis in patients with multiple myeloma. *Leuk. Res.* 36:1004–1008. https://doi.org/10.1016/j.leukres.2012.03.012

Fu, J., H. Shi, T. Zhan, H. Li, L. Ye, L. Xie, Z. Wang, B. Wang, and L. Zheng. 2021. BST-2/Tetherin is involved in BAFF-enhanced proliferation and survival via canonical NF-κB signaling in neoplastic B-lymphoid cells. *Exp. Cell Res.* 398:112399. https://doi.org/10.1016/j.yexcr.2020.112399

Gordon, N.C., S. Lien, J. Johnson, H.J.A. Wallweber, T. Tran, B. Currell, M. Mathieu, C. Quan, M.A. Starovasnik, S.G. Hymowitz, and R.F. Kelley. 2010. Multiple novel classes of APRIL-specific receptor-blocking peptides isolated by phage display. *J. Mol. Biol.* 396:166–177. https://doi.org/10.1016/j.jmb.2009.11.041

Grasset, E.K., A. Chorny, S. Casas-Recasens, C. Gutzeit, G. Bongers, I. Thomsen, L. Chen, Z. He, D.B. Matthews, M.A. Oropallo, et al. 2020. Gut T cell-independent IgA responses to commensal bacteria require engagement of the TACI receptor on B cells. *Sci. Immunol.* 5:eaat7117. https://doi.org/10.1126/sciimmunol.aat7117

Greenstein, S., N.L. Krett, Y. Kurosawa, C. Ma, D. Chauhan, T. Hideshima, K.C. Anderson, and S.T. Rosen. 2003. Characterization of the MM.1 human multiple myeloma (MM) cell lines: A model system to elucidate the characteristics, behavior, and signaling of steroid-sensitive and -resistant MM cells. *Exp. Hematol.* 31:271–282. https://doi.org/10.1016/s0301-472x(03)00023-7

Hatzoglou, A., J. Roussel, M.F. Bourgeade, E. Rogier, C. Madry, J. Inoue, O. Devergne, and A. Tsapis. 2000. TNF receptor family member BCMA (B cell maturation) associates with TNF receptor-associated factor (TRAF) 1, TRAF2, and TRAF3 and activates NF-κ B, elk-1, c-Jun N-terminal kinase, and p38 mitogen-activated protein kinase. *J. Immunol.* 165:1322–1330. https://doi.org/10.4049/jimmunol.165.3.1322

Hymowitz, S.G., D.R. Patel, H.J.A. Wallweber, S. Runyon, M. Yan, J. Yin, S.K. Shriver, N.C. Gordon, B. Pan, N.J. Skelton, et al. 2005. Structures of APRIL-receptor complexes: Like BCMA, TACI employs only a single cysteine-rich domain for high affinity ligand binding. *J. Biol. Chem.* 280:7218–7227. https://doi.org/10.1074/jbc.M411714200

Ingolia, N.T., J.A. Hussmann, and J.S. Weissman. 2019. Ribosome profiling: Global views of translation. *Cold Spring Harb. Perspect. Biol.* 11:a032698. https://doi.org/10.1101/cshperspect.a032698

Ingolia, N.T., L.F. Lareau, and J.S. Weissman. 2011. Ribosome profiling of mouse embryonic stem cells reveals the complexity and dynamics of mammalian proteomes. *Cell.* 147:789–802. https://doi.org/10.1016/j.cell.2011.10.002

Jurado, S., L.A. Conlan, E.K. Baker, J.L. Ng, N. Tenis, N.C. Hoch, K. Gleeson, M. Smeets, D. Izon, and J. Heierhorst. 2012a. ATM substrate Chk2-interacting Zn^{2+} finger (ASCIZ) Is a bi-functional transcriptional activator and feedback sensor in the regulation of dynein light chain (DYNLL1) expression. *J. Biol. Chem.* 287:3156–3164. https://doi.org/10.1074/jbc.M111.306019

Jurado, S., K. Gleeson, K. O'Donnell, D.J. Izon, C.R. Walkley, A. Strasser, D.M. Tarlinton, and J. Heierhorst. 2012b. The Zinc-finger protein ASCIZ regulates B cell development via DYNLL1 and Bim. *J. Exp. Med.* 209:1629–1639. https://doi.org/10.1084/jem.20120785

Jurado, S., I. Smyth, B. van Denderen, N. Tenis, A. Hammet, K. Hewitt, J.L. Ng, C.J. McNees, S.V. Kozlov, H. Oka, et al. 2010. Dual functions of ASCIZ in the DNA base damage response and pulmonary organogenesis. *PLoS Genet.* 6:e1001170. https://doi.org/10.1371/journal.pgen.1001170

Kariolis, M.S., Y.R. Miao, A. Diep, S.E. Nash, M.M. Olcina, D. Jiang, D.S. Jones, S. Kapur, I.I. Mathews, A.C. Koong, et al. 2017. Inhibition of the GAS6/AXL pathway augments the efficacy of chemotherapies. *J. Clin. Invest.* 127:183–198. https://doi.org/10.1172/JCI85610

Kassambara, A., and J. Moreaux. 2018. Analysis of global gene expression profiles. *Methods Mol. Biol.* 1792:157–166. https://doi.org/10.1007/978-1-4939-7865-6_11

Keats, J.J., R. Fonseca, M. Chesi, R. Schop, A. Baker, W.J. Chng, S. Van Wier, R. Tiedemann, C.X. Shi, M. Sebag, et al. 2007. Promiscuous mutations activate the noncanonical NF-κB pathway in multiple myeloma. *Cancer Cell.* 12:131–144. https://doi.org/10.1016/j.ccr.2007.07.003

Kuo, S.H., P.Y. Yeh, L.T. Chen, M.S. Wu, C.W. Lin, K.H. Yeh, Y.S. Tzeng, J.Y. Chen, P.N. Hsu, J.T. Lin, and A.L. Cheng. 2008. Overexpression of B cell-activating factor of TNF family (BAFF) is associated with Helicobacter pylori-independent growth of gastric diffuse large B-cell lymphoma with histologic evidence of MALT lymphoma. *Blood.* 112:2927–2934. https://doi.org/10.1182/blood-2008-02-137513

Lee, W.S., and O. Amengual. 2020. B cells targeting therapy in the management of systemic lupus erythematosus. *Immunol. Med.* 43:16–35. https://doi.org/10.1080/25785826.2019.1698929

Leszczynska, K.B., E.L. Gottgens, D. Biasoli, M.M. Olcina, J. Ient, S. Anbalagan, S. Bernhardt, A.J. Giaccia, and E.M. Hammond. 2016. Mechanisms and

consequences of ATMIN repression in hypoxic conditions: Roles for p53 and HIF-1. *Sci. Rep.* 6:21698. https://doi.org/10.1038/srep21698

Liu, Y., X. Hong, J. Kappler, L. Jiang, R. Zhang, L. Xu, C.H. Pan, W.E. Martin, R.C. Murphy, H.B. Shu, et al. 2003. Ligand-receptor binding revealed by the TNF family member TALL-1. *Nature*. 423:49–56. https://doi.org/10.1038/nature01543

Lonial, S., H.C. Lee, A. Badros, S. Trudel, A.K. Nooka, A. Chari, A.O. Abdallah, N. Callander, N. Lendvai, D. Sborov, et al. 2020. Belantamab mafodotin for relapsed or refractory multiple myeloma (DREAMM-2): A two-arm, randomised, open-label, phase 2 study. *Lancet Oncol.* 21:207–221. https://doi.org/10.1016/S1470-2045(19)30788-0

Lyu, M.A., D. Rai, K.S. Ahn, B. Sung, L.H. Cheung, J.W. Marks, B.B. Aggarwal, R.C.T. Aguiar, V. Gandhi, and M.G. Rosenblum. 2010. The rGel/BLyS fusion toxin inhibits diffuse large B-cell lymphoma growth in vitro and in vivo. *Neoplasia*. 12:366–375. https://doi.org/10.1593/neo.91960

Marsters, S.A., M. Yan, R.M. Pitti, P.E. Haas, V.M. Dixit, and A. Ashkenazi. 2000. Interaction of the TNF homologues BLyS and APRIL with the TNF receptor homologues BCMA and TACI. *Curr. Biol.* 10:785–788. https://doi.org/10.1016/s0960-9822(00)00566-2

McNees, C.J., L.A. Conlan, N. Tenis, and J. Heierhorst. 2005. ASCIZ regulates lesion-specific Rad51 focus formation and apoptosis after methylating DNA damage. *EMBO J.* 24:2447–2457. https://doi.org/10.1038/sj.emboj.7600704

Miao, Y.R., K.N. Thakkar, J. Qian, M.S. Kariolis, W. Huang, S. Nandagopal, T.T.C. Yang, A.N. Diep, G.M. Cherf, Y. Xu, et al. 2021. Neutralization of PD-L2 is essential for overcoming immune checkpoint blockade resistance in ovarian cancer. *Clin. Cancer Res.* 27:4435–4448. https://doi.org/10.1158/1078-0432.CCR-20-0482

Moreaux, J., D. Hose, M. Jourdan, T. Reme, M. Hundemer, M. Moos, N. Robert, P. Moine, J. De Vos, H. Goldschmidt, and B. Klein. 2007. TACI expression is associated with a mature bone marrow plasma cell signature and C-MAF overexpression in human myeloma cell lines. *Haematologica*. 92:803–811. https://doi.org/10.3324/haematol.10574

Moreaux, J., E. Legouffe, E. Jourdan, P. Quittet, T. Reme, C. Lugagne, P. Moine, J.F. Rossi, B. Klein, and K. Tarte. 2004. BAFF and APRIL protect myeloma cells from apoptosis induced by interleukin 6 deprivation and dexamethasone. *Blood*. 103:3148–3157. https://doi.org/10.1182/blood-2003-06-1984

O'Connor, B.P., V.S. Raman, L.D. Erickson, W.J. Cook, L.K. Weaver, C. Ahonen, L.L. Lin, G.T. Mantchev, R.J. Bram, and R.J. Noelle. 2004. BCMA is essential for the survival of long-lived bone marrow plasma cells. *J. Exp. Med.* 199:91–98. https://doi.org/10.1084/jem.20031330

Ozadam, H., M. Geng, and C. Cenik. 2020. RiboFlow, RiboR and RiboPy: An ecosystem for analyzing ribosome profiling data at read length resolution. *Bioinformatics*. 36:2929–2931. https://doi.org/10.1093/bioinformatics/btaa028

Pelletier, M., J.S. Thompson, F. Qian, S.A. Bixler, D. Gong, T. Cachero, K. Gilbride, E. Day, M. Zafari, C. Benjamin, et al. 2003. Comparison of soluble decoy IgG fusion proteins of BAFF-R and BCMA as antagonists for BAFF. *J. Biol. Chem.* 278:33127–33133. https://doi.org/10.1074/jbc.M305754200

Pham, L.V., L. Fu, A.T. Tamayo, C. Bueso-Ramos, E. Drakos, F. Vega, L.J. Medeiros, and R.J. Ford. 2011. Constitutive BR3 receptor signaling in diffuse, large B-cell lymphomas stabilizes nuclear factor-κB-inducing kinase while activating both canonical and alternative nuclear factor-κB pathways. *Blood*. 117:200–210. https://doi.org/10.1182/blood-2010-06-290437

Raje, N., J. Berdeja, Y. Lin, D. Siegel, S. Jagannath, D. Madduri, M. Liedtke, J. Rosenblatt, M.V. Maus, A. Turka, et al. 2019. Anti-BCMA CAR T-cell therapy bb2121 in relapsed or refractory multiple myeloma. *N. Engl. J. Med.* 380:1726–1737. https://doi.org/10.1056/NEJMoa1817226

Rapali, P., M.F. Garcia-Mayoral, M. Martinez-Moreno, K. Tarnok, K. Schlett, J.P. Albar, M. Bruix, L. Nyitray, and I. Rodriguez-Crespo. 2011. LC8 dynein light chain (DYNLL1) binds to the C-terminal domain of ATM-interacting protein (ATMINASCIZ) and regulates its subcellular localization. *Biochem. Biophys. Res. Commun.* 414:493–498. https://doi.org/10.1016/j.bbrc.2011.09.093

Robinson, M.D., and A. Oshlack. 2010. A scaling normalization method for differential expression analysis of RNA-seq data. *Genome Biol.* 11:R25. https://doi.org/10.1186/gb-2010-11-3-r25

Rodriguez, J.M., J. Rodriguez-Rivas, T. Di Domenico, J. Vazquez, A. Valencia, and M.L. Tress. 2018. APPRIS 2017: Principal isoforms for multiple gene sets. *Nucleic Acids Res.* 46:D213–D217. https://doi.org/10.1093/nar/gkx997

Rossi, J.F., J. Moreaux, D. Hose, G. Requirand, M. Rose, V. Rouille, I. Nestorov, G. Mordenti, H. Goldschmidt, A. Ythier, and B. Klein. 2009. Atacicept in relapsed/refractory multiple myeloma or active Waldenstrom's macroglobulinemia: A phase I study. *Br. J. Cancer*. 101:1051–1058. https://doi.org/10.1038/sj.bjc.6605241

Samy, E., S. Wax, B. Huard, H. Hess, and P. Schneider. 2017. Targeting BAFF and APRIL in systemic lupus erythematosus and other antibody-associated diseases. *Int. Rev. Immunol.* 36:3–19. https://doi.org/10.1080/08830185.2016.1276903

Schuepbach-Mallepell, S., D. Das, L. Willen, M. Vigolo, A. Tardivel, L. Lebon, C. Kowalczyk-Quintas, J. Nys, C. Smulski, T.S. Zheng, et al. 2015. Stoichiometry of heteromeric BAFF and APRIL cytokines dictates their receptor binding and signaling properties. *J. Biol. Chem.* 290:16330–16342. https://doi.org/10.1074/jbc.M115.661405

Shin, W., H.T. Lee, H. Lim, S.H. Lee, J.Y. Son, J.U. Lee, K.Y. Yoo, S.E. Ryu, J. Rhie, J.Y. Lee, and Y.S. Heo. 2018. BAFF-neutralizing interaction of belimumab related to its therapeutic efficacy for treating systemic lupus erythematosus. *Nat. Commun.* 9:1200. https://doi.org/10.1038/s41467-018-03620-2

Shrestha, S., P. Budhathoki, Y. Adhikari, A. Marasini, S. Bhandari, W.A.Y. Mir, and D.B. Shrestha. 2021. Belimumab in lupus nephritis: A systematic review and meta-analysis. *Cureus*. 13:e20440. https://doi.org/10.7759/cureus.20440

Swerdlow, S.H., E. Campo, S.A. Pileri, N.L. Harris, H. Stein, R. Siebert, R. Advani, M. Ghielmini, G.A. Salles, A.D. Zelenetz, and E.S. Jaffe. 2016. The 2016 revision of the World Health Organization classification of lymphoid neoplasms. *Blood*. 127:2375–2390. https://doi.org/10.1182/blood-2016-01-643569

Tai, Y.T., and K.C. Anderson. 2019. B cell maturation antigen (BCMA)-based immunotherapy for multiple myeloma. *Expert Opin. Biol. Ther.* 19:1143–1156. https://doi.org/10.1080/14712598.2019.1641196

Weber, T., and R. Schmitz. 2022. Molecular subgroups of diffuse large B cell lymphoma: Biology and implications for clinical practice. *Curr. Oncol. Rep.* 24:13–21. https://doi.org/10.1007/s11912-021-01155-2

Wu, Y., D. Bressette, J.A. Carrell, T. Kaufman, P. Feng, K. Taylor, Y. Gan, Y.H. Cho, A.D. Garcia, E. Gollatz, et al. 2000. Tumor necrosis factor (TNF) receptor superfamily member TACI is a high affinity receptor for TNF family members APRIL and BLyS. *J. Biol. Chem.* 275:35478–35485. https://doi.org/10.1074/jbc.M005224200

Yu, G., T. Boone, J. Delaney, N. Hawkins, M. Kelley, M. Ramakrishnan, S. McCabe, W.R. Qiu, M. Kornuc, X.Z. Xia, et al. 2000. APRIL and TALL-I and receptors BCMA and TACI: System for regulating humoral immunity. *Nat. Immunol.* 1:252–256. https://doi.org/10.1038/79802

Supplemental material

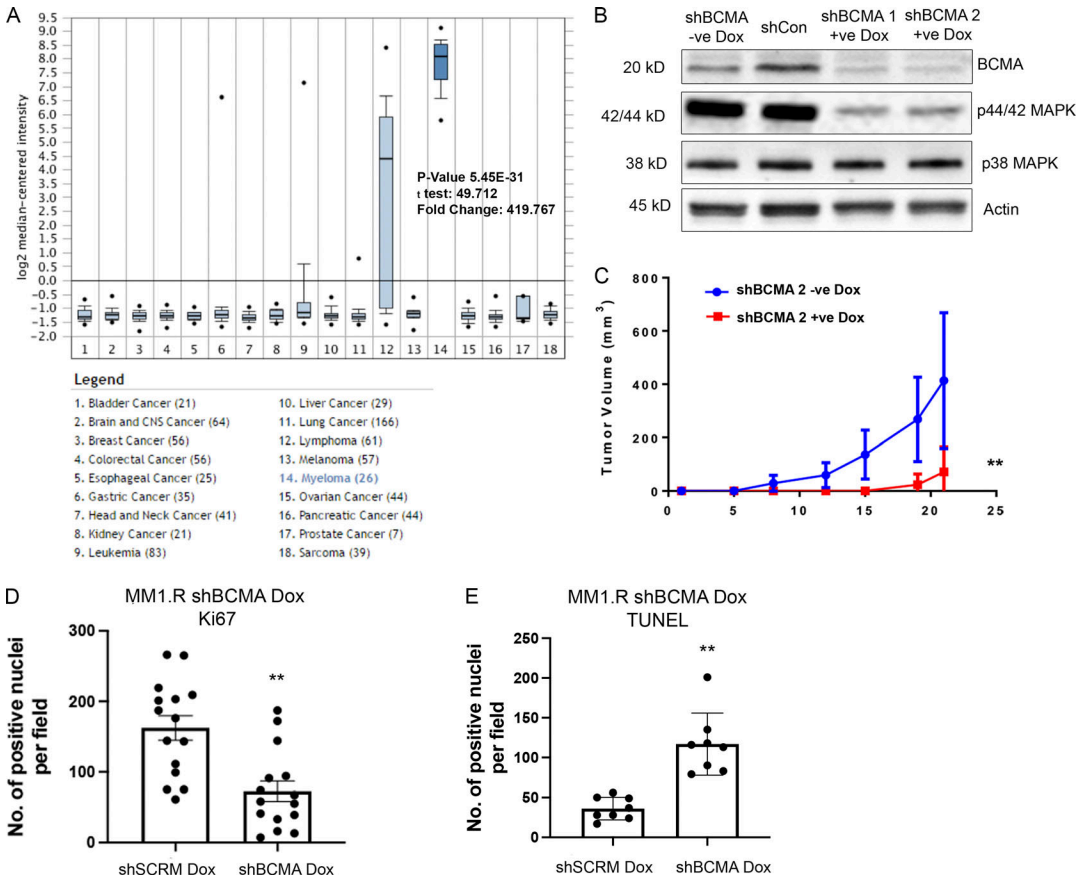

Figure S1. **BCMA signaling is essential for the growth and survival of MM. (A)** BCMA mRNA expression in a panel of 18 tumor cell lines queried through Oncomine. BCMA expression is significantly elevated in myeloma cell line; $P = 5.45 \times 10^{-31}$. **(B)** Western blotting analysis confirming knockdown of BCMA in MM cell line by dox-inducible shRNA. **(C)** Tumor growth kinetics in MM1.R MM cells transfected with inducible dox shBCMA, mice were given drinking water with or without dox (5 mg/ml); P = 0.007. **(D)** Quantitative analysis of Ki67-positive cells in the harvested tumors of dox-inducible shSCRM and shBCMA, represented as the average number of positive nuclei per image field; P = 0.0055. **(E)** Quantitative analysis of TUNEL-positive cells in the harvested tumors of dox-inducible shSCRM and shBCMA, represented as the average number of positive nuclei per image field; P = 0.0026. Statistical analysis was conducted using one-way ANOVA for comparing between treatment groups and repeated ANOVA for changes occurring over time. *, P < 0.05; **, P < 0.01; ***, P < 0.001. Source data are available for this figure: SourceData FS1.

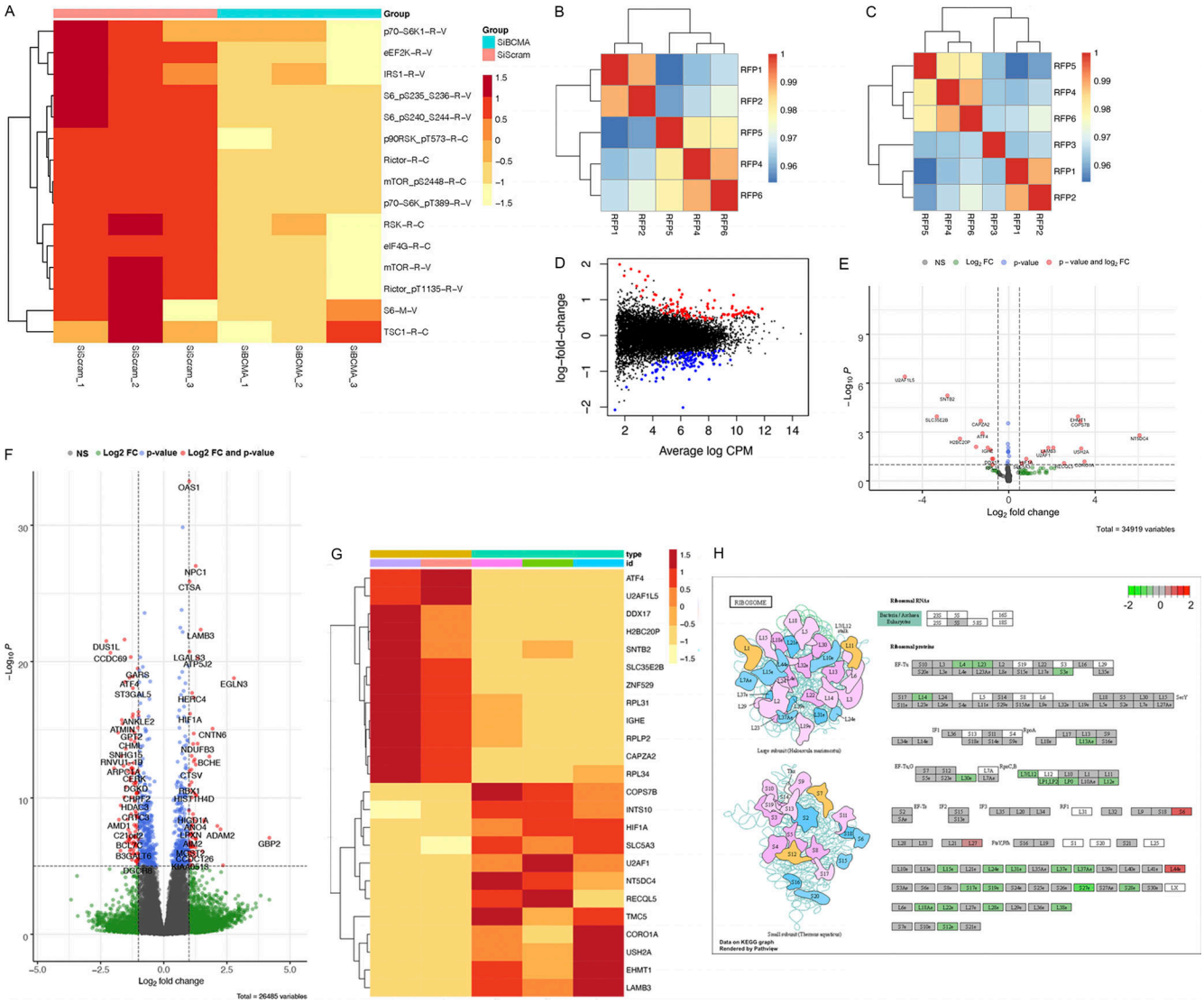

Figure S2. **BCMA is a critical regulator of protein translation machinery. (A)** Loss of BCMA-induced changes in downstream targets associated with protein translation analyzed through RPPA. **(B)** Spearman correlation analysis of ribosome profiling samples showing consistent reads across all samples with the exception of RFP3. **(C)** Spearman correlation analysis after RFP3 was removed from the dataset. **(D)** Distribution plot of changes in mRNA expression associated with genetic knockdown of BCMA. **(E)** Volcano plot analysis identifying significant changes of downstream targets within total RNA transcript associated with BCMA knockdown. Color-coded dots show statistical significance associated with log_{10}Fc, P value, or both. FC, fold-change. **(F)** Volcano plot analysis identifying significant changes of downstream targets within ribosome-bound RNA associated with BCMA knockdown. Color-coded dots show statistical significance associated with identified targets categorized into log_{10}Fc, P value, or both. **(G)** Representative heatmap of RPPA analysis showing subset of the significant changes in protein expression landscape associated with BCMA signaling axis. **(H)** Graphic illustration of large ribosome subunits (top) and small ribosome subunits (bottom). Each subunit shows changes in translation abundance upon BCMA loss. Decreased expression (green), no change (gray), or increased expression (red).

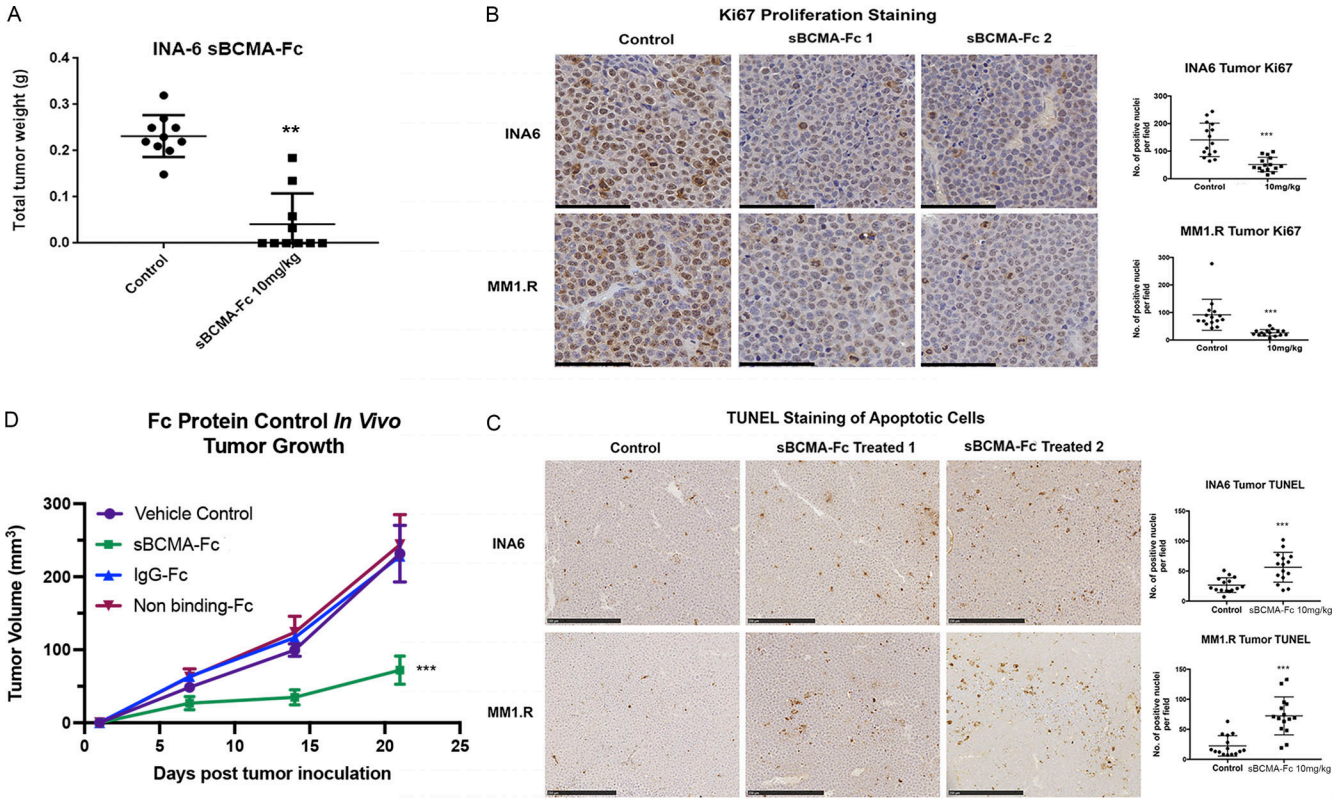

Figure S3. **Wild-type sBCMA decoy receptor treatment inhibits proliferation and promotes tumor cell death in MM. (A)** Terminal tumor weight of mice inoculated with INA-6 MM tumors and treated with vehicle control or 10 mg/kg of sBCMA-Fc (n = 10); P = 0.0082. **(B)** Representative images of Ki67-positive cells in the vehicle control and sBCMA-Fc–treated INA-6 (top panels) and MM1.R (bottom panels) MM tumors analyzed by IHC staining. Scale bar, 50 µm. Quantification of Ki67 staining on right. INA-6, P < 0.0001; MM1.R, P < 0.0001. **(C)** Representative images of TUNEL-positive cells in the vehicle control and sBCMA-Fc–treated INA-6 (top panels) and MM1.R (bottom panels) MM tumors analyzed by IHC staining. Quantification of TUNEL staining on right. INA-6, P = 0.0001; MM1.R, P < 0.0001. Scale bar, 50 µm. **(D)** Tumor growth kinetics of MM1.R tumors treated with vehicle control, sBCMA-Fc V3 (10 mg/kg; P < 0.0001), IgG-Fc control (10 mg/kg), and nonbinding Fc control (10 mg/kg; n = 5). Statistical analysis was conducted using t test and one-way ANOVA for comparing between treatment groups. Repeated ANOVA used for changes in tumor growth over time. *, P < 0.05; **, P < 0.01; ***, P < 0.001.

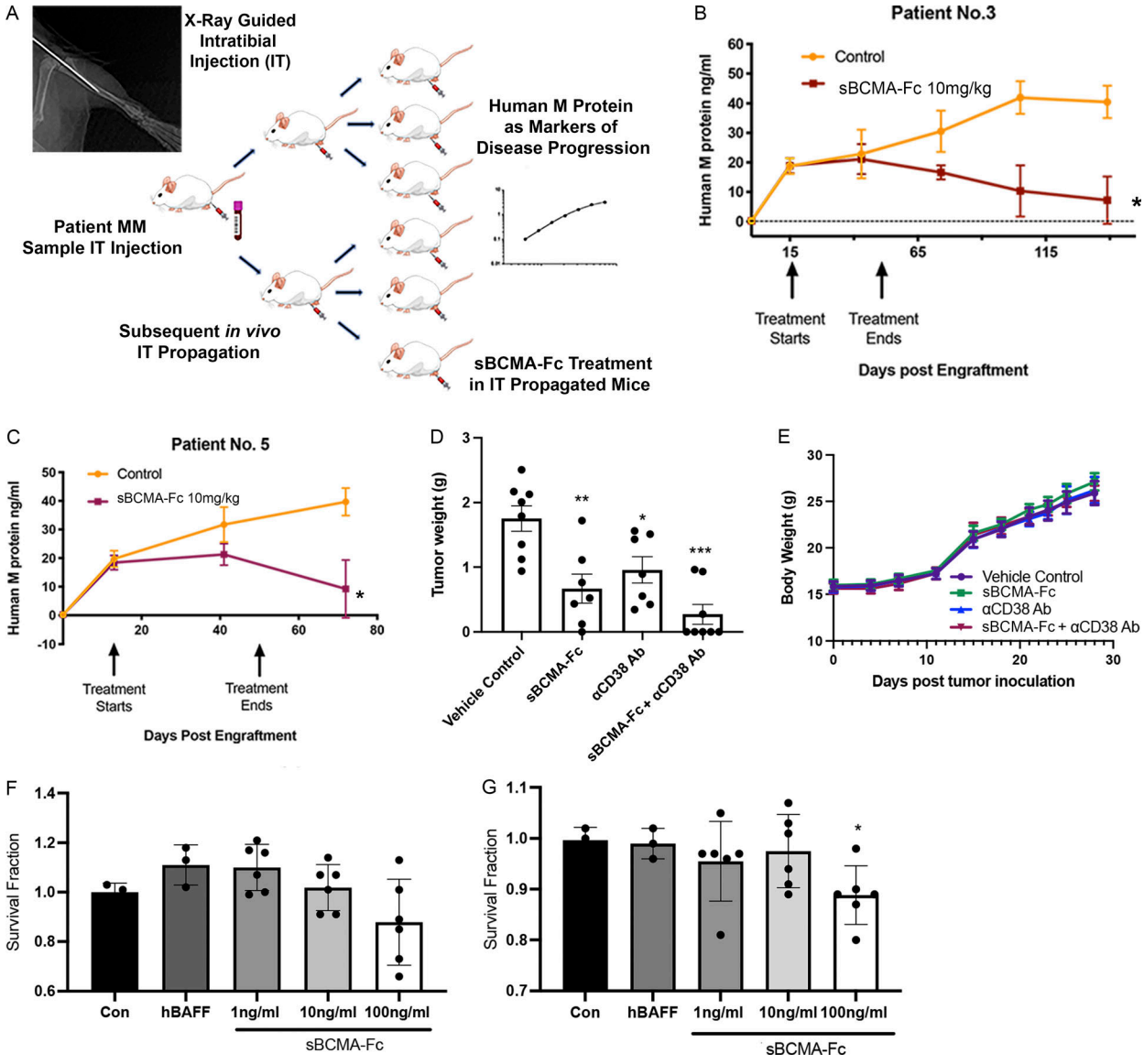

Figure S4. **Wild-type sBCMA decoy receptor inhibits MM growth in vivo but lacks efficacy in BAFF-driven DLBCL. (A)** Schematic flowchart of in vivo MM PDX propagation. Patient tumor cells were isolated from patient bone marrow biopsies and injected into the tibias of NSG mice. PDX were subsequently propagated in vivo using the same intratibial inoculation procedure and treated with vehicle control or sBCMA-Fc. Human IgG protein in mouse serum was continuously monitored over time as a marker of tumor progression. **(B)** Human IgG protein in mouse serum detected in animals successfully engrafted with MM cells from patient 3, showing reduction in human M protein level after sBCMA-Fc treatment (n = 8) compared with vehicle control (n = 7); P = 0.012. **(C)** Human IgG protein in mouse serum detected in animals successfully engrafted with MM cells from patient 5, showing reduction in human IgG protein level after sBCMA-Fc treatment (n = 10) compared with vehicle control (n = 10); P = 0.026. **(D)** Terminal tumor weight of MM1.R MM cells in mice dosed with sBCMA-Fc 10 mg/kg every 48 h (n = 7; P = 0.0078), αCD38 10 mg/kg weekly (n = 7; P = 0.01), sBCMA-Fc and αCD38 combination (n = 8; P < 0.0001), and vehicle control (n = 8) in 6-wk-old female NSG mice. **(E)** Changes in body weight of animals from study described in D. **(F)** sBCMA-Fc dose-dependent cytotoxicity assay validating in vitro cell survival in the presence of increasing doses of sBCMA-Fc and hBAFF (100 ng/ml) in SU-DHL-6 DLBCL cells. **(G)** sBCMA-Fc dose-dependent cytotoxicity assay validating in vitro cell survival in the presence of increasing doses of sBCMA-Fc and hBAFF (100 ng/ml) in Daudi DLBCL cells. Treatment with 100 ng/ml sBCMA-Fc led to significant reduction in cell number; P = 0.045. Statistical analysis was conducted using t test and one-way ANOVA for comparing between treatment groups. Repeated ANOVA used for changes in tumor growth over time. *, P < 0.05; **, P < 0.01; ***, P < 0.001.

A

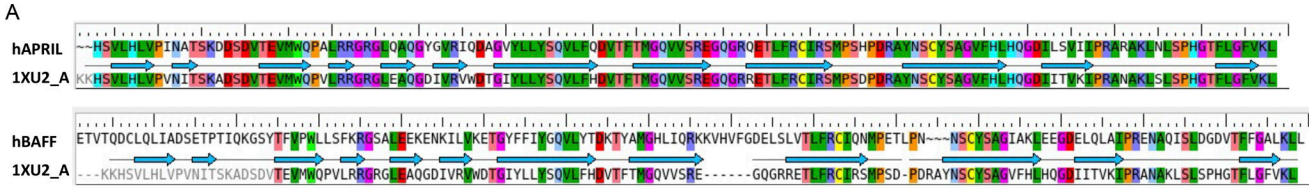

B

Sequence Alignment	Identities	Positives
hAPRIL(115-250) vs. 1XU2_A	86%	91%
hBAFF(140-285) vs. 1XU2_A	40%	58%

C

Structural Alignment	Score	RMSD(Å)
hAPRIL(4ZCH) vs. 1XU2_A	0.032	0.893
hBAFF(4ZCH) vs. 1XU2_A	0.062	1.248
hAPRIL(4ZCH) vs. hBAFF(4ZCH)	0.057	1.189

D

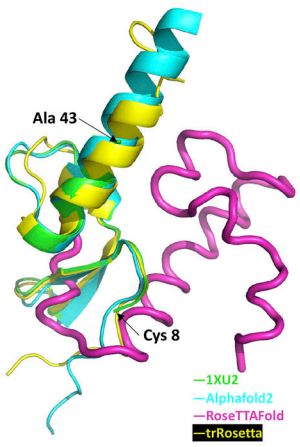

E

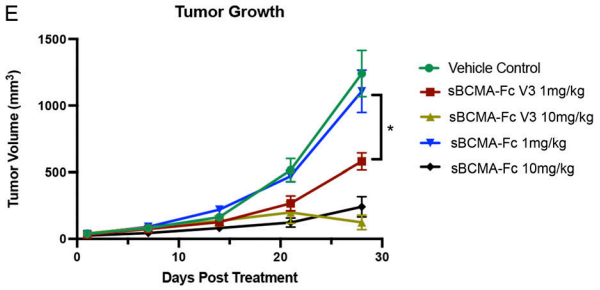

F

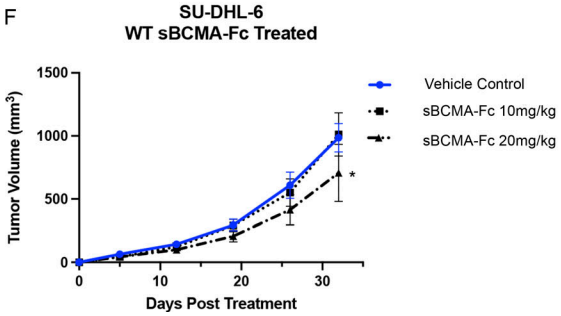

G

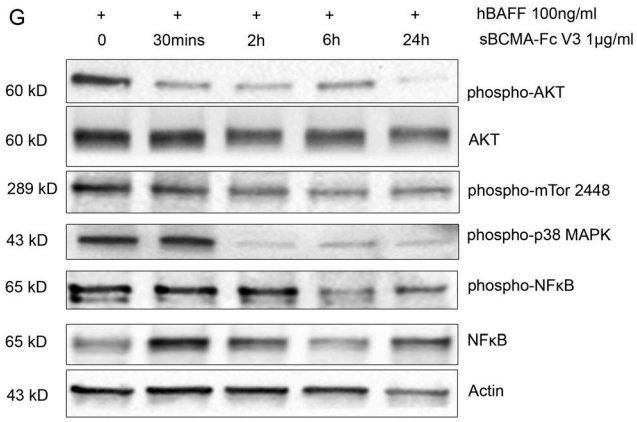

Figure S5. **Affinity-enhanced sBCMA-Fc V3 treatment inhibits tumor growth in models of MM and DLBCL. (A)** Amino acid sequence alignment between hAPRIL (top) or hBAFF (bottom) and Protein Data Bank structural ID 1XU2 (structure of mAPRIL and human sBCMA cocomplex). PDB 4ZCH reported a single-chain human APRIL-BAFF-BAFF heterotrimer structure. **(B)** Quantification of sequence alignment between hAPRIL/hBAFF and published structure 1XU2. **(C)** Quantification of structural alignment between hAPRIL/hBAFF and published structure 1XU2 as well as between predicted hAPRIL and hBAFF structures. **(D)** Structure overlay of extracellular BCMA flexible region (aa 44–54) between 1XU2 and structures predicted using Alphafold2 (cyan), RoseTTAfold (magenta), and trRosetta (yellow). **(E)** Subcutaneous tumor growth of MM1.R MM tumors in 6-wk-old female NSG mice dosed with wild-type sBCMA-Fc at 1 and 10 mg/kg every 48 h (n = 5), sBCMA-Fc V3 at 1 and 10 mg/kg every 48 h (n = 5), and vehicle control (n = 5). sBCMA-Fc V3 treatment significantly reduced tumor growth at 1 mg/kg; P = 0.031. **(F)** Subcutaneous tumor growth of SU-DHL-6 DLBCL in mice dosed with vehicle control, sBCMA-Fc 10 mg/kg, and sBCMA-Fc 20 mg/kg every 48 h (n = 5). sBCMA-Fc treatment significantly reduced tumor growth at 20 mg/kg; P = 0.043. **(G)** Analysis of BCMA downstream protein expression in SU-DHL-6 DLBCL cells upon sBCMA-Fc V3 treatment at multiple time points. Statistical analysis was conducted using t test and one-way ANOVA for comparing between treatment groups. Repeated ANOVA used for changes in tumor growth over time. *, P < 0.05; **, P < 0.01; ***, P < 0.001. Source data are available for this figure: SourceData FS5.

Provided online are Table S1, Table S2, Table S3, Table S4, Table S5, Table S6, Table S7, Table S8, and Table S9. Table S1 shows demographic information and treatment status of patient samples collected for establishing the MM PDX model. Table S2 shows clones selected from round 3. Table S3 shows clones selected from round 4. Table S4 shows clones selected from round 5. Table S5

shows clones selected from round 6. Table S6 shows male hematology results, part I. Table S7 shows male hematology results, part II. Table S8 shows female hematology results, part I. Table S9 shows female hematology results, part II.